

**INVESTIGATIONS ON THE STRUCTURAL, SPECTRAL AND
MAGNETIC INTERACTIONS OF TRANSITION METAL COMPLEXES
OF MULTIDENTATE LIGANDS FROM DI-2-PYRIDYL KETONE AND
N(4)-SUBSTITUTED THIOSEMICARBAZIDES**

Thesis submitted to

Cochin University of Science and Technology

*in partial fulfillment of the requirements
for the degree of*

DOCTOR OF PHILOSOPHY

in

CHEMISTRY

by

SUNI V.



**Department of Applied Chemistry
Cochin University of Science and Technology
Kochi - 682022**

August 2005

To my Mookāmbika...



DEPARTMENT OF APPLIED CHEMISTRY
COCHIN UNIVERSITY OF SCIENCE AND TECHNOLOGY
KOCHI - 682 022, INDIA


Phone Off. 0484-2575804
Phone Res. 0484-2576904
Telex: 885-5019 CUIN
Fax: 0484-2577595
Email: mrp@cusat.ac.in
mrp_k@yahoo.com

Prof. M.R. Prathapachandra Kurup
Head

29th August 2005

CERTIFICATE

This is to certify that the thesis entitled **“Investigations on the Structural, Spectral and Magnetic Interactions of Transition Metal Complexes of Multidentate Ligands from Di-2-pyridyl ketone and *N*(4)-substituted Thiosemicarbazides”** submitted by Ms. Suni V., in partial fulfillment of the requirements for the degree of Doctor of Philosophy, to the Cochin University of Science and Technology, Kochi-22, is an authentic record of the original research work carried out by her under my guidance and supervision. The results embodied in this thesis, in full or in part, have not been submitted for the award of any other degree.


M. R. Prathapachandra Kurup
(Supervisor)

DECLARATION

I hereby declare that the work presented in this thesis entitled “**Investigations on the Structural, Spectral and Magnetic Interactions of Transition Metal Complexes of Multidentate Ligands from Di-2-pyridyl ketone and N(4)-substituted Thiosemicarbazides**” is entirely original and was carried out independently under the supervision of Professor M. R. Prathapachandra Kurup, Department of Applied Chemistry, Cochin University of Science and Technology, and has not been included in any other thesis submitted previously for the award of any degree.



Suni V.

Kochi-22,
29th August 2005.

A few words of gratitude...

Interdependence is a higher value than independence, and hence here I place on record some of the many instances where people bestowed their wholehearted support upon me.

I am indebted to my supervising guide, Dr. M. R. Prathapachandra Kurup, Professor and Head, for his valuable suggestions and timely support and for providing the necessary facilities. Throughout my research tenure, his kind and approachable attitude helped me a lot. I am very much grateful to Dr. K. K. Mohammed Yusuff, Professor of Catalysis, for his wholehearted support as my doctoral committee member. I also deeply acknowledge the support received from all the teaching and non-teaching staff of the Dept. of Applied Chemistry, CUSAT.

I am grateful to the Cochin University of Science and Technology and the Kerala State Council for Science, Technology and Environment, for their financial support in the form of Junior Research Fellowships.

My sincere thanks are due to Dr. M. Nethaji, Dept. of Inorganic and Physical Chemistry, IISc Bangalore, for the help in single crystal X-ray diffraction studies. To Dr. M. V. Rajasekharan, School of Chemical Sciences, University of Hyderabad, I owe much for providing the program 'suscep.for', which contributed a lot towards my studies. I am much thankful to Dr. Suja Haridas, Mr. Arun V. and Mr. John P. R. for the help received in DRS and IR measurements. I acknowledge the head of the institutions of IIT Mumbai, IIT Roorkee, IISc Bangalore, CDRI Lucknow and SAIF Cochin for the services they provided in analytical measurements.

I owe much to Dr. Rohith P. John and Dr. Varughese Philip for their valuable suggestions during the early stages of my work. To Dr. Marthakutty Joseph and Dr. S. Sivakumar, I am immensely thankful for providing the necessary text book materials. I am much thankful to Dr. Sreeja P. B. for her love and affection. I always enjoyed the enthusiasm shared with my colleague, Dr. A. Sreekanth. To my dearest senior Dr. Chandini R. Nayar, I am indebted for the power of her words, which provided instant solutions to many of my unrelenting problems.

Among my labmates, I always enjoyed the light company and sisterly affection of Minikutty. Bessy dear was there to get as busy and tensed as myself at the final stages of this thesis, committing her wholehearted efforts towards its timely submission. To Raphael Sir, Seena, Manoj, Sreesha, Binu, Leji and Suja, I am deeply thankful for their warm support and encouragement.

My friends were always there to boost up my confidence. I am much obliged to Veena and Vifzi for being my constant source of inspiration and support. To my roommate Daby, I am immensely grateful for her ready to help attitude in all circumstances. I am much thankful to Rosh for her help in NMR measurements. I owe much to all my friends, especially Dinny, Smitha, Vidya, Radhika and Lala for their sweet affection and support. Last but not the least, I heartily acknowledge my dear parents and little brother for always being there with me.

Suni V.

CONTENTS

Chapter 1

A Prologue on the chemistry of thiosemicarbazones

1.1.	Thiosemicarbazones- why they are important?	2
1.2.	Thiosemicarbazones: applications	5
1.3.	Objectives and scope of the present work	8
1.4.	Physical measurements	9
1.5.	Crystallographic data collection and structure analyses	9
	References	10

Chapter 2

Syntheses, crystal structures and spectral characterization of ligands from di-2-pyridyl ketone and *N*(4)-substituted thiosemicarbazides

2.1.	Di-2-pyridylmethanone <i>N</i> (4)-phenylthiosemicarbazone, HL ¹	14
2.2.	<i>N</i> (4)-Cyclohexyl-2-[hydroxy(di-2-pyridyl)methyl]hydrazine-carbothioamide, HL ²	24
2.3.	Di-2-pyridylmethanone <i>N</i> (4)-cyclohexylthiosemicarbazone, HL ³	33
2.4.	<i>N</i> -[di-2-pyridylmethylene]morpholine-4-carbothiohydrazide, HL ⁴	37
2.5.	Experimental	38
	References	42

Chapter 3

Studies of structural, EPR spectral and magnetic interactions of Cu(II) complexes synthesized from di-2-pyridyl ketone *N*(4)- phenyl- and *N*(4)-cyclohexylthiosemicarbazones

3.1.	Stereochemistry of the complexes	46
3.1.1.	Cu ₂ TdCl ₃	46
3.1.2.	CuL ¹ N ₃	58
3.1.3.	Cu ₂ (L ¹) ₂ Br ₂ ·7H ₂ O	63
3.1.4.	Cu ₂ (L ¹) ₂ (SCN) ₂ ·4H ₂ O	66
3.1.5.	Cu ₂ (L ¹) ₂ (SO ₄)·1.5 H ₂ O	70
3.1.6.	Cu(L ³) ₂ ·4H ₂ O	71
3.1.7.	CuL ³ Cl·5H ₂ O	73
3.1.8.	Cu ₂ (L ³) ₂ (N ₃) ₂ ·2H ₂ O	74

3.2.	Magnetochemistry of the complexes	80
3.2.1.	Cu_2TdCl_3	82
3.2.2.	$\text{Cu}_2(\text{L}^1)_2\text{Br}_2 \cdot 7\text{H}_2\text{O}$	85
3.2.3.	CuL^1N_3	87
3.2.4.	$\text{Cu}_2(\text{L}^1)_2(\text{SCN})_2 \cdot 4\text{H}_2\text{O}$, $\text{Cu}(\text{L}^3)_2 \cdot 4\text{H}_2\text{O}$, $\text{CuL}^3\text{Cl} \cdot 5\text{H}_2\text{O}$ and $\text{Cu}_2(\text{L}^3)_2(\text{N}_3)_2 \cdot 2\text{H}_2\text{O}$	89
3.2.5.	$\text{Cu}_2(\text{L}^1)_2(\text{SO}_4) \cdot 1.5 \text{H}_2\text{O}$	89
3.3.	Experimental	91
	References	97

Chapter 4

Syntheses, structural, EPR and magnetic studies of Mn(II) and VO(IV) complexes of di-2-pyridyl ketone *N*(4)-substituted thiosemicarbazones

4.1.	Stereochemistry of the complexes	101
4.1.1.	$\text{Mn}(\text{L}^1)_2 \cdot \text{H}_2\text{O}$	101
4.1.2.	$\text{Mn}(\text{L}^3)_2$	108
4.1.3.	$\text{Mn}(\text{L}^4)_2$	110
4.1.4.	$\text{VOL}^1(\text{acac}) \cdot 2\text{H}_2\text{O}$	112
4.1.5.	$\text{VOL}^3(\text{acac})$	114
4.2.	Magnetochemistry of the complexes	117
4.2.1.	$\text{Mn}(\text{L}^1)_2 \cdot \text{H}_2\text{O}$	117
4.2.2.	$\text{Mn}(\text{L}^3)_2$	119
4.2.3.	$\text{VOL}^3(\text{acac})$	120
4.3.	Experimental	121
	References	129

Chapter 5

Ni(II) complexes of di-2-pyridyl ketone *N*(4)-cyclohexyl- and *N*(4)-phenylthiosemicarbazones - Syntheses, structural and spectral investigations

5.1.	Stereochemistry of the complexes	133
5.1.1.	$\text{Ni}(\text{L}^1)_2 \cdot 2\text{H}_2\text{O}$	133
5.1.2.	$\text{NiL}^1\text{NCS} \cdot 2\text{H}_2\text{O}$	137
5.1.3.	$\text{NiL}^1\text{Cl} \cdot 3\text{H}_2\text{O}$	141
5.1.4.	$\text{NiL}^1\text{N}_3 \cdot 4.5 \text{H}_2\text{O}$	142

5.1.5.	$\text{Ni}_2(\text{L}^1)_2\text{SO}_4 \cdot 4\text{H}_2\text{O}$	143
5.1.6.	$\text{NiL}^2\text{NCS} \cdot 2\text{H}_2\text{O}$	144
5.1.7.	$\text{NiL}^2\text{ClO}_4 \cdot 2\text{H}_2\text{O}$	147
5.1.8.	$\text{NiL}^2\text{Cl} \cdot 0.5\text{H}_2\text{O}$	150
5.2.	Magnetochemistry of the complexes	152
5.2.1.	$\text{Ni}(\text{L}^1)_2 \cdot 2\text{H}_2\text{O}$	153
5.2.2.	$\text{NiL}^1\text{N}_3 \cdot 4.5 \text{H}_2\text{O}$	155
5.2.3.	$\text{Ni}_2(\text{L}^1)_2\text{SO}_4 \cdot 4\text{H}_2\text{O}$	157
5.2.4.	$\text{NiL}^2\text{Cl} \cdot 0.5\text{H}_2\text{O}$	158
5.2.5.	$\text{NiL}^1\text{NCS} \cdot 2\text{H}_2\text{O}$, $\text{NiL}^1\text{Cl} \cdot 3\text{H}_2\text{O}$, $\text{NiL}^2\text{ClO}_4 \cdot 2 \text{H}_2\text{O}$ and $\text{NiL}^2\text{NCS} \cdot 2\text{H}_2\text{O}$	159
5.3.	Experimental	160
	References	167

Chapter 6

Syntheses and studies on some Co(II) and Co(III) complexes of di-2-pyridyl ketone *N*(4)-cyclohexyl- and *N*(4)-phenylthiosemicarbazones

6.1.	Stereochemistry of the complexes:	170
6.1.1.	$\text{Co}_2(\text{L}^1)_2\text{Cl}_2 \cdot 4\text{H}_2\text{O}$	171
6.1.2.	$\text{CoL}^1(\text{NCS})_2 \cdot 3\text{H}_2\text{O}$	172
6.1.3.	$[\text{Co}(\text{L}^1)_2]\text{NO}_3 \cdot 3\text{H}_2\text{O}$	173
6.1.4.	$\text{CoL}^1\text{Br}_2 \cdot 4.5\text{H}_2\text{O}$	174
6.1.5.	$\text{CoL}^3\text{NCS} \cdot 2\text{H}_2\text{O}$	175
6.1.6.	$[\text{Co}(\text{L}^3)_2]\text{ClO}_4$	177
6.1.7.	$[\text{Co}(\text{dpk})_2]\text{Br} \cdot 4\text{H}_2\text{O}$	178
6.2.	Magnetochemistry of the complexes	182
6.2.1.	$\text{CoL}^1\text{Cl} \cdot 2\text{H}_2\text{O}$	182
6.2.2.	$\text{CoL}^3\text{NCS} \cdot 2\text{H}_2\text{O}$	183
6.3.	Experimental	184
	References	188

Chapter 7

Zn(II) and Cd(II) complexes of di-2-pyridyl ketone *N*(4)-substituted thiosemicarbazones: Syntheses and spectral investigations

7.1.	Stereochemistry of the complexes	191
7.1.1.	ZnL^1Cl	191
7.1.2.	$\text{ZnL}^1\text{NCS} \cdot 2\text{H}_2\text{O}$	194
7.1.3.	ZnL^1NO_3	196
7.1.4.	$\text{ZnL}^1\text{N}_3 \cdot \text{CH}_3\text{OH}$	198

7.1.5.	ZnL ¹ OAc · 1.5H ₂ O	199
7.1.6.	ZnL ¹ Br	201
7.1.7.	ZnL ² Cl	203
7.1.8.	ZnL ² NCS · 2H ₂ O	204
7.1.9.	ZnL ² OAc	207
7.1.10.	CdL ¹ Cl · 2H ₂ O	208
7.1.11.	(CdL ¹ NCS) ₂	210
7.1.12.	CdL ¹ N ₃	212
7.1.13.	CdL ¹ Br · 2H ₂ O	213
7.1.14.	CdL ³ Cl · 2H ₂ O	213
7.1.15.	(CdL ³ N ₃) ₂	215
7.1.16.	(CdL ³ NCS) ₂	217
7.1.17.	CdL ³ Br · 4H ₂ O	218
7.1.18.	CdL ³ OAc	219
7.2	Experimental	222
	References	227
	Summary and Conclusion	228

CHAPTER 1

A prologue on the chemistry of thiosemicarbazones

Metallo-organic chemistry, incorporating the frontiers of both inorganic and organic chemical aspects, is a topic of utility concern. The first exploration of coordinated metal complexes dates back to the nineteenth century, during the days of Alfred Werner [1]. Thereafter, the inorganic chemistry witnessed a great outflow of coordination compounds, with unique structural characteristics and diverse applications. In the modern ages, the stereochemistry of most of the coordination compounds can be explored by accommodating the concepts of electronic energy levels and bonding, but however there are several instances where unusual structures and theoretical challenges are observed.

The stereochemistry of coordination compounds is one of the major interests of the coordination chemist. Coordination complexes can assume a wide variety of structures depending on the metal ion, its coordination number and the denticity of the ligands used. The ligands also range from monodentate to polydentate based on the potential donor sites available in their structural skeleton. The presence of more electronegative nitrogen, oxygen or sulfur atoms on the ligand structure is established to enhance the coordinating possibilities of ligands. Hence there has been a continuous quest over the many years for nitrogen or sulfur donor ligands, which possess a variety of coordination possibilities.

In this aspect, the thiosemicarbazides having the general formula $\text{NH}_2\text{-C(S)-NH-NH}_2$ are of note, since they have potential donor sites available for coordination. The chemistry of thiosemicarbazides and their substituted derivatives are well explored. Condensation of these thiosemicarbazides with aldehydes or ketones with potential donor sites yield Schiff bases termed as thiosemicarbazones, and they are having extended conjugation and enhanced activity. Complexation of these active Schiff bases or thiosemicarbazones with transition or main group metals improve their activities and thus further extend the chemistry of thiosemicarbazones in their versatile stereochemistries and applications.

1.1. Thiosemicarbazones- why they are important?

The beginning of the exploration of thiosemicarbazone chemistry dates back to many decades. Thiosemicarbazones are thiourea derivatives with the following general formula (Fig. 1.1). The numbering scheme shown in the figure is in accordance with the IUPAC system of numbering for thiosemicarbazones:

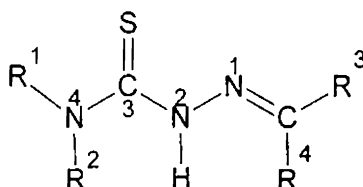


Fig. 1. 1. General formula of a substituted thiosemicarbazone

However it should be noted that the numbering schemes in the crystal structures are based on the types of different atoms present, and in the present study, since di-2-pyridyl ketone occupies the ketonic part, the nitrogen atom at *N*(4) is labelled as *N*5.

An interesting attribute of the thiosemicarbazones is that in the solid state, they predominantly exist in the thione form, whereas in solution state, they exhibit a thione-thiol tautomerism (Fig. 1. 2). The thiol form predominates in the solution state, and a deprotonation at the thiolate sulfur render the thiosemicarbazone an anionic ligand, which can effectively coordinate to a metal atom.

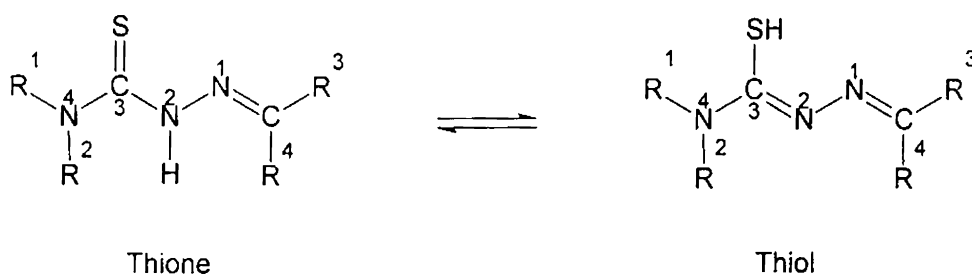
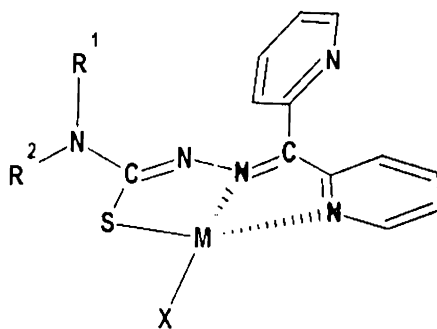


Fig. 1. 2. Thiol-thione equilibrium of a substituted thiosemicarbazone

In addition, it should be noted that in the thiol form, there is an effective conjugation along the thiosemicarbazone skeleton thus giving rise to an efficient electron delocalization along the moiety. Aromatic substituents on the skeleton can

further enhance the delocalization of electron charge density. Due to this reason, we have chosen di-2-pyridyl ketone to occupy the ketonic part of our ligands. Upon coordination to a metal centre, the delocalization is further increased through the metal chelate rings. Thus it can be inferred that the di-2-pyridyl ketone thiosemicarbazones and their metal complexes are highly conjugated systems, which offer a variety of potential applications.

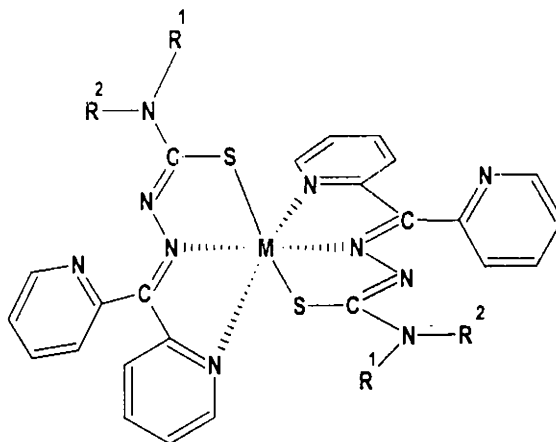
Interestingly, thiosemicarbazones show a variety of coordination modes with transition metals. The coordination mode is influenced by the number and type of the substituents. This is because, the active donor sites of the ligand varies depending upon the substituents. The presence of di-2-pyridyl ketone at the ketonic part attributes many interesting coordinating possibilities for the ligands under study. Due to the deprotonation, a metal–sulfur covalent bond is formed in the complex. In addition to this, coordination occurs through the azomethine nitrogen and one of the pyridyl nitrogens, thus the thiosemicarbazone acting as a tridentate ligand (Structure I). The anionic coligand is denoted by 'X' in the structures (I-IV) below:



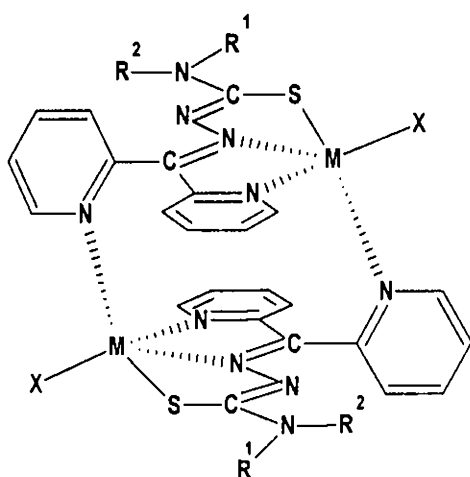
Structure I

However, in some cases, thiosemicarbazone exhibits potential quadridentate attributes, when the second pyridyl nitrogen of a four-coordinated metal complex shows some tendency to form a coordinate bond with the metal centre of an adjacent metal complex in the lattice. This gives rise to dimeric five-coordinated structures. Dimeric structures also result when two metal centres are bridged through anions such as chloride, bromide, azide etc. There are also reports on the thiolate sulfur bridging in

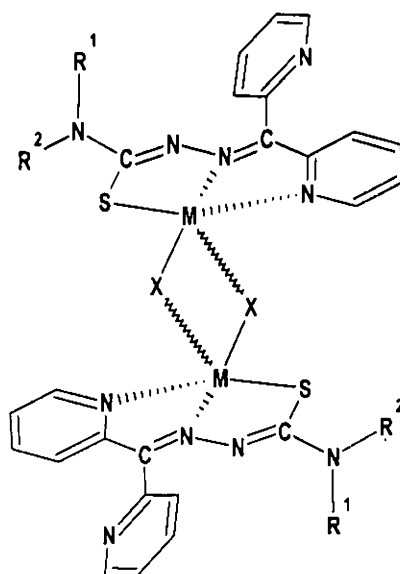
dimeric structures of thiosemicarbazones [2]. Some of the possible coordination modes of di-2-pyridyl ketone thiosemicarbazones are shown below:



Structure II



Structure III



Structure IV

1.2. Thiosemicarbazones: Applications

The chief motive in many a research work on thiosemicarbazones is still, its versatile biological activities. The magic influence of the sulfur atom in the structural skeleton plays the key role in enabling thiosemicarbazones biologically important. However, the lipophilicity, which controls the rate of entry into the cell, is modified by coordination [3]. Also the metal complex can be more active than the free ligand, and some side effects may decrease upon complexation [4]. The resultant is that there are many volumes of literature on the study of bioactive thiosemicarbazones.

The antiviral activity of thiosemicarbazones was first reported in 1950 by Hamre *et al.*, who found that derivatives of benzaldehyde thiosemicarbazone were active against neurovaccinial infection in mice when given orally [5]. A clinical trial of the *N*-methyl derivative of isatin- β -thiosemicarbazone (methisazone) was carried out in India [6-8], and the studies indicated that the drug was effective in the prevention of smallpox in persons exposed to the disease. Sidwell and co-workers in 1969 evaluated a series of purine analogs as antiviral agents and demonstrated that purine-6-carboxaldehyde thiosemicarbazone was effective in suppressing both the cytopathic effect and the titers of human cytomegalo virus [9] and this was the first report of a substituted thiosemicarbazone being active against a herpes virus. However, Shipman *et al.* [10] in 1981 reported the selective antiviral activity of 2-acetylpyridine thiosemicarbazones against HSV-1 and HSV-2. Meanwhile, some thiosemicarbazone derivatives of (\pm)-3-menthone are reported to show antiviral effects against the replication of HIV-1 (IIIB) and HIV-2 (ROD) in acutely infected MT-4 cells [11]. It was found that thiosemicarbazones with chlorobenzene substituents at the *N*(4) position revealed the highest activity among the various (\pm)-3-menthone thiosemicarbazones. The effect of heterocyclic thiosemicarbazones against HSV was examined by Brockman and co-workers [12]. A series of thiosemicarbazones derived from 2-acetylpyridine, 2-acetylquinoline and 1-acetylquinoline were evaluated as inhibitors of type 1 and type 2 herpes simplex virus and some of them were highly active [13]. The selective inhibition of HSV ribonucleotide diphosphate reductase by 2-acetylpyridine thiosemicarbazone derivatives was investigated and the results

supported the hypothesis that the HSV-induced RDR is an important target for the design of antiviral drugs [14]. Some transition metal complexes of thiosemicarbazones of β -diketones are also reported to exhibit antitumour activity [15].

Thiosemicarbazones and their metal complexes present a wide spectrum of antimicrobial activity. As early as in 1946, Domagk reported that some thiosemicarbazones of cyclic aldehydes and ketones possessed antitubercular activity *in vitro* [16]. Later, 2-formylpyridine thiosemicarbazones and their VO(IV) complexes exhibited powerful *in vitro* antibacterial activities towards *E. coli* [17] and aryl thiosemicarbazones showed good activity against *Aeromonas Hydrophilia* and *Salmonella typhimurium* [18]. A recent work reports slight antibacterial activity of thiosemicarbazones and thiocarbohydrazones of 1-adamantyl 2-pyridyl ketone and 1-adamantyl methyl ketone [19]. Base adducts of Cu(II) complexes synthesized from salicylaldehyde *N*(4)-phenylthiosemicarbazone showed growth inhibitory activity against the human pathogenic bacteria *Salmonella typhi*, *Shigella dysenteriae*, non-coagulace *Staphylococcus*, *Photobacterium* sp. and *S. aureus* and the complexes against plant pathogenic fungi. An increase in coordination number from 4 to 5 in the complexes led to higher activity, probably due to increase in lipophilicity [20].

In 1963, French *et al.* formulated hypotheses about the mode of action of the α (*N*)-heterocyclic thiosemicarbazones. The first was that they were acting as tridentate ligands and the second was that modifying the ring system while retaining the ligand pattern could lead to improved activity and decreased toxicity. The electron densities, substituents and geometry could have critical effects on activity [21]. According to this prediction, the pyrazine carboxaldehyde thiosemicarbazone exhibited greater activity on L-1210 cells than 2-formylpyridine thiosemicarbazone and was active on Lewis lung carcinoma (LLC). Sartorelli *et al.* showed that 2-formylpyridine thiosemicarbazones caused marked inhibition of the incorporation of 3H-thymidine into the DNA of several tumor lines. The syntheses of RNA and protein were considerably less sensitive to these agents [22]. The site of metabolic lesion on the DNA biosyntheses was supposed to be the conversion of ribonucleotides to deoxyribonucleotides, catalysed by the enzyme ribonucleoside diphosphate reductase.

Some thiosemicarbazone derivatives are also reported to show second-harmonic generation (SHG) abilities. Non-linear optical materials exhibiting efficient SHG abilities at short wavelengths are needed in the fields of high-density optical recording, laser printing, and optical measurement systems and for other applications [23-25]. The large non-linearities of π -conjugated organics and favourable crystal growth characteristics and mechanical properties of ionic salts should combine to give an ideal NLO crystal. Semiorganic compounds have the potential for combining the high optical nonlinearity and chemical flexibility of organics with the physical ruggedness of inorganics. Consequently, some zinc halide complexes synthesized from 4-methoxybenzaldehyde thiosemicarbazone are found to possess non-linear optical properties [26]. Similarly, theoretical and experimental second order optical nonlinearity studies on cadmium halides of bis(2-chlorobenzaldehyde thiosemicarbazone) are also reported [27], and it was concluded that the intermolecular contacts are the main factors controlling the SHG efficiencies of these compounds.

Thiosemicarbazone derivatives and their metal complexes are also reported to have diverse analytical applications [28]. Pavon *et al.* reported the 4-phenyl-3-thiosemicarbazone of biacetylmonoxime as an analytical reagent [29]. The Mn(II) complexes of the above thiosemicarbazone was suggested for the selective spectrophotometric determination of manganese, by means of extraction in amyl alcohol, at pH 10, where interference of iron(III) is eliminated by masking with tartrate. 2-Hydroxy-5-methoxybenzaldehyde thiosemicarbazone and 2-hydroxy-5-chlorobenzaldehyde thiosemicarbazone formed fluorescent complexes with gallium, and are recommended as selective reagents for gallium [30]. Some nickel complexes of thiosemicarbazones are reported to function as effective homogeneous catalysts for the alcoholysis of silanes [31] and for the reduction of imines to primary and secondary amines [32]. Thiosemicarbazones are also reported to have corrosion inhibition properties [33]. There are also some studies on the electrochemical and positron annihilation studies of thiosemicarbazones [34]. However, the field of molecular magnetism appears to be little contributed by studies on thiosemicarbazone systems. This is rather surprising, when considering the appreciable electron

delocalization effects in thiosemicarbazone systems and the diverse structural possibilities of their metal complexes.

1.3. Objectives and scope of the present work

The magnetochemistry of di-2-pyridyl ketone complexes is a current hot subject of research, which mainly owes to the excellent structural diversity of the complexes ranging from cubanes to clusters, with promising ferromagnetic outputs. Some of these research endeavours worth quoting include the copper and bismuth complexes reported by Breeze *et al.*, which yielded ferromagnetically coupled tetranuclear Cu(II) chains [35]. Here the di-2-pyridyl ketone was observed to undergo a reversible addition with water in presence of acetic acid to form di-2-pyridyl methanediol and the complex exhibited long-range ferromagnetic ordering below 2 K. The case of a Cu₄ rhombus in molecular magnetism was described by Tangoulis *et al.* using a tetrameric Cu(II) cluster of monomethylated diol of di-2-pyridyl ketone [36]. The magnetic susceptibility data here was fitted with a 3-*J* magnetic model, simultaneously affording a very strong antiferromagnetic, a weak ferromagnetic and a very weak antiferromagnetic interactions. There are many other similar reports of di-2-pyridyl single molecule magnets [37-40], however, all these reports were concerned with either the di-2-pyridyl ketone or its mono- or dimethylated anion as the principal ligand. Little efforts were aimed at the magnetochemistry of metal complexes of di-2-pyridyl ketone thiosemicarbazones. The only comparable work was reported by Cheng *et al.*, [41] where a macrocyclic tetranuclear Cu(II) complex of bis[phenyl(2-pyridyl)methanone]thiocarbazone was studied for its variation of magnetic susceptibility with temperature. However, as far as the monothiosemicarbazones are concerned, the magnetochemistry of transition metal complexes of di-2-pyridyl ketone thiosemicarbazones turned up quite unexplored. Consequently, an investigation into it appeared novel and promising to us, which prompted this study, which can be regarded as the initial step towards the exploration of magnetochemistry of metal complexes of thiosemicarbazones, especially the di-2-pyridyl ketone derivatives.

Hence, we synthesized four new ligands and their metal complexes and characterized them using spectroscopic, EPR and/or crystallographic methods.

Paramagnetic metal complexes are also studied for their magnetic behavior. The instrumental details of the various analyses are given below.

1.4. Physical Measurements

Elemental analyses are carried out at Central Drug Research Institute, Lucknow using a Heraeus Elemental Analyser and at Sophisticated Analytical Instruments Facility, Kochi using VarioEL III CHNS. The magnetic susceptibility measurements are carried out in the polycrystalline state on a Vibrating Sample Magnetometer (VSM) at 5.0 kOe field strength at various temperatures between 80 to 298 K at Indian Institute of Technology, Roorkee. The magnetic susceptibility values are then fitted into various magnetic equations by least square fitting methods using the program *suscep.for* developed by Dr. M. V. Rajasekharan, School of Chemistry, University of Hyderabad. Infrared spectral measurements are done on an ABB Bomem FTIR instrument using KBr pellets for spectra in the region 4000 - 500 cm^{-1} . The far IR spectra are recorded using polyethylene pellets in the 500-100 cm^{-1} region on a Nicolet Magna 550 FTIR instrument at Regional Sophisticated Instrumentation Facility, Indian Institute of Technology, Bombay. Ocean Optics SD 2000 Fiber Optic Spectrometer is used to measure solid-state reflectance spectra in the range 200 – 900 nm. NMR spectra were recorded using Bruker AMX 400 FT-NMR Spectrometer using TMS as the internal standard at Sophisticated Instruments Facility, Indian Institute of Science, Bangalore. EPR spectral measurements are carried out on a Varian E-112 X-band spectrometer using TCNE as standard at Regional Sophisticated Instrumentation Facility, Indian Institute of Technology, Bombay.

1.5. Crystallographic data collection and structure analyses

Single crystal X-ray diffraction measurements are carried out on a Bruker Smart Apex CCD diffractometer equipped with fine-focused sealed tube at the Dept. of Inorganic and Physical Chemistry, Indian Institute of Science, Bangalore. The unit cell parameters are determined and the data collections are performed using a graphite-monochromated $\text{Mo K}\alpha$ ($\lambda = 0.71073 \text{ \AA}$) radiation. The data collected are reduced using SAINT program [42] and the empirical absorption corrections are carried out

using the SADABS program [43]. The trial structure was obtained by direct methods [44] using SHELXS-97, which revealed the position of all non-hydrogen atoms and refined by full-matrix least squares on F^2 (SHELXL-97) [45] and the graphics tool used is DIAMOND [46]. All non-hydrogen atoms are refined anisotropically, while the hydrogen atoms are treated with a mixture of independent and constrained refinements.

References

1. J. E. Huheey, E. A. Keiter, R. L. Keiter, *Inorganic Chemistry, Principles of Structure and Reactivity*, 4th ed., Harper Collins College Publishers, New York, 1993.
2. M. Joseph, V. Suni, M. R. P. Kurup, M. Nethaji, A. Kishore, S. G. Bhat, *Polyhedron* 23 (2004) 3069.
3. N. Farrel, *Coord. Chem. Rev.* 1 (2002) 232.
4. H. Beraldo, D. Gambino, *Mini Rev. Med. Chem.* 4 (2004) 159.
5. D. Hamre, J. Bernstein, R. Donovan, *Proc. Soc. Exp. Biol. Med.* 73 (1950) 275.
6. D. J. Bauer, *Ann. N. Y. Acad. Sci.* 130 (1965) 110.
7. D. J. Bauer, L. St. Vincent, C. H. Kempe, A. W. Downie, *Lancetii* (1963) 494.
8. D. J. Bauer, L. St. Vincent, C. H. Kempe, P. A. Young, W. Downie, *Am. J. Epidemiol.* 90 (1969) 130.
9. R. W. Sidwell, G. Arnett, G. J. Dixon, F. M. Schabel, Jr., *Proc. Soc. Exp. Biol. Med.* 131 (1969) 1223.
10. C. Shipman, Jr., S. H. Smith, J. C. Drach, D. L. Klayman, *Antimicrob. Agents Chemother.* 19 (1981) 682.
11. V. Mishra, S. N. Pandeya, C. Pannecouque, M. Witvrouw, E. De Clercq, *Arch. Pharm. Pharm. Med. Chem.* 5 (2002) 183.

12. R. W. Brockman, R. W. Sidwell, G. Arnett, S. Shaddix, *Proc. Soc. Exp. Biol. Med.* 133 (1970) 609.
13. C. Shipman, Jr., S. H. Smith, J. C. Drach, D. L. Klayman, *Antiviral Research* 6 (1986) 197.
14. S. R. Turk, C. Shipman, J. C. Drach, *Biochem. Pharmacol.* 35 (1986) 1539.
15. S. Jayasree, K. K. Aravindakshan, *Polyhedron*, 12 (1993) 1187.
16. G. Domajk, R. Behnish, F. Mietzch, H. Schimidt, *Naturwissenschaften* 33 (1946) 315.
17. A. Maiti, A. K. Guha, S. Ghosh, *J. Inorg. Biochem.* 33 (1988) 57.
18. S. K. Singh, S. N. Pandeya, *Boll. Chim. Farm.* 140 (2001) 238.
19. A. Kolocouris, K. Dimas, C. Pannecouque, M. Witvrouw, G. B. Boscolos, G. Stamatou, G. Fytas, G. Zoidis, N. Kolocouros, G. Andrei, R. Snoeck, E. De Clerq, *Biorg. Med. Chem. Lett.* 12 (2002) 723.
20. P. Bindu, M. R. P. Kurup, T. R. Satyakeerty, *Polyhedron* 18 (1999) 321.
21. F. A. French, E. J. Blanz, Jr., *Cancer Res.* 25 (1965) 1454.
22. A. C. Sartorelli, E. C. Moore, K. C. Agrawal, *Biochem. Pharmacol.* 20 (1971) 3119.
23. J. Zyss, I. Ledoux, *Chem. Rev.* 94 (1994) 77.
24. W. E. Maerner, S. M. Silence, *Chem. Rev.* 94 (1994) 127.
25. T. Verbiest, S. Houbrechts, M. Kauranen, A. Persoons, *J. Mater. Chem.* 7 (1997) 2175.
26. Y. -P. Tian, W. -T. Yu, C. -Y. Zhao, M. -H. Jiang, Z. -G. Cai, H. -K. Fun, *Polyhedron* 21 (2002) 1217.
27. Y. -P. Tian, C. -Y. Duan, C. -Y. Zhao, X. -Z. You, T. C. W. Mak, Z. -Y. Zhang, *Inorg. Chem.* 36 (1997) 1247.
28. R. B. Singh, B. S. Garg, R. P. Singh, *Talanta* 25 (1978) 619.
29. J. N. C. Pavon, J. C. J. Sanchez, F. Pino, *Anal. Chim. Acta* 75 (1975) 335.
30. K. Morisige, *Anal. Chim. Acta* 72 (1974) 295.
31. D. E. Barber, Z. Lu, T. Richardson, R. H. Crabtree, *Inorg. Chem.* 31 (1992) 4709.

32. A. H. Vetter, A. Berkessel, *Synthesis* (1995) 419.
33. E. E. Ebenso, U. J. Ekpe, B. I. Ita, O. E. Offiong, U. J. Ibok, *Mat. Chem. Phys.* 60 (1999) 79.
34. J. E. J.C. Graudo, C. A. L. Filgueiras, A. Marques-Netto, A. A. Batista, *J. Braz. Chem. Soc.* 11 (2000) 237.
35. S. R. Breeze, S. Wang, J. E. Greedan, N. P. Raju, *Inorg. Chem.* 35 (1996) 6944.
36. V. Tangoulis, C. P. Raptopoulou, S. Paschalidou, A. E. Tsohos, E. G. Bakalbassis, A. Terzis, S. P. Perlepes, *Inorg. Chem.* 36 (1997) 5270.
37. A. N. Papadopoulos, V. Tangoulis, C. P. Raptopoulou, A. Terzis, D. P. Kessissoglou, *Inorg. Chem.* 35 (1996) 559.
38. A. E. Tsohos, S. Dionyssopoulou, C. P. Raptopoulou, A. Terzis, E. G. Bakalbassis, S. P. Perlepes, *Angew. Chem. Int. Ed.* 38 (1999) 983.
39. Z. E. Serna, M. K. Urriaga, M. G. Barandika, R. Cortes, S. Martin, L. Lezama, M. I. Arriortua, T. Rojo, *Inorg. Chem.* 40 (2001) 4550.
40. Z. E. Serna, M. G. Barandika, R. Cortes, M. K. Urriaga, G. E. Barberis, T. Rojo, *J. Chem. Soc., Dalton Trans.* (2000) 29.
41. H. Cheng, D. Chun-ying, F. Chen-jie, L. Yong-jiang, M. Qing-jin, *J. Chem. Soc., Dalton Trans.* (2000) 1207.
42. Siemens, SMART and SAINT, Area Detector Control and Integration Software, Siemens Analytical X-ray Instruments Inc., Madison, Wisconsin, USA, 1996.
43. G. M. Sheldrick, SADABS, Program for Empirical absorption correction of Area Detector Data., University of Göttingen, Göttingen, Germany, 1997.
44. G. M. Sheldrick, *Acta Crystallogr.* A46 (1990) 467.
45. G. M. Sheldrick, SHELXS-97 Program for the Solution of Crystal Structures, University of Göttingen, Göttingen, Germany, 1997.
46. K. Brandenburg, H. Putz, DIAMOND Version 3.0, Crystal Impact, GbR, Postfach 1251, D-53002 Bonn, Germany, 2004.

CHAPTER 2

Syntheses, crystal structures and spectral characterization of ligands from di-2-pyridyl ketone and *N*(4)-substituted thiosemicarbazides

For the past three decades, thiosemicarbazones with the general formula $R_2N-C(S)-NH-N=CR_2$ have remained as important ligand construction units in both the neutral and anionic forms [1-18]. These organic molecules with potential donor atoms in their structural skeleton fascinate coordination chemists with their versatile chelating behaviour. The coordinating ability of thiosemicarbazides to both transition and main group metallic cations is attributed to the extended delocalization of electron density over the thiosemicarbazone skeleton, which is enhanced by substitution at the *N*(4) position. Condensation of thiosemicarbazides with aromatic aldehydes or ketones extends the electron delocalization along the azomethine bond. Presence of additional donor sites in the ketonic part as in the case of di-2-pyridyl ketone, offer much more coordination possibilities for the thiosemicarbazone ligand.

Interestingly, di-2-pyridyl ketone (*dpk*), as such can function as a ligand construction unit, chelating with metal ions and forming promising clusters and cubanes with excellent ferromagnetic characteristics [19-21]. The hydrolysed derivative of *dpk*, commonly referred to as the gem-diol form of di-2-pyridyl ketone coordinates to metals either in the monoanionic or dianionic form, giving rise to infinite arrays. Hence, incorporation of di-2-pyridyl ketone into an *N*(4)-substituted thiosemicarbazone chain offers a variety of binding modes with possible extension into polymeric structures. However, the coordination chemistry of substituted or unsubstituted thiosemicarbazones of di-2-pyridyl ketone is quite unexplored with a few previous reports [22-26]. This prompted our study into the synthesis and characterization of di-2-pyridyl ketone thiosemicarbazones and their metal complexes [10, 13-14]. Here we have synthesized four new ligands using di-2-pyridyl ketone, *N*(4)-phenylthiosemicarbazone, *N*(4)-cyclohexylthiosemicarbazone and *N*-morpholylcarbothiohydrazide.

2.1. Di-2-pyridylmethanone *N*(4)-phenylthiosemicarbazone, HL¹

The compound HL¹ is newly synthesized from di-2-pyridyl ketone and *N*(4)-phenylthiosemicarbazide (Fig. 2.1).

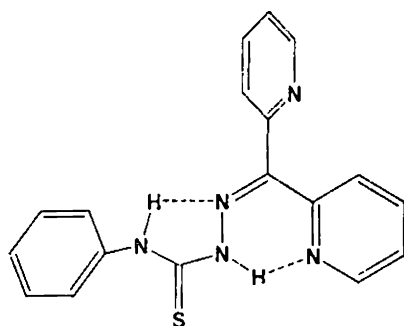
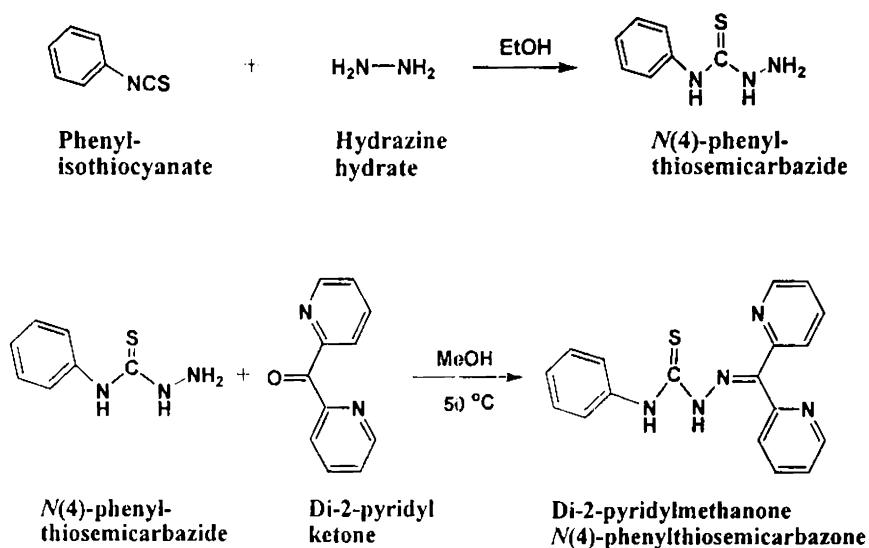


Fig. 2.1. Structure of compound HL¹

Preparation of HL¹ was carried out as in Scheme 1, by the condensation of di-2-pyridyl ketone with *N*(4)-phenylthiosemicarbazide, adapting a reported procedure of preparation of similar thiosemicarbazones [27]. The compound was obtained as a light yellow coloured crystalline product.



Scheme 1

Crystal studies

The molecular structure of HL¹ along with atom numbering scheme is given in Fig. 2.2. The crystal data and structural refinement parameters are given in Table 2.1 and selected bond lengths and angles are given in Table 2.2. The compound crystallizes into a monoclinic lattice with space group *C2/c*. The molecule exists in the *ZE* conformation of thiosemicarbazones since *Z* and *E* configurations are perceived with respect to C6–N3 and C12–N4 bonds respectively. A torsion angle of 171.58(5)° corresponding to the S1–C12–N4–N3 moiety confirms the *trans* configuration of the thiocarbonyl S1 atom [28]. The thiosemicarbazone skeleton comprising of atoms N3, N4, C12, S1 and N5 is almost planar with a maximum deviation of –0.0650(4) Å from the mean plane. The C6–N3 bond distance (1.2858(8) Å) is appreciably close to that of a C=N double bond (1.28 Å) [29], which confirms the azomethine bond formation.

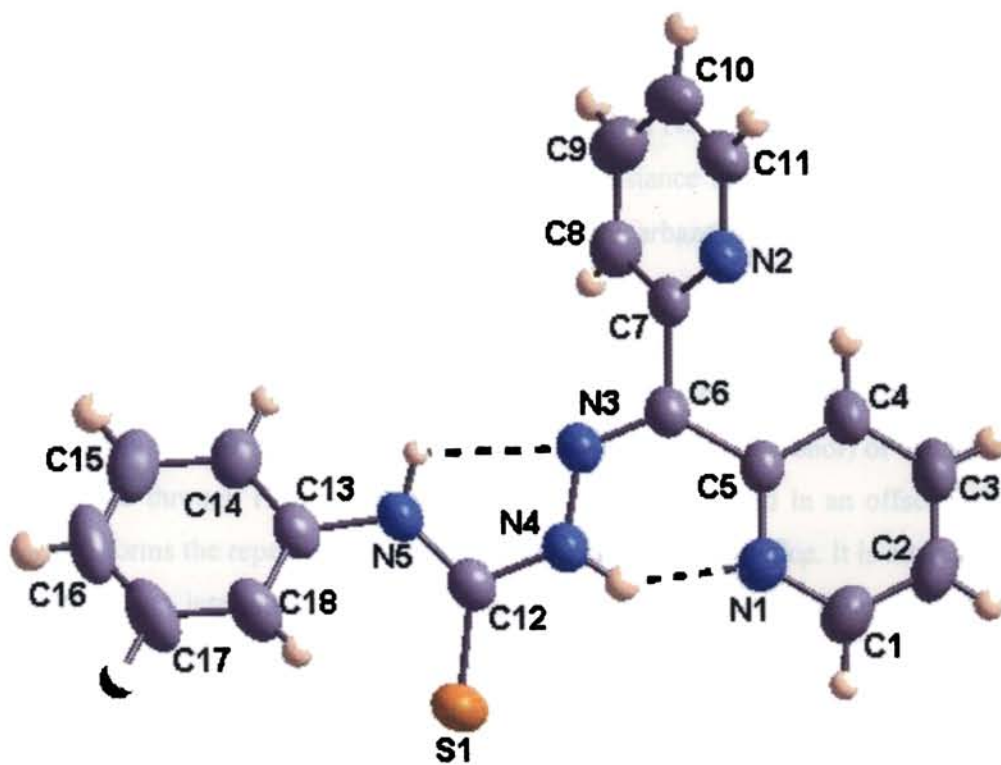


Fig. 2.2. Molecular structure of HL¹. Intramolecular hydrogen bonding interactions are shown as dashed lines

The existence of the thiosemicarbazone in the thione form in the solid state is evidenced by the C12–S1 bond distance of 1.6763(12) Å, which is very close to a formal C=S bond length (1.60 Å) [30]. However, the N3–N4 (1.3573(10)) and N4–C12 (1.3616(9)) bond distances have values intermediate between the ideal values of corresponding single [N–N; 1.45 Å and C–N; 1.47 Å] and double bonds [N=N; 1.25 Å and C=N; 1.28 Å] [31], which are in support of an extended π delocalization along the thiosemicarbazone chain. Among the three aromatic rings, the pyridyl ring Cg(1) with the N1 nitrogen on it, suffers least deviation from the thiosemicarbazone moiety at a dihedral angle of 17.65(1)° between the two corresponding planes. The pyridyl ring Cg(2) and the phenyl ring Cg(3) make a dihedral angle of 60.81(2)° between each other and they are deviated from the central thiosemicarbazone moiety at angles 35.98(1)° and 57.34(2)° respectively. The largest deviation is observed between the planes of the two pyridyl rings positioned at a dihedral angle of 67.66(2)° between each other, which owes mainly to the steric interactions of the bulky pyridyl groups. Two prominent intramolecular hydrogen bonding interactions, *viz.*, N4–H4N---N1 and N5–H5N---N3 lead to the formation of one six-membered ring and one five-membered ring comprising of atoms N1, C5, C6, N3, N4, H4N and N3, N4, C12, N5, H5N respectively. A short interatomic contact, C8–H8---N2, at a C8–N3 distance of 2.919(2) Å also helps to stabilize the present conformation of the thiosemicarbazone.

The packing of the molecules of HL¹ is shown in Fig. 2.3, where the unit cell is viewed down the 'b' axis. The basic unit of the crystal packing consists of a set of two molecules, which are held together by intermolecular hydrogen bonding interactions involving N2 (acceptor) of one molecule and N5 (donor) of the adjacent molecule through H5N. Two adjacent sets are then aligned in an offset fashion, which forms the repeating unit of the packing in the crystal lattice. It is interesting to note that no intermolecular interactions are perceived between these adjacent sets and the overall packing in a two-dimensional manner is effected by the offset alignment of neighboring sets in the unit cell. Some weak C–H--- π and π – π interactions, *viz.*, C15–H15--[1]--Cg(1)ⁱ [Cg(1): N1, C1, C2, C3, C4, C5; $d_{C15...Cg} = 3.5800$ Å; $i = -x, 2-y, 1-z$] and Cg(2)--[1]--Cg(2)ⁱⁱ; [Cg(2): N2, C7, C8, C9, C10,

C11; $d_{Cg \cdots Cg} = 3.5809 \text{ \AA}$; ii = $-x, y, \frac{1}{2} -z$] are the shortest interactions observed of the type in the lattice. However, the two intramolecular hydrogen bonding interactions observed are much effective, operating at appreciably short distances, viz., N5–H5N \cdots N3ⁱⁱⁱ [$d_{D \cdots A} = 2.596(2) \text{ \AA}$; $\angle_{D-H-A} = 101.99^\circ$; iii = x, y, z] and N(4)–H(4)N \cdots N(1)ⁱⁱⁱ [$d_{D \cdots A} = 2.670(2) \text{ \AA}$; $\angle_{D-H-A} = 135.65^\circ$]. These intramolecular hydrogen bonding interactions have substantial effects upon the structural as well as spectral properties of the thiosemicarbazone.

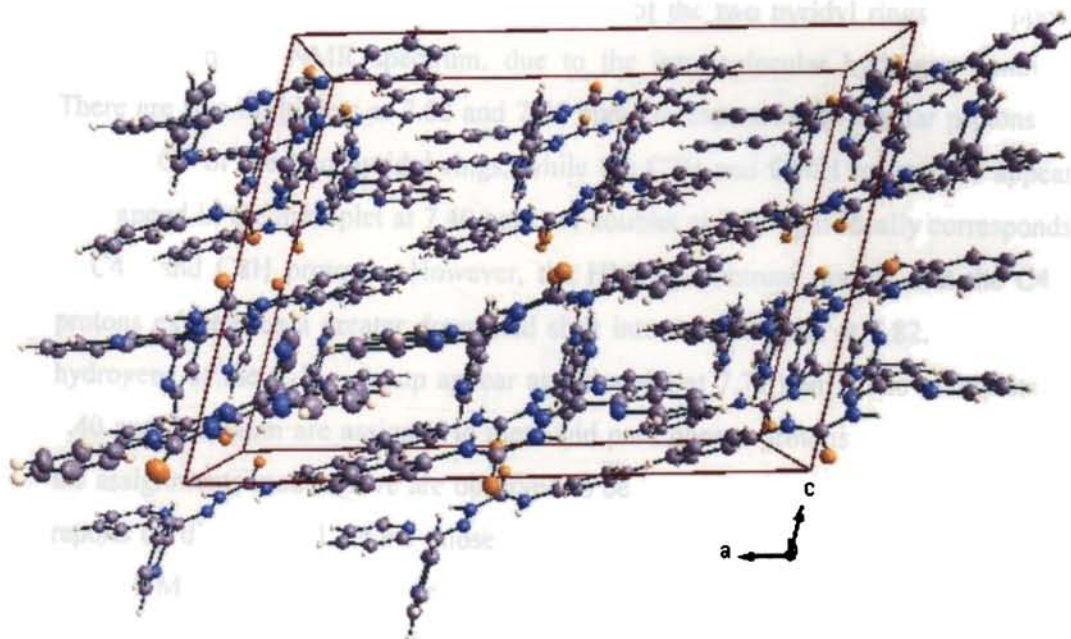


Fig. 2.3. Molecular packing diagram of HL¹, the unit cell is viewed down the 'b' axis

Spectral studies

Proton magnetic resonance spectroscopy is a helpful tool for the identification of organic compounds in conjunction with other spectrometric informations. The ¹H NMR spectrum of HL¹ along with the spectral assignments is given in Fig. 2.4. A sharp singlet, which integrates as one hydrogen at $\delta = 14.55$ ppm is assigned to the proton attached to the nitrogen atom N4, while another similar singlet at 9.55 ppm is assigned to the N5H proton. The downfield shifts of these protons are assigned to their hydrogen bonding interactions with adjacent

nitrogen atoms N1 and N3. Hydrogen bonding decreases the electron density around the proton, and thus moves the proton absorption to a lower field [32]. Absence of any coupling interactions by N4H and N5H protons due to the lack of availability of protons on neighboring atoms render singlet peaks for the imine protons. Two doublets at 8.84 and 8.68 ppm are assigned to the C1H and C11H protons respectively. These signals are shifted to lower field due to electronic effect of the adjacent electronegative pyridyl nitrogens and the more downfield shift of C1H can be attributed to the increased charge density on N1 resulted by its hydrogen bonding to N4H. Coupling of these protons with the C2 and C10 protons splits their signals into doublets. The proton resonances of the two pyridyl rings also appear separately in the NMR spectrum, due to the intramolecular hydrogen bonding. There are two multiplets at 7.82 and 7.86 ppm corresponding to similar protons on C3 and C9 of the two pyridyl rings, while the C2H and C10H resonances appear overlapped in the multiplet at 7.40 ppm. A doublet at 7.57 ppm ideally corresponds to C4H and C8H protons. However, the HMQC spectrum reveals that the C4H protons experience a greater downfield shift into the multiplet at 7.82. The ortho hydrogens of the C₆H₅- group appear as a doublet at 7.71 ppm. The multiplets at 7.40 and 7.24 ppm are assigned to meta and para phenyl protons respectively. All the assignments made above are observed to be in general agreement with previous reports on di-2-pyridyl ketone thiosemicarbazones [22,23]. However, interestingly, the ¹H NMR spectrum of the present compound reveals some more singlet peaks in the higher field region beyond 2.2 ppm. A comparatively weak signal at 2.18 ppm may be assigned to an -SH peak attributable to the possible presence of the thiol tautomer in solution. Thiosemicarbazones are believed to exhibit a thione – thiol equilibrium in the solution state. However, in all the previous reports mentioned above, such an -SH signal was absent and the compounds were established to retain their structure in solution. A sharp peak at 1.6 ppm is characteristic of the dissolved water content in the solvent [32]. Another interesting singlet at 1.25 ppm, which integrates as two protons, is typical of the present compound and it is assigned to be of the protons on the hetero atoms N(4) and N(5), which are subjected to hydrogen bonding in CDCl₃ solvent [32]. To the best of our knowledge, such a typical

evidence for the intramolecular hydrogen bonding in *N*(4)-substituted thiosemicarbazones has never been previously obtained from the ^1H NMR spectrum.

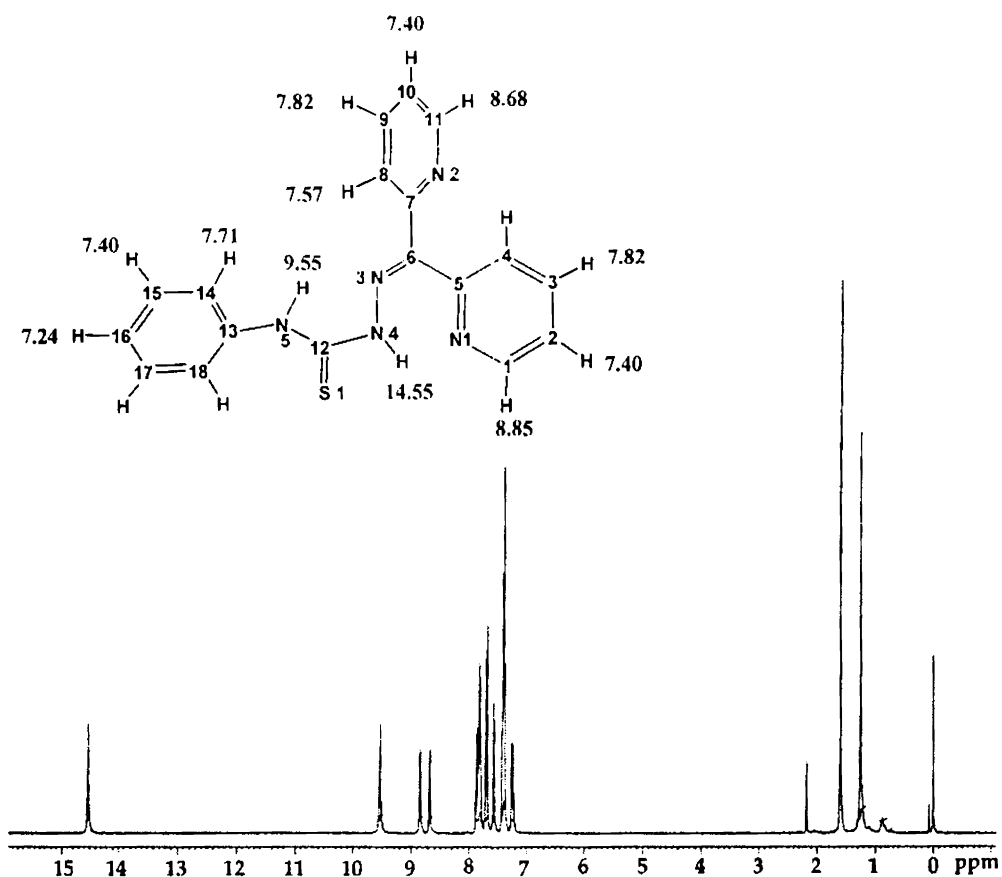


Fig. 2.4. ^1H NMR spectrum of HL¹

In order to get a direct information about the carbon skeleton of the molecule, the ^{13}C NMR spectrum of the compound was taken. Assignment of different resonant peaks to respective carbon atoms is presented in Fig. 2.5. Considering the two pyridyl rings non-equivalent, since one of them is involved in hydrogen bonding interactions, there are sixteen unique carbon atoms in the molecule, which give a total of sixteen different peaks in the ^{13}C NMR spectrum. In both the pyridyl rings, the C1 and C11 carbon atoms adjacent to the more electronegative nitrogen atoms N1 and N2 are shifted further downfield when compared to the neighboring carbon atoms. Also, the carbon atoms at para position to the hetero atoms, viz., C3 and C9 resonate at lower field values when compared to

the meta positioned carbons, C2, C4, C8 and C10. However, the non-protonated carbons C5 and C7 are showing more downfield shift in the pyridyl rings due to an increased electron density resulting from the presence of electronegative nitrogen atom and π electron delocalization in the magnetic environment. Hence the ^{13}C peaks of the two pyridyl rings are assigned as follows: C1, 148.93; C2, 124.43; C3, 137.68; C4, 125.02; C5, 155.03; C7, 156.67; C8, 127.51; C9, 137.80; C10, 124.72; C11, 149.56 ppm.

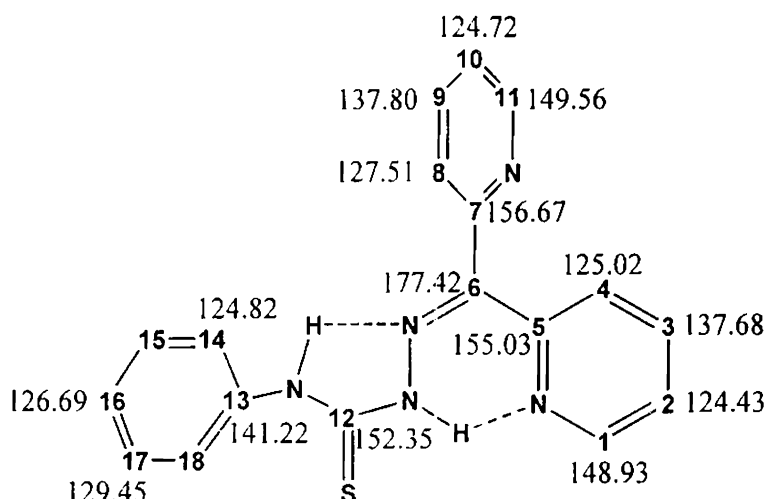


Fig. 2.5. ^{13}C NMR assignments of HL¹

The non-protonated carbon atom at C6 is shifted farthest downfield in the spectrum ($\delta = 177.42$ ppm), effected by the magnetic interaction of two bulky pyridyl rings and the π electron delocalization on the C6=N3 bond. Similarly, the C12 carbon atom resonance is also observed at a lower field of 152.35 ppm, resultant of the conjugative effect of the -N3-N4-CS-N5- thiosemicarbazone skeleton. The three different types of aromatic carbons on the substituted phenyl ring are clearly distinguishable in the ^{13}C NMR spectrum. The peak corresponding to the para positioned carbon atom C16 is observed rather upfield when compared to its ortho [C14 and C18] and meta [C15 and C17] counterparts. The phenyl resonances are: C14 and C18, 124.82; C15 and C17, 129.45; C16, 126.69 ppm.

The COSY spectrum reveals the ^1H - ^1H coupling interactions in the molecule. It is usually plotted as three-dimensional contours, where the conventional spectrum is represented along the diagonal (Fig. 2.6). The cross-peaks along both the sides of the diagonal identify the nuclei that are coupled to each other. On the contrary, the protons that are decoupled from the adjacent ones due to the lack of α -protons will show no correlation in the spectrum. For instance, in the COSY spectrum of the present compound, absence of any off-diagonal peaks extending from 14.55 and 9.55 ppm confirm their assignment to N4H and N5H protons respectively. However, extending horizontal and vertical lines from 8.84 ppm [C1H] and 8.68 ppm [C11H] encounter cross-peaks at 7.40 ppm, where the C2H and C10H resonances are merged into multiplets along with the phenyl ring proton resonances.

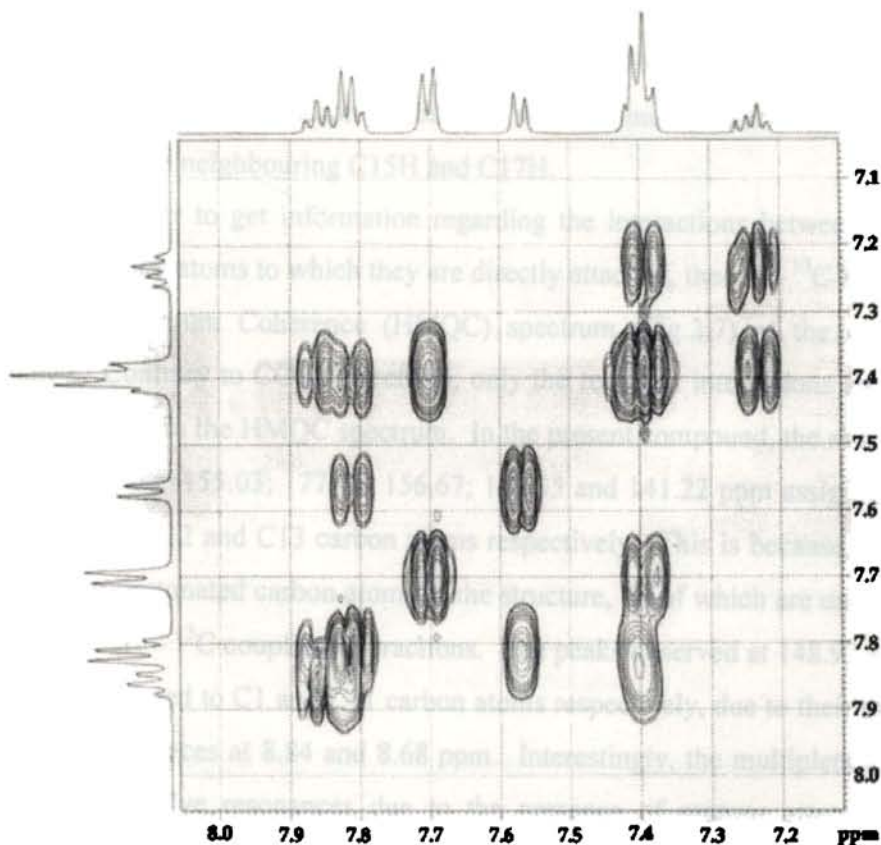


Fig. 2.6. ^1H - ^1H COSY spectrum of compound HL¹

The comparatively weaker coupling interactions of C1H and C11H with the β -positioned C3H and C9H protons are shown by the poorly resolved cross peaks at 7.82 and 7.86 ppm. This also helps to accurately assign C3H ($\delta = 7.82$ ppm) and C9H ($\delta = 7.86$ ppm) protons to their respective values, which is contrary to the expected more downfield shift of C3H proton of the hydrogen bonded pyridine ring. COSY spectrum also turns out very helpful in the accurate assignment of proton resonances in the aromatic region. The multiplets of the C3H and C9H protons show coupling interactions with the doublet at 7.57 ppm [C4H and C8H] and with the multiplet at 7.40 ppm [C2H and C10H]. However, the C3 and C9 protons show no interactions with the doublet at 7.71 ppm, which helps to assign the latter peak to the phenyl protons at the ortho position, i.e., C14H and C18H. Coupling interactions of these protons are observed at 7.40 ppm, thus assigning the multiplet to the meta positioned phenyl protons C15H and C17H also. Assignment of the multiplet at 7.24 ppm to the para phenyl proton C16H is clearly evident from the COSY, as its only correlation is observed with the multiplet at 7.40 ppm, which is assigned to the neighbouring C15H and C17H.

In order to get information regarding the interactions between the protons and the carbon atoms to which they are directly attached, the $^1\text{H} - ^{13}\text{C}$ Heteronuclear Multiple Quantum Coherence (HMQC) spectrum (Fig.2.7) of the compound is studied. Contrary to COSY spectrum, only the resultant interactions are plotted as contour peaks in the HMQC spectrum. In the present compound, the absence of any contours at $\delta = 155.03$; 177.42; 156.67; 152.35 and 141.22 ppm assign them to the C5, C6, C7, C12 and C13 carbon atoms respectively. This is because, they belong to the non-protonated carbon atoms in the structure, all of which are unable to show any direct $^1\text{H} - ^{13}\text{C}$ coupling interactions. The peaks observed at 148.93 and 149.56 ppm are assigned to C1 and C11 carbon atoms respectively, due to their interactions with ^1H resonances at 8.84 and 8.68 ppm. Interestingly, the multiplets at 7.86 and 7.82 ppm involve resonances due to the presence of protons attached to three different types of carbon atoms. The evidence for this is obtained from the $^{13}\text{C} - ^1\text{H}$ HMQC spectrum, which gives three contours at ^{13}C signals 137.68 (C3); 137.81 (C9) and 124.43 (C2) ppm. The doublets at 7.71 and 7.57 ppm and the quartet at

7.24 ppm show contours at 124.81 (C14) and (C18), 127.51 (C8) and 126.69 (C16) ppm, which help to distinguish these ^{13}C resonances, which are close to each other. The multiplet at 7.40 ppm in the ^1H NMR shows two different resultant contour peaks around 124 and 129 ppm, which reveals the presence of both the phenyl and pyridyl ring proton resonances in the multiplet. With the help of these contours, the carbon atoms at meta positions of the phenyl ring are assigned to the ^{13}C resonance at 129.45 ppm, while the carbon atoms at meta positions to the nitrogen atoms on the two pyridyl rings are assigned at 124.72 and 124.43 ppm.

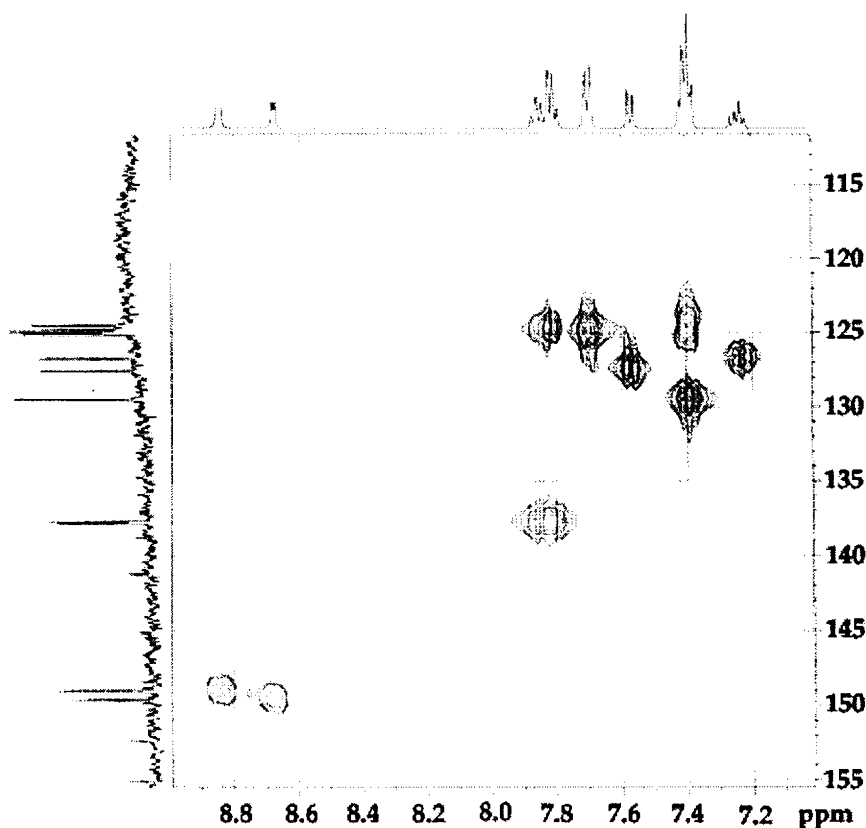


Fig. 2.7. $^1\text{H} - ^{13}\text{C}$ HMQC spectrum of HL^1

In the IR region, the thioamide function in the thiosemicarbazone skeleton usually exhibit free $-\text{NH}$ stretching vibrations as multiple bands near $3300 - 3060 \text{ cm}^{-1}$. Multiple bands result from the association of thioamide groups in different molecules to form dimers or polymers [33]. However, the samples in the solid state

can give rise to a widened band near 3400 cm^{-1} , as in the case of the present compound, HL^1 . Absence of any bands in the $2800\text{-}2550\text{ cm}^{-1}$ region points towards the lack of -SH stretching vibrations in the molecule. It reveals the presence of only the thione tautomer in the solid state. The azomethine stretching vibration, characteristic of a Schiff base, is observed at 1592 cm^{-1} [32]. The band at 1529 cm^{-1} is the resultant of the interactions between N-H bending and C-N stretching vibrations of the C-N-H group of the thioamide function. A weak band at 1253 cm^{-1} also results from the N-H bending and C-N stretching interactions. The thiocarbonyl group shows vibrations at 1320 and 806 cm^{-1} , while additional bands in the broad region of $1400\text{-}700\text{ cm}^{-1}$ are due to the combinations of bands involving the interactions between $\nu(\text{CS})$ and $\nu(\text{CN})$ vibrations of the C=S group attached to a nitrogen atom.

In contrast to the infrared spectrum, the electronic spectrum is rather used to show the relationship between functional groups, chiefly conjugation [34]. The UV-visible spectra of organic compounds are associated with the electronic transitions between energy levels, and at wavelengths above 200 nm , excitation of electrons from the π -orbitals usually occurs giving rise to informative spectra [35]. Solid-state reflectance spectrum of the present thiosemicarbazone reveals the spectral bands in close proximity with similar systems reported earlier. The $\pi \rightarrow \pi^*$ transitions of the pyridyl ring and the thiosemicarbazone imine function are rather weak, observed at 283 nm . However, an intense band at 358 nm is attributed to the $\pi \rightarrow \pi^*$ transition of the thiocarbonyl group and the $n \rightarrow \pi^*$ transition of the pyridine ring [32].

2.2.N(4)-Cyclohexyl-2-[hydroxy(di-2-pyridyl)methyl]hydrazinecarbothioamide, HL^2

Unlike HL^1 , the ligand HL^2 is having a hemiaminal structure with the di-2-pyridyl ketone part existing in the enolic form. These types of compounds are termed as hemiaminals and the product HL^2 is isolated as single crystals from the condensation reaction of di-2-pyridyl ketone with 4-cyclohexyl-3-thiosemicarbazide.

The mechanistic pathway for the condensation of amines with carbonyl compounds involves the formation of a tetrahedral addition intermediate followed

by its dehydration to yield imines [36]. These reaction intermediates, formerly referred to as ‘carbinolamines’, are thermodynamically unstable and are presently termed as ‘hemiaminals’ by IUPAC. The rate of formation of hemiaminals with the effect of substituents and pH has been the subject of several investigations and many conclusions were established with regard to their mechanisms. Isolation of the hemiaminal product was immaterial in the above studies and the products of the reactions of aldehydes with thiosemicarbazides were the corresponding thiosemicarbazones. However, here we observed the isolation of the hemiaminal derivative, HL² of a substituted thiosemicarbazone as crystalline product from a reaction between 4-cyclohexyl-3-thiosemicarbazide and di-2-pyridyl ketone (Scheme 2). The structure of the compound (Fig. 2.8) is established by spectral and single crystal X-ray diffraction studies.

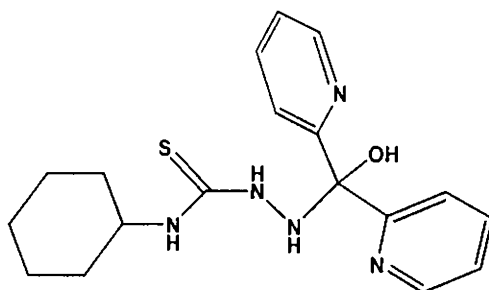
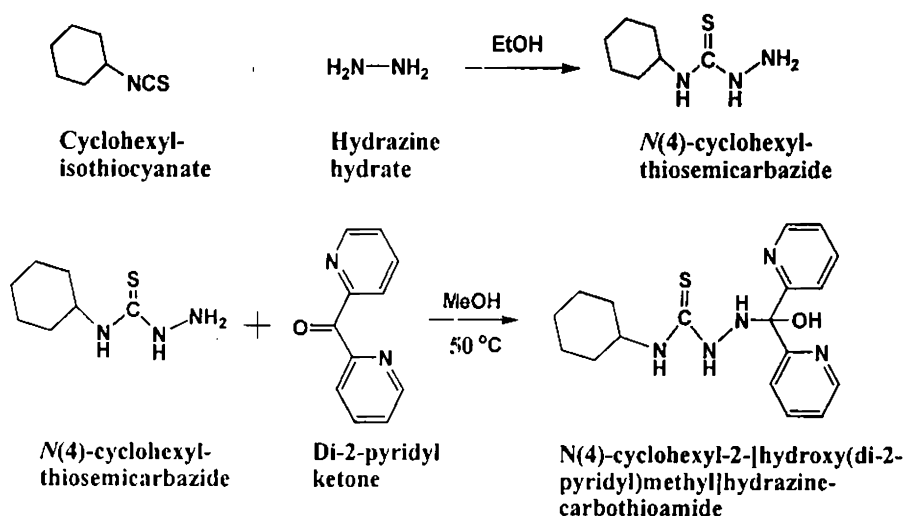


Fig. 2.8. Structure of compound HL²



Scheme 2

Unsubstituted or alkyl substituted imines are highly reactive and imines are stabilized by one or more aryl groups attached to carbon or nitrogen. In such cases, the compounds are easily isolated and are called Schiff bases. Enhanced stability is imparted by aryl substituents due to the conjugative effect of the aryl group and the carbon-nitrogen double bond. For Schiff bases such as hydrazones and semicarbazones, additional stability is imparted by a second nitrogen attached to the azomethine nitrogen [36]. In the light of these facts, a stable thiosemicarbazone is always expected as the final product of the condensation between a thiosemicarbazide and a carbonyl compound with the support of voluminous literature. However, in spite of the stability factors such as aromatic substitution and hydrazinic nitrogen linkage, which favour the imine product, the hemiaminal derivative is isolated here, which makes the present study particularly interesting. Previous report of a stable hemiaminal crystal was in the form of covalent intermediate during the reaction of an aldehyde with lysine [37]. However, to the best of our knowledge, the compound HL² is the first report of the isolation of a hemiaminal product as single crystals from the condensation of a substituted thiosemicarbazide with any carbonyl compound.

The carbonyl addition of both weakly and moderately basic amines at weakly acidic pH values corresponds to a stepwise mechanism involving the formation of an unstable zwitterionic form of hemiaminal, which undergoes an intramolecular 'proton switch' or a proton transfer from a molecule of acid in order to convert into the hemiaminal product [38]. Usually, dehydration of the hemiaminal readily occurs as the next step yielding imines. A mechanistic approach towards the hemiaminal formation can be made by a possible hydrolysis of the thiosemicarbazone. The hemiaminal is then obtained as the intermediate product, which finally yields the corresponding amine and carbonyl compounds. However, this mechanistic prediction seems to be unreliable in the present case, since once the imine, i.e., the di-2-pyridyl ketone 4-cyclohexyl-3-thiosemicarbazone is formed, it is expected to be stabilized by substituent effects and electron delocalization, which contradicts the possibility for getting hydrolysed. Hence, here the stabilization of the hemiaminal derivative can be rationalized only by taking into account the different electron

transfer processes in the transition state during the condensation of di-2-pyridyl ketone with *N*(4)-cyclohexylthiosemicarbazone. A suggestive mechanistic approach would be that the double bond formation and the rehybridisation of carbon and nitrogen atoms from tetrahedral sp^3 structure of the hemiaminal intermediate to the planar sp^2 structure of the imine product lag behind other processes such as proton removal and electron delocalization in the transition state. As stated by Sayer and Jencks [39], the energetic advantage of maintaining significant overlap and bonding with the departing oxygen and hydrogen atoms in an sp^3 hybridised transition state is more than enough to offset the stabilization achieved through a carbon-nitrogen double bond by rehybridisation towards a planar sp^2 structure.

Crystal studies

The compound crystallizes into a triclinic lattice with space group $P\bar{1}$ and the molecular structure of HL² along with atom numbering scheme is given in Fig.2.9.

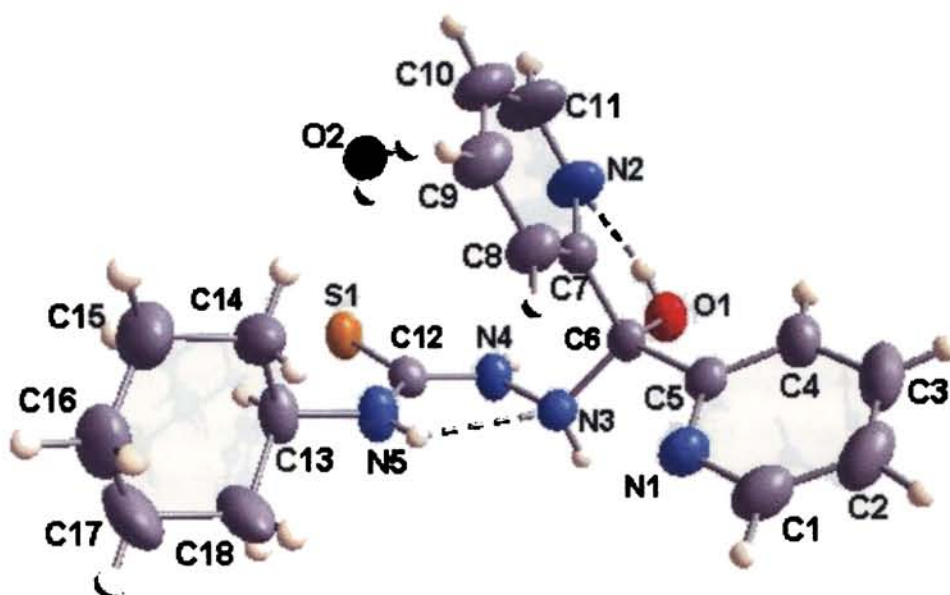


Fig. 2.9. Molecular structure of HL². The ellipsoids are drawn at 50% probability and the intramolecular hydrogen bonding interactions are shown as dashed lines

The crystal data parameters are given in Table 2.1 and selected bond distances and angles are given in Table 2.2. The molecule is non-planar as a whole, whereas the central moiety comprising of atoms N3, N4, C12, S1 and N5 is almost

planar with a maximum deviation of 0.0211(3) Å from the mean plane. A torsion angle of 177.86(11)° corresponding to the S1–C12–N4–N3 moiety confirms the trans configuration of the thiocarbonyl S1 atom [28]. Unlike the azomethine double bond in thiosemicarbazones, the C6–N3 bond distance (1.464(2) Å) is more close to that of a C–N single bond [29], supporting the hemiaminal structure of the compound. In order to minimize the steric stain, the bulky pyridyl groups are deviated farthest with a dihedral angle of 75.31(1)° between each other. The intramolecular hydrogen bonding interactions, *viz.*, N5–H401---N3 and O1–H101---N2 lead to the formation of two five membered rings comprising of atoms N3, N4, C12, N5, H401 and N2, C7, C6, O1, H101 respectively. Ring puckering analyses and least square planes calculations show that the cyclohexyl ring, Cg(3) adopts a chair conformation ($Q_T = 0.5404$ Å).

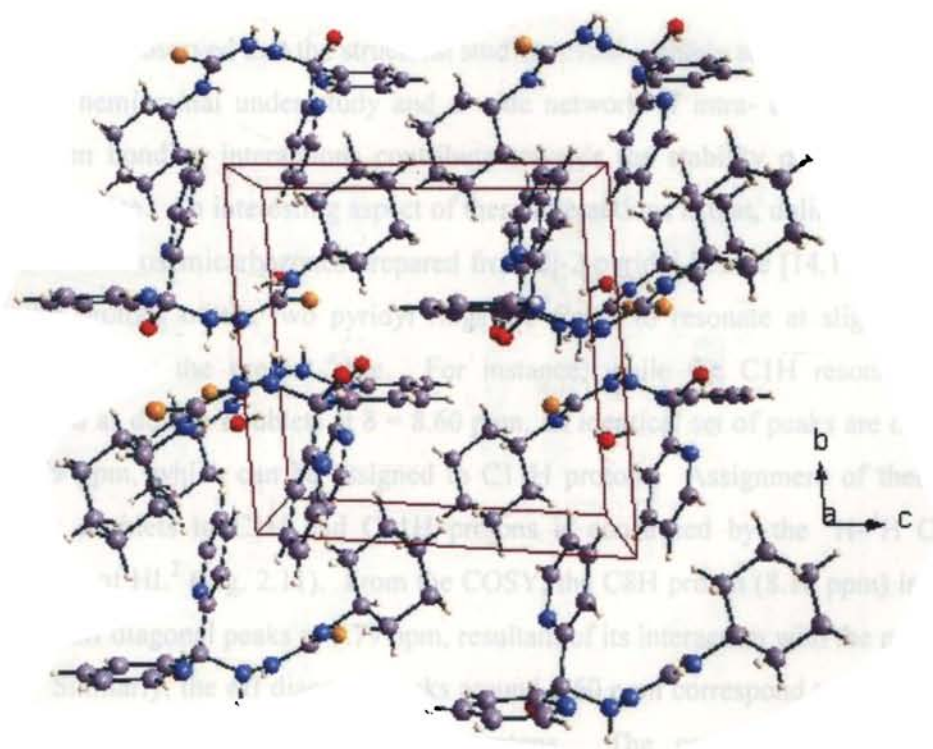


Fig. 2.10. Molecular packing diagram of HL², the unit cell is viewed down the 'a' axis

The molecular packing of compound HL² is shown in Fig. 2.10. The unit cell is viewed down the 'a' axis and the repeating unit consists of two molecules set

in an offset fashion, arranged one-dimensionally in the crystal lattice. A residual water molecule in the crystal lattice is involved in extensive hydrogen bonding interactions with three of its adjacent molecules. Each thiocarbonyl sulfur atom is involved in two intermolecular hydrogen bonding interactions, N4-H301---S1ⁱ [$d_{D...A}$ = 3.410(1) Å; \angle_{D-H-A} = 91.04°; $i = -x+1, -y+1, -z+2$] and O2-H202---S1ⁱⁱ [$d_{D...A}$ = 3.490(1) Å; \angle_{D-H-A} = 164.37°; $ii = +x, +y, +z$]. The water molecule residue reveals two more intermolecular hydrogen bonds, *viz.*, N5-H401---O2ⁱⁱⁱ [$d_{D...A}$ = 3.035(2) Å; \angle_{D-H-A} = 103.46°; $iii = +x, +y, +z$] and O2-H201---N1^{iv} [$d_{D...A}$ = 2.823(2) Å; \angle_{D-H-A} = 115.82°; $iv = x-1, +y, +z$]. These intermolecular hydrogen bonding interactions are mainly operational in the packing of the molecules in the crystal lattice, since $\pi - \pi$ and C-H--- π interactions are weak, perceived at rather longer distances.

Spectral studies

It is observed that the structural studies reveal a highly strained conformation for the hemiaminal under study and a wide network of intra- and intermolecular hydrogen bonding interactions contribute towards the stability of packing in the crystal lattice. An interesting aspect of these interactions is that, unlike the previous reports of thiosemicarbazones prepared from di-2-pyridyl ketone [14,17,22-24], the similar protons of the two pyridyl rings are found to resonate at slightly varied frequencies in the present case. For instance, while the C1H resonances are observed as double doublets at $\delta = 8.60$ ppm, an identical set of peaks are observed at 8.79 ppm, which can be assigned to C11H protons. Assignment of these two double doublets to C1H and C11H protons is confirmed by the ¹H-¹H COSY spectrum of HL² (Fig. 2.11). From the COSY, the C8H proton (8.10 ppm) is found to give off diagonal peaks at 8.79 ppm, resultant of its interaction with the proton on C11. Similarly, the off diagonal peaks around 8.60 ppm correspond to the coupling interaction between C1H and C4H protons. The prominent intramolecular interaction O1-H101-N2 observed at a donor-acceptor distance of 2.577(1) Å from the crystal structure is instrumental in bringing about the different resonant frequencies. An increased charge density is experienced at N2 as a result of the

hydrogen bonding, which shifts the C11H resonance to more downfield compared to that of the C1H proton.

The molecule as a whole adopts a conformation in which the pyridyl ring with N2 is highly strained with active participation in the hydrogen bonding interactions. This results in a redistribution of electron density over the entire ring causing slight variations in the resonating frequencies of similar protons on the two pyridyl rings. Hence the C2H and C10H peaks are observed as triplets at 7.28 and 7.38 ppm respectively, while the C3H and C9H resonances are perceived as multiplets centred around 7.71 and 7.50 ppm respectively. Similarly, the doublets at 8.10 ppm and the doublet of a triplet at 7.90 ppm are assigned to C8 and C4 protons respectively. Assignment of these peaks to the respective protons is carried out with the help of ^1H - ^1H correlation data available from the COSY spectrum.

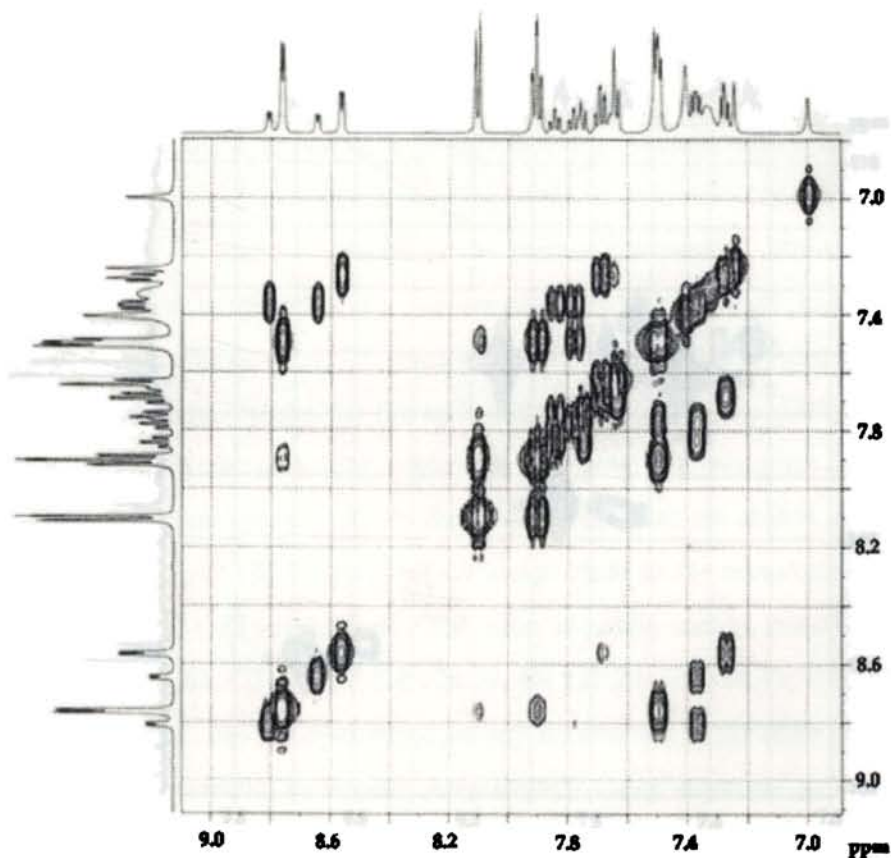


Fig. 2.11. ^1H - ^1H COSY spectrum of HL^2

Two sets of double doublets observed at 8.79 and 8.60 ppm for protons α to pyridyl nitrogens attribute interesting features to the compound under study. The ^1H NMR spectrum of the present compound follows strictly first order with well-separated chemical shift positions for protons with different environments. For example, the signal for C1H proton appears as a double doublet around 8.60 ppm due to the following coupling pattern observed between adjacent protons. At first, the proton at C1 couples with C2 proton, which splits the C1H signal into a doublet. But C1H also couples with C3H so that each line of the C1H is further split into two, giving a double doublet [33]. Although doublets and double doublets are reported previously [22] two well-defined sets of double doublets corresponding to two similar pyridyl protons are observed for the first time in substituted thiosemicarbazones.

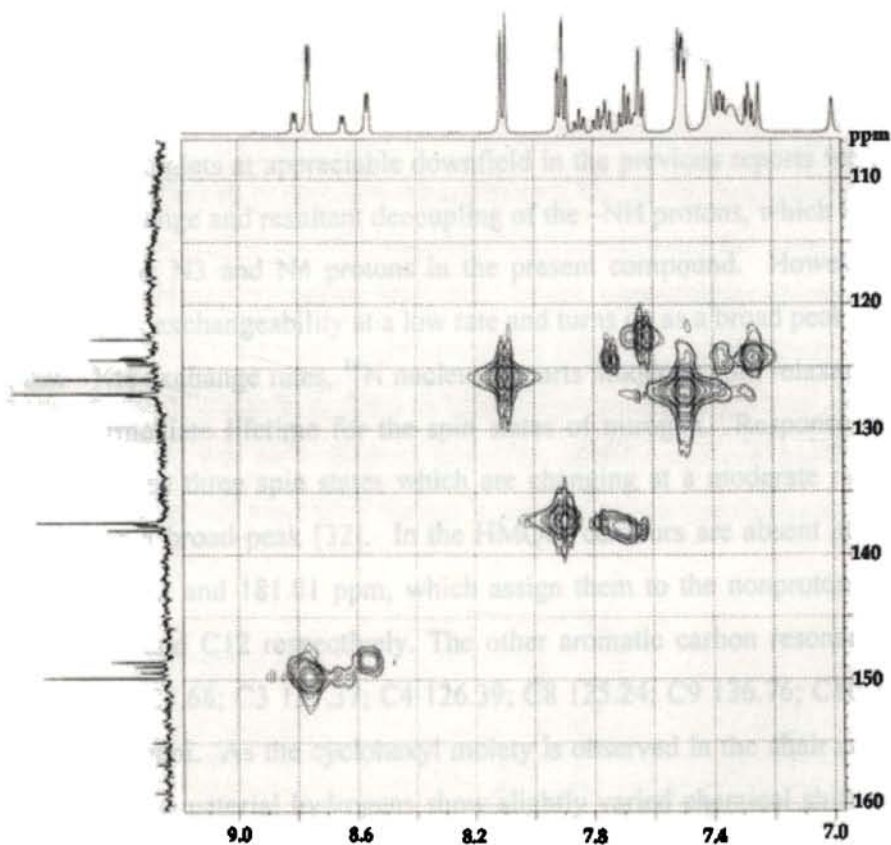


Fig. 2.12. $^1\text{H} - ^{13}\text{C}$ HMQC spectrum of HL^2

More distinctive features are associated with the resonance peaks of the protons on N3 and N4 atoms, which appear as a triplet at 7.84 ppm corresponding to the two protons of identical chemical environments. Contrary to this, in a previous report of a di-2-pyridyl ketone thiosemicarbazone, a sharp singlet at appreciable downfield values ($\delta = 13\text{--}15$ ppm) is observed for the N3H proton [22]. Hence, in order to confirm the assignment of these triplets to --NH protons, the $^1\text{H}\text{--}^{13}\text{C}$ correlation data were scrutinized. Absence of coupling of the triplets at 7.84 ppm with the ^{13}C peaks in the HMQC experiments (Fig. 2.12) authenticated its assignment to the protons on N3 and N4. The triplet is in accordance with the 2I+1 splitting ($I=1$ for ^{14}N) of the resonance peak of the proton attached to the ^{14}N nucleus. The appreciable electrical quadrupole moment at N3 and N4 nitrogens is able to induce an efficient spin relaxation to observe three well-defined spin states of the nitrogen nucleus, to which the proton responds by giving a triplet in the ^1H NMR spectrum.

The singlets at appreciable downfield in the previous reports were the result of rapid exchange and resultant decoupling of the --NH protons, which is found to be absent for the N3 and N4 protons in the present compound. However, the N5H proton shows exchangeability at a low rate and turns up as a broad peak at 7.33 ppm. At low --NH exchange rates, ^{14}N nucleus imparts moderate spin relaxation resulting in an intermediate lifetime for the spin states of nitrogen. Response of the --NH proton to these three spin states which are changing at a moderate rate is usually observed as a broad peak [32]. In the HMQC, contours are absent at $\delta = 158.52$, 193.01, 154.52 and 181.01 ppm, which assign them to the nonprotonated carbons C5, C6, C7 and C12 respectively. The other aromatic carbon resonances are: C1 149.20; C2 123.68; C3 137.37; C4 126.39; C8 125.24; C9 136.76; C10 122.07 and C11 147.92 ppm. As the cyclohexyl moiety is observed in the chair conformation, the axial and equatorial hydrogens show slightly varied chemical shift values with the equatorial protons observed at more downfield ($\delta = 2.05\text{--}1.73$ ppm) compared to their axial counterparts ($\delta = 1.42\text{--}1.22$ ppm). However, the C13H is deshielded by the adjacent electronegative nitrogen resulting in a multiplet at 4.21 ppm, which couples with the proton on N5. Assignment of the broad peak to N5 proton is

confirmed by the ^1H - ^1H correlation experiments, since coupling of the N5H proton with the C13H proton of the cyclohexyl ring is clearly evident from the COSY.

The compound reveals well-defined molecular vibrations in the IR region. The -OH stretching vibration of the hydroxyl group at C6 is observed as a distinct band at 3516 cm^{-1} in the IR spectrum [33]. The -NH stretching vibration is perceived as another distinct band at 3187 cm^{-1} , while the -CH stretching vibration of the cyclohexyl moiety is observed at 2930 and 2853 cm^{-1} . The absence of $\nu(\text{SH})$ band around 2600 cm^{-1} suggests the existence of the thiosemicarbazone in the thione form. The $\nu(\text{CS})$ vibration appears as a sharp band at 1237 cm^{-1} , while the $\delta(\text{CS})$ vibration is observed at 802 cm^{-1} . In the solid state electronic spectrum of the compound, the $\pi\rightarrow\pi^*$ transitions of the pyridyl ring and the thiosemicarbazone moiety are observed at 259 and 268 nm respectively, while the $n\rightarrow\pi^*$ transition of the pyridyl nitrogen is observed as a broad band at 353 nm .

2.3. Di-2-pyridylmethanone *N*(4)-cyclohexylthiosemicarbazone, HL^3

It is interesting to note that the compound HL^3 is also synthesized from di-2-pyridyl ketone and *N*(4)-cyclohexylthiosemicarbazone, using the same procedure as that of HL^2 . However, unlike HL^2 , HL^3 is not immediately obtained after the reaction. The product immediately turned out from the condensation reaction has always been HL^2 , which is isolated as light yellow prismatic crystals. However, in some cases, there was no immediate formation of the compound and nevertheless, when the solution was kept aside for one week, colourless needle shaped crystals of HL^3 are isolated (Fig. 2.13).

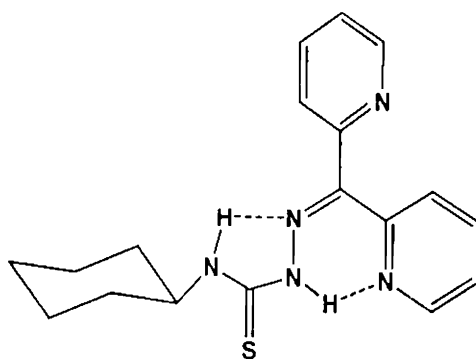


Fig. 2.13. Structure of compound HL^3

However, the yield of the compound HL^3 is observed to be very low. Hence for the preparation of some of the complexes of HL^3 , a one-pot method is employed successfully. Here, equimolar solutions of di-2-pyridyl ketone and *N*(4)-cyclohexylthiosemicarbazone are allowed to react for four hours, after that a solution of the stoichiometric amount of the metal salt is directly added to the solution and the refluxing continued for more than six hours, which produced the complexes in good yield.

Crystal studies

We could successfully isolate X-ray quality single crystals from a methanolic solution of the compound. The molecular structure of HL^3 along with atom numbering scheme is given in Fig. 2.14. The crystal data and structural refinement parameters are given in Table 2.1 and selected bond lengths and angles are given in Table 2.2.

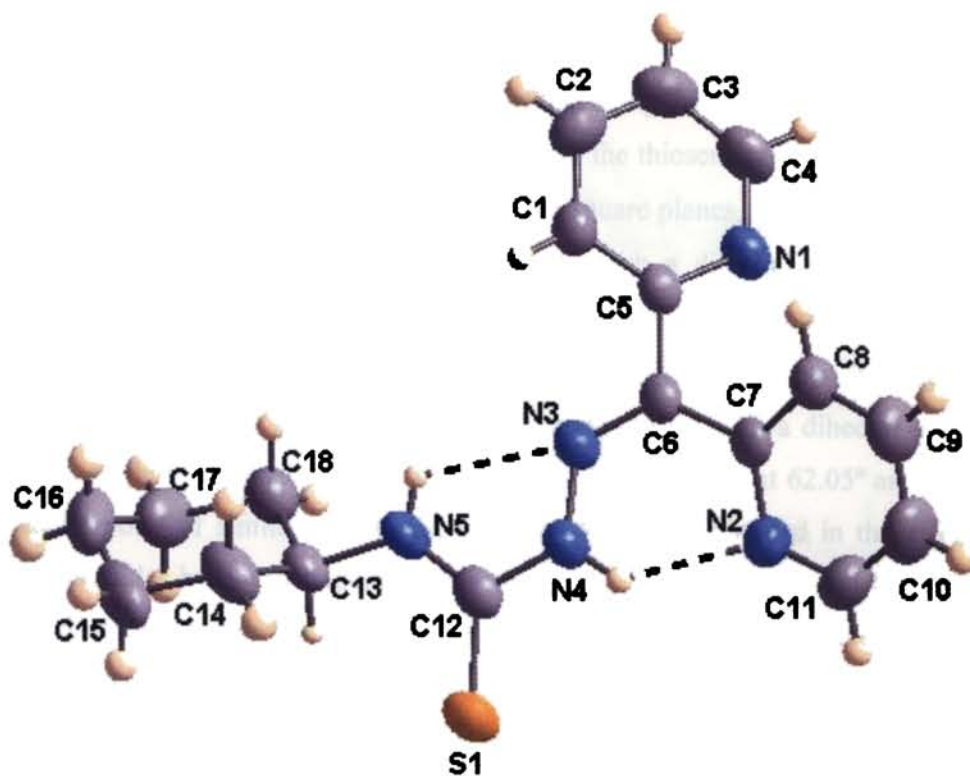


Fig. 2.14. Molecular structure of HL^3 . Ellipsoids are drawn at 50% probability and intramolecular hydrogen bonding interactions are shown as dashed lines

The compound crystallizes into a monoclinic lattice with space group $P2_1$. The structure of HL^3 shows conformational similarity with the structure of HL^1 in many aspects. Similar to HL^1 , the molecule of HL^3 also exists in the ZE conformation of thiosemicarbazones with Z and E configurations about $C6-N3$ and $C12-N4$ bonds. The thiosemicarbazone moiety comprising of atoms $N3$, $N4$, $C12$, $S1$ and $N5$ in HL^3 is more planar compared to that of HL^1 , since a lesser value for the maximum mean plane deviation ($-0.0375(1)$ Å) is observed here. The thiocarbonyl $S1$ atom is more *trans* aligned in HL^3 due to a higher torsion angle value of $175.21(16)^\circ$ corresponding to the $S1-C12-N4-N3$ moiety. The azomethine bond, $C6-N3$ ($1.297(3)$ Å) is in conformity with a formal $C=N$ double bond (1.28 Å) [29]. The $C12-S1$ bond distance of $1.672(2)$ Å, is very close to a formal $C=S$ bond length (1.60 Å), and is slightly shorter than that of HL^1 , which shows its increased bond strength in HL^3 . However, it confirms the existence of the thiosemicarbazone in the thione form in the solid state. Similar to HL^1 , the $N3-N4$ and $N4-C12$ bond distances of $1.359(3)$ and $1.372(3)$ respectively in HL^3 are intermediate between the formal single $N-N$, $C-N$ and double $N=N$, $C=N$ bonds, giving evidence for an extended π delocalization along the thiosemicarbazone chain. The cyclohexyl moiety is deviated farthest from the thiosemicarbazone moiety, at a dihedral angle of 55.41° between the two least square planes, while the pyridyl ring $Cg(2)$ with the $N2$ nitrogen is least deviated with a dihedral angle of 28.32° . Maximum deviation is observed between the pyridyl ring $Cg(2)$ and the cyclohexyl moiety, with a dihedral angle of 80.57° between the planes. The pyridyl ring $Cg(1)$ shows least deviation with the thiosemicarbazone moiety with a dihedral angle of 38.34° , while it deviates from the $Cg(2)$ and cyclohexyl rings at 62.05° and 52.75° . Another point of similarity with the structure of HL^1 is revealed in the effective intramolecular hydrogen bonding interactions, *viz.*, $N4-H4A\cdots N2$ and $N5-H5A\cdots N3$, which lead to the formation of one six-membered ring and one five-membered ring comprising of atoms $N2$, $C7$, $C6$, $N3$, $N4$, $H4A$ and $N3$, $N4$, $C12$, $N5$, $H5A$ respectively. The cyclohexyl moiety exists in a chair conformation with the axial and equatorial hydrogen atoms on it, which is clearly observed in Fig. 2.14.

The molecular packing of HL³ is shown in Fig. 2.15. The unit cell is viewed down the 'a' axis. The repeating unit consists of a set of two molecules aligned in an offset fashion, which are aligned in such a way that the cyclohexyl rings of both the molecules are positioned close to each other. Each molecule repeats separately in a one-dimensional manner in the crystal lattice, and since these one-dimensional arrays are aligned in an offset fashion, a two-dimensional zig-zag packing is effected in the unit cell. The $\pi - \pi$ interactions observed in the crystal are rather weak, as they are observed at distances longer than 4.0 Å. Similarly, the C-H \cdots π interactions are also observed to be weak, since they are observed at distances greater than 3.7 Å. The intermolecular hydrogen bonding interactions are observed at a minimum donor-acceptor distance of 3.6 Å, which decreases the efficiency of the contact. However, the two prominent intramolecular hydrogen bonding interactions are observed in the crystal structure, viz., N5-H5A \cdots N3ⁱ [$d_{D\cdots A} = 2.614$ Å; $\angle_{D-H-A} = 110.14^\circ$; $i = x, y, z$] and N4-H4A \cdots N2ⁱ [$d_{D\cdots A} = 2.695$ Å; $\angle_{D-H-A} = 131.29^\circ$].

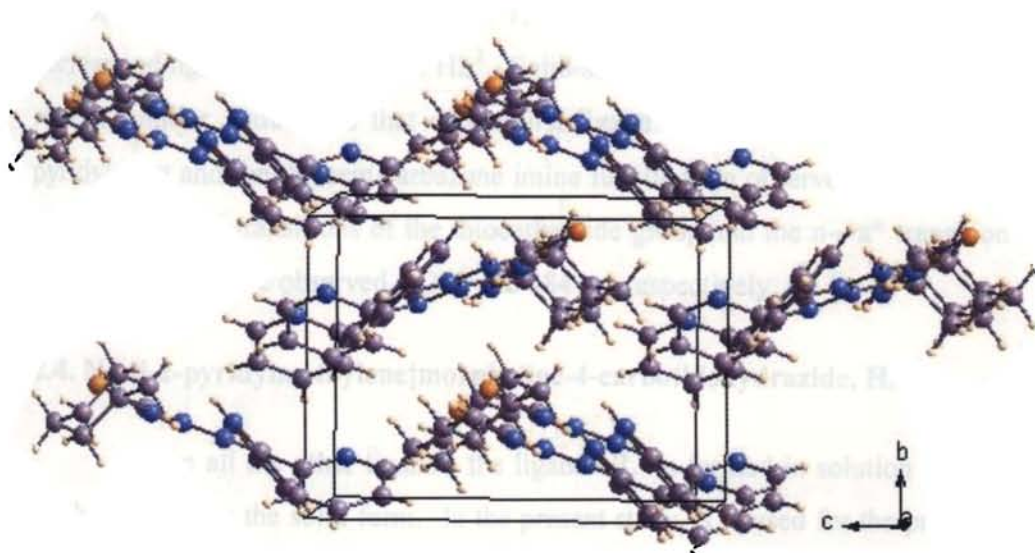


Fig. 2.15. Molecular packing diagram of HL³, the unit cell is viewed down the 'a' axis

Spectral studies

The compound is also characterized using infrared and electronic spectral studies. The low yield of HL³ denied the possibility for the NMR characterization of the compound. However, as far the structure of the compound is concerned, the

single crystal X-ray diffraction data alone is sufficient for accurate assignment of the stereochemistry of the molecule. The infrared spectral data is observed to be in conformity with the structural results. Unlike in the compound HL¹, the present compound exhibits no widened band near 3400 cm⁻¹, instead a few weak discrete bands are observed at 3749, 3646 and 3326 cm⁻¹. A possible explanation could be that it may arise due to the association of thioamide groups in different molecules. The bands around 3300 cm⁻¹ can also be due to the –NH stretching vibrations at N(4). The –CH stretching vibrations of the cyclohexyl moiety are observed as two sharp bands at 2929 and 2850 cm⁻¹, similar to the observations in ligand HL². These bands confirm the existence of cyclohexyl ring in the molecular structure. Absence of any bands at in the 2800-2550 cm⁻¹ region reveals the presence of only the thione tautomer in the solid state, as they imply the lack of –SH stretching absorptions in the molecule. The $\nu(\text{C}=\text{N})$ vibrations is observed at 1585 cm⁻¹ [33]. The N–H bending and C–N stretching vibrations of the thioamide function give rise to weak bands at 1563 and 1547 cm⁻¹ and a strong combination band at 1529 cm⁻¹. The $\nu(\text{CS})$ and $\delta(\text{CS})$ vibrations are observed at 1323 and 801 cm⁻¹, which are close to the corresponding values in HL¹ and HL². Solid-state reflectance spectrum of HL³ also reveals similar features as that of the first ligand. The $\pi \rightarrow \pi^*$ transitions of the pyridyl ring and the thiosemicarbazone imine function are observed at 263 and 291 nm. The $\pi \rightarrow \pi^*$ transitions of the thiocarbamide group and the $n \rightarrow \pi^*$ transition of the pyridine ring are observed at 364 and 384 nm respectively.

2.4. N-[di-2-pyridylmethylene]morpholine-4-carbothiohydrazide, HL⁴

Unlike all the other ligands, the ligand HL⁴ is formed in solution and could not be isolated in the solid form. In the present study, it is used for the preparation of only one complex, Mn(L⁴)₂. During the preparation of the complex, a solution of the stoichiometric amount of the Mn(II) acetate is directly added to the ligand solution and refluxed, and room temperature slow evaporation of the reaction mixture finally gave the complex as crystalline products. Detailed description of the synthesis and complexation of HL⁴ is provided in Chapter 4 of this thesis.

2.5. Experimental

2.5.1. Materials

Commercial reagents, phenyl isothiocyanate (Fluka), cyclohexyl isothiocyanate (Fluka), hydrazine hydrate (Lancaster), di-2-pyridyl ketone (Aldrich) and methanol (Ranchem) were used as received. Ethyl alcohol was repeatedly distilled before use.

2.5.2. Synthesis of HL¹

A solution of phenyl isothiocyanate (0.675 g, 5 mmol) in 20 ml of ethanol was continuously stirred with an ethanolic solution of hydrazine hydrate (0.250 g, 5 mmol) for one hour. The white product of *N*(4)-phenylthiosemicarbazide thus formed was washed, dried and recrystallized from ethanol. An ethanolic solution of *N*(4)-phenyl thiosemicarbazide (0.502 g, 3 mmol) was then refluxed with methanolic solution of di-2-pyridyl ketone (0.553 g, 3 mmol) continuously for 4 hrs after adding one drop of acetic acid. Light yellow crystals of the thiosemicarbazone were separated upon cooling, which were filtered and washed with methanol. The compound was recrystallized from ethanol and dried over P₄O₁₀ *in vacuo*. Single crystals suitable for X-ray analysis were grown by slow evaporation of its dilute solution in methanol. Elemental analyses, Found (Calcd): C 64.79(64.84); H 4.53(4.46); N 21.11(21.01), m. p. 135 °C, yield 1.23 g (62%).

2.5.3. Synthesis of HL²

Ethanolic solutions of cyclohexyl isothiocyanate (0.706 g, 5 mmol) and hydrazine hydrate (0.250 g, 5 mmol) were mixed with constant stirring. The stirring was continued for one more hour and the white product, *N*(4)-cyclohexylthiosemicarbazide formed was filtered, washed, dried and recrystallized from ethanol. A methanolic solution of the *N*(4)-cyclohexylthiosemicarbazide (0.519 g, 3 mmol) was then refluxed with di-2-pyridyl ketone (0.553 g, 3 mmol) in 5 ml methanol continuously for 4 hrs after adding few drops of acetic acid and the pH

of the solution was measured to be 4.7. Pale yellow crystals separated on cooling the solution were filtered and washed with methanol. The crystals were recrystallized from ethanol and dried over P_4O_{10} *in vacuo*. Single crystals suitable for X-ray diffraction were obtained by slow evaporation of a methanolic solution of HL^2 . Elemental analyses, Found (Calcd): C 60.98(60.48); H 6.54(6.49); N 19.02(19.59), m. p. 124 °C, yield 1.04 g (52%).

2.5.4. Synthesis of HL^3

The compound HL^3 was synthesized using the same procedure as that of HL^2 . The only difference is that there was no immediate formation of the product. After refluxing for six hours continuously, the reaction mixture was kept aside for slow evaporation at room temperature. After one week, needle shaped light yellow crystals suitable for single crystal analyses turned out, which were carefully separated. M.p. 104 °C, yield 0.95 g (47%).

To conclude, four new ligands were synthesized and used for complexation with various transition metals. Di-2-pyridyl ketone occupied the ketonic part in all the ligands. The use of di-2-pyridyl ketone was selected based on the possible magnetic attributes of its metal complexes. All the ligands were successfully synthesized and the complexes revealed interesting magnetic characteristics.

Table 2.1
Crystal data and structural refinement for HL¹, HL² and HL³

Parameters	HL ¹	HL ²	HL ³
Empirical Formula	C ₁₈ H ₁₅ N ₅ S	C ₁₈ H ₂₅ N ₅ O ₂ S	C ₁₈ H ₂₁ N ₅ S
Formula weight, M	333.41	375.49	339.46
Crystal system	Monoclinic	Triclinic	Monoclinic
Space group	C2/c	P $\bar{1}$	P2 ₁
Lattice constants			
a (Å)	22.073(19)	8.571(5)	9.9281(17)
b (Å)	9.740(8)	10.700(6)	8.4668(15)
c (Å)	16.380(14)	11.104(6)	10.9480(19)
α (°)	90.00	95.089(9)	90.00
β (°)	104.766(13)	104.996(8)	101.331(3)
γ (°)	90.00	91.481(9)	90.00
Volume V (Å ³)	3405(5)	978.5(9)	902.3(3)
Z	8	2	2
Calculated density, ρ (Mg m ⁻³)	1.301	1.274	1.249
Absorption coefficient, μ (mm ⁻¹)	0.199	0.188	0.188
F(000)	1392	400	360
Crystal size (mm)	0.80 x 0.64 x 0.61	0.35 x 0.33 x 0.30	0.66 x 0.24 x 0.05
θ Range for data collection	1.91 - 27.32	1.91 - 26.25	1.90 - 27.03
Limiting Indices	-28 $\leq h \leq$ 25, -11 $\leq k \leq$ 12, -20 $\leq l \leq$ 20	-10 $\leq h \leq$ 10, -13 $\leq k \leq$ 13, -13 $\leq l \leq$ 13	-12 $\leq h \leq$ 12, -10 $\leq k \leq$ 10, -13 $\leq l \leq$ 13
Reflections collected	12701	10253	7228
Unique Reflections	3534 [R _{int} = 0.0184]	3978 [R _{int} = 0.0145]	3650 [R _{int} = 0.0207]
Completeness to θ	27.32 (91.8%)	26.25 (91.1%)	27.31 (93.3%)
Absorption correction	None	Multi-scan	Multi-scan
Data / restraints / parameters	3534/0/278	3978/0/335	3650/0/301
Goodness-of-fit on F ²	1.057	1.029	1.081
Final R indices [I > 2 σ (I)]	R ₁ = 0.0521, wR ₂ = 0.1525	R ₁ = 0.0443, wR ₂ = 0.1165	R ₁ = 0.0440, wR ₂ = 0.0905
R indices (all data)	R ₁ = 0.0599, wR ₂ = 0.1621	R ₁ = 0.0496, wR ₂ = 0.1211	R ₁ = 0.0557, wR ₂ = 0.0949

Table 2.2

Selected bond lengths (Å) and bond angles (°) of HL¹, HL² and HL³

	HL ¹	HL ²	HL ³
C6–N3	1.2858(8)	1.464(2)	1.297(3)
N3–N4	1.3573(10)	1.406(1)	1.359(3)
N4–C12	1.3616(9)	1.340(2)	1.372(3)
C12–S1	1.6763(12)	1.702(1)	1.672(2)
N3–N4	1.3573(10)	1.371(4)	1.359(3)
C12–N5	1.3392(8)	1.327(2)	1.318(3)
N5–C13	1.4137(10)	1.461(2)	1.461(3)
C6–C7	1.4935(12)	1.537(2)	1.478(3)
C5–C6	1.4806(9)	1.527(2)	1.489(3)
O1–C6		1.410(1)	
C7–C6–C5	118.88(4)	111.25(12)	119.22(18)
C5–C6–N3	127.81(6)	108.96(12)	113.83(18)
C6–N3–N4	120.51(5)	110.06(12)	120.05(18)
N3–N4–C12	120.03(4)	120.68(13)	119.7(2)
N4–C12–S1	117.44(4)	118.67(12)	118.18(18)
N4–C12–N5	114.27(6)	117.22(15)	115.5(2)
C12–N5–C13	128.50(6)	125.38(16)	126.9(2)
O1–C6–N3		111.50(13)	
O1–C6–C7		110.03(13)	

References:

1. D. H. Petering, *Bioinorg. Chem.* 1 (1972) 255.
2. D. L. Klayman, J. P. Scovill, J. F. Bartosevich, J. Bruce, *J. Med. Chem.* 26 (1983) 39.
3. B. S. Garg, M. R. P. Kurup, S. K. Jain, Y. K. Bhoon, *Transition Met. Chem.* 13 (1988) 247.
4. B. S. Garg, M. R. P. Kurup, S. K. Jain, Y. K. Bhoon, *Transition Met. Chem.* 16 (1991) 111.
5. B. S. Garg, M. R. P. Kurup, S. K. Jain, Y. K. Bhoon, *Synth. React. Inorg. Met.-Org Chem.* 28 (1998) 1415.
6. J. R. Dilworth, J. S. Lewis, J. R. Miller, Y. Zheng, *J. Chem. Soc. Dalton Trans.* (1995) 1357.
7. P. Bindu, M. R. P. Kurup, T. R. Satyakeerthy, *Polyhedron* 18 (1999) 321.
8. J. S. Casas, A. Castineiras, M. C. Rodriguez-Arguelles, A. Sanchez, J. Sordo, A. Vazquez-Lopez, E. M. Vazquez-Lopez, *J. Chem. Soc. Dalton Trans.* (2000) 2267.
9. H. Beraldo, W. F. Nacif, L. R. Teixeira, J. S. Reboucas, *Transition Met. Chem.* 27 (2002) 85.
10. A. Usman, I. A. Razak, S. Chantrapromma, H. K. Fun, V. Philip, A. Sreekanth, M. R. P. Kurup, *Acta Crystallogr. C* 58 (2002) o652.
11. A. Sreekanth, M. R. P. Kurup, *Polyhedron* 22 (2003) 3321.
12. A. Sreekanth, S. Sivakumar, M. R. P. Kurup, *J. Mol. Struct.* 655 (2003) 47.
13. V. Philip, V. Suni, M. R. P. Kurup, *Acta Crystallogr. C* 60 (2004) o856.
14. V. Philip, V. Suni, M. R. P. Kurup, M. Nethaji, *Polyhedron* 23 (2004) 1225.
15. R. P. John, A. Sreekanth, V. Rajakannan, T. A. Ajith, M. R. P. Kurup, *Polyhedron* 23 (2004) 2549.
16. M. Joseph, V. Suni, M. R. P. Kurup, M. Nethaji, A. Kishore, S. G. Bhat, *Polyhedron* 23 (2004) 3069.
17. M. Joseph, V. Suni, C. R. Nayar, M. R. P. Kurup, H.-K. Fun, *J. Mol. Struct.* 705 (2004) 63.

18. A. Sreekanth, H.-K. Fun, M. R. P. Kurup, *Inorg. Chem. Commun.* 7 (2004) 1250.
19. M. L. Tong, S. L. Zheng, J. X. Shi, Y. X. Tong, H. K. Lee, X. M. Chen, *J. Chem. Soc. Dalton Trans.* (2002) 1727.
20. Z. E. Serna, M. K. Urriaga, M. G. Barandika, R. Cortes, S. Martin, L. Lezama, M. I. Arriortua, T. Rojo, *Inorg. Chem.* 40 (2001) 4550.
21. S. R. Breeze, S. Wang, J. E. Greedan, N. P. Raju, *Inorg. Chem.* 35 (1996) 6945.
22. J. K. Swearingen, W. Kaminsky, D. X West, *Transition Met. Chem.* 27 (2002) 724.
23. J. K. Swearingen, D. X West, *Transition Met. Chem.* 26 (2001) 252.
24. C. Duan, X. You, T. C. Mak, *Acta Crystallogr. C* 54 (1998) 1395.
25. M. Maji, M. Chatterjee, S. Ghosh, S. K. Chattopadhyay, B. M. Wu, T. C. W. Mak, *J. Chem. Soc. Dalton Trans.* (1999) 135.
26. C. Duan, B. Wu, T. C. Mak, *J. Chem. Soc. Dalton Trans.* (1996) 3485.
27. D. L. Klayman, J. F. Bartosevich, T. S. Griffin, C. J. Mason, J. P. Scovill, *J. Med. Chem.* 22 (1979) 855.
28. D. Chattopadhyay, T. Banerjee, S. K. Mazumdar, S. Ghosh, R. Kuroda, *Acta Crystallogr. C* 43 (1987) 974.
29. G. J. Palenik, D. F. Rendle, W. S. Carter, *Acta Crystallogr. B* 30 (1974) 2390.
30. J. March, *Advanced Organic Chemistry, Reactions, Mechanisms and Structure*, 4th ed., Wiley, New York, 1992.
31. J. E. Huheey, E. A. Keiter, R. L. Keiter, *Inorganic Chemistry, Principles of Structure and Reactivity*, 4th ed., Harper Collins College Publishers, New York, 1993.
32. R. M. Silverstein, G. C. Bassler, T. C. Morrill, *Spectrometric Identification of Organic Compounds*, 4th ed., John Wiley & Sons, New York, 1981.
33. W. Kemp, *Organic Spectroscopy*, 3rd ed., Macmillan, Hampshire, 1996.
34. R. T. Morrison, R. N. Boyd, *Organic Chemistry*, 4th ed., Allyn and Bacon Inc., London, 1990.

35. D. H. Williams, I. Fleming, *Spectroscopic Methods in Organic Chemistry*, 4th ed., McGraw-Hill, London, 1989.
36. T. H. Lowry, K. S. Richardson, *Mechanism and Theory in Organic Chemistry*, 3rd ed., Harper Collins, New York, 1987.
37. A. Heine, G. DeSantis, J. G. Luz, M. Mitchell, C. H. Wong, I. A. Wilson, *Science* 294 (2001) 369.
38. J. M. Sayer, B. Pinsky, A. Schonbrunn, W. Washtien, *J. Am. Chem. Soc.* 96 (1974) 7998.
39. J. M. Sayer, W. P. Jencks, *J. Am. Chem. Soc.* 99 (1977) 464.

CHAPTER 3

Studies of structural, EPR spectral and magnetic interactions of Cu(II) complexes synthesized from di-2-pyridyl ketone *N*(4)-phenyl- and *N*(4)-cyclohexylthiosemicarbazones

"The reasons for trying to make magnets from molecules are numerous: processing from solution at low temperatures, coupling magnetism with optical properties, looking for new lattice topologies and interactions mechanisms, and finally, the thrill of making architectures of molecules that never existed before and finding that they have quite unlooked for properties..."

Peter Day

The concept of 'Magnetochemistry' was introduced by de Jongh in 1982 during a summer school on "Magneto-structural correlations in exchange-coupled systems". This new philosophy in magnetism consisted of synthesizing materials for a given purpose, instead of studying magnetic properties of materials 'as available' in nature. This impact had a great effect on the chemical community, which continues today. The molecular design and synthesis of simple magnetic systems of low dimensionality, *viz.* dimers and chains helps to use them as model systems to establish useful magneto-structural correlations. This background helps the chemists to increase the structural and magnetic complexities of systems with the aim to control, as much as possible, the passage from molecular properties to collective phenomena, from molecular assemblies to magnetic materials and from molecular engineering to crystal engineering [1].

When Michael Faraday published the first picture of the lines of magnetic flux around a magnet [2], the magnetic material was undoubtedly, iron [3]. Over the succeeding decades, the number of substances showing spontaneous magnetization has increased enormously, and among them, the Cu(II) complexes and clusters contribute a major lot. So in our quest towards exploring the magnetochemistry of transition metal complexes of di-2-pyridyl ketone thiosemicarbazones, we first deal with the Cu(II) complexes in the series. Detailed description on the synthesis of the ligands was given previously, and with two of these ligands eight new Cu(II) complexes are synthesized. As the complexes are newly synthesized, in the first part, the stereochemistry of the

complexes is elucidated, in order to establish their structural attributes, and then in the next section, the magnetic interactions in the complexes are explored.

3.1. Stereochemistry of the complexes

The Cu(II) complex with d^9 electronic configuration is subject to Jahn-Teller distortion if placed in an environment of cubic (i.e. regular octahedral or tetrahedral) symmetry, and this has a pronounced effect on its stereochemistry. The typical distortion is an elongation along one four fold axis, so that there is a planar array of four short Cu – L bonds and two *trans* long bonds [4]. But the additional out-of-plane bonding potential of the CuL_4 chromophore may then be satisfied in a number of ways, viz, by coordination of a single fifth ligand (square pyramidal), by semi-coordination of a fifth and sixth ligand (elongated tetragonal octahedral), by out-of-plane π -bonding (square coplanar) or by off-the-z-axis coordination from one to four additional ligands to give the range of coordination numbers from five to eight [5].

3.1.1. Cu_2TDCl_3 (1)

The bimetallic Cu(II) complex Cu_2TDCl_3 (1), turned out with a unique stereochemistry. To the best of our knowledge, there are no previous reports of a structure of this type, not only in thiosemicarbazones, but also in the whole of the coordinated metal complexes. Hence a detailed discussion on the synthetic and structural aspects of the compound Cu_2TDCl_3 is provided here.

Synthesis

It is interesting to note that the method employed for the preparation of Cu_2TDCl_3 (1) was the direct condensation method usually employed for the synthesis of coordination metal complexes. However, there was no immediate formation of the products, the solution was kept aside and was allowed to evaporate at room temperature and after two days, blue crystalline product was separated out. This points to the fact that the development of an unusual structure for the complex can be explained in relation to some possible reaction mechanisms involving the reactants in the solution state, catalysed by the presence of copper.

Among the N, N'-donors, the di-2-pyridyl ketone ligand exhibits certain singularities that explain its tendency to give rise to unusual structures to coordination metal complexes. As already mentioned in Chapter 2, the di-2-pyridyl ketone can exist as the hydrolysed derivative in alcoholic medium. We are also convinced with this fact by the single crystal X-ray diffraction studies of the ligand, HL². In the case of HL¹, even though the crystal studies revealed a conventional Schiff base structure for it, the possibility of it converting into the hydrolysed form in alcoholic solution is still relevant, as has been observed for HL².

During the formation of Cu₂TlCl₃, in addition to the solvolysis of the di-2-pyridyl ketone part, an oxidative cyclization reaction of the thiosemicarbazone moiety also takes place, which is explained with the support from the literature. Among the reactions involving the thiosemicarbazones, some published mechanisms of the oxidative cyclization give rise to thiadiazoles, thiadiazolines, pyrazolones, 1,2,4-triazoline-5-thiones and other compounds [6-8]. Cyclization of different aliphatic and aromatic aldehyde or ketone thiosemicarbazones under acetylating conditions are also observed to yield substituted 1,3,4-thiadiazolines and thiadiazoles [9-15]. It is reported that 100% conversion was yielded during the synthesis of some substituted steroidal (6*R*)-spiro- Δ^2 -1',3',4'-thiadiazolines by the acetylation of steroidal-6-ketone thiosemicarbazones with acetic anhydride and pyridine at 80 °C [16]. Thiosemicarbazones are also successfully employed in the solid phase synthesis of substituted 1,3,4-thiadiazoles. Resin-bound thiosemicarbazides are treated with aldehydes to form immobilized thiosemicarbazones, which on a subsequent oxidative cyclodehydration and acid mediated cleavage yielded 1,3,4-thiadiazoles. Another similar approach involved the cyclization of the resin-bound thiosemicarbazides with di-(2-pyridyl)thionocarbonate to yield substituted 5-amino-3H-1,3,4-thiadiazole-2-thiones [17]. All these observations correspond to a rearrangement in the uncomplexed thiosemicarbazones in the absence of a metal.

Metal-induced cyclization of thiosemicarbazones is also reported to give oxadiazoles and thiadiazoles in good yield. For instance, pyridine-2-carbaldehyde thiosemicarbazone and its substituted derivatives are observed to undergo an oxidative cyclization when treated with bromate or iodate, leading to 2-amino-5-pyridin-2-yl-

1,3,4-oxadiazole and 2-methylamino-5-pyridin-2-yl-1,3,4-oxadiazole. It is observed that this reaction occurs either with free ligands or when coordinated to Cu(II) [18]. Oxidative cyclization of substituted thiosemicarbazones are also achieved with iron(III) chloride to yield substituted 1,3,4-thiadiazoles [19]. The formation of heterocyclic ring systems upon reactions with tetrachloroaurate(III) had been observed with thiourea derivatives such as N-thiocarbamoylbenzamidines which gave 1,2,4-thiadiazolium cations with the reduction of gold [20]. Similarly, reactions of $[\text{NBu}_4][\text{AuX}_4]$ with diphenylthiocarbazone resulted in a reduction of the metal and the formation of gold(I) complex of the composition $[\text{AuX}(\text{SCN}_4\text{-3,4-Ph}_2)]$ where $\text{SCN}_4\text{-3,4-Ph}_2$ is 3,4-diphenyltetrazole thione which is formed from the cyclization of diphenylthiocarbazone [21].

In the case of pyridine-2-carbaldehyde thiosemicarbazones, the cyclization of the free ligands takes place either with bromate (KBrO_3) or iodate, and it requires a pH $\approx 0 - 1$. For the corresponding Cu(II) complexes, the oxidation with bromate occurs even at pH = 6, but not with iodate at the same pH. However, in the present case, the reaction pathway for the formation of Cu_2TdCl_3 turns out to be unique, as it does not involve any oxidising agents such as KBrO_3 .

Previously, during the preparation of 2-aminoacetophenone 3-piperidyl thiosemicarbazone, an unusual product of thiadiazole derivative was obtained [22]. The formation of this undesired product was explained with regard to the possibility of a second 3-piperidylthiosemicarbazide reacting with the 2-aminoacetophenone 3-piperidylthiosemicarbazone. Similar strategy can be taken into account in the present case also. Here, the addition of a second ligand unit to di-2-pyridyl ketone *N*(4)-phenylthiosemicarbazone (HL^1) takes place through mechanistic pathways very similar to that of a nucleophilic substitution reaction, which constitutes the first step during the formation of the unusual complex.

The second step is mediated by metallic copper, Cu(II), which involves a cleavage of the hydrazinic N – N bond in the thiosemicarbazone moiety. The two-electron reductive cleavage of the N – N bond is one of the elementary reaction steps in the reduction of nitrogen to ammonia [23]. Examples of the metal-induced cleavage of N – N bond in thiosemicarbazones are available in the literature. For instance,

when rhenium precursors are treated with 4-phenyl-3-thiosemicarbazides under reflux for more than three hours, acid promoted cleavage of the N – N bond occurs yielding a nitrido complex of rhenium(V) [24].

The first report of reductive cleavage of the hydrazinic N – N bond of the thiosemicarbazone moiety is observed in 1999 [25], where a Ru(II) complex of methyl(2-pyridyl)-methyleneimine was isolated. Complex redox processes were involved in the reductive cleavage of N–N bond of 2-acetylpyridine-thiosemicarbazone to give rhenium(V) complex of methyl-(2-pyridyl)-methyleneimine where the anionic part of the complex is $[\text{ReO}_4]^-$ [26]. Similarly, rhenium(V) complexes of dithiocarbazic acid precursors also undergo N – N bond cleavage resulting in a Re(V) nitrido complex [27].

In the present reaction, step 2 consists of a number of rearrangement and elimination reactions occurring simultaneously, which makes it difficult to interpret them separately. A possible description of reactions in the second step can be given as follows. The intermediate ligand form incorporating two ligand moieties undergoes a two-electron reductive cleavage at the hydrazinic N – N bonds by one molecule of CuCl_2 each and as a result, one part of the di-2-pyridyl methyleneimine leaves presumably due to the bulky pyridyl interactions. The metal-induced cyclization of the thiosemicarbazone moiety also is effected in this step. It is interesting to note that these metal-induced cyclization and N – N cleavage reactions are highly favoured in this step on stability grounds. These reactions result in highly conjugated ring systems, one metal chelate ring and a thiadiazidine ring in the resulting complex, imparting a high level of electron delocalization along the entire system. This high delocalization of electron density over the entire coordination network imparts enough stability for the complex Cu_2TDCl_3 to be isolated as stable crystalline products from the reaction mixture.

However, some interesting novel aspects of the present complex are:

- The compound Cu_2TDCl_3 is the first report of a coordination complex, where the formation is assisted by a simultaneous metal-induced cyclization and N – N bond cleavage. Previous observations were concerned with either the cyclization or the N – N bond cleavage alone, but a combination of both the

rare phenomena during the formation of a coordination complex is observed for the first time.

- It is the first observation of a Cu(II) induced N – N cleavage in any Schiff base. Examples of previous reports of hydrazinic N – N cleavage are limited to Ru(II), Re(III), and Re(V) [23-26].
- In all the previous reports, the metal catalysed N – N cleavage resulted in monometallic complexes. In the present case, the resultant compound is a bimetallic Cu(II) complex, where the two copper centres are bridged by a chloride anion.
- As regards to cyclization, it is the first report of a conversion involving two thiosemicarbazone moieties, where the ketonic part of one of the thiosemicarbazones is removed after the cyclization.

All these features establish the uniqueness of the structure of Cu_2TDCl_3 . Attempts were carried out to synthesize similar structures with CuBr_2 and other metal salts of Cu(II). But, unfortunately, these efforts failed, which points to a strong influence of the chloride anion in the formation of the unique structure.

Crystal studies

Single crystals suitable for X-ray analyses were grown by slow evaporation from an ethanolic solution. The molecular structure of the compound is given in Fig. 3.1. The structural data refinement details are given in Table 3.1 and selected bond lengths and angles are given in Table 3.2. Both the Cu(II) atoms exhibit distorted square pyramidal geometry and are bridged through the chlorine atom Cl3 at the apical position and the nitrogen atom N3 at the basal plane.

The percentage of trigonal distortion from square pyramidal geometry is described by the parameter τ , defined as $[(\theta - \phi)/60] \times 100$, where θ and ϕ are angles between the donor atoms forming the basal plane in a square pyramidal geometry. While $\tau = 0$ for an ideal square pyramidal geometry, $\tau = 100$ for the ideal trigonal bipyramidal geometry [28]. The τ parameters for the complex ($\tau = 25.6$ at Cu1; $\tau = 23.83$ at Cu2) indicates that the coordination geometry around both the copper atoms are more of square pyramidal in nature.

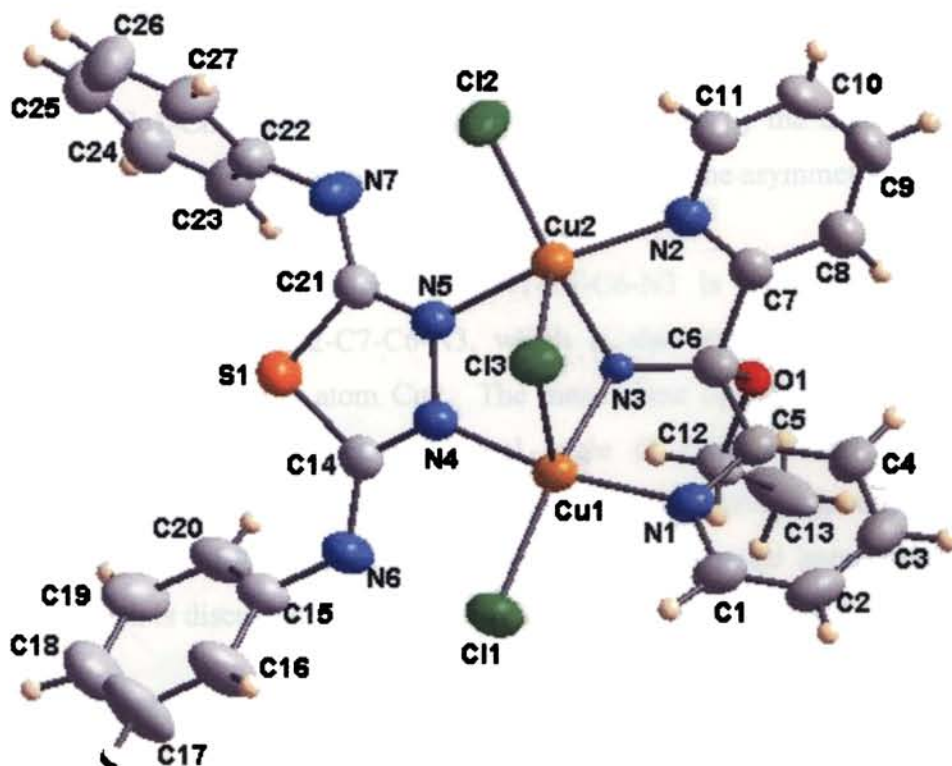


Fig. 3.1. Molecular structure of Cu_2TDCl_3 . The ellipsoids are drawn at 50% probability level

The skeletal structure at the metal centres can be regarded as two edge-sharing square pyramids. The $\text{Cu1}-\text{Cl3}-\text{Cu2}$ and the $\text{Cu1}-\text{N3}-\text{Cu2}$ angles are observed at $70.79(3)$ and $96.73(8)^\circ$ respectively and the bridging is found to be asymmetric with unequal apical bond lengths of the square pyramids ($\text{Cu1}-\text{Cl3} = 2.5790(13)$ Å; $\text{Cu2}-\text{Cl3} = 2.5347(17)$ Å). Also, Cu1 is $0.2132(4)$ Å out of the mean basal plane (atoms N1, N3, N4 and Cl1), whereas Cu2 is deviated at $0.2761(3)$ Å from its basal plane (atoms N2, N3, N5 and Cl2) towards the apical chlorine atom Cl3. This reveals greater pull on the chlorine Cl3 by Cu2 rather than Cu1, thus giving rise to asymmetry in bridging.

Interestingly, the overall structure of the molecule is composed of a number of six-membered and five-membered rings, mostly aromatic, which attribute much electron delocalization along the overall molecule, imparting stability to the structure. The thiazole ring is very nearly planar with a maximum deviation of $-0.0021(3)$ Å

at N5 from the mean plane, while the Cremer and Pople ring puckering analyses reveals that the two metal chelate rings, composed of N3, Cu1, N4, N5 & Cu2 and Cl3, Cu1, N4, N5 & Cu2 are observed to form envelopes on N3 and Cl3 respectively. The bridging plane Cu1-Cl3-Cu2-N3 is non-planar, as evidenced by the maximum mean deviation value of $-0.2961(5)$ Å. This is in accordance with the asymmetry in the Cu – Cl3 bonding suggested earlier.

Also, the metal chelate ring Cu1-N1-C5-C6-N3 is more puckered when compared to the ring Cu2-N2-C7-C6-N3, which is also attributed to the stronger Cu–Cl3 interaction of copper atom Cu2. The mean plane of the bridging Cu1-Cl3-Cu2-N3 moiety is positioned at a dihedral angle of $79.95(2)^\circ$ with the planar thiadiazole ring. However, the most interesting aspect of the bridging, coupled with a Cu1–Cu2 separation of $2.9591(13)$ Å is the strong spin-exchange interactions in the compound, which is discussed in detail at a later section of this chapter.

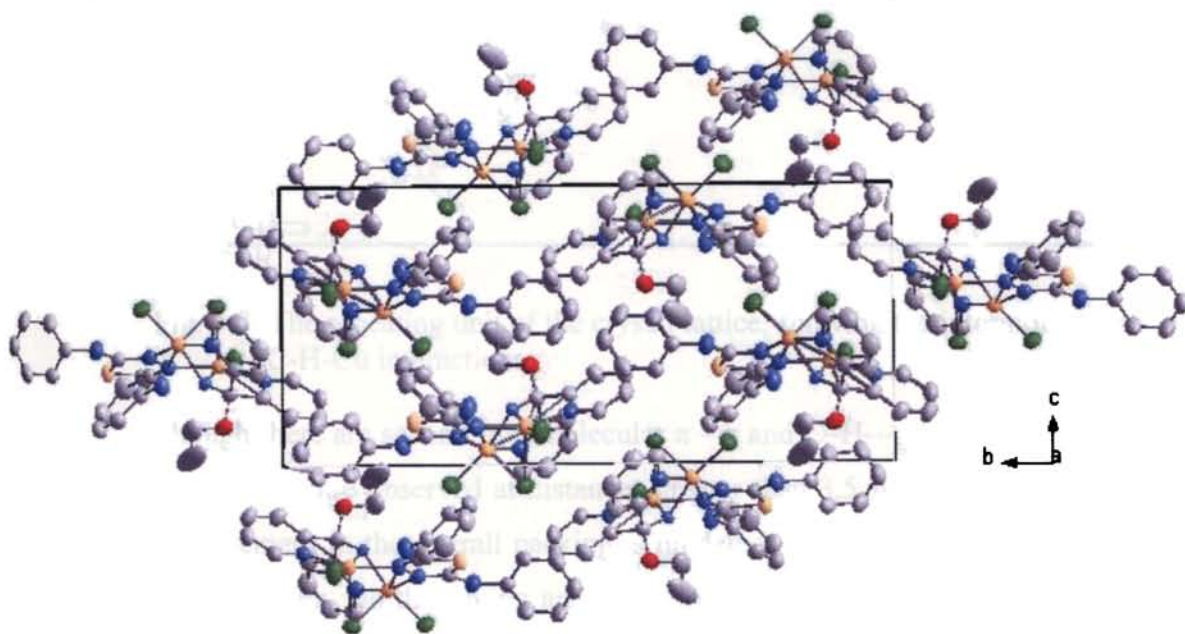


Fig. 3.2. Molecular packing diagram of Cu_2TdCl_3 , hydrogen atoms are omitted for clarity

Much stability is attributed to the structure through hydrogen bonding, $\pi - \pi$ and CH – π interactions in the crystal lattice. The molecular packing diagram of Cu_2TdCl_3 is given in Fig. 3.2, and the unit cell is viewed down the 'a' axis. The basic repeating unit in the crystal lattice is a set of two molecules, which are held together by

intermolecular C–H–Cu bonding interactions (Fig. 3.3) involving the hydrogens on C16 and C17 atoms of one molecule with the Cu2 atom of the adjacent molecule [C17–H17---Cu2 = 3.387 Å; C16–H16---Cu2 = 3.133 Å]. Two such adjacent units are then arranged in an offset fashion to each other, and in the crystal lattice, these two sets repeat one-dimensionally along the ‘c’ axis, contributing towards a zig-zag packing of the molecule.

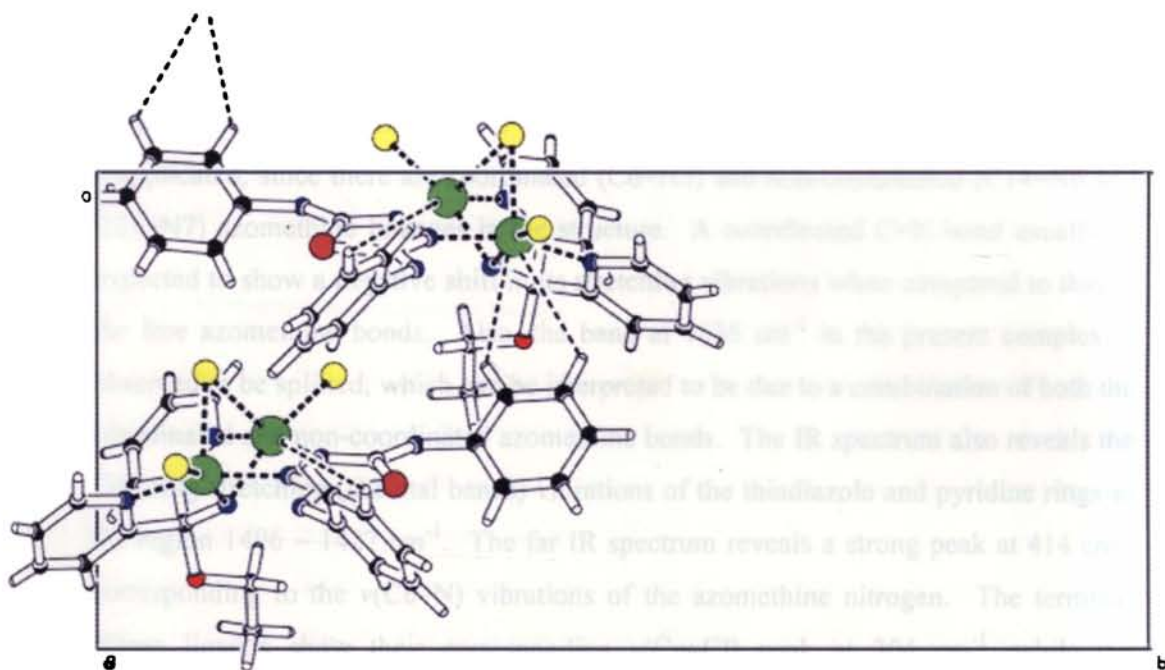


Fig. 3.3. The repeating unit of the crystal lattice, showing the intermolecular C-H-Cu interactions

Although there are several intermolecular $\pi - \pi$ and C–H--- π interactions in the lattice, most of them are observed at distances greater than 3.5 Å, due to which their effective involvement in the overall packing is hindered. Some of the weak C–H--- π and $\pi - \pi$ interactions, worth quoting are the following: C(12)–H(12A)–[1]–Cg(11)ⁱ [Cg(11): Cu(1), N(1), C(5), C(6), N(3); $d_{C(12)\cdots Cg} = 2.7987$ Å; $i = x, y, z$]; C(17)–H(17)–[1]–Cg(19)ⁱⁱ [Cg(19): N(2), C(7), C(8), C(9), C(10), C(11); $d_{C(17)\cdots Cg} = 3.5447$ Å; $ii = x, \frac{1}{2}-y, \frac{1}{2}+z$]; C(23)–H(23)–[1]–Cg(15)ⁱⁱⁱ [Cg(15): S(1), C(14), N(4), N(5), C(21); $d_{C(23)\cdots Cg} = 2.7987$ Å; $iii = x, \frac{1}{2}-y, -\frac{1}{2}+z$] and Cg(11)–[1]–Cg(19)ⁱ; $d_{Cg\cdots Cg} = 3.8363$ Å]. Three appreciable intra-molecular hydrogen bonding interactions are observed, viz., C(8)–H(8)---O(1)ⁱ [$d_{D\cdots A} = 2.797(1)$ Å, $\angle_{D-H-A} = 97.77^\circ$]; C(12) – H(12)B ---N(3)ⁱ

$[d_{D...A} = 2.809(1) \text{ \AA}, \angle_{D-H-A} = 86.59^\circ]$ and $C(20)-H(20)---S(1)^I [d_{D...A} = 2.996(1) \text{ \AA}, \angle_{D-H-A} = 96.98^\circ]$.

Spectral studies

The infrared spectral assignments confirm the functional groups on the structural skeleton of the molecule. Absence of a broad band near 3400 cm^{-1} is consistent with the lack of lattice water content in the sample as suggested by the elemental analyses data. The azomethine stretching vibrations are observed in the combination band at 1636 cm^{-1} . However, the assignment of this band is a bit complicated, since there are coordinated (C6=N3) and non-coordinated (C14=N6 and C21=N7) azomethine linkages in the structure. A coordinated C=N bond usually, is expected to show a negative shift in its stretching vibrations when compared to that of the free azomethine bonds. Also, the band at 1636 cm^{-1} in the present complex is observed to be splitted, which can be interpreted to be due to a combination of both the coordinated and non-coordinated azomethine bonds. The IR spectrum also reveals the C-N ring stretching (skeletal bands) vibrations of the thiadiazole and pyridine rings in the region $1496 - 1427 \text{ cm}^{-1}$. The far IR spectrum reveals a strong peak at 414 cm^{-1} corresponding to the $\nu(\text{Cu}-\text{N})$ vibrations of the azomethine nitrogen. The terminal chloro ligands show their corresponding $\nu(\text{Cu}-\text{Cl})$ peak at 304 cm^{-1} , while the vibration of the bridging chlorine is observed as a strong peak at 227 cm^{-1} . The bands at 246 and 280 cm^{-1} correspond to the $\nu(\text{Cu} - \text{N})$ vibrations of the coordinated pyridine nitrogen.

Another useful tool for the characterization of the compound is its electronic spectrum. A d^9 metal ion has an electron vacancy or 'hole' in its d level and thus can be regarded as the inverse of the d^1 arrangement. These two configurations also have identical ground state free ion terms, 2D which will be split by an octahedral field into two levels, $^2T_{2g}$ and 2E_g [27]. However, due to the relatively low symmetry of the environments in which the Cu^{2+} ion is characteristically found, detailed interpretations of the spectra and magnetic properties are somewhat complicated, even though we are dealing with the equivalent of a one-electron case. Cu(II) ion in the present compound

is observed to exist in a bridged square pyramidal environment by the crystal structure studies. During the formation of metal complexes, there occur linear combinations of metal and ligand atomic orbitals having appropriate symmetry giving rise to σ and π bonding molecular orbitals. The observed peaks in the UV-visible spectra of complexes are often interpreted in terms of transitions between these molecular energy levels. Thus in the electronic spectra of the complexes, small peaks at 272 and 282 nm are attributed to the $\pi \rightarrow \pi^*$ transitions of the pyridyl and imine functions, while the $n \rightarrow \pi^*$ transitions in the complex are observed at 300 and 367 nm. A shoulder at 325 nm is assigned to Cl \rightarrow Cu charge transfer transitions, and the S \rightarrow Cu and Py \rightarrow Cu charge transfer transitions are observed at 468 and 497 nm. The bands in the visible region, at 543 and 588 nm correspond to the $d-d$ transitions.

Electron Paramagnetic Resonance studies

Electron Paramagnetic Resonance (EPR) phenomenon was discovered by E. Zavoisky in 1944 and in the beginning it was used by physicists to study the paramagnetic metal ions in crystal lattices. It is based on the absorption of electromagnetic radiation, usually in the microwave region, which causes transitions between energy levels produced by the action of a magnetic field on an unpaired electron. In the case of a Cu(II) ion, it has an effective spin of $S = \frac{1}{2}$ and is associated with a spin angular momentum $m_s = +\frac{1}{2}$, leading to a doubly degenerate spin state in the absence of a magnetic field. When a sufficient magnetic field is applied, this degeneracy is removed, and the energy difference between two resultant states is given by

$$E = h\nu = g\beta H$$

where h is Planck's constant, ν is the frequency, g is the Lande splitting factor, β is the electron Bohr magneton and H is the magnetic field [29].

The factors that determine the type of EPR spectrum observed are:

- (a) the nature of the electronic ground state
- (b) the symmetry of the effective ligand field about the Cu(II) ion

(c) the mutual orientations of the local molecular axes of the separate Cu(II) chromophores in the unit cell.

The third factor determines the amount of exchange coupling present, which is a major factor in reducing the amount of stereochemical information available from the EPR spectrum [30].

The X-band EPR spectra of Cu_2TDCl_3 (**1**) reveal rhombic features with three g values, *viz.*, $g_1 = 2.174$, $g_2 = 2.073$, $g_3 = 2.041$ at 298 K (powder) (Fig. 3.4) and $g_1 = 2.221$, $g_2 = 2.115$, $g_3 = 2.079$ in DMF at 77 K (Fig. 3.5).

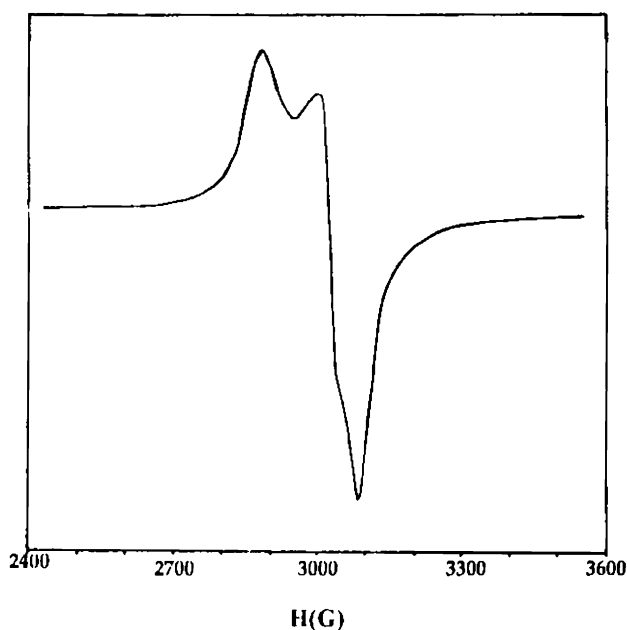


Fig.3.4. EPR spectrum of Cu_2TDCl_3 at 298 K

The spectrum at 77 K is complicated due to the rhombic features of the complex, which contains three non-equivalent nitrogen ligands. The nitrogen super-hyperfine splittings by aromatic nitrogen donors are commonly observed at 77 K, and in the EPR spectrum of **1** the seven hyperfine splittings characteristic of the bimetallic Cu(II) complex are poorly resolved, which can be attributed to the distorted structure. At room temperature, the EPR spectrum shows relatively lesser g -tensor anisotropy presumably due to larger spin-lattice relaxation time and smaller spin-orbit coupling interactions.

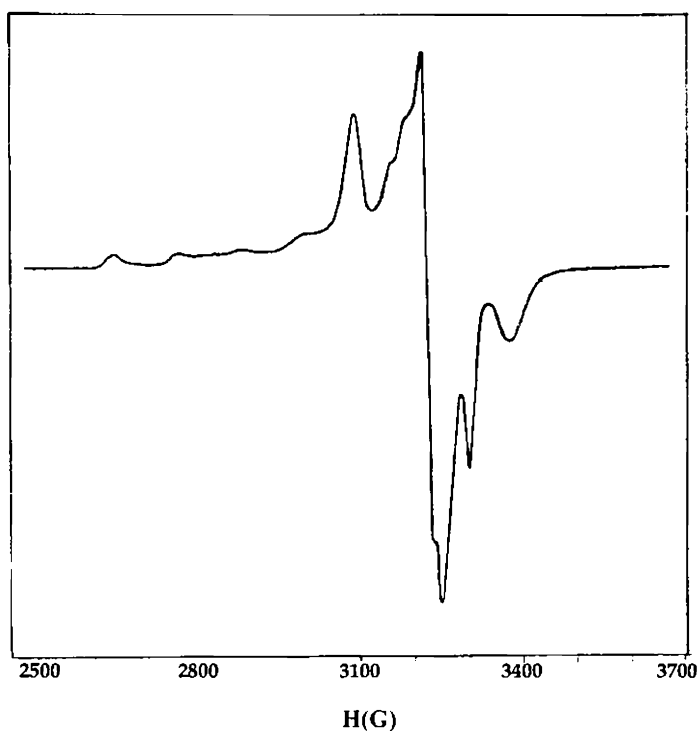


Fig.3.5. EPR spectrum of Cu_2TDCl_3 at 77 K in DMF

The lowest g value is greater than 2.04, which points towards a $d_{x^2-y^2}$ ground state [30], consistent with the distorted square pyramidal geometry observed in the X-ray crystal structure studies. The shifting of g values from 2.0023 in a transition metal complex is due to the mixing, via spin-orbit coupling of the metal orbitals involved in molecular orbitals containing the unpaired electrons, with the empty or filled ligand orbitals. Since the g values here suffer a positive shift, it indicates mixing with the filled ligand orbitals. The magnitude of shift is a measure of the degree of covalency of the complex. Since $g_{\min} > 2.04$, a possible trigonal bipyramidal alignment of the ligands around Cu(II) is ruled out. The anisotropic rhombic g -tensors with $G < 4.0$ [$G = (g_1 - 2.0023)/(g_1 - 2.0023)$; $g_1 = (g_2 + g_3) / 2$; $G = 3.13$ at 298 K and 2.31 at 77 K] suggest exchange coupling interactions in the complex [30]. A lower G value in DMF at 77 K characteristic of complexes more of a square planar nature, indicates lesser bridging interactions due to weakened Cu-Cl3 bonds in solution. The magnetically

less-concentrated disposition of the complex in solution at 77 K is evidenced by the absence of zero-field splitting with no half field signal corresponding to $\Delta M_s = \pm 2$ transition at 77 K in DMF, which implies weaker spin-spin exchange interactions in the dimer in the solution state.

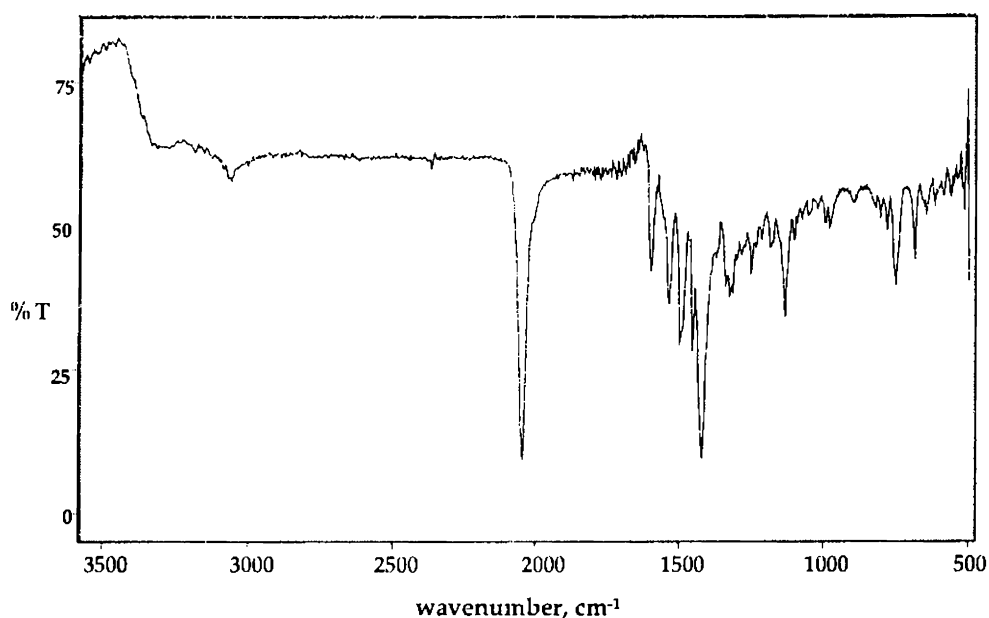
However, the single crystal X-ray diffraction studies reveal that at room temperature, the separation between the two Cu(II) ions is 2.9 Å, which is only slightly greater than the interatomic distance in metallic copper (~2.56 Å). A metal-metal bond distance <4.0 Å in a coordination compound is indicative of magnetic exchange interactions, and hence in the solid state, the presence of antiferromagnetic interactions in Cu₂ Cl₃ is accounted.

3.1.2. CuL¹N₃ (2)

The elemental analyses data are in conformity with a CuL¹N₃ stoichiometry for the compound **2**. The compound was synthesized by the metathetical displacement of the acetate ion by azide anion in the Cu(II) complex. As we were unable to obtain a single crystal suitable for X-ray diffraction of the compound, the main tools used for the study of the molecule are IR, electronic and EPR spectra.

Spectral studies

IR spectrum of CuL¹N₃ shows no broad band near 3500 cm⁻¹ supporting the absence of lattice water content consistent with the elemental analyses data. However, a weak band at 3056 cm⁻¹ corresponds to the $\nu(\text{N-H})$ vibrations of the nitrogen at the N(4)-position (Fig. 3.6). A sharp band is observed at 2045 cm⁻¹ corresponding to the antisymmetric $\nu(\text{NNN})$ vibration. The symmetric bending vibration of the azido group also appears as a very weak band at *ca.* 600 cm⁻¹. The $\nu(\text{M-N})$ vibration of the Cu-azide bond is obtained as a sharp band at 420 cm⁻¹ in the far IR region. The $\delta(\text{CS})$ band at 806 cm⁻¹ in the ligand is shifted to regions near 781 cm⁻¹ in the complex implying the enolization of thiosemicarbazone moiety upon coordination. Similarly the $\nu(\text{CS})$ band at 1251 cm⁻¹ also suffers a negative shift upon complexation.

Fig. 3.6. IR spectrum of CuL^1N_3

Conventionally, coordination of azomethine nitrogen to a metal ion has been proposed on the basis of the shifting of the azomethine $\nu(\text{C}=\text{N})$ band. The azomethine stretching band in HL^1 (1592 cm^{-1}) suffers a negative shift of *ca.* 60 cm^{-1} in the complex. It is believed that, upon complexation, the stretching vibration of the azomethine bond is weakened due to coordination with $\text{Cu}(\text{II})$ atom. However, the shifting of this band has been reported to be to both higher [31] and lower [32] energies. Since this band is unlikely to be exclusively $\nu(\text{C}=\text{N})$, but a combination band, a shift is difficult to be predicted with accuracy. Both the types of shifts can occur due to the different mixing of the $\nu(\text{C}=\text{N})$ band with other bands [33]. However, a new sharp band at *ca.* 1595 cm^{-1} is observed, which is assigned to the stretching vibration of the newly formed $\text{N}=\text{C}$ bond in the thiolate form of thiosemicarbazone.

Solid state diffused reflectance spectrum of the compound is also used for spectral studies. In the case of square planar complexes, three allowed transitions are expected in the visible region, but often these theoretical expectations are overlooked in practice, and these bands usually appear overlapped due to the very small energy difference between the d levels. However, for the complexes under study, useful information available from the electronic spectra are the energies of the transitions to

anti-bonding π molecular orbitals from the non-bonding and π -bonding molecular orbitals, which have characteristic values for thiosemicarbazones. Other useful bands are the charge transfer bands, which support coordination. Thus the molecule reveals $\pi \rightarrow \pi^*$ transitions of the pyridyl and imine functions at 268 and 278 nm, while the $n \rightarrow \pi^*$ transitions in the compound are observed at 326 and 365 nm. The charge transfer transitions are observed as shoulders at 424 and 448 nm. The $d-d$ transitions appear at 558 and 627 nm in the visible region. However, the Cu(II) complexes appear to exist in a wide range of stereochemistry making it difficult to use electronic spectroscopy alone as a definitive tool for identifying the geometry. In the absence of crystal data, EPR is regarded as an essential tool to complement electronic spectroscopic data [34].

Electron Paramagnetic Resonance studies

The EPR spectrum of compound CuL^1N_3 in DMF at 77 K reveals axial features with g values, $g_{\parallel} = 2.162$ and $g_{\perp} = 2.084$ (Fig.3.7).

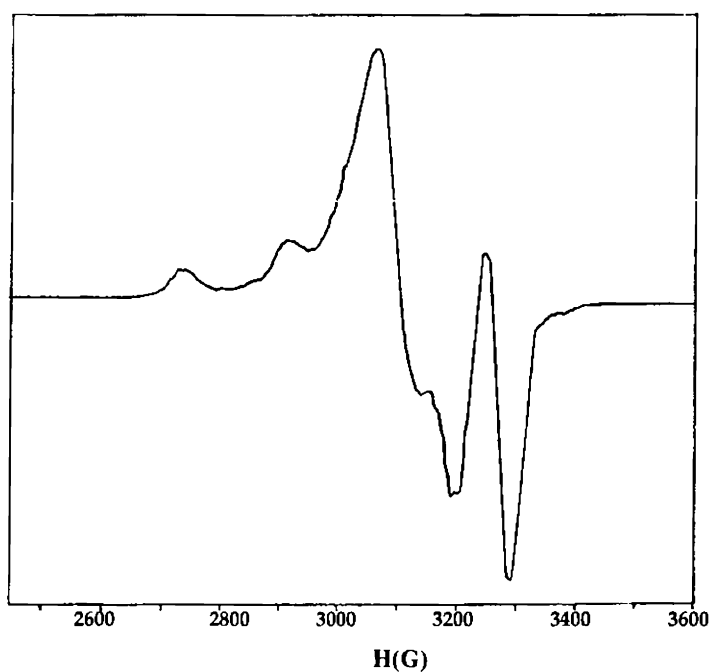


Fig. 3. 7. EPR spectrum of CuL^1N_3 in DMF at 77 K

All the g values are less than 2.3, which indicate considerable covalent character to the M-L bonds. The elemental analyses and spectroscopic data are in conformity with CuL^1N_3 stoichiometry for the compound. The EPR spectrum also is in strong support of this four coordinate stereochemistry. The f value, ($f = \frac{g_{\perp}}{A_{\parallel}}$), which reveals the extent of tetragonal distortion, is equal to 120.11 for the complex. The f values are reported to be in the range of 105-135 cm for square planar complexes [35]. Also, the value of $g_{\perp} < g_{\parallel}$ is characteristic of square planar complexes. Based on the above observations, the Cu(II) complex CuL^1N_3 is assigned a four-coordinated distorted square planar geometry, consistent with other spectroscopic evidences.

According to Frago *et al.*, [36] considering the magnetic parameters from Table 3.3, and using the theoretical basis of Maki and McGarvey for Cu(II) complexes [37], it is possible to apply a semi-empirical LCAO-MO scheme and express anisotropic g values and hyperfine constants as a function of MO coefficients. The anti-bonding molecular orbital of Cu(II) ions can be related to the spin Hamiltonian parameters by means of the following equations:

$$A_{\parallel} = P \left[-k - \frac{4\alpha^2}{7} + (g_{\parallel} - 2.0023) + \frac{3(g_{\perp} - 2.0023)}{7} \right] \quad (3.1)$$

$$A_{\perp} = P \left[-k + \frac{2\alpha^2}{7} + \frac{11(g_{\perp} - 2.0023)}{14} \right] \quad (3.2)$$

where P is taken as 0.036 cm^{-1} and by solving the two equations, we get the values for α^2 and k . The factor α^2 arises from the dipole-dipole interaction between magnetic moments associated with the spin motion of the electron and the nucleus and its value decreases with increasing covalency [38]. The term k arises from the Fermi contact interaction that has its origin in a non vanishing probability of finding the unpaired electron at the site of the nucleus. k is assumed to be independent to the direction of the magnetic field and the maximum value is obtained at an intermediate

covalence of α^2 . In other words, the stronger covalence should result in smaller hyperfine interaction.

However, Jezierska *et al.* [39] regarded α^2 as the MO index of in-plane σ bonding, which can be calculated from the expression,

$$\alpha^2 = -\frac{A_{\parallel}}{0.036} + (g_{\parallel} - 2.0023) + \frac{3(g_{\perp} - 2.0023)}{7} + 0.04 \quad (3.3)$$

Hathaway [5] investigated the evidence for out-of-plane bonding of ligands in axial copper(II) complexes to assess the out-of-plane bonding potential in a strictly square coplanar CuL_4 chromophore. He inferred that since there is no crystallographic evidence for a strictly square coplanar CuL_4 chromophore, in such complexes, some out-of-plane bonding potential still remains to be satisfied. In complexes with ligands capable of π -bonding the four ligands may satisfy the additional bonding potential of the CuL_4 chromophore by out-of-plane π -bonding. Hathaway derived the orbital reduction factors from the electronic and ESR spectral data and then related them to the MO coefficients through the following equations:

$$K_{\parallel}^2 = (g_{\parallel} - 2.0023) \frac{\Delta E(d_{xy} \rightarrow d_{x^2-y^2})}{8\lambda_0} \quad (3.4)$$

$$K_{\perp}^2 = (g_{\perp} - 2.0023) \frac{\Delta E(d_{xz}, d_{yz} \rightarrow d_{x^2-y^2})}{2\lambda_0} \quad (3.5)$$

$$K_{\parallel} = \alpha\beta \quad (3.6)$$

$$\text{and } K_{\perp} = \alpha\gamma \quad (3.7)$$

where K_{\parallel} and K_{\perp} are orbital reduction factors, α the σ bonding, β in-plane π -bonding and γ , the out-of-plane π -bonding MO coefficients. However, it should be noted that, the term α in (3.6) and the term α^2 in (3.3) are essentially the same, and hence in the present study we will consider the MO index of in-plane σ bonding as α itself.

Efforts were carried out to calculate the orbital reduction and covalency parameters for all the EPR active compounds. However the complicated nature of the spectrum restricted the calculation of bonding parameters in Cu_2TdCl_3 while the lack of hyperfine interactions prevented the calculation in some other complexes. The covalency parameters calculated for the present compound **2** are as follows: $\alpha = 0.7128$; $\beta = 0.8699$; $\gamma = 0.9963$; $K_{\parallel} = 0.6201$ and $K_{\perp} = 0.7102$. The extent of covalency is expressed in relation to the value of α , where the value of 1.0 corresponds to a purely ionic nature, and a decreased value indicates increased covalency of the M-L bonds. Also, as postulated by Hathaway, for pure σ bonding, $K_{\parallel} \sim K_{\perp} \sim 0.77$; for in-plane π -bonding, $K_{\parallel} < K_{\perp}$ and for out-of-plane π -bonding, $K_{\perp} < K_{\parallel}$. The trend in the calculated values in present complexes reveals that there is significant covalency in the M-L bonds as suggested by the values of $\alpha < 1$, while the chance for pure σ bonding is denied by $K_{\parallel} \neq K_{\perp} \neq 0.77$.

3.1.3. $\text{Cu}_2(\text{L}^1)_2\text{Br}_2 \cdot 7\text{H}_2\text{O}$ (**3**)

The elemental analyses results revealed a $\text{CuL}^1\text{Br} \cdot 3.5\text{H}_2\text{O}$ stoichiometry for the compound. However, the magnetic studies revealed some antiferromagnetic interactions in the compound, which proposed exchange-coupled interactions between two metal centres. Also the EPR spectrum in the polycrystalline state revealed $g_{\text{min}} < 2.04$. However, the IR spectrum revealed no characteristic bonds corresponding to a bridged -Br group. Hence a possible dimeric geometry is suggested where the non-coordinating pyridyl nitrogen of the first molecule effects a bridged structure for the complex by getting involved in a coordinate bond with the Cu(II) nucleus of the

second molecule (see Fig.3.17). The magnetochemistry of the complex is discussed in detail in a later section of this chapter.

Spectral studies

The compound **3** reveals a broad band around 3460 cm^{-1} in the IR spectrum, which arises due to the symmetric and antisymmetric -OH stretching vibrations of lattice water. It is interesting to note that the broad band around 3200 cm^{-1} in the ligand HL¹ corresponding to N-H vibration disappears in the complex, supporting the enolization of the ligand during complexation. The shift of the $\delta(\text{CS})$ band at 806 cm^{-1} in the ligand to 759 cm^{-1} in the complex supports the enolization of thiosemicarbazone moiety upon coordination. Similar to the case of compound **1**, the azomethine stretching vibration is observed as a strong combination band at 1641 cm^{-1} . In addition to the $\nu(\text{C}=\text{N})$ vibrations, the N-H bending and C-N stretching vibrations of the C-N-H group of the thioamide function can also contribute to this combination band, and hence an accurate assignment of the shift of the azomethine band cannot be carried out. Well-defined peaks are obtained in the far IR region, the Cu - N_{azomethine} and Cu - S_{thiolate} stretching vibrations are observed at 416 and 337 cm^{-1} . The $\nu(\text{Cu} - \text{N}_{py})$ vibrations appear as a strong band splitted at 282 and 255 cm^{-1} . Another strong band at 228 cm^{-1} supports the presence of terminal bromine in the complex and no characteristic bands corresponding to a bridging bromine are observed. The solid-state diffused reflectance spectrum reveals the $\pi \rightarrow \pi^*$ transitions of the pyridyl and imine functions at 269 and 280 nm . The $n \rightarrow \pi^*$ transitions in the complex are observed as shoulders at 305 and 319 nm and the Py \rightarrow Cu charge transfer transitions are observed at 481 nm . The $d-d$ transitions appear at 523 , 546 , and 584 nm in the visible region.

Electron Paramagnetic Resonance studies

The X-band EPR spectra of the compound reveal rhombic features with three g values, viz., $g_1 = 2.148$, $g_2 = 2.079$, $g_3 = 2.029$ at 298 K (Fig. 3.8) and $g_1 = 2.173$, $g_2 = 2.082$, $g_3 = 2.073$ at 77 K (Fig. 3.9).

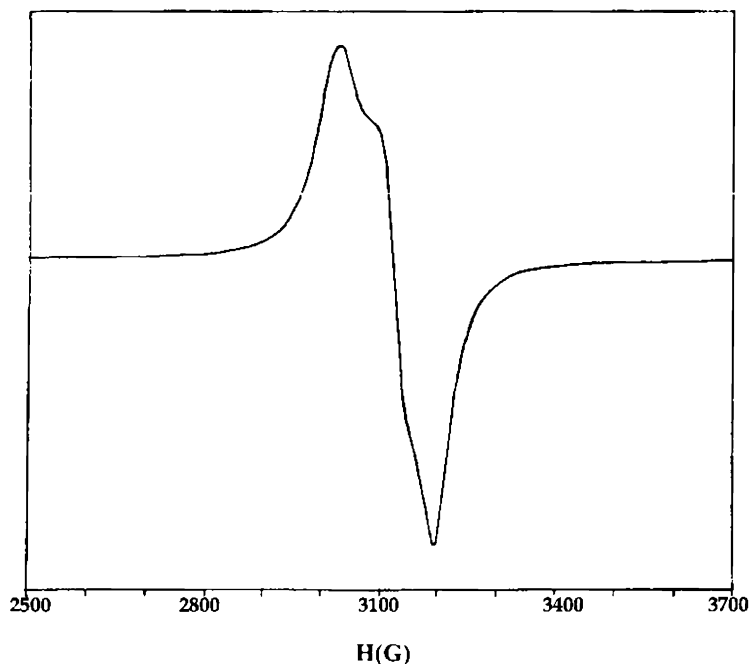


Fig. 3. 8. EPR spectrum of compound $\text{Cu}_2(\text{L}^1)_2\text{Br}_2 \cdot 7\text{H}_2\text{O}$ at 298 K

The rhombic features point towards the distorted environment around the metal centre, supporting the proposed structure. It may be noted that $g_{min} < 2.04$ at 298 K whereas $g_{min} > 2.04$ at 77 K. Hence the geometry of the compound is more distorted at 298 K, which supports the more magnetically concentrated nature of the compound in the polycrystalline state at room temperature.

The G values are calculated to be 2.82 and 2.27 at 298 and 77 K. The G value at 77 K indicates the more square planar nature of the compound in the frozen state. This may due to the fact that the bridging interactions in the bulk powder state are weakened in the frozen state at liquid nitrogen temperature. The covalency parameters calculated for **3** at 77 K is as follows: $\alpha = 0.7504$; $\beta = 0.8853$; $\gamma = 0.9971$; $K_{\parallel} = 0.6643$ and $K_{\perp} = 0.7482$.

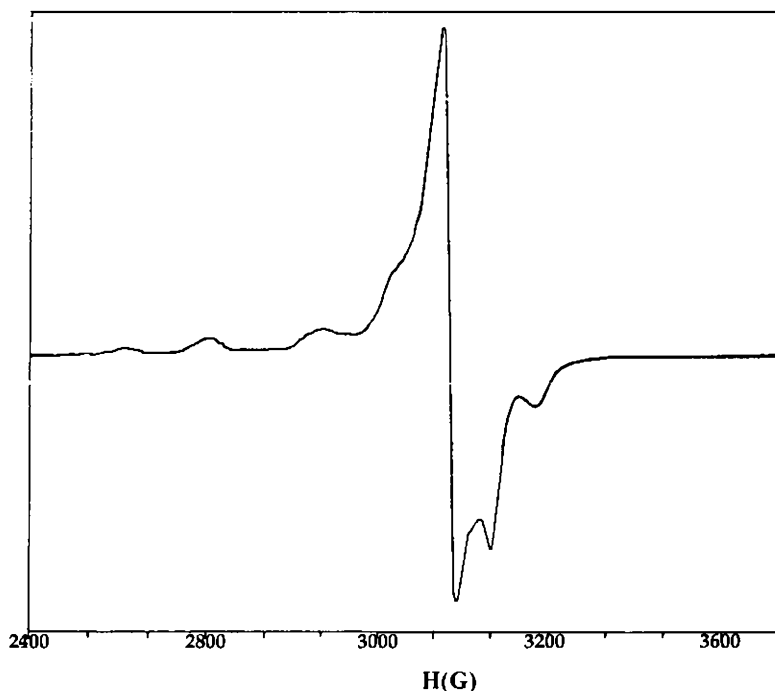


Fig. 3. 9. EPR spectrum of compound $\text{Cu}_2(\text{L}^1)_2\text{Br}_2 \cdot 7\text{H}_2\text{O}$ at 77 K in DMF

3.1.4. $\text{Cu}_2(\text{L}^1)_2(\text{SCN})_2 \cdot 4\text{H}_2\text{O}$ (**4**)

The elemental analyses data revealed a $\text{CuL}^1\text{SCN} \cdot 2\text{H}_2\text{O}$ stoichiometry for the compound **4**, however, the IR data showed some bridging characteristics for the thiocyanate group. Magnetic studies revealed the compound to be diamagnetic, however it appeared to be EPR active. Hence the diamagnetism here is attributed to a net spin pairing through effective antiferromagnetic interactions.

Spectral studies

The IR spectrum of compound **4** reveals that the $-\text{SCN}$ group is coordinated to $\text{Cu}(\text{II})$ through the sulfur atom since the characteristic bands are observed at $\sim 2150 \text{ cm}^{-1}$ (Fig.3.10). A coordination through the nitrogen atom of the $-\text{NCS}$ usually reveals a band near and below 2050 cm^{-1} [40]. The presence of a $\nu(\text{CS})$ band at 691 cm^{-1}

further supports the S-bonded nature of the thiocyanate group [41-43]. This type of coordination through the sulfur atom of thiocyanate group is rarely observed since metals of first transition series generally form $M-N_{SCN}$ bonds, where M corresponds to the metal atom [44]. The spectrum of compound **4** shows the $-N_{SCN}$ stretching vibration splitted into two peaks, one at 2127 cm^{-1} and other at 2159 cm^{-1} . This point towards the possibility of an unusual coordination mode of the $-SCN$ group.

It is established that the bridging ($M-NCS-M$) complexes, exhibit $\nu(CN)$ well above 2100 cm^{-1} [40]. Correlating this fact with the nature of the thiocyanate stretching bands leads to the assignment of a bridged structure to compound **4**. It is also possible that the splitted bands are the resultant of $\nu(MN)$ and $\nu(MS)$ bands. The S-bonded nature of the thiocyanato group is further supported by several low intensity bands around 420 cm^{-1} , since a single sharp $\delta(NCS)$ band would have been observed near 480 cm^{-1} if the thiocyanate group were end-on N-bonded to Cu(II).

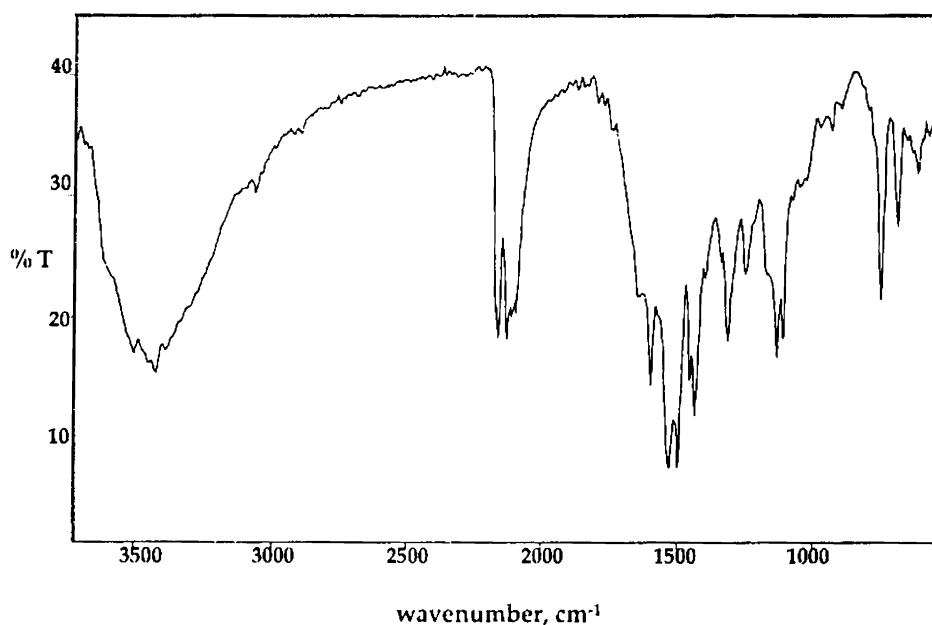


Fig. 3.10. IR spectrum of compound $Cu_2(L^1)_2(SCN)_2 \cdot 4H_2O$

Similar to other compounds, the bands due to lattice water and $N(4)-H$ nitrogen appear at 3424 and 3050 cm^{-1} respectively. The azomethine stretching vibration suffers a negative shift to 1526 cm^{-1} , while the new $N=C$ bond formed due to

deprotonation resonate at 1596 cm^{-1} . The $\nu(\text{CS})$ and $\delta(\text{CS})$ bands in the complex are observed at 1314 and 752 cm^{-1} . The electronic spectrum of the compound reveals the $\pi \rightarrow \pi^*$ transitions at 281 nm . The $n \rightarrow \pi^*$ transitions are observed as shoulders at 318 and 341 nm and the $\text{S} \rightarrow \text{Cu}$, $\text{NCS} \rightarrow \text{Cu}$ and $\text{Py} \rightarrow \text{Cu}$ charge transfer transitions are revealed as low intensity peaks at 407 , 433 and 456 nm . The $d-d$ transitions in complex **4** are observed as shoulders at 517 and 555 nm .

Electron Paramagnetic Resonance studies

The EPR spectra of compound **4** reveals rhombic features at both 298 (Fig.3.11) and 77 K (Fig.3.12). The g values are calculated from the spectra $g_1 = 2.178$, $g_2 = 2.081$, $g_3 = 2.034$ at 298 K and $g_1 = 2.287$, $g_2 = 2.072$, $g_3 = 2.029$ at 77 K .

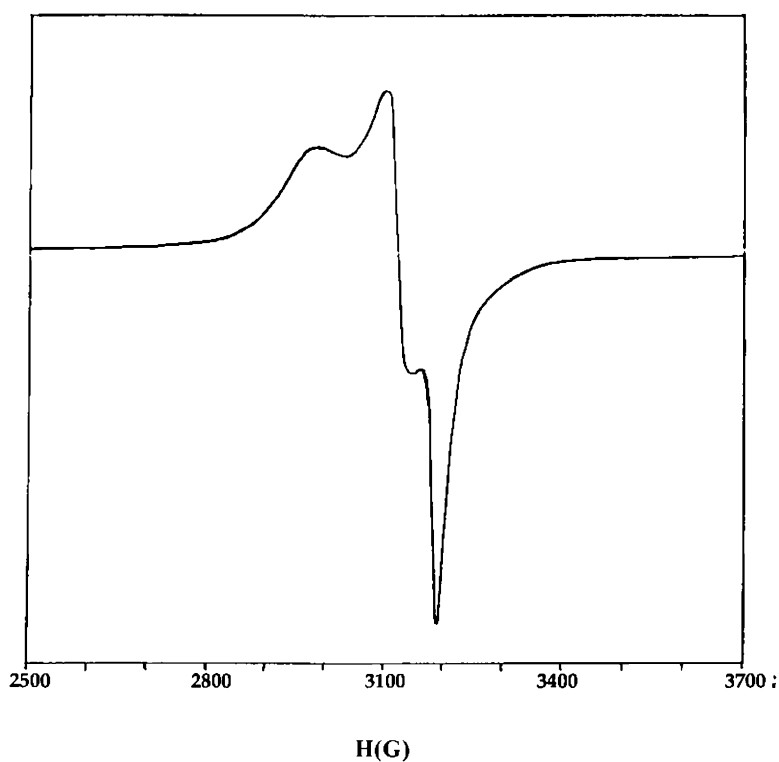


Fig. 3. 11. EPR spectrum of compound $\text{Cu}_2(\text{L}^1)_2(\text{SCN})_2 \cdot 4\text{H}_2\text{O}$ at 298 K

Due to the Jahn-Teller distortion, the molecules undergo a slight compression or elongation of the axial ligands in order to attain stability. In the case of the present compound, an effective distortion is predicted, due to the bridged nature of the complex. All the g values are less than 2.3, which indicate considerable covalent character to the M – L bonds.

Another interesting observation is that the G values calculated [$G = 3.18$ at 298 K and 5.91 at 77 K] rule out the possibility for a possible square planar nature of the compound. This, in turn supports the proposed bridged nature of the compound. However even at 77 K in DMF solution, the hyperfine interactions are rather weak, which indicates low tumbling rate and less paramagnetic nature of the Cu(II) ion. This is in accordance with the diamagnetic nature of the complex from susceptibility measurements. The covalency parameters calculated for **4** at 77 K is as follows: $\alpha = 0.8395$; $\beta = 0.9889$; $\gamma = 0.8984$; $K_{\parallel} = 0.8302$ and $K_{\perp} = 0.7542$.

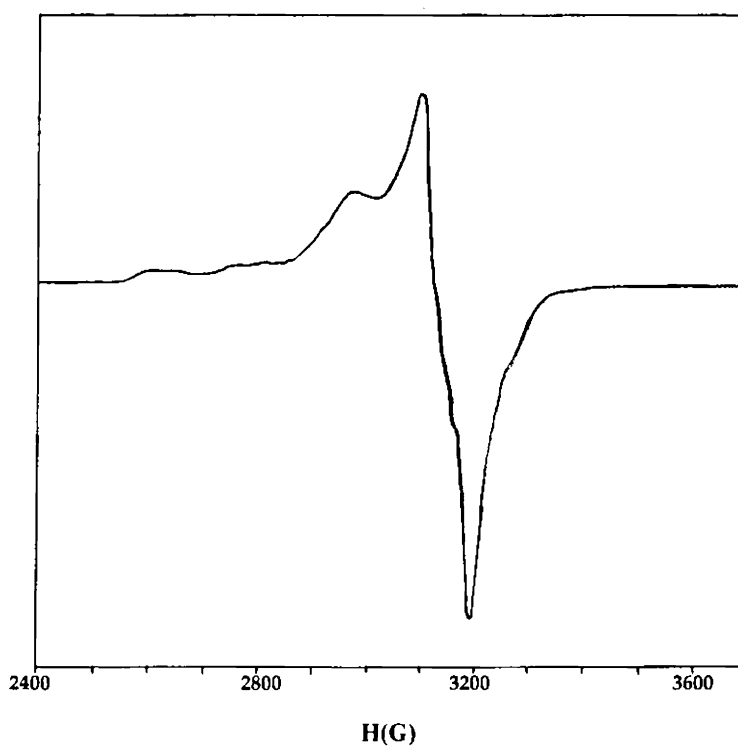


Fig. 3.12. EPR spectrum of compound $\text{Cu}_2(\text{L}^1)_2(\text{SCN})_2 \cdot 4\text{H}_2\text{O}$ at 77 K

3.1.5. $\text{Cu}_2(\text{L}^1)_2(\text{SO}_4)\cdot 1.5 \text{H}_2\text{O}$ (5)

A bridged stereochemistry is suggested for compound **5** also, where a sulfate group bridges two CuL^1 units. As in the case of **4**, the infrared spectrum of the compound is the chief support for this structure. The compound **5** is both diamagnetic and EPR silent in the polycrystalline state.

Spectral studies

Coordination lowers the high T_d symmetry of the sulfate anion. Complexation split the degenerate vibrations and all the ν_1 , ν_2 , ν_3 and ν_4 bands appear in the infrared spectra. However, depending upon the mode of coordination of the sulfate anion, i.e., whether unidentate, bidentate or bridged bidentate, the intensity and frequency of the bands are slightly varied, and hence with the help of established structures, we can distinguish the nature of the linkage of the sulfate anion in the complex [40]. Bridged bidentate structure of the sulfate anion is having the C_{2v} symmetry. The ν_1 and ν_2 vibrations are observed at 998 and 465 cm^{-1} , in the IR spectrum of $\text{Cu}_2(\text{L}^1)_2(\text{SO}_4)\cdot 1.5 \text{H}_2\text{O}$, which suggests the bridged bidentate nature of the sulfate anion. However, these bands are of very low intensity, appearing as weak bands, which is in accordance with the change of symmetry from T_d to C_{2v} of the sulfate anion. The ν_3 vibrations observed as medium bands at 1172 and 1115 cm^{-1} , and the ν_4 vibrations at 628 and 538 cm^{-1} , are also in conformity with the corresponding values of other complexes where the sulfate anion exists in the bridged bidentate form. Other IR vibrations are quite similar to those commonly observed in the present series. For instance, the lattice water stretching vibrations are observed at 3470 cm^{-1} , the azomethine stretching vibrations are included in the combination band at 1649 cm^{-1} and the $\nu(\text{CS})$ and $\delta(\text{CS})$ vibrations are observed at 1345 and 743 cm^{-1} . In the electronic spectrum, the compound reveals the $\pi \rightarrow \pi^*$ transitions at 271 and 285 nm, and the $n \rightarrow \pi^*$ transitions at 327 and 345 nm. The $\text{L} \rightarrow \text{Cu}$ charge transfer transitions are viewed at 448 and 481 nm. In the visible region, the $d-d$ transitions are observed as shoulders at 543 and 584 nm.

3.1.6. $\text{Cu}(\text{L}^3)_2 \cdot 4\text{H}_2\text{O}$ (6)

Spectral studies

The IR spectrum reveals a broad band around 3310 cm^{-1} and a medium band at 3056 cm^{-1} , which correspond to the lattice water content and the N(4)–H vibrations respectively. The characteristic cyclohexyl stretching vibrations are observed at 2928 and 2851 cm^{-1} . These two bands are unchanged in the complexes of HL^3 . The azomethine vibrations are observed at 1587 cm^{-1} . The $\nu(\text{CS})$ and $\delta(\text{CS})$ vibrations are observed as sharp bands at 1318 and 742 cm^{-1} . In the far IR region, $\nu(\text{CuN})$ vibration involving the azomethine bond, and the $\nu(\text{CuS})$ vibrations of the thiolate bond are observed at 418 and 302 cm^{-1} . Solid-state electronic spectrum of the compound reveals the $\pi \rightarrow \pi^*$ transitions at 280 and 299 nm , whereas the $n \rightarrow \pi^*$ transitions in the complex are observed as small peaks at 327 and 348 nm . The $\text{S} \rightarrow \text{Cu}$ and $\text{Py} \rightarrow \text{Cu}$ charge transfer transitions are observed at 416 , 451 and 461 nm , while the d - d transitions appear at 526 and 564 nm in the visible region.

Electron Paramagnetic Resonance studies

Rhombic features are revealed in the EPR spectrum in DMSO solution at 77 K (Fig.3.13) with three g values, $g_1 = 2.165$, $g_2 = 2.052$ and $g_3 = 2.041$.

Considerable covalent character is imparted to the M–L bonds, since all the g values are less than 2.3. Due to the d^9 configuration of the Cu(II) ion, in octahedral or tetrahedral symmetry, the odd d -electron occupies a degenerate d -orbital set, Cu(II) complexes are subject to Jahn-Teller distortions. In the octahedral case, the Jahn-Teller theorem splits the degeneracy of the 2E_g ground state, resulting in a concomitant elongation or compression of the Cu-ligand bonds parallel to one of the three molecular axes. Here, the $g_{\text{min}} > 2.04$, and hence a possible axial compression is ruled out. Usually, Jahn-Teller elongations are preferred owing to the $4s - 3d_{z^2}$ orbital mixing, which slightly lowers the energy of $3d_{z^2}$ when compared to $3d_{x^2-y^2}$.

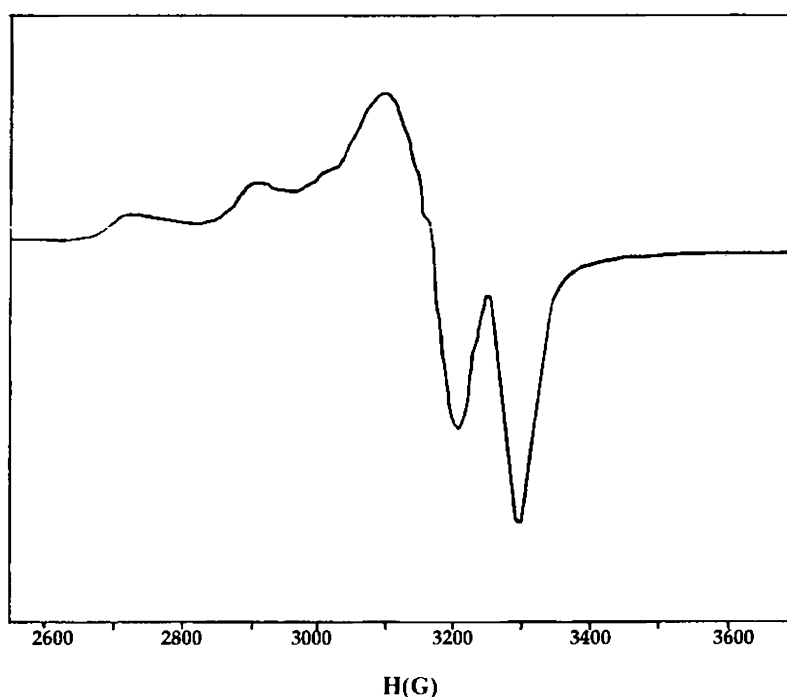


Fig. 3. 13. EPR spectrum of compound $\text{Cu}(\text{L}^3)_2 \cdot 4\text{H}_2\text{O}$ at 77 K in DMSO

However, the above factors strictly apply only to six-coordinate complexes with true O_h symmetry, where all the six ligands and all the three molecular axes are equivalent. Compounds of the type CuL_4X_2 typically undergo a structural elongation along one of the two molecular axes, caused by vibronic coupling of non-degenerate, but close in energy, $d_{x^2-y^2}$ and d_{z^2} energy levels. This is 'pseudo Jahn-Teller distortion', because if the compounds were not distorted, they would still not possess the d -orbital degeneracy [45]. However, in the present compound $\text{Cu}(\text{L}^3)_2 \cdot 4\text{H}_2\text{O}$, the EPR spectral details confirm a Jahn-Teller elongation along the molecular axes, since a $g_{\min} > 2.04$ pattern is expected of a Jahn-Teller elongated octahedral structure, with the ground state $d_{x^2-y^2}$. The f value is calculated to be 117 cm for the complex, which comes in the range of values corresponding to square planar complexes. Considering all the above factors, the six-coordinate complex **6** can be assigned an octahedral stereochemistry with a Jahn-Teller elongated D_{4h} symmetry. The covalency

parameters calculated for **6** at 77 K is as follows: $\alpha = 0.7413$; $\beta = 0.9218$; $\gamma = 0.9332$; $K_{\parallel} = 0.6833$ and $K_{\perp} = 0.6918$.

3.1.7. $\text{CuL}^3\text{Cl}\cdot 5\text{H}_2\text{O}$ (**7**)

Spectral studies

Contrary to the chloride complex of the ligand HL^1 , which turned out with an unprecedented structure, the compound **7** is found to exist in a four coordinate environment supported by the elemental and other spectroscopic data. The IR spectrum of the compound **7** is given in Fig. 3.14 below.

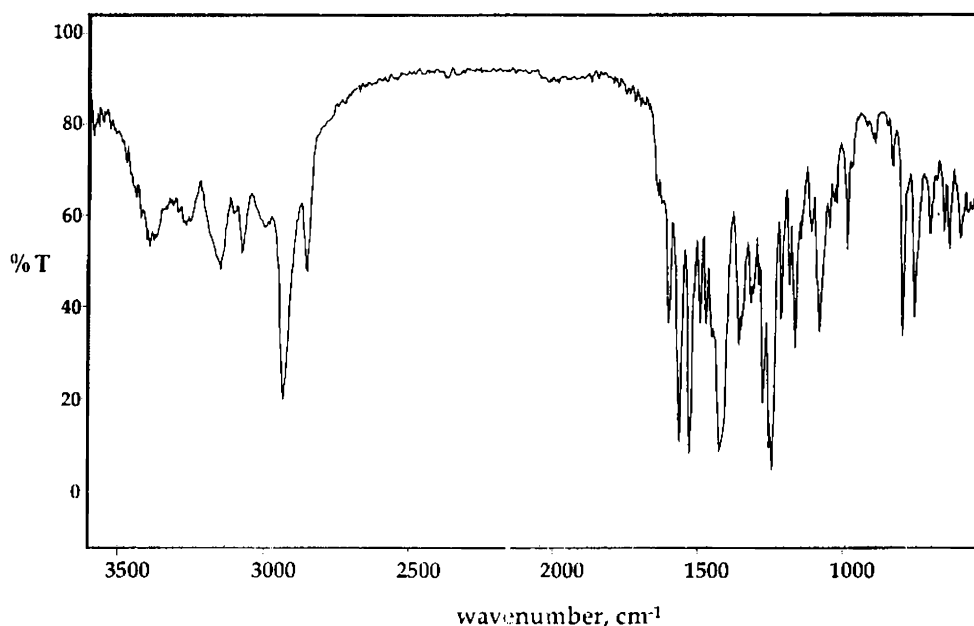


Fig. 3.14. IR spectrum of compound $\text{CuL}^3\text{Cl}\cdot 5\text{H}_2\text{O}$

The region of $3400 - 3200 \text{ cm}^{-1}$ in the IR spectra of complex is complicated due to the appearance of two, three or four distinct bands unlike one broad or sharp band usually observed in other complexes of this series. This can be attributed to the differences in the hydrogen bonding interactions of the complexes. An alternative explanation could be that the band at lower frequency is an overtone of the N - H bending vibrations found in the region near 1600 cm^{-1} , which is intensified by Fermi

resonance [46, 47]. The cyclohexyl stretching vibrations appear as two sharp bands at 2932 and 2852 cm^{-1} . The newly formed N=C bond due to enolization of the ligand resonate at 1598 cm^{-1} , while the azomethine stretching vibration is observed at 1559 cm^{-1} . The stretching and bending vibrations of the thiocarbonyl group appear at 1356 and 751 cm^{-1} . The $\nu(\text{CuCl})$ vibration of the terminal chloro ligand is observed at 304 cm^{-1} . In the solid-state diffused reflectance spectrum, the $n \rightarrow \pi^*$ transitions are observed as shoulders at 336, and 385 nm. The L \rightarrow M charge transfer transitions are observed at 415, 433 and 461 nm, and the $d-d$ transitions appear at 519 and 565 nm.

Electron Paramagnetic Resonance studies

The EPR spectra of the compound 7 gave poorly resolved peaks, however, the magnetic studies revealed the compound to be diamagnetic. Even if the net magnetic moment is negative in a molecule, i.e., diamagnetic, the presence of a paramagnetic Cu(II) ion even in very small concentrations can give rise to electron paramagnetic resonance absorptions. This is the case here with compound 7, since the spectrum appears with more of an isotropic nature even in the frozen state at 77 K. Ideally, in the dissolved state at 77 K in a suitable solvent, the intermolecular interactions are reduced, and the EPR spectrum is well resolved. In the EPR spectrum of the present compound, not only the hyperfine interactions are absent, but it also does not provide for the accurate assignment of the g values. The EPR study of the compound thus returned poor results, which are not worth mentioning here.

3.1.8. $\text{Cu}_2(\text{L}^3)_2(\text{N}_3)_2 \cdot 2\text{H}_2\text{O}$ (8)

In accordance with the elemental analyses data, an empirical formula $\text{CuL}^3\text{N}_3 \cdot \text{H}_2\text{O}$ is assigned for compound 8. Synthesis of the compound is achieved by the metathetical displacement of the acetate ion by azido anion in the Cu(II) complex. However, the infrared spectrum of the compound reveals some bridging aspects for the coordinated azido anion in the complex. Hence the diamagnetic attribute may be explained by a possible spin pairing through effective antiferromagnetic interactions in

the compound. However, the reason for the EPR active nature of the compound is explained in detail in a later section of this chapter.

Spectral studies

In contrast to that of compound **2** mentioned earlier, the IR spectrum of the compound (Fig.3.15) shows that the asymmetric stretching vibrations of the coordinated azido group appear as two sharp bands at 2173 and 2080 cm^{-1} . This may possibly arise due to the non-linear nature of the azido group, which give different asymmetric stretching frequencies. However, comparison with the reported IR frequencies of other azido complexes reveals that the presence of more than one azido group in the complex usually give rise to two or more sharp bands near 2100 cm^{-1} region. Hence, a reasonable explanation could be that the complex exists as a dimer in which the azido anion in each unit is involved in an end-on bridging with the second Cu(II) centre (see Fig. 3.18).

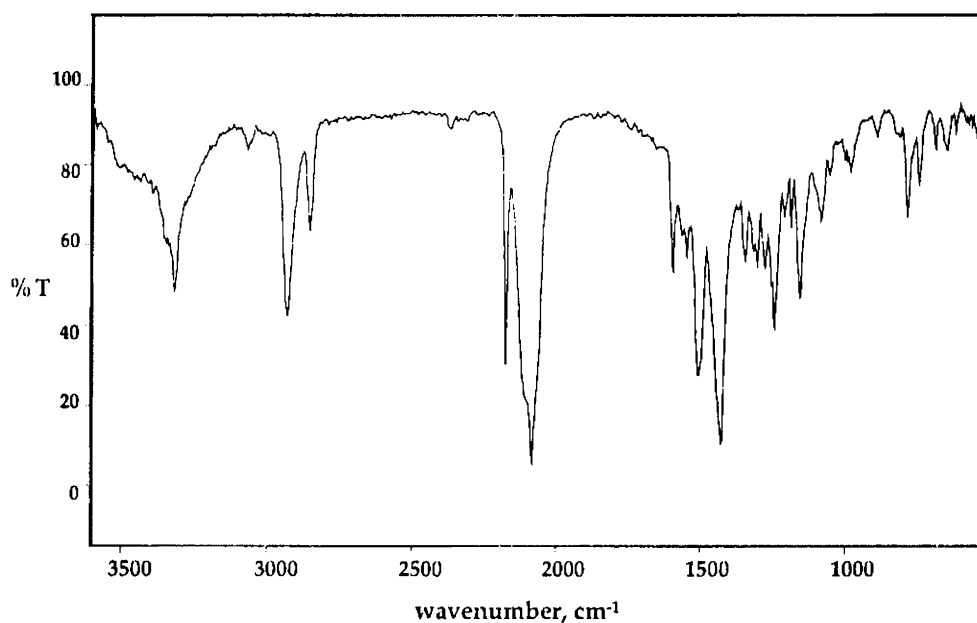


Fig. 3.15. IR spectrum of compound $\text{Cu}_2(\text{L}^3)_2(\text{N}_3)_2 \cdot 2\text{H}_2\text{O}$

The symmetric stretching vibration of the azido groups is observed as a sharp band at 1272 cm^{-1} . The $\delta(\text{NNN})$ vibration is observed as a medium band near 660

cm^{-1} , while the $\nu(\text{Cu-N})$ vibration of the coordinated azido group is observed near 410 cm^{-1} . The other bands are assigned similar to that of the other compounds. The non-hydrogen bonded lattice water appear as a sharp band at 3313 cm^{-1} , the cyclohexyl stretching vibrations appear at 2930 and 2851 cm^{-1} , the azomethine stretching bands are observed at 1533 cm^{-1} and the stretching and bending vibrations of the thiocarbonyl group appear at 1344 and 745 cm^{-1} respectively. The solid-state diffused reflectance spectrum reveals the $\pi \rightarrow \pi^*$ transitions of the pyridyl and imine functions at 265 and 282 nm . The $n \rightarrow \pi^*$ transitions in the complex are observed at 310 and 331 nm . The $\text{S} \rightarrow \text{Cu}$ and $\text{Py} \rightarrow \text{Cu}$ charge transfer transitions are observed at 420 and 432 nm . In the visible region, appreciable $d-d$ transitions are only observed at wavelengths higher than 600 nm .

Electron Paramagnetic Resonance studies

The EPR spectrum of the compound in DMF at 77 K is given in Fig. 3.16.

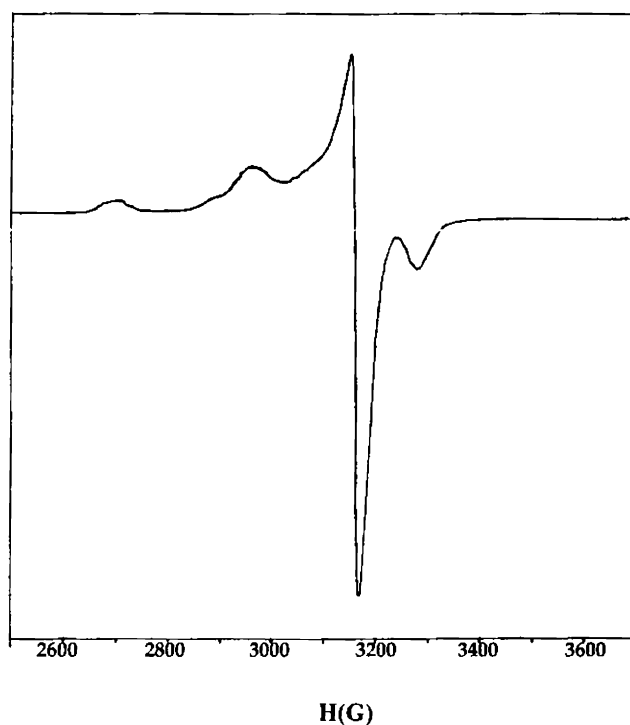
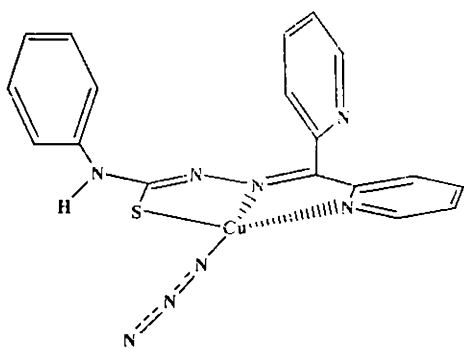


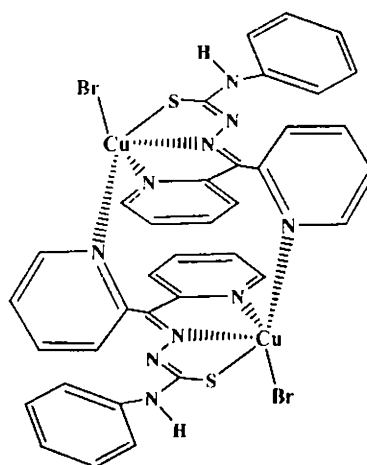
Fig. 3.16. EPR spectrum of compound $\text{Cu}_2(\text{L}^3)_2(\text{N}_3)_2 \cdot 2\text{H}_2\text{O}$ at 77 K

The EPR spectrum of the compound is found to be more of an axial type, with some weak hyperfine interactions observed at low fields. The g values are calculated to be $g_{\parallel} = 2.173$ and $g_{\perp} = 2.053$. Since $g_{min} > 2.04$, a possible axial compression and a consequent trigonal bipyramidal alignment of the Cu(II) complex is ruled out [30]. The f value of 112.42 cm for the complex points towards the weaker bridging interactions in the compound, since a square planar stereochemistry reveals an f value in the range of 105-135 cm [35].

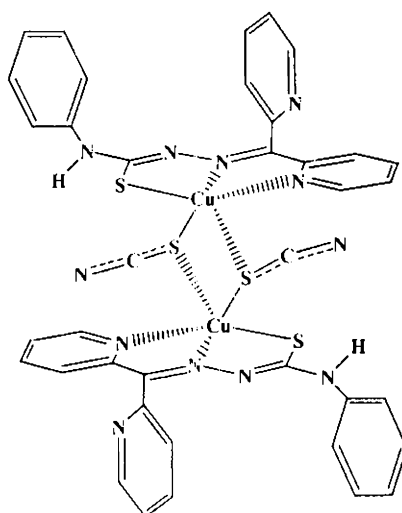
Thus the stereochemistry of the complexes reveals possible square planar, square pyramidal and octahedral geometries for the compounds, all distorted from the ideal geometries. Compound **1** possesses crystal structure evidence, while EPR and spectroscopic evidence are the useful tools for elucidating the stereochemistry of other complexes. Compounds **3**, **4**, **5** and **8** are assigned bridged stereochemistries with evidences from magnetic and IR data. However, the EPR spectra of these bridged structures at 77 K hardly revealed any bimetallic features, which may be due to the weakened bridging interactions in solution in the frozen state. In this context, it is interesting to note that even for the compound **1**, which is essentially bimetallic as revealed by the crystal structure, the EPR did not reveal any half-field transition. The tentative structures of the complexes (**2** - **8**) are given in Figs 3.17 and 3.18.



Compound 2

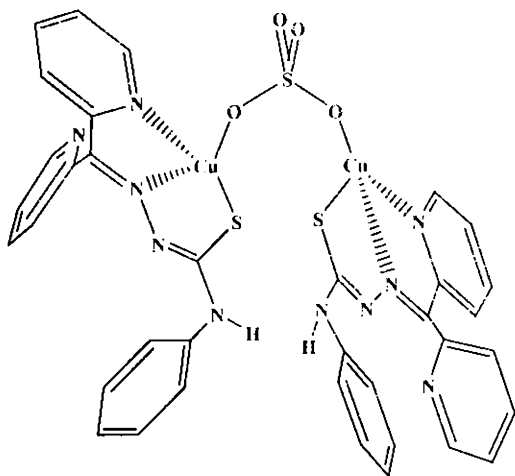


Compound 3

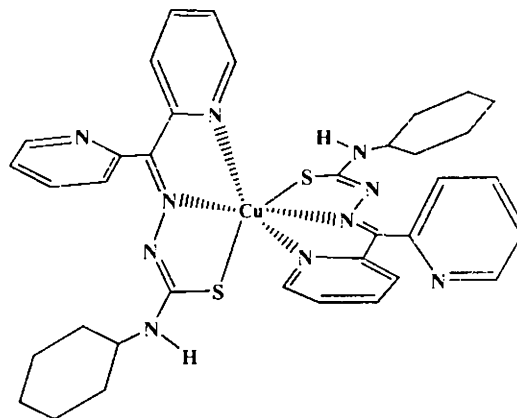


Compound 4

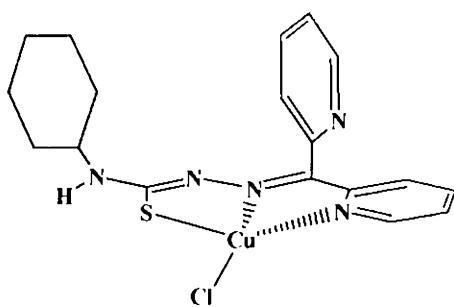
Fig. 3.17. Tentative structures of the complexes 2, 3 and 4
Water of hydration is omitted for convenience



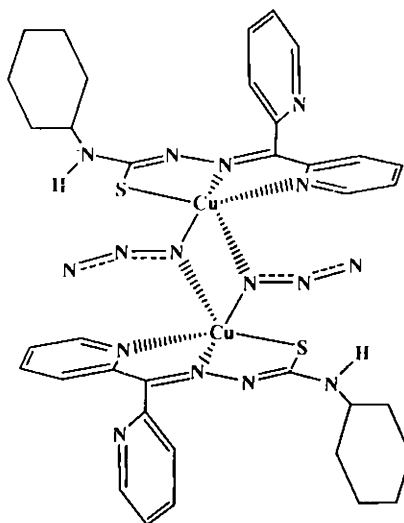
Compound 5



Compound 6



Compound 7



Compound 8

Fig. 3.18. Tentative structures of the complexes 5, 6, 7 and 8
Water of hydration is omitted for convenience

3.2. Magnetochemistry of the complexes

When the neighbouring magnetic centers in a complex are close enough for direct or indirect orbital overlap, they are termed as magnetically concentrated complexes. This interaction affects the magnetic property of the complex, and sometimes, swamps the ligand field effect. When two spin carriers, I and J with the spins i and j respectively, are close enough to each other, they interact with the quantum numbers associated with the total spin of the system being the integer or half-integer values from $|i-j|$ to $i+j$. In most cases, the ground state has the lowest spin $|i-j|$; the interaction between I and J is antiferromagnetic, which for simplicity concerns, can be accounted as the two spins being arranged antiparallel to each other. In some cases, the ground state has the highest spin $i+j$, the interaction is then ferromagnetic, with the spins being aligned parallel [48]. Magnetic susceptibility measurements reveal the nature of the interaction. When this interaction is antiferromagnetic, the low spin ground state is more and more populated as the temperature is lowered, and the product $\chi_M \cdot T$, where χ_M is the molar magnetic susceptibility and T the absolute temperature, decreases. When the interaction is ferromagnetic, the high-spin state is more and more populated as temperature is lowered, and $\chi_M \cdot T$ increases, reaches very high values at low temperature, and eventually may show a maximum due to magnetic saturation effects. An antiferromagnet has a characteristic Neel temperature (T_N) above which it behaves like a paramagnet, but below this temperature, with the lowering of T , the magnetic susceptibility decreases. A ferromagnet retains a characteristic Curie temperature (T_C) above which it behaves like a paramagnet, but below this temperature, its magnetic susceptibility increases rapidly. A third case arises where the antiferromagnetic interactions occur between two different spin lattices, with unequal spins, then the system is said to be ferrimagnetic. The spontaneous antiparallel alignment occurs also in a ferrimagnetic substance at the transition temperature, but since the non-equivalent sublattices in the structure do not balance each other, the compound retains a small permanent magnetic moment.

The majority of coordination complexes are magnetically dilute as in these complexes the paramagnetic centres are usually linked to ligands where other atoms reasonably separate the donor atoms from each other. As a result, no secondary magnetic interaction is possible between the neighbouring paramagnetic centres. Of the magnetically concentrated coordination complexes, most are antiferromagnetic and very few are ferromagnetic. Antiferromagnetism can arise due to either intramolecular or intermolecular spin exchange interactions.

A quantitative approach for the calculation of the effect of a magnetic field to the energy levels is developed taking into account two factors, viz. the effect of magnetic field on the individual Kramer's doublets and the mixing of these doublets together. The two effects are known, respectively as the first- and second- order Zeeman effects. Van Vleck derived the magnetic susceptibility equation taking into account the two Zeeman effects as [49]:

$$\chi_M = \frac{N \sum_n \left[\frac{(E_n(1))^2}{kT} - 2E_n(2) \right] \cdot \exp \frac{(-E_n(0))}{kT}}{\sum_n \exp \frac{(-E_n(0))}{kT}} \quad (3.8)$$

where $E_n(0)$ is the energy of the n^{th} level in the absence of field, and $E_n(1)$ and $E_n(2)$ are the first order and second order Zeeman coefficients, respectively.

For coordination compounds, we will incorporate the Van Vleck's equation with large multiplet width, where the first order Zeeman coefficient is replaced by the appropriate magnetic moment operator $\hat{\mu}$, which is equal to $\hat{J} \cdot g \beta H$ and the second order Zeeman effect approaches zero. For a binuclear complex, with two paramagnetic ions undergoing antiferromagnetic interaction, $S^z=0$ is the ground state with zero energy and $S^z=1$ is the excited state with an energy $-2J$ above the ground state level. In the case of a binuclear complex, the population of the excited states also need to be considered. Hence, taking all the possible levels of S^z and their

multiplicities $(2S' + 1)$ into consideration and including the temperature independent paramagnetism term, $N\alpha$, the magnetic susceptibility equation assumes the form,

$$\chi_M = \frac{Ng^2\beta^2}{3kT} \frac{\sum S(S'+1)(2S'+1)\exp\left[\frac{-E_{(0)}}{kT}\right]}{\sum (2S'+1)\exp\left[\frac{-E_{(0)}}{kT}\right]} + N\alpha \quad (3.9)$$

For the d^1 and d^9 systems, $S = 1/2$ so that $S' = 0, 1$, for which the exchange interaction energies are $3/2J$ and $-1/2J$ respectively. Thus the equation (9) above can be modified as,

$$\chi_M = \frac{2Ng^2\beta^2}{kT} \left[\frac{1}{3 + \exp\left(\frac{-2J}{kT}\right)} \right] + N\alpha \quad (3.10)$$

The above equation gives the magnetic susceptibility of a dimer. The magnetic susceptibility per gram atom (χ_A) of the interacting ions will be half the first term in equation (3.10) above.

$$\chi_A = \frac{Ng^2\beta^2}{3kT} \left[1 + \frac{1}{3} \exp\left(\frac{-2J}{kT}\right) \right]^{-1} + N\alpha \quad (3.11)$$

This is known as Bleaney-Bowers equation [50]. Fitting the experimental magnetic susceptibility data at various temperatures in the above equation using the least squares fitting methods will provide the magnetic parameters $-2J$, g and $N\alpha$.

3.2.1. Cu_2TDCl_3

The compound Cu_2TDCl_3 reveals subnormal magnetic moment value per Cu ion at room temperature, suggesting possible exchange-coupled interactions between the Cu(II) ions. The magnetic susceptibility data are collected at various temperatures between 80 and 298 K. The magnetic parameters are well interpreted in terms of the modified Bleaney-Bowers equation corrected for paramagnetic impurities, with the best fit values of $2J = -376 \text{ cm}^{-1}$, $g = 2.058$, $N\alpha = -40 \times 10^{-6} \text{ emu}$ and ρ (impurity

factor) = 0.1470 with an agreement factor $R \left\{ \frac{\sum (\chi_{calc} - \chi_{obs})^2}{\sum \chi_{obs}^2} \right\} = 8.0 \times 10^{-4}$. The variation of magnetic susceptibility with temperature is plotted as points in Fig. 3.19 and the theoretical best fit curve is shown as in the solid line.

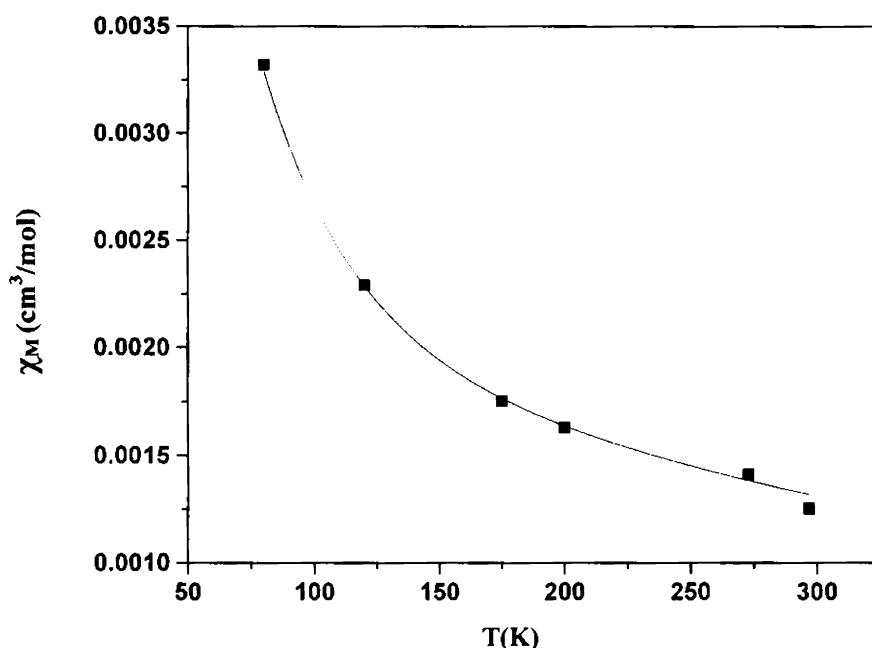
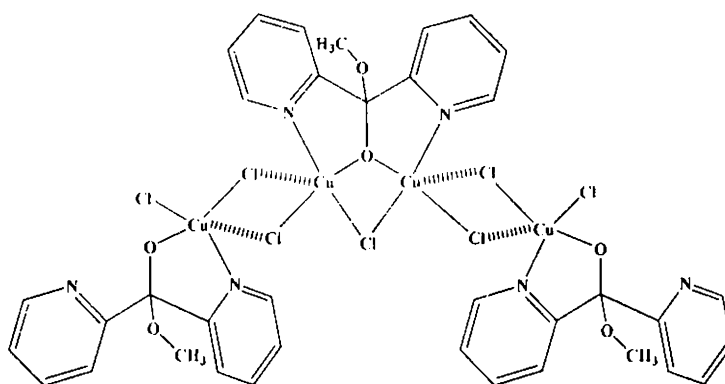


Fig. 3.19. Temperature dependence of χ_M for compound Cu_2TDCl_3 . The squares are the experimental points and the solid line is the theoretical best fit of the experimental data

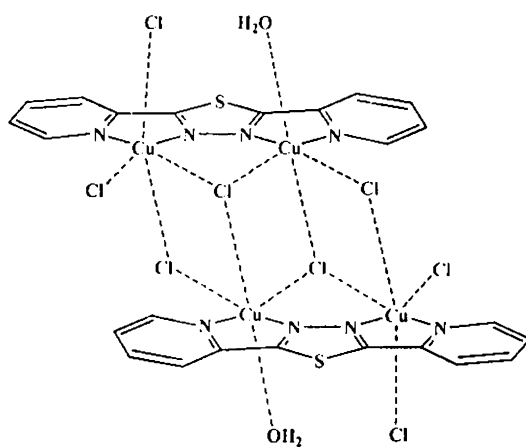
The antiferromagnetic behaviour is as expected in the compound based on its structural features revealed by single crystal X-ray diffraction. The two Cu(II) nuclei are much close to each other, and are bridged by one nitrogen and one chlorine atoms. This leads to an effective coupling of the neighbouring spins via an indirect super-exchange mechanism, involving the π -overlap of the $d_{x^2-y^2}$ orbitals of the two Cu(II) nuclei through the filled p_z orbital of the ligand atom along the Cu1–N3–Cu2 bridge, giving rise to strong antiferromagnetic interactions. The separation between the two Cu(II) nuclei at 2.9591(13) Å is only slightly higher than the Cu–Cu interatomic distance of 2.56 Å in metallic copper lattice, also plays a significant role in the

magnetic exchange since the super exchange interaction is highly sensitive to the metal-metal distance. Another factor is the positioning of the bridging nitrogen atom on the equatorial plane of both the Cu(II) nuclei, which provides for the spin-exchange between the metal ions.

It is interesting to compare the present results with previous reports of structures similar to that of Cu_2Cl_3 . Only two comparable structures are observed in the literature, compound A [51] and compound B [52].



Compound A



Compound B

The complex A consisted of tetrameric Cu(II) repeating units with alternating Cu_2Cl_2 and Cu_2ClO bridging subunits, and the magnetic susceptibility measurements

revealed a ferromagnetic behaviour coupled with an intercluster antiferromagnetic interaction. This was explained on the basis of the intermolecular interactions in the tetramer, which saturate into spin-aligned $S=1/2$ states at low temperature. In the second compound **B**, the intradimer Cu1 – Cu2 couplings are not observed since one of the Cu(II) atoms of the dimer retains a paramagnetic character at low temperature, as evident from the experimental magnetic susceptibility values. Hence it is the intermolecular magnetic exchange interactions involving pairs of dinuclear complexes related by a centre of symmetry, which give rise to antiferromagnetic interactions with singlet-triplet splitting value of $2J = -360 \text{ cm}^{-1}$ in compound **B**. As these two complexes are of tetrameric structure, which offer diverse interaction possibilities, an effort to generalise the magnetic behaviour of the present complex cannot be unerringly carried out. However, these complexes **A** and **B** are worth mentioning here, since they are the only structural findings comparable to Cu_2DCl_3 so far.

3.2.2. $\text{Cu}_2(\text{L}^1)_2\text{Br}_2 \cdot 7\text{H}_2\text{O}$

Although no crystal structure evidence was obtained for the dimeric nature of the compound **3**, the room temperature magnetic moment values are appreciably reduced from the spin-only values, which suggest possible antiferromagnetic exchange interactions in the compound. The magnetic parameters are then fitted into the modified Bleaney-Bowers equation, which further supports the assignment of antiferromagnetic nature to complex **2**, with the best fit values of $2J = -148 \text{ cm}^{-1}$, $g = 2.142$, $N\mu = -40 \times 10^{-6} \text{ emu}$ and ρ (impurity factor) = 0.0365 with $R \left\{ \frac{\sum (\chi_{\text{calc}} - \chi_{\text{obs}})^2}{\sum \chi_{\text{obs}}^2} \right\} = 5.3 \times 10^{-4}$. The magnetic susceptibility data collected at various temperatures between 80 and 278 K are plotted in Fig. 3.20 together with the theoretical best fit.

The antiferromagnetism in compound **3** may arise either due to the intramolecular Cu – Cu interaction or due to the intermolecular interaction between copper centres in the lattice. As there is no crystal structure support for the present compound, we have to look into the spectral data of **3**, where we find the IR spectrum supportive of a dimeric nature for the complex in the solid state.

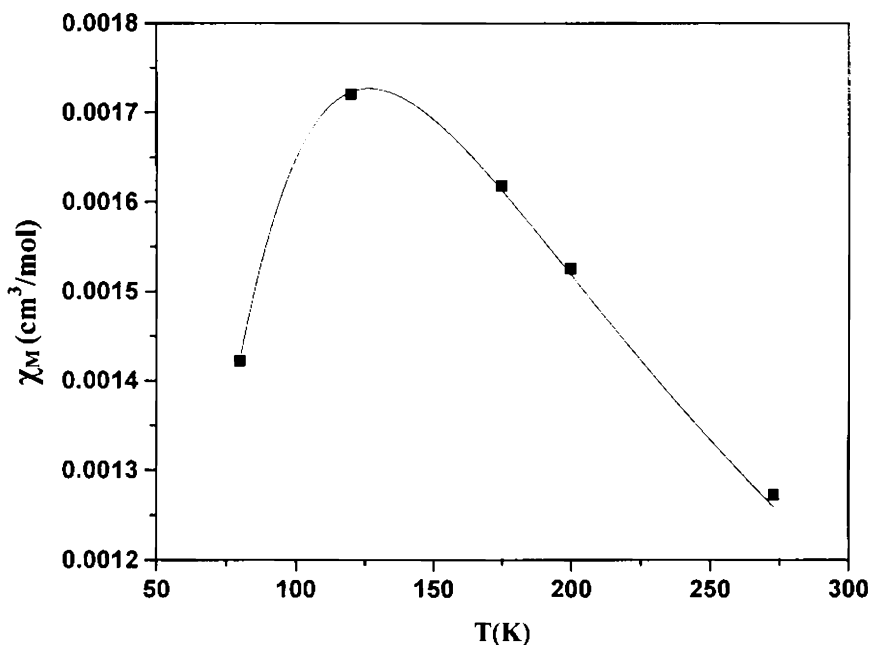


Fig. 3.20. Temperature dependence of χ_M for compound $\text{Cu}_2(\text{L}^1)_2\text{Br}_2 \cdot 7\text{H}_2\text{O}$. The squares are the experimental points and the solid line is the theoretical best fit of the experimental data

Taking into account the proposed structure (Fig. 3.17), where bridging through the non-coordinated pyridyl nitrogen is suggested, the moderately strong antiferromagnetic behaviour of the complex can be accounted. The structure points towards possible intra-dimer spin exchange interactions in the molecule, giving rise to reduced magnetic moments per copper ion. The proposed bridged structure also provides reasons for the weaker antiferromagnetic interactions in compound **3** when compared to that of compound **1**. The super-exchange mechanism is not effective in compound **3**, since the bridging nitrogen here is the part of a pyridyl ring. Unlike in the case of Cu–O–Cu or Cu–N–Cu bridges, where the super-exchange pathway is provided by the metal orbitals containing the unpaired electron and the filled p-orbital of the bridging ligand atom, here the electron density on the non-hybridised p-orbital of the bridging nitrogen atom is delocalized over the pyridyl ring. Also, the Cu–Cu

distance in compounds of similar structures are observed to be 5.307 [53] and 5.297 [54], which are higher than the separation between the two Cu(II) nuclei in compound 1. In addition to these, the strong ligand field effect of the bulky pyridyl groups plays the major role in quenching the spin-spin exchange interactions between the copper centres in compound 3.

3.2.3. CuL^1N_3

The situation is different in CuL^1N_3 , where the experimental magnetic susceptibility values (Fig.3.21) showed no regular gradation with temperature. However, at low temperatures, the curve shows characteristics similar to antiferromagnetic exchanges. Efforts were carried out to fit the experimental values to theoretical values of Curie-Weiss equation, which turned out unsuccessful. The values did not fit to a theoretical curve and returned subnormal g values of the order of 1.4. Hence it can be concluded that the compound CuL^1N_3 is magnetically dilute. The compound is, however paramagnetic, showing irregular magnetic moments with the variation of temperature, due to which it does not obey the Curie-Weiss law.

The inconsistent magnetic behaviour can be attributed to a possible equilibrium between the two spin states in the molecule. According to Orgel, in the vicinity of that interval within which the pairing energy is comparable to the excess stabilisation energy of the spin-paired state, the two spin states are expected to coexist [55,56]. This is a commonly observed phenomenon in Ni(II) complexes [57,58], where some amount of paramagnetic behaviour is observed at low temperatures in d^8 nickel complexes, which is explained to be due to an equilibrium between the singlet-triplet states. However, in the present case, additive contributions to the magnetic moments of the compound may result due to the square planar nature of the compound since the Cu(II) ion exists in a weak tetragonal field, where a possible spin-state equilibrium can be suggested. The magnetic property is then determined by the thermal population of the two spin states, $S = 0$ and $S = 1$. However, if there were a fixed mixture of the two spin states, a linear Curie-Weiss plot would have been obtained. But if the spin-state

equilibrium is temperature dependent, the composition of the mixture will change with a change in temperature, and the Curie-Weiss plot will be non-linear, as in the present case.

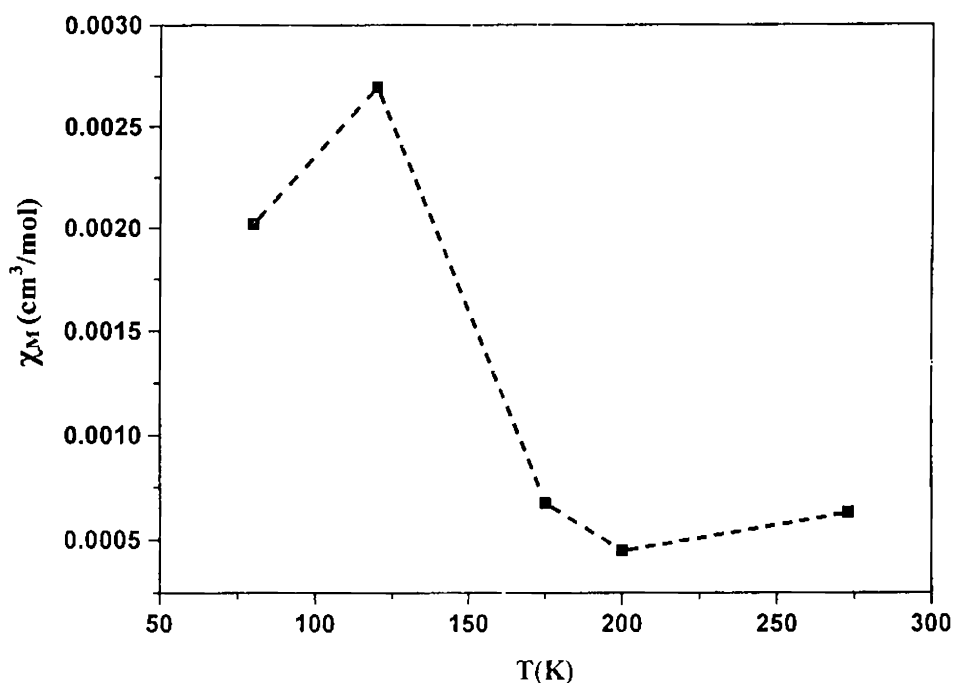


Fig. 3.21. Temperature dependence of χ_M for compound CuL^1N_3

A second reason for the unusual magnetic behaviour may be the presence of magnetically non-equivalent sites in the unit cell. In a unit cell, the metal ions may have the same coordination number and the same set of ligands with different geometries. There is also possibility that the metal ions in the entire lattice may have different coordination numbers and consequently different geometries, and the strength of some weak interatomic contacts can be temperature-dependent. The anomalous magnetic moments observed in the present compound CuL^1N_3 can thus be accounted to a total contribution of these effects.

3.2.4. $\text{Cu}_2(\text{L}^1)_2(\text{SCN})_2 \cdot 4\text{H}_2\text{O}$, $\text{Cu}(\text{L}^3)_2 \cdot 4\text{H}_2\text{O}$, $\text{CuL}^3\text{Cl} \cdot 5\text{H}_2\text{O}$ and $\text{Cu}_2(\text{L}^3)_2(\text{N}_3)_2 \cdot 2\text{H}_2\text{O}$

The compounds 4, 6, 7 and 8 reveal another special case, since the magnetic susceptibility measurements assign a diamagnetic nature for the complexes, whereas the EPR studies revealed the presence of a paramagnetic Cu(II) ion. This rare phenomenon can be accounted as follows. The observed magnetic susceptibility is the sum of the diamagnetic and paramagnetic contributions from the ligands and the central metal ion in a metal complex. Also, the paramagnetic terms may be the sum of effects due to several species or due to the same species in non-equivalent positions in a crystal lattice. Sometimes, the diamagnetic influence of the ligand fields can be considerably enhanced by the resonance effects so that the assumptions made on the diamagnetic corrections may go wrong [59]. Each type of centre in resonance will show its own characteristic moment independent of the presence of paramagnetic impurities. This is particularly true with compound $\text{Cu}(\text{L}^3)_2 \cdot 4\text{H}_2\text{O}$, since the compound is assigned a distorted octahedral structure with two bulky ligands of high field strength. However, the presence of a paramagnetic substance, even in amounts approaching 10^{-11} moles, will show its positive evidence as an absorption line or its derivative in EPR. The susceptibility measurements actually give only an effective magnetic moment of the compound in a lattice, whereas the electron paramagnetic resonance absorptions allows the 'g' to be calculated unequivocally, a value characteristic of the geometry of the molecule. Accordingly, as far as the stereochemistry of a compound is concerned, the EPR turns out to be a better tool when compared to the magnetic susceptibility measurements.

3.2.5. $\text{Cu}_2(\text{L}^1)_2(\text{SO}_4) \cdot 1.5 \text{H}_2\text{O}$

In the case of compound 5, the complex is found to be diamagnetic and EPR silent. This is contrary to the expectations, since a sulfate bridging is postulated based on IR analyses. Had the compound were EPR active, in spite of being diamagnetic, it could have been assumed that it is magnetically dilute, i.e., there is no secondary magnetic interaction between the neighbouring molecules as in the case of complexes

mentioned just above. However, here the compound is EPR silent also, which provides support for the magnetically concentrated nature of the complex. Thus, the magnetic behaviour can be accounted on the basis of the proposed bridged structure for the compound, where the bridging sulfate group, with available filled p -orbitals on the atoms, can effectively carry out an exchange-coupled spin-pairing between two adjacent Cu(II) nuclei in a magnetically concentrated system, through super-exchange pathways. A complete coupling of the spins can give rise to an effective anti-ferromagnetic interaction, leading to a diamagnetic ground state. This is similar to the effect observed in bis(diazoaminobenzenato)copper(II) complex, where the diazoaminobenzene functions as a bridging ligand. Another example is the ligand arylazooxime, $C_6H_5N=NC(R)=NO$, which reacts with copper(II) to give the dimeric bis(arylazooximato)copper(II) complex, which is diamagnetic.

Thus, it can be inferred that the Cu(II) complexes of di-2-pyridyl ketone thiosemicarbazones reveal a variety of magnetic behaviour, some of them being strongly antiferromagnetic. No ferromagnetic interactions were encountered in the present complexes, which may be attributed to their structural features. The bridging structure most commonly observed in these complexes gives way to strong super-exchange mechanistic attributes, resulting in the reversal of spins in neighbouring Cu(II) nuclei, thus giving rise to antiferromagnetic interactions. The diamagnetic nature of some bridged complexes is also assigned to their structure, where a complete spin-reversal by antiferromagnetic interactions can give rise to spin-pairing. One of the compounds, CuL^1N_3 turned out to be paramagnetic, however, some antiferromagnetic-like variation in its molar magnetic susceptibilities is observed with temperature. Chances are there, that the potential anti-ferromagnetic interactions in CuL^1N_3 are being suppressed by some paramagnetic impurities in the lattice. A possible prediction can thus be suggested, based on these observations that the magnetic exchange interactions in Cu(II) complexes of di-2-pyridyl ketone thiosemicarbazones turn out mostly antiferromagnetic in nature. Since there are no previous reports available for generalisation, only future experiments with similar compounds can substantiate this prediction. However, when considering the prevalent

bridged nature of these compounds, which is well-established in literature [53], the prediction of predominant antiferromagnetic exchange interactions in di-2-pyridyl ketone thiosemicarbazone complexes of Cu(II) turns out to be quite relevant.

3.3. Experimental

Materials

Di-2-pyridyl ketone (Fluka), Cu(OAc)₂·H₂O (Qualigens), CuSO₄·5H₂O (Merck), CuBr₂ (Merck), CuCl₂·2H₂O (Merck), NaN₃ (Reidel-De Haen), KSCN (BDH) and methanol (Ranchem) were used as received. When ethyl alcohol was used as the solvent, repeated distillation was carried out to ensure purity.

Synthesis of ligands

The ligands used were HL¹ and HL³, and their preparations were done as described previously in Chapter 2.

Preparation of complexes

Cu₂^I·Cl₃ (1): Ethanolic solutions of HL¹ (0.317 g, 1 mmol) and CuCl₂·2H₂O (0.171 g, 1 mmol) were mixed and heated under reflux for four hours. Room temperature slow evaporation yielded blue crystalline complex, **1**, which was separated, washed with a small amount of cold dilute ethanol followed by ether and dried over P₄O₁₀ *in vacuo*. Single crystals suitable for X-ray diffraction were grown by room temperature slow evaporation of an ethanolic solution of the complex. Yield: 0.27 g (55%). Elemental Anal. Found (Calc.): C, 44.84 (44.60); H, 3.48 (3.19); N, 14.24 (13.49)%.

CuL¹N₃ (2): To ethanolic solution of HL¹ (0.317 g, 1 mmol), 1 mmol of Cu(OAc)₂·H₂O (0.199 g) dissolved in ethanol (10 ml) was added and refluxed. Aqueous solution of NaN₃ (0.0651 g, 1 mmol) was then added to the solution followed

by a further refluxing for three hours. Olive green product separated out was collected, washed with ether and dried *in vacuo*. Yield: 0.34 g (59%). Elemental Anal. Found (Calc.): C, 49.39 (49.36); H, 2.44 (3.22); N, 25.26 (25.58)%.

Cu₂(L¹)₂Br₂·7H₂O (3) : Ethanolic solutions of HL¹ (0.317 g, 1 mmol) and CuBr₂ (0.223 g, 1 mmol) were mixed and refluxed continuously for four hours. Light green product was separated out, which was collected, washed with dilute ethanol followed by ether and dried *in vacuo*. Yield: 0.33 g (61%). Elemental Anal. Found (Calc.): C, 39.14 (40.12); H, 3.15 (3.93); N, 12.82 (13.00)%.

Cu₂(L¹)₂(SCN)₂·4H₂O (4): Cu(OAc)₂·H₂O (0.199 g, 1 mmol) dissolved in ethanol (10 ml) was added to HL¹ (0.317 g, 1 mmol) under hot conditions. KSCN (0.097 g, 1 mmol) was then added to the solution and refluxed for three hours. Olive green product separated out was collected, washed with ether and dried *in vacuo*. Yield: 0.40 g (65%). Elemental Anal. Found (Calc.): C, 47.66 (46.57); H, 3.66 (3.70); N, 16.42 (17.15)%.

Cu₂(L¹)₂SO₄·1.5H₂O (5): HL¹ (0.317 g, 1 mmol) was dissolved in ethanol (15 ml) and refluxed with a solution of CuSO₄·5H₂O (0.249 g, 1 mmol) in 10 ml of water. Dark green crystal separated out, which was filtered and washed with ether and dried over P₄O₁₀ *in vacuo*. Yield: 0.39 g (68%). Elemental Anal. Found (Calc.): C, 47.69 (47.26); H, 4.05 (3.41); N, 14.54 (15.31)%.

Cu(L³)₂·4H₂O (6): CuBr₂ (0.223 g, 1 mmol) in ethanol was mixed with an ethanolic solution of HL³ (0.323 g, 1 mmol) and heated under reflux for four hours. The solution was then cooled at room temperature and left overnight. Green product of complex, 6 was then formed, which were separated, washed with ether and dried over P₄O₁₀ *in vacuo*. Yield: 0.29 g (52%). Elemental Anal. Found (Calc.): C, 52.94 (53.22); H, 5.80 (5.95); N, 17.02 (17.24)%.

CuL³Cl·5H₂O (7): A solution of CuCl₂·2H₂O (0.171 g, 1 mmol) in 10 ml of water was added to HL³ (0.323 g, 1 mmol) and refluxed for three hours. The resulting green precipitate was washed with water followed by ether and dried over P₄O₁₀ *in vacuo*. Yield: 0.28 g (56%). Elemental Anal. Found (Calc.): C, 40.32 (40.98); H, 5.36 (5.73); N, 12.50 (13.28)%.

Cu₂(L³)₂(N₃)₂·2H₂O (8): Ethanolic solutions of HL³ (0.323 g, 1 mmol), and Cu(OAc)₂·H₂O (0.199 g, 1 mmol) dissolved in ethanol (10 ml) was added and refluxed for the preparation of compound 8. Aqueous solution of NaN₃ (0.0651 g, 1 mmol) was then added to the solution followed by a further refluxing for three hours. Olive green product separated out was collected, washed with ether and dried *in vacuo*. Yield: 0.26 g (45%). Elemental Anal. Found (Calc.): C, 44.96 (45.04); H, 4.20 (5.04); N, 23.22 (23.34)%.

Table 3.1. Crystal data and structure refinement for Cu₂ Cl₃

Parameters	Cu ₂ Cl ₃
Empirical Formula	C ₂₇ H ₂₃ Cl ₃ Cu ₂ N ₇ OS
Formula weight (M)	727.01
Temperature (T) K	293(2)
Wavelength (Mo K α) (Å)	0.71073
Crystal system	Monoclinic
Space group	<i>P</i> 2 ₁ / <i>c</i>
Lattice constants	
<i>a</i> (Å)	11.023(7)
<i>b</i> (Å)	24.552(14)
<i>c</i> (Å)	12.140(7)
α (°)	90
β (°)	113.161(8)
γ (°)	90
Volume <i>V</i> (Å ³)	3021(3)
<i>Z</i>	4
Calculated density (ρ) (Mg m ⁻³)	1.599
Absorption coefficient (μ) (mm ⁻¹)	1.777
<i>F</i> (000)	1468
Crystal size (mm)	0.30 x 0.21 x 0.06
θ Range for data collection	1.66-27.26
Limiting Indices	-14 $\leq h \leq$ 13, -30 $\leq k \leq$ 28, -15 $\leq l \leq$ 15
Reflections collected	23405
Unique Reflections	6246 [<i>R</i> _{int} = 0.0235]
Completeness to θ	26.26 (100 %)
Absorption correction	Multi-Scan
Maximum and minimum transmission	0.9086 and 0.6159
Data / restraints / parameters	6246/0/442
Goodness-of-fit on <i>F</i> ²	1.075
Final <i>R</i> indices [<i>I</i> > 2 σ (<i>I</i>)]	<i>R</i> ₁ = 0.0372, <i>wR</i> ₂ = 0.1013
<i>R</i> indices (all data)	<i>R</i> ₁ = 0.0492, <i>wR</i> ₂ = 0.1079
Largest difference peak and hole (e Å ⁻³)	0.823 and -0.338

Table 3.2. Selected bond lengths (Å) and bond angles (°) of Cu_2TdCl_3

	Cu_2TdCl_3
Cu1-Cu2	2.9591(13)
Cu1-Cl1	2.2724(12)
Cu1-Cl3	2.5740(13)
Cu1-N1	1.997(3)
Cu1-N3	1.979(2)
Cu1-N4	2.028(3)
Cu2-Cl2	2.2423(16)
Cu2-Cl3	2.5347(17)
Cu2-N2	2.011(3)
Cu2-N3	1.980(2)
Cu2-N5	2.046(3)
N4-N5	1.404(3)
N4-C14	1.302(4)
S1-C14	1.742(3)
S1-C21	1.743(3)
N5-C21	1.306(4)
N6-C14	1.365(4)
N3-C6	1.382(4)
N7-C21	1.344(4)
N7-C22	1.435(4)
C6-O1	1.426(4)
C6-C5	1.557(4)
C6-C7	1.527(4)
Cu1-Cl3-Cu2	70.79(3)
N1-Cu1-N3	81.93(9)
N1-Cu1-Cl1	95.97(8)
N3-Cu1-N4	82.73(9)
Cl1-Cu1-N4	97.29(8)
Cl2-Cu2-N2	96.10(8)
N2-Cu2-N3	81.49(9)
N3-Cu2-N5	82.54(9)
N3-C6-O1	112.1(2)
N3-C6-C7	110.1(2)
N4-N5-C21	112.7(2)
Cl2-Cu2-N5	95.79(7)
C14-S1-C21	87.13(15)
C14-N4-N5	112.3(2)
C15-N6-C14	122.9(3)
C22-N7-C21	123.6(3)

Table 3.3. Magnetic parameters from the EPR spectra of complexes

Compound	g_1	g_2	g_3	g_{\parallel}	g_{\perp}	g_{av}	A_{xz}	A_{yz}	A_{zz}	A_{\parallel}	A_{\perp}	A_{av}
1 (298 K, powder)	2.174	2.073	2.041			2.096						
1 (77 K, DMF)	2.221	2.115	2.079			2.138	48.5	59.6	133.9			80.67
2 (77 K, DMF)				2.162	2.084	2.110				173.6	43.3	86.75
3 (298 K, powder)	2.148	2.079	2.029			2.085						
3 (77 K, DMF)	2.173	2.082	2.073			2.109	19.05	45.5	179.88			81.48
4 (298 K, powder)	2.178	2.081	2.034			2.111						
4 (77 K, DMF)	2.287	2.072	2.029			2.129	17.3	76.8	189.2			94.4
6 (77 K, DMSO)	2.165	2.052	2.041			2.086	19.0	96.4	187.4			100.93
8 (77 K, DMF)				2.173	2.053	2.093				193.3	5.05	67.8

References

1. E. Coronado, M. Clemente-Leon, J. R. Galan-Mascaros, C. Gimenez-Saiz, C. J. Gomez-Garcia, E. Martinez-Ferrero, *J. Chem. Soc., Dalton Trans.* (2000) 3955.
2. M. Faraday, *Phil. Trans. R. Soc. Lond.* 122 (1832) 125.
3. P. Day, A. E. Underhill *in* Metal Organic and Organic Molecular Magnets, P. Day and A. E. Underhill Eds., Royal Society of Chemistry, Cambridge, 1999.
4. F. A. Cotton, G. Wilkinson, *Advanced Inorganic Chemistry*, 5th ed., John Wiley & Sons, Inc., New York, 1988.
5. B. J. Hathaway, *J. Chem. Soc., Dalton Trans.* (1972) 1196.
6. L. Somogyi, *Liebigs Ann. Chem.* (1991) 1267.
7. R. Milcent, T. -H. Nguyen, *J. Heterocyclic Chem.* 23 (1986) 881.
8. J. S. Casa, M. V. Castano, E. E. Castellano, J. Ellena, M. S. Garcia-Tasende, A. Gato, A. Sanchez, L. M. Sanjuan, J. Sordo, *Inorg. Chem.* 41 (2002) 1150.
9. S. Kubota, K. Fujikane, M. Uda, T. Yoshika, *Heterocycles* 4 (1976) 1909.
10. S. Kubota, Y. Ueda, K. Fujikane, T. Toyooka, M. Shibuya, *J. Org. Chem.* 45 (1980) 1473.
11. S. Andreae, E. Schimitz, H. Seeboth, *J. Prakt. Chem.* 328 (1986) 205.
12. L. Somogyi, *Tetrahedron* 47 (1991) 9305.
13. L. Somogyi, *Carbohydr. Res.* 75 (1979) 325.
14. K. Toyooka, Y. Takeuchi, Z. Taira, S. Kubota, *Heterocycles* 29 (1989) 1233.
15. S. Andreae, E. Schmitz, *Z. Chem.* 23 (1983) 450.
16. Shamsuzzaman, M. Aslam, A. Salim, *J. Chem. Research (S)* (1998) 824.
17. J. P. Kilburn, J. Lau, R.C.F. Jones, *Tetrahedron Letters* 44 (2003) 7825.
18. P. Gomez-Saiz, J. Garcia-Tojal, M. A. Maestro, J. Mahia, F. J. Arnaiz, L. Lezama, T. Rojo, *Eur. J. Inorg. Chem.* (2003) 2639.
19. G. Werber, F. Buccheri, M. Gentile, L. Librici, *J. Heterocycl. Chem.* 14 (1977) 853.
20. U. Schroder, R. Richter, J. Hartung, U. Abram, L. Beyer, *Z. Naturforsch., Teil B*, 30 (1997) 620.

-
21. I. G. Santos, A. Hagenbach, U. Abram, Dalton Trans. (2004) 677.
 22. D. X. West, A. A. Nassar, F. A. El-Saied, M. I. Ayad, Transition Met. Chem. 23 (1998) 321.
 23. M. Maji, M. Chatterjee, S. Ghosh, S. K. Chattopadhyay, B. –M. Wu, T. C. W. Mak, J. Chem. Soc., Dalton Trans. (1999) 135.
 24. J. R. Dilworth, J. S. Lewis, J. R. Miller, Y. Zheng, J. Chem. Soc., Dalton Trans. (1995) 1357.
 25. A. R. Cowley, J. R. Dilworth, P. S. Donnelly, J. Woollard –Shore, Dalton Trans. (2003) 748.
 26. F. Mevellec, N. Lepareur, A. Roucoux, N. Noiret, H. Patin, G. Bandoli, M. Porchia, F. Tisato, Inorg. Chem. 41 (2002) 1591.
 27. J. E. Huheey, E. A. Keiter, R. L. Keiter, Inorganic Chemistry, Principles of Structure and Reactivity, 4th ed., Harper Collins College Publishers, New York, 1993.
 28. A. W. Addison, T. N. Rao, J. Reedijk, J. Chem. Soc., Dalton Trans. (1984) 1349.
 29. B. J. Hathaway, Coord. Chem. Rev. 53 (1983) 87.
 30. B. J. Hathaway, D. E. Billing, Coord. Chem. Rev. 5 (1970) 143.
 31. M. Mohan, P. Sharma, Inorg. Chim. Acta 106 (1985) 197.
 32. P. Bindu, M. R. P. Kurup, Transition Met. Chem. 22 (1997) 578.
 33. M. A. Ali, A. H. Mirza, M. Nazimuddin, H. Rahman, R. J. Butcher, Transition Met. Chem. 27 (2002) 268.
 34. A. B. P. Lever, Inorganic Electronic Spectroscopy, 2nd ed., Elsevier Science Publishers B. V., Netherlands, 1984.
 35. R. Pogni, M. C. Baratto, A. Diaz, R. Basosi, J. Inorg. Biochem. 79 (2000) 333.
 36. A. Fragoso, M. C. Baratto, A. Diaz, Y. Rodriguez, R. Pogni, R. Basosi, R. Cao, Dalton Trans. (2004) 1456.
 37. A. H. Maki, B. R. McGarvey, J. Chem. Phys. 29 (1958) 31.
 38. A. Rockenbauer, J. Magn. Reson. 35 (1979) 429.
 39. J. Jezierska, B. Jezowska-Trzebiatowska, G. Petrova, Inorg. Chim. Acta 50 (1981) 153.

40. K. Nakamoto *in* Infrared and Raman Spectra of Inorganic and Coordination Compounds, 4th ed., John Wiley & Sons, New York, 1986.
41. A. Turco, C. Pecile, *Nature* 191 (1961) 66.
42. J. Lewis, R. S. Nyholm, P. W. Smith, *J. Chem. Soc.* (1961) 4590.
43. A. Sabatini, I. Bertini, *Inorg. Chem.* 4 (1965) 959.
44. S. Ahrland, J. Chatt, N. R. Davies, *Quart. Rev.* 12 (1958) 265.
45. M. A. Halcrow, *Dalton Trans.* (2003) 4375.
46. R. M. Silverstein, G. C. Bassler, T. C. Morrill, *Spectrometric Identification of Organic Compounds*, 4th ed., John Wiley & Sons, New York, 1981.
47. K. J. Tubbs, A. L. Fuller, B. Benette, A. M. Arif, M. M. Makowska-Grzyska, L. M. Berreau, *Dalton Trans.* (2003) 3111.
48. O. Kahn, J. Larionova, J. V. Yakhmi, *Chem. Eur. J.* 1999, 5, 3443.
49. S. F. A. Kettle, *Coordination Compounds*, ELBS, Great Britain, 1975.
50. O. Kahn, *Molecular Magnetism*, VCH: Weinheim, Germany, 1993.
51. F. Bentiss, M. Lagrenee, O. Mentre, P. Conflant, H. Vezin, J. P. Wignacourt, E. M. Holt, *Inorg. Chem.* 43 (2004) 1865.
52. A. N. Papadopoulos, V. Tangoulis, C. P. Raptopoulou, A. Terzis, D. P. Kessissoglou, *Inorg. Chem.* 35 (1996) 559.
53. V. Philip, V. Suni, M. R. P. Kurup, M. Nethaji, *Polyhedron* 24 (2005) 1133.
54. V. Philip, V. Suni, M. R. P. Kurup, M. Nethaji, unpublished results.
55. R. C. Stouffer, D. H. Busch, W. B. Hadley, *J. Am. Chem. Soc.* 83 (1961) 3732.
56. L. E. Orgel, *J. Chem. Phys.*, 23 (1955) 1810.
57. S. L. Holt (Jr.), R. J. Bouchard, R. L. Carlin, *J. Am. Chem. Soc.* 86 (1964) 519.
58. S. C. Nyburg, J. S. Wood, *Inorg. Chem.* 3 (1964) 468.
59. J. E. Wertz, *Chem. Rev.* 55 (1955) 829.



CHAPTER 4

Syntheses, structural, EPR and magnetic studies of Mn(II) and VO(IV) complexes of di-2-pyridyl ketone *N*(4)-substituted thiosemicarbazones

Manganese coordination chemistry with a diverse range of ligands has much relevance in biological systems with a number of model manganese complexes. There are also fascinating cluster compounds, which exhibit unusual magnetic properties, and elegant supramolecular arrays. For instance, the Mn^{2+} complexes of benzimidazolyl derivatives are reported to exhibit superoxide dismutase activity [1]. Manganese coordination compounds are also of growing importance as homogeneous catalysts in oxidation reactions [2-5]. The manganese porphyrins are very efficient catalysts for fractionalization of hydrocarbons in processes that involve high valent intermediates [6-8]. Manganese is identified in metalloenzymes such as oxygen evolving centre of photosystem-II, catalases and superoxide dismutases [9-13]. Manganese complexes are also studied for their magnetic behavior. Cubane like Mn(II) complexes of di-2-pyridyl ketone in the gem-diol form are reported with single crystal X-ray structural analyses, and this complex is observed to be antiferromagnetic [14]. However, there are only few reports on manganese complexes of thiosemicarbazones [15-20], and there is only one report with a di-2-pyridyl ketone thiosemicarbazone [21]. Surprisingly, the magnetic behavior of these manganese complexes are never studied in these reports and here we attempt to find out the magnetic behavior of some of the Mn(II) complexes synthesized from di-2-pyridyl ketone thiosemicarbazones.

Oxovanadium complexes with vanadium in the oxidation state IV are reported to have insulin mimetic effects in animal model systems in the treatment for diabetes [22-25]. However, there are only few reports on VO(IV) complexes of thiosemicarbazones [26]. Most of the vanadyl complexes of thiosemicarbazones are compounds of dioxovanadium(V) [27, 28]. Although VO(IV) thiosemicarbazone complexes are widely studied for their biological applications [26], their magnetic properties are least explored. Hence an investigation into the magnetic attributes of some newly synthesized VO(IV) complexes also is attempted here.

4.1. Stereochemistry of the complexes

The electronic structure of manganese reveals that it can have a maximum oxidation state of +7. However, the manganese complexes under the present study exist in the +2 oxidation state. The characteristic coordination number of Mn(II) is six in the present complexes, which corresponds to octahedral stereochemistry.

4.1.1. $\text{Mn}(\text{L}^1)_2 \cdot \text{H}_2\text{O}$ (9)

We could successfully isolate a single crystal suitable for X-ray diffraction for the compound, which revealed a distorted octahedral structure. Other major tools used for the characterisation include IR, electronic and EPR spectra.

Crystal studies

A single crystal suitable for X-ray diffraction was isolated by the slow evaporation of a solution of the compound in a 1:1:2 mixture of DMF, CH_2Cl_2 and acetone. There are two crystallographically independent molecules in the asymmetric unit of the compound (Fig. 4. 1).

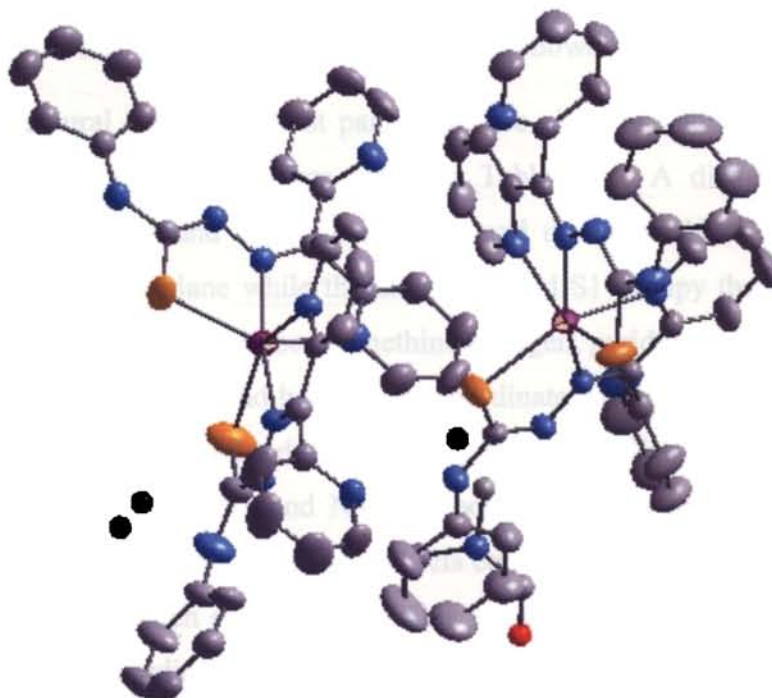


Fig. 4.1. Molecular structure of the compound $\text{Mn}(\text{L}^1)_2 \cdot 1.5(\text{H}_2\text{O}) \cdot 0.5(\text{DMF})$
Hydrogen atoms are omitted for clarity

There are four solvent molecules in the lattice, *viz*, three water molecules and one DMF molecule. The molecular structure of the compound with the atom numbering scheme is given in Fig. 4.2.

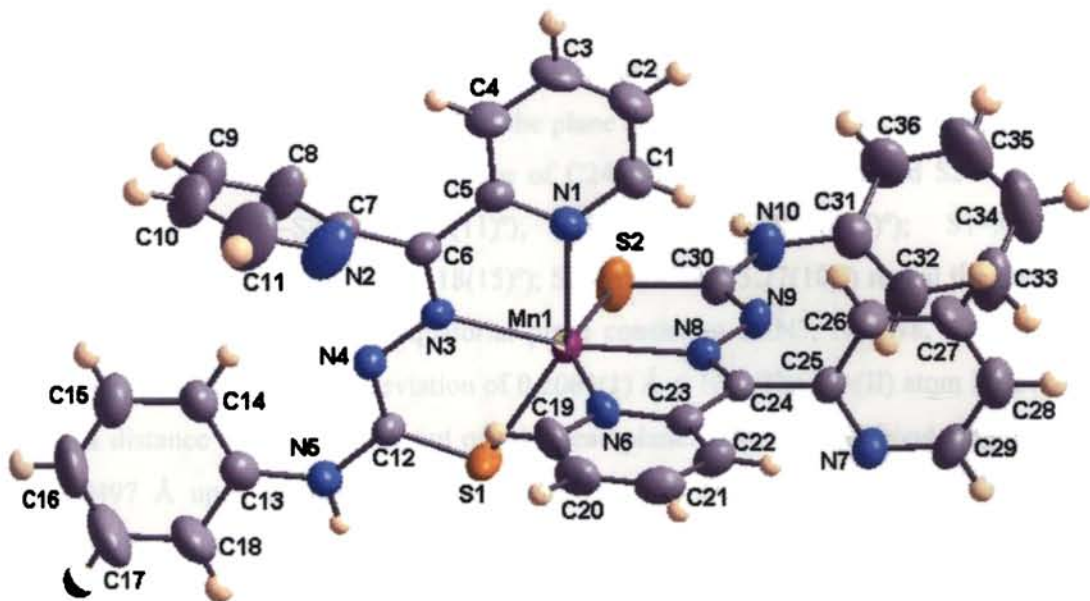


Fig. 4. 2. Molecular structure of one independent molecule $Mn(L^1)_2$ in the unit cell with the atom numbering scheme. The ellipsoids are shown with 50% probability.

The structural data refinement parameters are given in Table 4.1 and selected bond distances and bond angles are given in Table 4.2. A distorted octahedral geometry is observed around each metal center and the atoms N3, N6, N8 and S2 constitute the equatorial plane while the atoms N1 and S1 occupy the axial position. The coordination occurs through the azomethine nitrogen, pyridyl nitrogen and thiolate sulfur of two ligand moieties and hence a six-coordinate environment is present about the metal center. The thiosemicarbazone moiety in the free ligand [29] shows an *ZE* conformation about the C6–N3 and N4–C12 bonds, whereas in the present Mn(II) complex, it reveals an *ZZ* conformation with *cis* configurations about both the C6–N3 and N4–C12 bonds, which suggests a possible rotation occurs about the azomethine double bond during coordination. The S1–C12–N4–N3 torsion angle value of $-3.0(6)^\circ$ also evidences that the thiocarbonyl S1 atom is positioned *cis* to the hydrazinic N3 atom. *ZZ* conformation is rarely observed in complexes of di-2-pyridyl ketone derivatives of mono substituted thiosemicarbazones. Earlier, similar *ZZ* conformations

were reported, when the *N*(4) position is either disubstituted [30] or when it is part of a ring system [31, 32]. An *ZE* conformation is observed for unsubstituted or monosubstituted 2-dipyridyl ketone thiosemicarbazones [33].

The molecule consists of two main fragments, *viz.*, two thiosemicarbazone ligand moieties, and it is interesting to note that the two ligand moieties are arranged in such a way that they are almost perpendicular to each other, as revealed from the dihedral angle value of $89.38(0)^\circ$ of the plane defined by atoms C6, N3, N4, C12, N5 and S1 with the corresponding plane of C24, N8, N9, C30, N10 and S2. The bite angles N3–Mn1–S2 ($115.34(11)^\circ$); N1–Mn1–N3 ($71.30(15)^\circ$); S1–Mn1–N3 ($75.88(10)^\circ$); N6–Mn1–N8 ($71.18(15)^\circ$); S2–Mn1–N8 ($75.77(10)^\circ$) reveal the distorted octahedral geometry. The equatorial plane consisting of N3, N6, N8, S2 and Mn1 shows a maximum mean deviation of $0.2063(1) \text{ \AA}$ at N8. The Mn(II) atom is deviated at a distance of $0.1602(1) \text{ \AA}$ out of this mean plane. The C12–S1 bond lengthens by 0.0497 \AA upon coordination to the Mn(II). The free ligand exists as the thione tautomer, and it coordinates to Mn(II) in the deprotonated thiolate form, thus rendering a single bond character for the C–S bond. Similarly, the coordination of azomethine nitrogen to central Mn(II) atom results in a redistribution in the electron density along the thiosemicarbazone chain, giving rise to changes in the bond distances along the moiety when compared to that of the uncoordinated thiosemicarbazone. For instance, the azomethine bond distance is increased by 0.0112 \AA and the N3–N4 bond distance is increased by 0.0207 \AA while the N4–C12 bond distance is decreased by 0.0346 \AA in compound **9** from the corresponding values of the free ligand. The bonding parameters in the second individual molecule are also similar.

The packing of the molecules of **9** is shown in Fig. 4.3., where the unit cell is viewed down the ‘a’ axis. The basic unit of the crystal packing consists of four molecules, which are two sets, each consisting of two individual molecules in the asymmetric unit. Each set of two molecules is arranged in an off-set fashion, and this whole unit of four molecules repeat one-dimensionally in the lattice. The repeating unit in the crystal lattice is shown in Fig. 4. 4. It is interesting to note that although the intermolecular $\pi - \pi$ interactions are rather weak, as they are observed at distances greater than 3.5 \AA , there are appreciable C–H $\cdots\pi$ interactions in the lattice. Some

hydrogen bonding interactions are also significant and the list of the intermolecular interactions is given in Table 4.3.

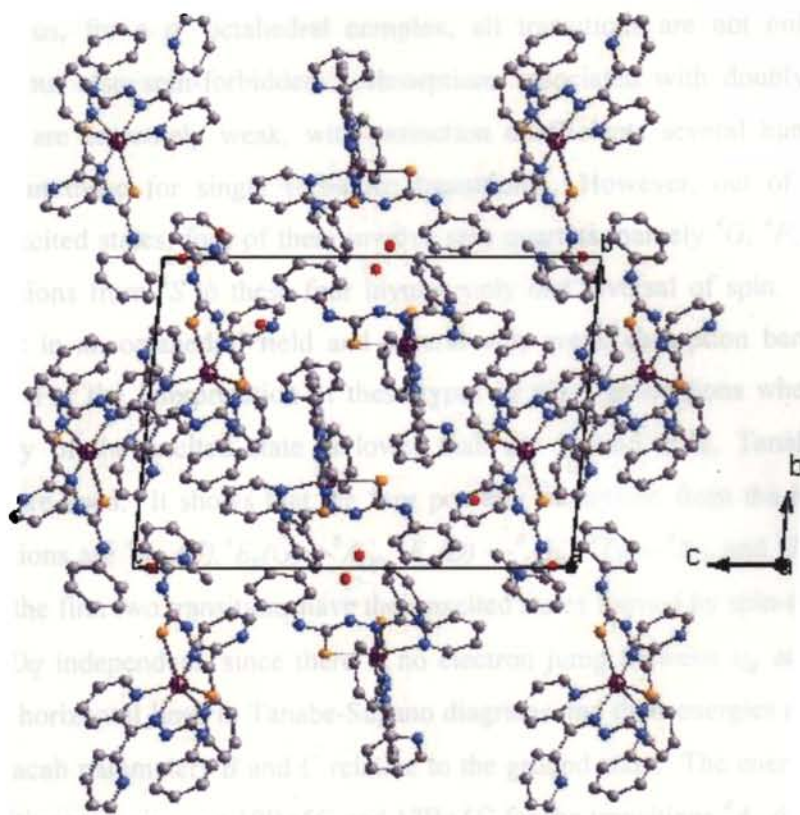


Fig. 4.3. Molecular packing diagram of $\text{Mn}(\text{L}^1)_2 \cdot 1.5(\text{H}_2\text{O})0.5(\text{DMF})$, the unit cell is viewed down the 'a' axis

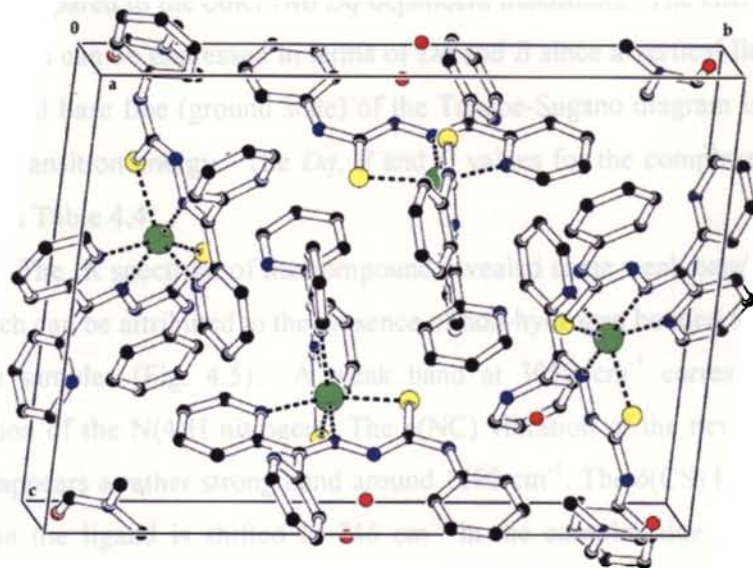


Fig. 4.4. The repeating unit in the lattice of $\text{Mn}(\text{L}^1)_2 \cdot 1.5(\text{H}_2\text{O})0.5(\text{DMF})$

Spectral studies

The high spin d^5 configuration of Mn(II) with five unpaired electrons reveals the ${}^6A_{1g}$ ground state, which is an orbital singlet with no possible spin-sextet excited states. Thus, for a d^5 octahedral complex, all transitions are not only Laporte-forbidden but also spin-forbidden. Absorptions associated with doubly forbidden transitions are extremely weak, with extinction coefficients several hundred times smaller than those for singly forbidden transitions. However, out of the eleven possible excited states, four of them involve spin quartets, namely 4G , 4F , 4D and 4P . The transitions from 6S to these four involve only one reversal of spin. These four states split in an octahedral field and several very weak absorption bands may be observed. For the interpretation of these types of weak absorptions where the spin multiplicity of the excited state is lower than the ground state, Tanabe-Sugano diagrams are used. It shows that the four possible transitions from the high-spin d^5 configurations are ${}^4A_{1g}(G), {}^4E_g(G) \leftarrow {}^6A_{1g}$, ${}^4E_g(D) \leftarrow {}^6A_{1g}$, ${}^4T_{1g} \leftarrow {}^6A_{1g}$ and ${}^4T_2(G) \leftarrow {}^6A_{1g}$. Of these, the first two transitions have their excited states formed by spin-reversal, and they are Dq independent, since there is no electron jump between t_{2g} and e_g . They appear as horizontal lines in Tanabe-Sugano diagrams and their energies are functions of only Racah parameters B and C relative to the ground state. The energies of these two transitions are given as $10B+5C$ and $17B+5C$ for the transitions ${}^4A_{1g}(G) \leftarrow {}^6A_{1g}$ and ${}^4E_g(D) \leftarrow {}^6A_{1g}$ respectively [34]. They generally appear as much sharper transitions when compared to the other two Dq dependent transitions. The energies of these latter transitions can be expressed in terms of Dq and B since a vertical line drawn from the horizontal base line (ground state) of the Tanabe-Sugano diagram is a direct measure of the transition energy. The Dq , B and C values for the complexes under study are given in Table 4.4.

The IR spectrum of the compound revealed some weak bands around 3300 cm^{-1} , which can be attributed to the presence of non-hydrogen bonded lattice water content in the samples (Fig. 4.5). A weak band at 3050 cm^{-1} corresponds to the $\nu(\text{NH})$ vibration of the N(4)H nitrogen. The $\nu(\text{NC})$ vibration of the newly formed N4=C12 bond appears a rather strong band around 1590 cm^{-1} . The $\delta(\text{CS})$ band observed at 806 cm^{-1} in the ligand is shifted to 746 cm^{-1} in the complex due to the enolization of

thiosemicarbazone moiety upon coordination. However, an interesting observation is that, the azomethine stretching vibration is very much weakened in intensity in the present Mn(II) complex. This point is noteworthy regarding the structure of the complex, which reveals that the bonding is more dominated by the thiosemicarbazone moieties around Mn(II), due to which the electron density on the coordinated azomethine bond is more delocalized towards the metal atom. The electronic spectral assignments of the compound $\text{Mn}(\text{L}^1)_2 \cdot \text{H}_2\text{O}$ are given in Table 4.4.

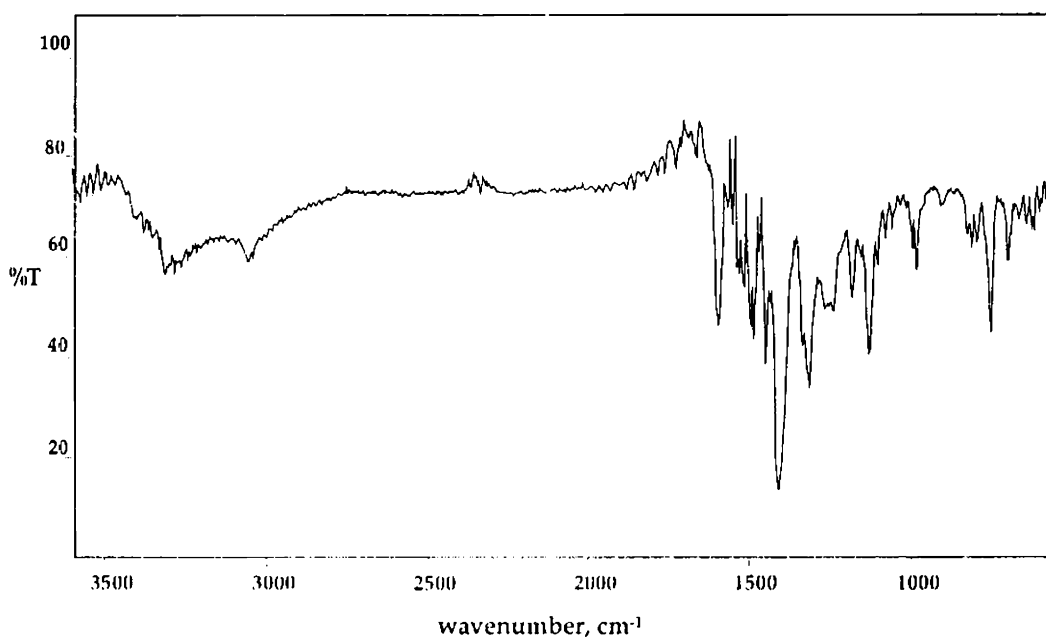


Fig. 4.5. IR spectrum of the compound $\text{Mn}(\text{L}^1)_2 \cdot \text{H}_2\text{O}$

Electron Paramagnetic Resonance studies

The spin Hamiltonian for the high spin Mn(II) is expressed as:

$$\mathcal{H} = g\beta H_s + D[S_z^2 - S(S+1)/3] + E(S_x^2 - S_y^2) \quad (4.1)$$

Where H is the magnetic field vector, D is the axial zero field splitting term, E is the rhombic zero field splitting parameter. If D and E are very small compared to $g\beta H_s$, five EPR transitions corresponding to $\Delta m_s = \pm 1$ are expected with a g value of 2.0. However, for the case where D or E is very large, the lowest doublet has

effective g values of $g_1 = 2$, $g_2 = 6$ for $D \neq 0$ and $E = 0$ but for $D = 0$ and $E \neq 0$, the middle Kramers doublet has an isotropic g value of 4.29 [35, 36].

Electron spin resonance of the compound **9** is measured in frozen solution of DMSO at 77 K (Fig. 4.6). A central hyperfine sextet corresponding to $g_{iso} = 2.021$ is observed. High spin Mn^{2+} ions with five unpaired electrons ($S=5/2$) have an orbitally non-degenerate ${}^6A_{1g}$ ground state. Hence the spin-orbit coupling is expected to be unimportant and the zero field splitting should be rather small. This is usually observed with complexes of weak field ligands, which give only one 'g' value close to 2.0023, the free electron 'g' value. However, in the present complex **9**, Mn(II) is present in a sufficiently strong ligand field of two thiosemicarbazone moieties, and distortions from the ideal octahedral geometry are observed in the crystal structure. Even then, only one resonance corresponding to $\Delta m_s = \pm 1$ is observed. This may mean that the manganese in compound **9** exists in a nearly cubic field with negligible zero field splitting, with low values of D and E , where D is the axial zero field splitting parameter and E is the rhombic zero field splitting parameter.

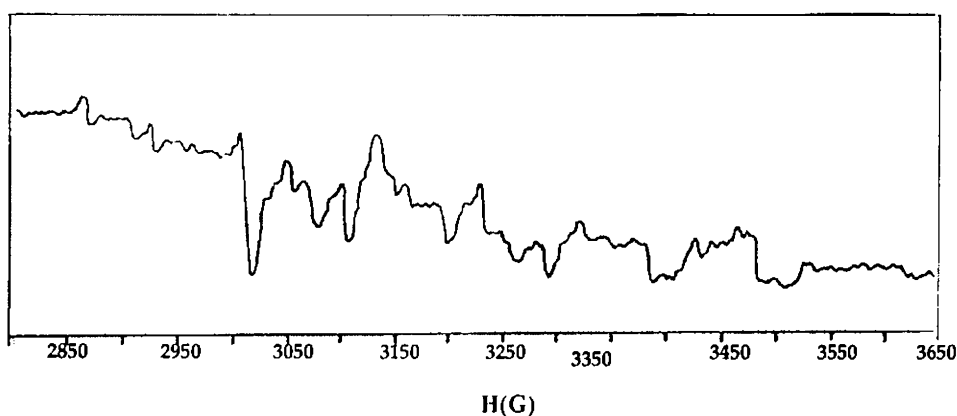


Fig. 4.6. EPR spectrum of the compound $Mn(L^1)_2 \cdot H_2O$ in DMSO at 77 K

There are some additional lines present in the central hyperfine sextet, which can be explained as follows. It is possible that ESR spectra, involving interaction with nuclei with quadrupole moments (nuclear spin $I > 1$), visualise a violation of the

selection rules. Thus in addition to the transition due to $\Delta m_s = \pm 1$, $\Delta m_l = 0$, transitions associated with $\Delta m_l \neq 0$ also occur. This effect is seen as weak lines midway between the principal hyperfine lines. The forbidden transitions are further split into doublets by spin-spin interaction of the sextuplet states and this causes variations in the hyperfine splitting separation of the forbidden transitions.

The axial zero field splitting parameter D can be calculated using the expression [37],

$$I_m \propto \left[2 - \frac{A^2(35-4m^2)}{2(g\beta H)^2} - \frac{5.334D^2}{(g\beta H)^2} - \frac{D^2(34.14)(35-4m^2)}{(g\beta H)^2} + \frac{D^4(208)(35-4m^2)^2}{(g\beta H)^4} \right] \quad (4.2)$$

where I_m is the resultant intensity for a hyperfine line corresponding to a given nuclear spin magnetic quantum number m , H is the magnetic field and β is the Bohr magneton. From a spectra such as that shown in Fig. 4.6., intensity ratios of the three allowed lines lying at the lowest field ($m=5/2, 3/2, 1/2$) are measured by peak-to-peak height of the derivative curve. The D value calculated for the complex is given in Table 4.4. It should be noted that among the three Mn(II) complexes, the compound **9** has the lowest value for D , i.e., the least zero field splitting effect. This is in accordance with the EPR spectrum, which shows only a single resonance with a hyperfine sextet with an effective g value at 2.021. Accordingly, this complex can be regarded as having less distortion from ideal octahedral symmetry when compared to the other two complexes $\text{Mn}(\text{L}^3)_2$ and $\text{Mn}(\text{L}^4)_2$.

4.1.2. $\text{Mn}(\text{L}^3)_2$ (**10**)

Spectral studies

The vibrational spectrum of the compound $\text{Mn}(\text{L}^3)_2$ also reveals features similar to the compound $\text{Mn}(\text{L}^1)_2 \cdot \text{H}_2\text{O}$ above (Fig. 4.7). However, the cyclohexyl stretching vibrations typical of the ligand moiety appear at 2928 and 2849 cm^{-1} . Similar to the compound **9** above, the $\nu(\text{NC})$ vibrations of the newly formed $\text{N}4=\text{C}12$ bond appears as a sharp band at 1584 cm^{-1} . The $\delta(\text{CS})$ band observed at 801 cm^{-1} in the ligand is shifted to regions near 742 cm^{-1} in the complex due to the enolization of

thiosemicarbazone moiety upon coordination. However, here also, the azomethine stretching vibrations are very much weakened in intensity which reveals that the bonding is dominated by the thiosemicarbazone moieties around Mn(II), as in the case of the compound **9**. The electronic spectral assignments of the compound $\text{Mn}(\text{L}^2)_2$ are given in Table 4.4.

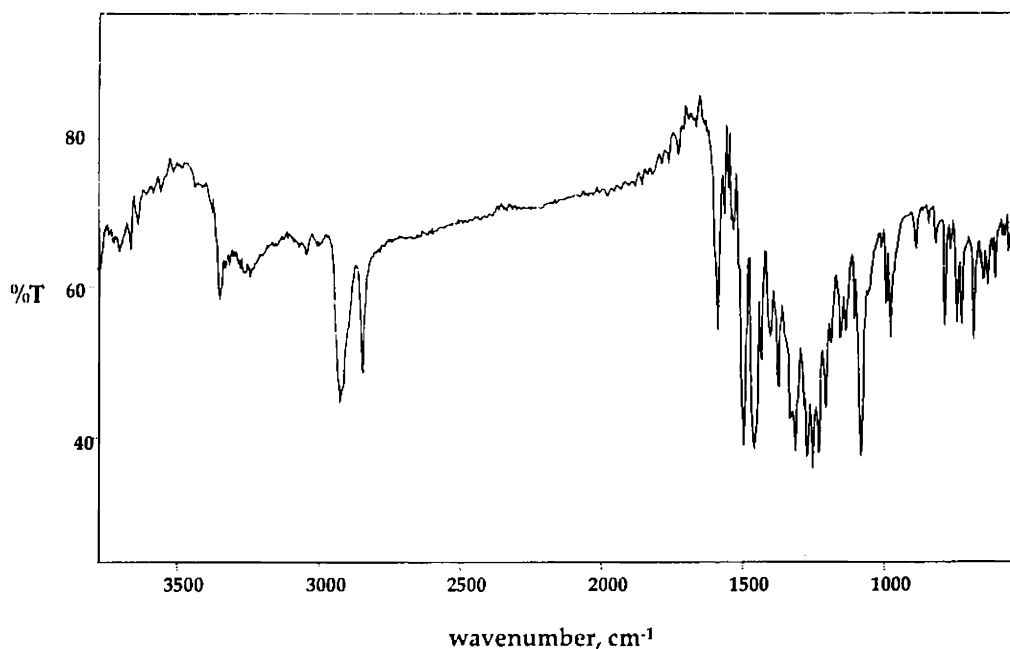


Fig. 4.7. IR spectrum of the compound $\text{Mn}(\text{L}^3)_2$

Electron Paramagnetic Resonance studies

The frozen state EPR spectrum of the compound **10** in DMSO at 77 K is shown in Fig. 4.8. Unlike in the case of $\text{Mn}(\text{L}^1)_2 \cdot \text{H}_2\text{O}$, the compound $\text{Mn}(\text{L}^3)_2$ reveals three ESR resonances corresponding to $g_1 = 5.691$, $g_2 = 2.871$, $g_3 = 2.021$, with the highest field resonance exhibiting a hyperfine sextet.

The presence of three g values can be attributed to an appreciable zero field splitting effects due to the strong field influence of the two ligand moieties. When the zero field splitting parameters D and E are appreciable between the Kramer's doublets, the 'cubic' symmetry of the ligand field around Mn(II) is tetragonally distorted. This gives rise to resonant absorptions being highly anisotropic with an effective g value of *ca.* 2.0 when the magnetic field is parallel to the tetragonal axis and near 6.0 when the

field is perpendicular to the axis. An additional resonance corresponding to an effective g value near 4.0 is also observed when the ligand field effect is appreciably strong. Since the spectrum shows three anisotropic g values, it reveals that there is appreciable zero field splitting effect in the coordination sphere with non-zero D and E values. The axial zero field splitting parameter D is calculated using the expression given above and it was found that the value is appreciably higher when compared to that of the compound **9**. Hence it can be concluded that the cubic symmetry of the ligands around Mn^{2+} is more distorted in the case of compound **10** when compared to that of compound **9**.

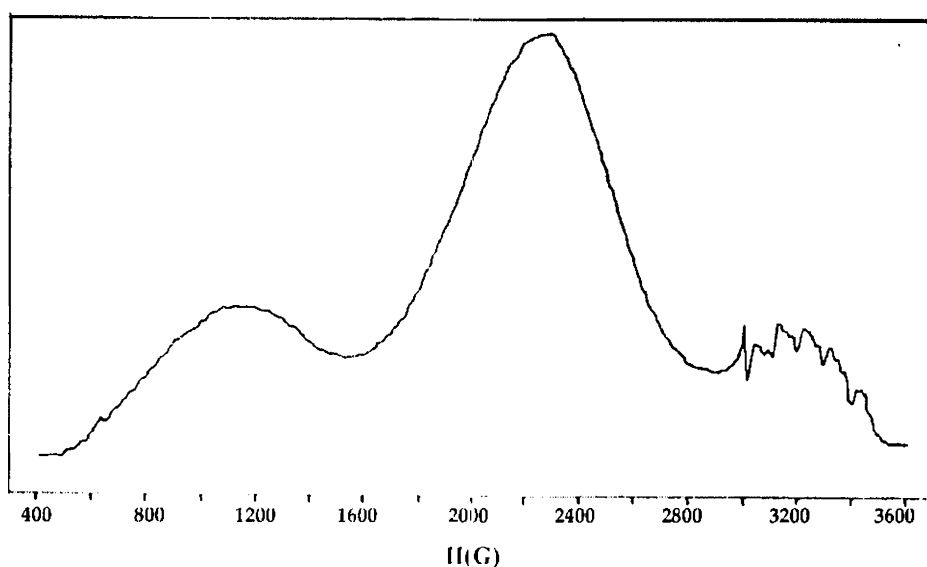


Fig. 4.8. EPR spectrum of the compound $\text{Mn}(\text{L}^3)_2$ in DMSO at 77 K

4.1.3. $\text{Mn}(\text{L}^4)_2$ (**11**)

Spectral studies

In the case of complex **11**, the ligand is not isolated in the solid form and hence a comparative assignment of the spectral features of the complex is not possible. However, the IR spectrum of the compound $\text{Mn}(\text{L}^4)_2$ reveals a very weak band at 3050 cm^{-1} , which can be assigned to the $\nu(\text{N4H})$ vibrations (Fig. 4.9). A weak band at 2972 cm^{-1} and a medium band at 2852 cm^{-1} are assigned to the aromatic C–H stretching vibrations of the morpholine ring. The sharp band at 1586 cm^{-1} can be assigned to the

$\nu(\text{NC})$ vibrations of the newly formed $\text{N4}=\text{C12}$ bond. Interestingly, similar to the other two manganese complexes, there are some very weak intensity bands around 1550 cm^{-1} , which can be presumably assigned to the stretching vibrations of the coordinated azomethine bond considering the proposed stereochemistry of the compound, which is very similar to the other two Mn(II) complexes. The electronic spectral assignments of the compound $\text{Mn}(\text{L}^4)_2$ are given in Table 4.4.

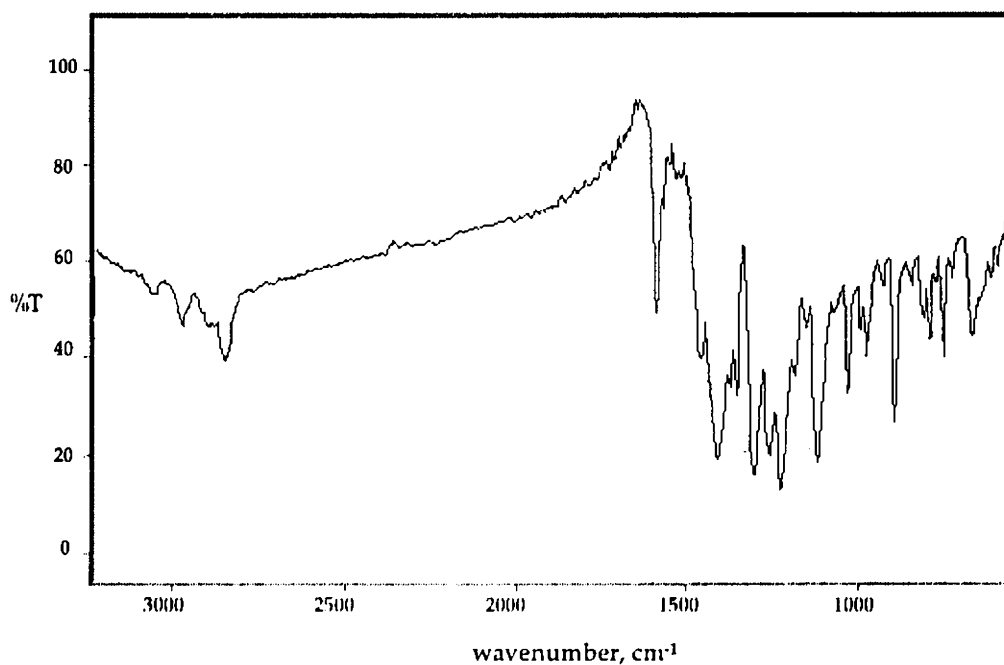


Fig. 4.9. IR spectrum of the compound $\text{Mn}(\text{L}^4)_2$

Electron Paramagnetic Resonance studies

In the case of compound **11**, the EPR spectrum in DMF at 77 K (Fig. 4.10) shows much resemblance to that of compound **10** rather than that of compound **9**. Three resonances corresponding to $g_1 = 5.659$, $g_2 = 3.099$ and $g_3 = 2.021$ are observed with the hyperfine sextet revealed only for the resonance at the highest field.

The presence of three resonant absorption reveals that, similar to compound **10**, an appreciable zero field splitting effect and a considerable distortion from the ideal 'cubic' alignment of the ligand field around Mn(II) can be attributed to compound **11** also. The axial zero field splitting parameter D calculated from the expression (4.2) is

found to be 5.42, which is of the highest magnitude among the three Mn(II) complexes studied here. This may be attributed to the stronger ligand field effect of the ligand HL^4 with the morpholine moiety.

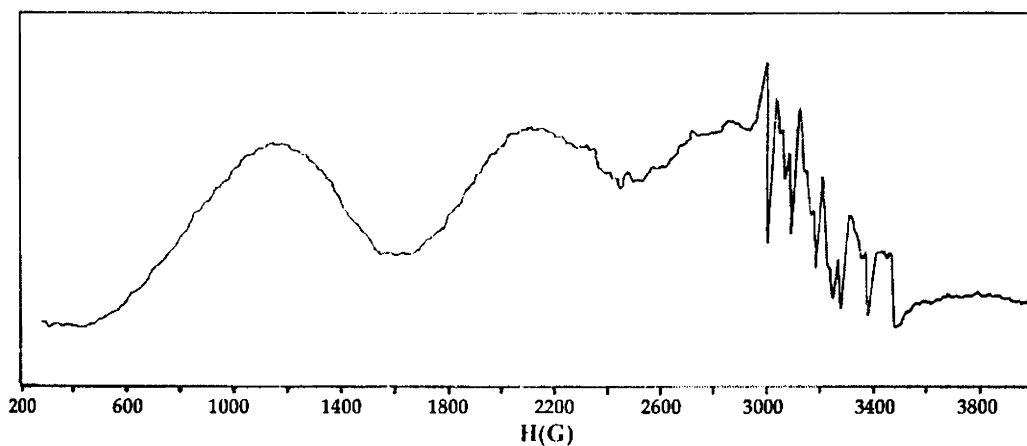


Fig. 4.10. EPR spectrum of the compound $Mn(L^4)_2$ in DMF at 77 K

In all the EPR spectra of Mn^{2+} complexes under study, it is observed that the separation between adjacent lines in the hyperfine multiplet differ slightly, and this can be attributed to the inequivalent spacing of the $2nI+1$ nuclear levels. $Mn(II)$ nuclei with $S=5/2$ has an appreciable quadrupole moment and the electric field gradient from the surrounding ligand ions compete with the magnetic hyperfine interaction in determining the orientation of the nuclear spin, due to which the degeneracy of the nuclear levels is lost resulting in difference in the separation between adjacent lines in the hyperfine splittings.

4.1.4. $VOL^1(acac) \cdot 2H_2O$ (12)

The chemistry of vanadium is dominated by the formation of the oxo species and a wide range of compounds with VO^{2+} groups are known. Almost all compounds containing the VO^{2+} units are blue and they display mostly square pyramidal structures as in the case of $VO(acac)_2$, with the possibility for a sixth ligand to be attached trans to $V=O$ yielding octahedral geometries. However, in a few cases, for eg., in some Schiff base complexes, the structure is found to be distorted trigonal bipyramidal, due to the dominant steric effect of the bulky ligand molecules and the color of the

complexes are not often blue, but instead yellow or maroon. There are also some reports on the reddish-brown colored VO(IV) complexes of thiosemicarbazones [38]. Hence, although it is ambiguous to make any supposition on the geometry of a complex considering the colour of the compound, the predominant reddish-brown color of the present VO(IV) complexes seems to question the assignment of a possible square pyramidal geometry to them. Another point is the potential tridentate nature of the ligands as observed in other metal complexes. Due to these reasons, it is reasonable to assign a distorted octahedral geometry around the central VO(IV) nuclei in the complexes.

Spectral studies

The IR bands of the compound $\text{VO}^{\text{IV}}(\text{acac})\cdot 2\text{H}_2\text{O}$ are less resolved when compared to that of the Mn(II) complexes discussed previously. However, the spectrum reveals some interesting attributes. For instance, two sharp bands near 2900 and 2800 cm^{-1} are observed in the present complex, even though the ligand moiety does not possess a cyclohexyl ring like some other complexes with similar bands in the IR region. Instead, in the present complex, these bands can be assigned to the $\nu(\text{CH}_3)$ vibrations of the acetylacetonato group. The bands near 1600 cm^{-1} are very poorly resolved, perhaps due to their appearance as a combination band owing to the probable presence of the $\nu(\text{C}=\text{C})$ and $\nu(\text{C}=\text{O})$ bands of the acetylacetonato group and the azomethine stretching vibrations of the thiosemicarbazone moiety in the same region. A strong band at 961 cm^{-1} can be assigned to the stretching vibration of the V=O group. The $\nu(\text{V}=\text{O})$ is observed at 999 cm^{-1} in $\text{VO}(\text{acac})_2$, and this band shifts to regions near 960 cm^{-1} in its complexes [39]. The solid state electronic spectrum reveals the $\pi \rightarrow \pi^*$ and $n \rightarrow \pi^*$ transitions at 271 and 337 nm. The charge transfer transitions are observed as a weak shoulder around 434 nm, while the $d-d$ transitions are observed to be very weak.

Electron Paramagnetic Resonance studies

The VO(IV) ion belongs to the $3d^1$ system and the vanadium nucleus has $I=7/2$. The unpaired electron is in the vicinity of $I = 7/2$ of its own nucleus and hence a

magnetically dilute VO(IV) complex will give eight $(2nI+1)$ lines in the isotropic EPR spectrum. The frozen state EPR spectrum of the complex at 77 K is taken in DMF solution (Fig. 4.11) and this reveals three rhombic g tensors, $g_1=2.015$, $g_2=1.995$ and $g_3=1.943$.

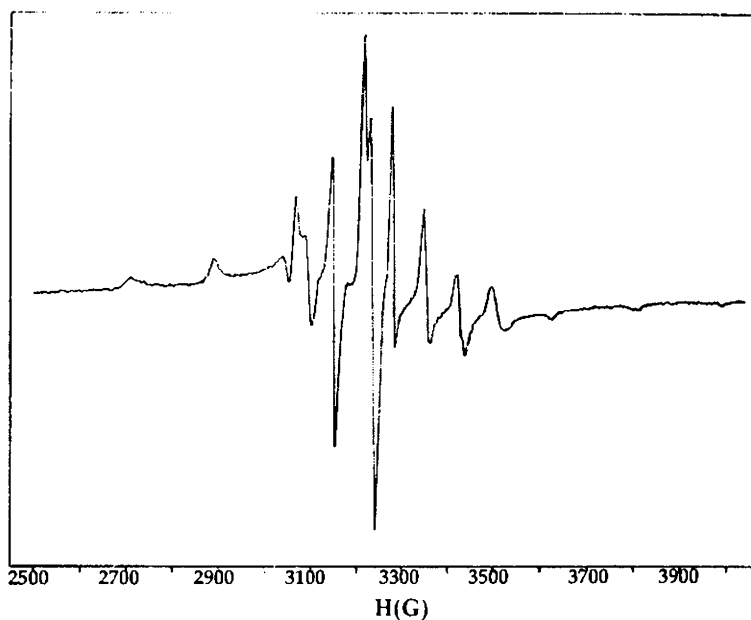


Fig. 4.11. EPR spectrum of the compound $\text{VOL}^1(\text{acac}):2\text{H}_2\text{O}$ in DMF at 77 K

Unlike in Cu(II) complexes, the super-hyperfine splittings are not observed in the VO(IV) complex with nitrogen donor ligands even at low temperature. This is because of essentially nonbonding d_{xy} ground state, where are usually are smaller than the natural peak-to-peak line width of about 10 G.

4.1.5. $\text{VOL}^3(\text{acac})$ (13)

Spectral studies

The compound $\text{VOL}^3(\text{acac})$ reveals similar bands in the IR region as that of the other VO(IV) complex discussed above. The stretching vibration of the V=O group appears as a medium band near 960 cm^{-1} . The azomethine stretching vibration is observed as a weak combination band at 1589 cm^{-1} . The $\delta(\text{CS})$ vibration is observed at

745 cm^{-1} , which is negatively shifted when compared to the corresponding vibration in the free ligand at 801 cm^{-1} . In the solid state electronic spectrum, the $\pi \rightarrow \pi^*$ and $n \rightarrow \pi^*$ transitions are observed at 276 and 345 nm. Shoulder peaks at 401 and 426 nm correspond to the charge transfer transitions. Broad peaks around 460 and 559 nm can be assigned to the $d-d$ transitions.

Electron Paramagnetic Resonance studies

Similar to the case of compound 12 above, the frozen state EPR spectrum of compound 13 also reveal rhombic features with three g values $g_1 = 2.021$, $g_2 = 1.998$ and $g_3 = 1.955$. A distorted octahedral geometry can be suggested in the present complex also, based upon the tridentate behavior of the ligand coordinating through the azomethine nitrogen, thiolate sulfur and pyridyl nitrogen. The EPR spectrum in DMF at 77 K solution is given below (Fig. 4. 12)

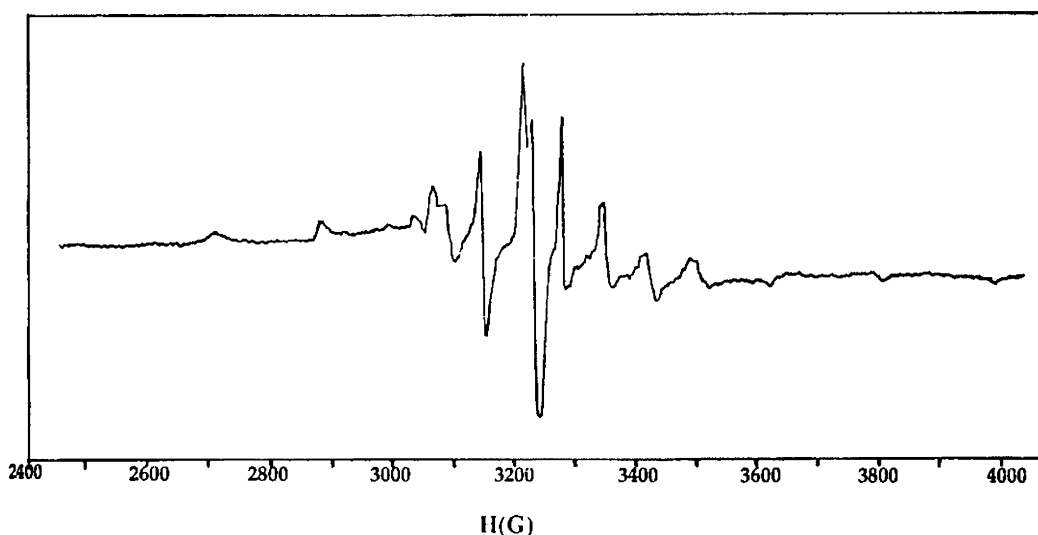
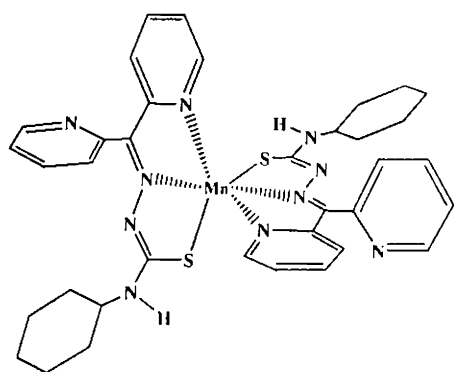


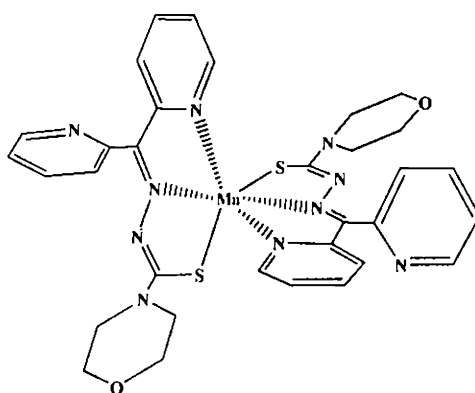
Fig. 4.12. EPR spectrum of the compound $\text{VOL}^3(\text{acac})$ in DMF at 77 K

An interesting point regarding the present VO(IV) complexes is that the EPR spectral features deny the possibility for a dimeric behavior in both the compounds. The oxovanadium(IV) complexes can be five or six coordinate with various degrees of interaction, forming dimeric structures bridged by the ligand units. In such a case,

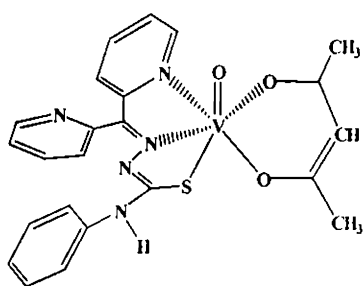
zero field splitting is observed since magnetic exchange is possible between the two unpaired electrons of the two bridged VO nuclei. This will eventually result in an ESR forbidden $\Delta m_s = 2$ transition at half the field of the allowed $\Delta m_s = \pm 1$ transitions. This forbidden transition, is however, absent in the present spectra. Another point is that a dimeric VO(IV) structure will split the resonant absorptions into 15 lines [$2n+1$; $n=2$, $I=7/2$] in the EPR, which is also not observed for both the complexes. Hence the EPR results are in accordance with the proposed monomeric distorted octahedral stereochemistry for the complexes (Fig. 4.13).



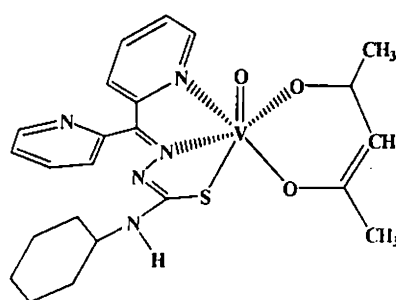
Compound 10



Compound 11



Compound 12



Compound 13

Fig. 4.13. Tentative structures of the complexes 10, 11, 12 and 13
Water of hydration is omitted for convenience.

4.2. Magnetochemistry of the complexes

The complexes that revealed paramagnetic behavior at room temperature are subjected to magnetic studies at variable temperatures up to liquid nitrogen temperature. However, the magnetic studies of the complexes $\text{Mn}(\text{L}^4)_2$ and $\text{VOL}^3(\text{acac})$ could not be carried out due to the low yield of the sample.

4.2.1. $\text{Mn}(\text{L}^1)_2 \cdot \text{H}_2\text{O}$

The magnetic susceptibility data for the compound $\text{Mn}(\text{L}^1)_2 \cdot \text{H}_2\text{O}$ are collected at various temperatures between 80 and 298 K. The magnetic parameters are then well interpreted in terms of the modified Bleaney-Bowers equation corrected for paramagnetic impurities, with the best fit values of $2J = -42.48 \text{ cm}^{-1}$, $g = 2.061$ and ρ (impurity factor) = 0.0095 with an agreement factor $R \left\{ \frac{\sum (\chi_{\text{calc}} - \chi_{\text{obs}})^2}{\sum \chi_{\text{obs}}^2} \right\} = 2.5 \times 10^{-5}$ (Fig. 4.14). Since there are no significant upper levels present for a high spin $d^5 \text{Mn}^{2+}$, the correction for temperature independent paramagnetism is not applied.

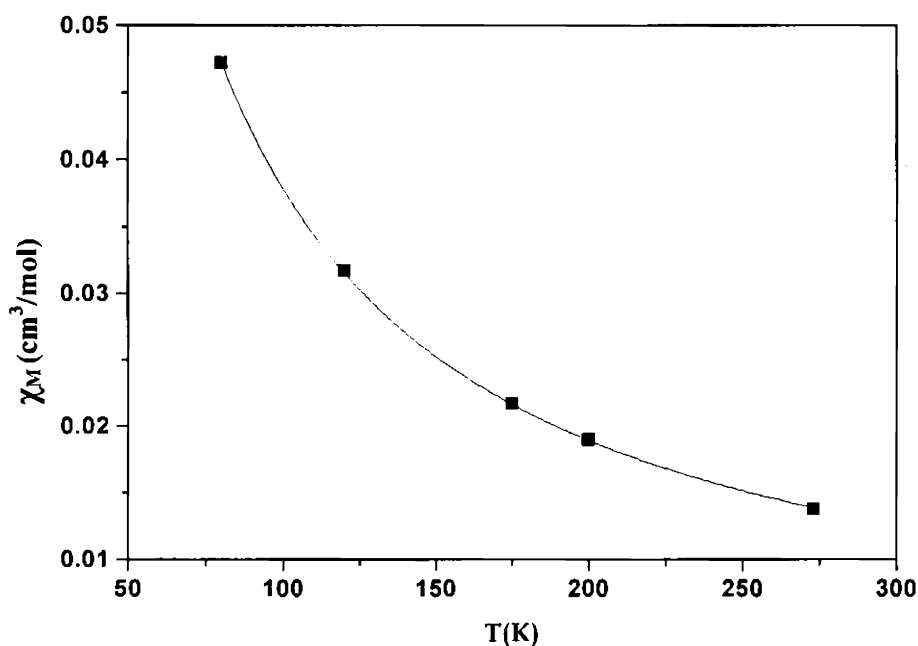


Fig. 4.14. Temperature dependence of χ_M for $\text{Mn}(\text{L}^1)_2 \cdot \text{H}_2\text{O}$. The squares are the experimental points and the solid line is the theoretical best fit of the experimental data

The antiferromagnetic interactions observed in the manganese complex can be explained in more than one way as follows:

- (1) As per the crystal field approach, since there is no bridging atoms between the two Mn(II) atoms as revealed by the crystal structure, the observed exchange coupled interactions can be accounted only on the basis of a possible 'through space' direct interaction of the metal orbitals. However, it is difficult to fit this argument here, since the metal-metal distance in the asymmetric unit is observed to be *ca.* 7.0 Å. Generally, 'through-space' direct metal-metal interaction are observed in the range 3–5 Å. Hence it is the quantum mechanical approach that provides more reliable reasons for the effect. Contradictory to the crystal field considerations, in the quantum mechanical approach, the directional vectors in space are not confined to any particular axes or distances, and hence a net coupling of the moments are very nearly possible.
- (2) Another explanation that can be given to the observed variation of magnetic susceptibility with temperature is that it is due to appreciable zero field splitting effect. Considering the relatively longer metal-metal distance, this argument appears to be logical here. However, this explanation does not fit to the complex $\text{Mn}(\text{l}^{\text{I}})_2\cdot\text{H}_2\text{O}$, since the EPR results and subsequent calculations revealed that the zero field splitting is negligible in the compound. However, since the magnetic data are collected only up to liquid nitrogen temperature, the effect of zero field splitting at very low temperatures, i.e., below 77 K could not be traced out.
- (3) A third, but least reliable viewpoint is based upon a weak hydrogen bonding interaction between the hydrogen atom on N5 nitrogen of one molecule with the nitrogen atom N57 of the neighboring molecule ($d_{\text{D}-\text{A}}=2.978$ Å). There are some reports in literature, where the magnetic exchange interaction is proposed through a hydrogen bonded pathway. However, taking into consideration of the fact that the thiosemicarbazone skeleton is a highly electron delocalized system, it would be better to treat the hydrogen bonding as an ancillary effect, which would enhance the interaction through the effects (1) and (2).

4.2.2. $\text{Mn}(\text{L}^3)_2$

The room temperature effective magnetic moment value was much reduced from the spin-only value for Mn^{2+} , and the magnetic susceptibility data for the compound are collected at various temperatures between 80 and 298 K. Fitting the magnetic susceptibility values into the modified Bleaney-Bowers equation corrected for paramagnetic impurities, gave best fit values of $2J = -41.06 \text{ cm}^{-1}$, $g = 2.053$ and ρ (impurity factor) = 0.1752 with an agreement factor $R \left\{ \frac{\sum (\chi_{\text{calc}} - \chi_{\text{obs}})^2}{\sum \chi_{\text{obs}}^2} \right\} = 1.0 \times 10^{-5}$. The variation of magnetic susceptibility with temperature is plotted as points in Fig. 4.15 and the theoretical best-fit curve is shown as the solid line.

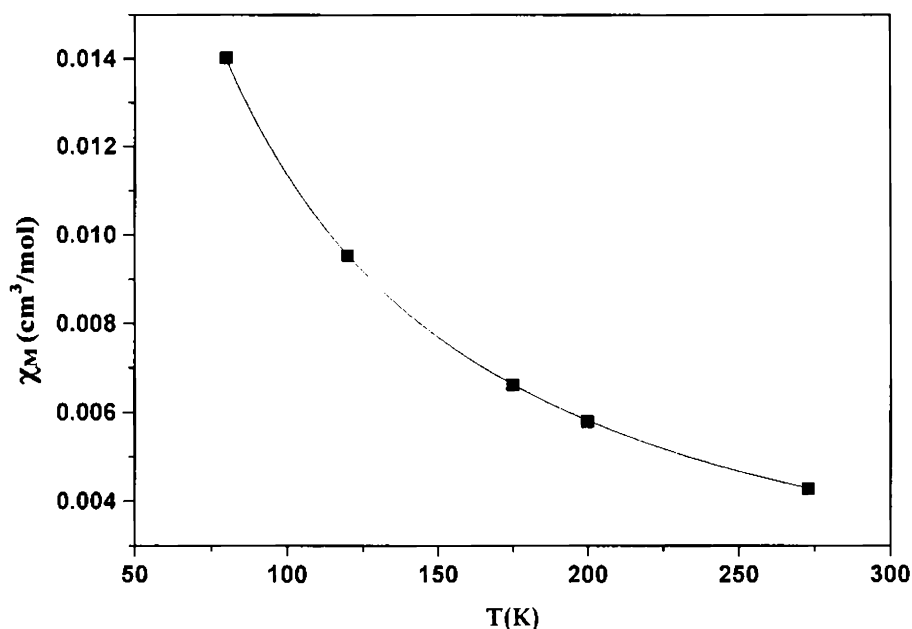


Fig. 4.15. Temperature dependence of χ_M for $\text{Mn}(\text{L}^3)_2$. The squares are the experimental points and the solid line is the theoretical best fit of the experimental data

Considering the stereochemistry assigned to the complex **10** similar to that of compound **9**, the antiferromagnetic interactions in **10** can be attributed to the same reasons as for **9**. However, unlike complex **9**, the compound **10** reveals some zero field splitting effects with three g values in the EPR and a D value of 4.68, which may

contribute to the observed variation in susceptibilities. As crystal structure evidence is not available for the present compound, a detailed investigation into the bonding interactions is not possible here.

4.2.3. VOL³(acac)

The effective magnetic moment value for the complex VOL³(acac) is found to be higher than the spin-only value. Hence, the magnetic susceptibility data for the compound are collected at various temperatures between 80 and 298 K. The variation of magnetic susceptibility with temperature is plotted as points in Fig. 4.16 and a solid dashed line is used only to interconnect the values at various temperatures.

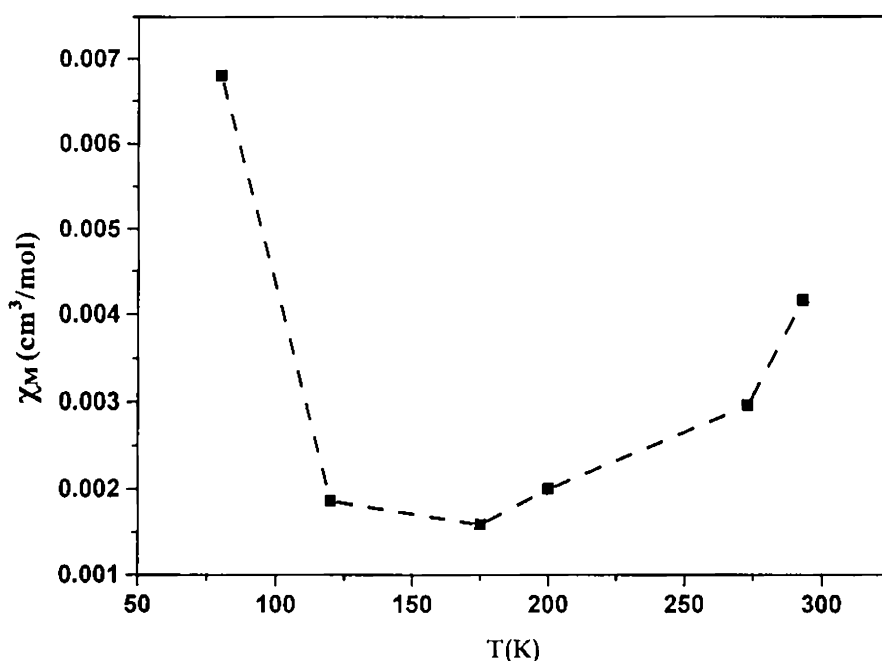


Fig. 4.16. Temperature dependence of χ_M for VOL³(acac)

However, the magnetic susceptibility values at various temperatures did not fit into Curie-Weiss equation. Hence it was concluded that the compound reveals no regular gradation with temperature, it is neither ferromagnetic nor antiferromagnetic.

4.3. Experimental

Materials

Di-2-pyridyl ketone (Fluka), morpholine (Merck), CS₂ (Merck), hydrazine hydrate (Ranchem), acetonitrile (Qualigens), Mn(OAc)₂ (Merck), VO(acac)₂ (Merck) and Methanol (Ranchem) were used as received. When the solvent used was ethyl alcohol, it was repeatedly distilled for purification.

Synthesis of ligands

Preparation of the ligands HL¹ and HL³ was done as described previously in Chapter 2. Another ligand, HL⁴ was obtained in solution state, and hence could not be separated out as solid product.

Preparation of complexes

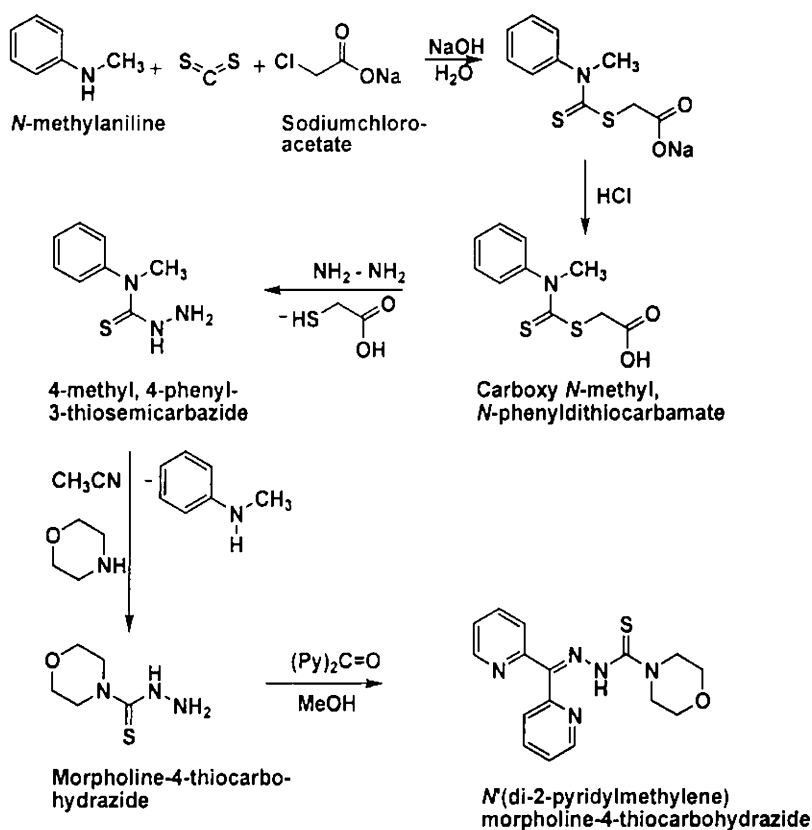
Mn(L¹)₂·H₂O (9): A solution of Mn(OAc)₂ (0.173 g, 1 mmol) in 10 ml of methanol was added to a methanolic solution of HL¹ (0.317 g, 1 mmol) and refluxed continuously. Shining bronze colored crystalline products were separated out after ten hours. The product was washed with dilute methanol followed by ether and dried over P₄O₁₀ *in vacuo*. Single crystals for X-ray diffraction were grown by room temperature slow evaporation of a solution of the complex in a 1:1:2 mixture of DMF, CH₂Cl₂ and acetone. Yield: 0.35 g (73%). Elemental Anal. Found (Calc.): C, 58.43 (58.61); H, 4.12 (4.10); N, 19.03 (18.99)%.

Mn(L³)₂ (10): HL³ (0.323 g, 1 mmol) was dissolved in methanol (15 ml) and refluxed with a solution of Mn(OAc)₂ (0.173 g, 1 mmol) in 10 ml of methanol for eight hours. Brown crystalline product separated out, which was filtered and washed with ether and dried over P₄O₁₀ *in vacuo*. Yield: 0.32 g (64%). Elemental Anal. Found (Calc.): C, 59.38 (59.08); H, 5.76 (5.51); N, 19.56 (19.14)%.

Mn(L⁴)₂ (11): The synthesis of Mn(L⁴)₂ was done (Scheme 3) as follows:

A mixture consisting of 12 ml (5.2 g, 0.2 ml) of carbon disulphide and 21.6 ml (21.2 g, 0.2 mol) of N-methylaniline was treated with a solution of sodium hydroxide (8.4 g, 0.21 mol) in 250 ml water. After stirring at room temperature for 4 hours, the organic

layer had completely disappeared and at this point the straw coloured solution was treated with 23.2 g (0.20 mol) of sodium chloroacetate and allowed to stand overnight (17 hours). The solution was acidified with 25 ml conc. HCl and the solid, which separated, was collected and dried. This afforded 39.7 g (82%) of pale buff colored carboxy N-methyl N-phenyl dithiocarbamate (m.p. 197 – 198 °C).



Scheme 3

A solution of 17.7 g (0.0733 mol) of carboxy N-methyl N-phenyl dithiocarbamate in 20 ml 98% hydrazine hydrate and 10 ml water was heated in the rings of a steam bath at 85 °C, after 3 minutes crystals began to separate. Heating was continued for additional 22 minutes. The crystals were collected by filtration, washed well with water and dried. The crude product was recrystallized from a mixture of 50 ml ethanol and 25 ml water. This gave 10.8 g (81%) of 4-methyl, 4-phenyl 3-thiosemicarbazide (m.p. 124 °C). A solution of 1 g of this product (5.52 mmol) in 5 ml

acetonitrile was treated 480 ml (5.52 mmol) of morpholine and the resulting solution was heated under reflux for four hours. The solution was chilled for one week, however, no solid products were separated out. Hence a solution of 10 mmol (1.84 g) of di-2-pyridyl ketone in 5 ml of ethanol was directly added into this solution and refluxed for six hours. There was no immediate formation of the products and hence this solution was again chilled for a few weeks in the freezer. However, the products did not separate out even after reducing the volume of the solution by concentration through evaporation. Hence a solution of $\text{Mn}(\text{OAc})_2$ (0.173 g, 1 mmol) in 10 ml of methanol was added to HL^4 in solution state and refluxed for twelve hours. No immediate formation of products was observed and the solution was kept aside undisturbed for two days at room temperature. Dark brown crystalline products separated out, which were filtered, washed with ether and dried over P_4O_{10} *in vacuo*. Yield: 0.28 g (39 %). Elemental Anal. Found (Calc.): C, 55.02 (54.31); H, 4.84 (4.56); N, 20.11 (19.79)%.

$\text{VOL}^1(\text{acac})\cdot 2\text{H}_2\text{O}$ (12): The reaction was carried out in a three-necked round bottom flask where two necks were fitted with stop-cocks. The first neck was connected to a vacuum pump and the second neck was connected to the piston less portion of a glass syringe. The third neck was tightly closed with a septum. At first, the R.B. was evacuated using a suction pump linked through the first stop-cock. After the completion of evacuation, the stop-cock was turned off and the connection to the pump was detached. Then the syringe at the second neck was injected into a bladder filled with nitrogen and the second stop-cock was turned on. Methanolic solutions of HL^1 (0.317 g, 1 mmol) followed by $\text{VO}(\text{acac})_2$ (0.265 g, 1 mmol) were injected into the flask through the septum. The solution was stirred continuously for twelve hours (magnetic pellets were inserted in the R.B. prior to evacuation). The resulting solution was kept aside for evaporation at room temperature for three days. Reddish brown crystalline products separated out, which were washed with ether and dried over P_4O_{10} *in vacuo*. Yield: 0.49 g (65%). Elemental Anal. Found (Calc.): C, 51.05 (51.68); H, 5.26 (4.71); N, 12.85 (13.10)%.

VOL³(acac) (13): Preparation of VOL³(acac) was carried out by the same procedure as that of compound **12** above, except that a methanolic solution of HL³ (0.323 g, 1 mmol) was used instead of HL¹. The resultant solution after reaction was evaporated at room temperature and reddish brown products separated out in two days, which were washed with ether and dried over P₄O₁₀ *in vacuo*. Yield: 0.36 g (62%). Elemental Anal. Found (Calc.): C, 56.68 (56.44); H, 5.39 (5.35); N, 12.02 (11.45)%.

Table 4.1.

Crystal data and structure refinement for $\text{Mn}(\text{L}^1)_2 \cdot 1.5(\text{H}_2\text{O}) \cdot 0.5(\text{DMF})$

Empirical Formula	$\text{C}_{37.5}\text{H}_{33.5}\text{N}_{10}\text{MnO}_{1.5}\text{S}_2$
Formula weight (M)	767.30
Temperature (T) K	293(2)
Wavelength (Mo $K\alpha$) (Å)	0.71073
Crystal system	Triclinic
Space group	$P\bar{1}$
Lattice constants	
a (Å)	13.4241(18)
b (Å)	14.2981(19)
c (Å)	20.254(3)
α (°)	95.073(3)
β (°)	99.802(2)
γ (°)	93.632(2)
Volume V (Å ³)	3803.5(9)
Z	4
Calculated density (ρ) (Mg m ⁻³)	1.340
Absorption coefficient (μ) (mm ⁻¹)	0.503
$F(000)$	1590
Crystal size (mm)	0.36 x 0.33 x 0.26
θ Range for data collection	1.68-28.04
Limiting Indices	$-17 \leq h \leq 17, -18 \leq k \leq 18, -26 \leq l \leq 26$
Reflections collected	44896
Unique Reflections	10537 [$R_{\text{int}} = 0.1005$]
Completeness to θ	28.04 (96.4 %)
Absorption correction	Multi-Scan
Maximum and minimum transmission	0.8821 and 0.8413
Data / restraints / parameters	17782 / 0 / 936
Goodness-of-fit on F^2	1.089
Final R indices [$I > 2\sigma(I)$]	$R_1 = 0.1036, wR_2 = 0.2359$
R indices (all data)	$R_1 = 0.1739, wR_2 = 0.2710$
Largest difference peak and hole (e Å ⁻³)	0.894 and -0.398

Table 4.2.
Comparison of selected bond lengths (Å)
and bond angles (°) of HL¹ and Mn(L¹)₂·1.5(H₂O)0.5(DMF)

	HL ¹	Mn(L ¹) ₂
Mn1-N1		2.302(4)
Mn1-N3		2.246(4)
Mn1-S1		2.4851(17)
Mn1-N6		2.305(5)
Mn1-N8		2.244(4)
Mn1-S2		2.5277(18)
S1-C12	1.6763(12)	1.726(5)
N3-C6	1.2858(8)	1.298(6)
N4-N3	1.3573(10)	1.378(5)
N4-C12	1.3616(9)	1.327(6)
S2-C30		1.730(5)
N8-C24		1.294(6)
N9-N8		1.379(6)
N9-C30		1.319(6)
N1-Mn1-N3		71.30(15)
N1-Mn1-S1		147.16(11)
N1-Mn1-N6		88.38(16)
N3-Mn1-S1		75.88(10)
N6-Mn1-N8		71.18(15)
N6-Mn1-S1		94.61(11)
N6-Mn1-S2		146.85(10)
N6-Mn1-N3		96.89(15)
N8-Mn1-S2		75.77(10)
N8-Mn1-N1		90.82(15)
S2-Mn1-N1		94.58(11)

Table 4.3.
H-bonding, π - π and CH \cdots π interaction parameters of the compound Mn(L¹)₂·1.5(H₂O)0.5(DMF)

H-bonding					
Donor--H---A	D--H (Å)	H---A (Å)	D---A (Å)	D--H---A (°)	
N5-H5---S1	0.860	2.566	2.615	83.64	
N5-H5---N57	0.860	2.126	2.978	170.88	
N10-H10---S2	0.860	2.598	2.618	81.84	
N55-H55-S3	0.860	2.549	2.605	84.09	
N60-H60-S4	0.860	2.633	2.639	81.04	
π-π interactions					
Cg(1)-Res(1)---Cg(J)	Cg-Cg(Å)	α °	β °		
Cg(9) [1] -> Cg(9) ^a	3.7600	0.02	20.71		
Equivalent position code					
a=2-x, 1-y, z					Cg(9)=N1, C1, C2, C3, C4, C5
CH$\cdots$$\pi$ interactions					
X-H(I)---Cg(J)	H..Cg(Å)	X-H---Cg (°)	X..Cg (°)		
C1-H1[1] -> Cg(2) ^a	2.8083	113.83	3.2957		
C1-H1[1] -> Cg(4) ^a	3.0927	102.05	3.4103		
C19-H19[1] -> Cg(1) ^a	3.0002	115.01	3.4964		
C36-H36[1] -> Cg(18) ^b	3.3801	86.88	3.4565		
C70-H70[2] -> Cg(11) ^c	3.2506	96.00	3.4732		
C84-H84[2] -> Cg(15) ^c	3.0256	107.85	3.4269		
					Cg(1)=Mn1, S1, C12, N4, N3
					Cg(2)=Mn1, S2, C30, N9, N8
					Cg(4)=Mn1, N6, C23, C24, N8
					Cg(11)=N6, C19, C20, C21, C22, C23
					Cg(15)=N56, C69, C70, C71, C72, C73
					Cg(18)=C31, C32, C33, C34, C35, C36
Equivalent position code					
a=x, y, z					
b=2-x, 1-y, -z					
c=1-x, 1-y, 1-z					

Table 4.4.
Electronic spectral data of Mn(II) complexes

Compound	${}^4T_{1g}(P) \leftarrow {}^6A_{1g}$ (nm)	${}^4E_g(D) \leftarrow {}^6A_{1g}$ (nm)	${}^4A_{1g}(G), {}^4E_g(G) \leftarrow {}^6A_{1g}$ (nm)	${}^4T_2(G) \leftarrow {}^6A_{1g}$ (nm)	$n \rightarrow \pi^*$ and $\pi \rightarrow \pi^*$ (nm)	B' (cm^{-1})	Dq (cm^{-1})	D
$\text{Mn}(\text{L}^1)_2 \cdot \text{H}_2\text{O}$ (9)	278	328	411	531	340 260	896.76	1434.82	0.52
$\text{Mn}(\text{L}^3)_2$ (10)	274	327	406	529	342sh 267	900.19	1458.31	4.68
$\text{Mn}(\text{L}^4)_2$ (11)	295	337sh	402	547	338sh 282	910.75	1548.28	5.42

sh = shoulder

References:

1. D. F. Xiang, C. Y. Duan, X. S. Tan, Q. W. Hang, W. X. Tang, *J. Chem. Soc. Dalton Trans.* (1998) 1201.
2. R. Hage, *Recl. Trav. Chim. Pays-Bays* 115 (1996) 385.
3. W. Zhang, J. L. Loebach, S. B. Wilson, E. N. Jacobsen, *J. Am. Chem. Soc.* 112 (1990) 2801.
4. J. Brinksma, R. Hage, J. Kerschner, B. L. Feringa, *Chem. Commun.* (2000) 537.
5. K. B. Jensen, E. Johansen, F. B. Larsen, C. J. McKenzie, *Inorg. Chem.* 43 (2004) 3801.
6. J. Bendix, H. B. Gray, G. Golubkov, Z. Gross, *Chem. Commun.* (2000) 1957.
7. B. Meunier, in *Metalloporphyrin Catalysed Oxidations*, ed. F. Montanari and L. Casella, Kluwer Academic Publishers, Dordrecht, 1994.
8. J. T. Groves, in *Cytochrome P450: Structure, Mechanism and Biochemistry*, Ed. P. R. Ortiz de Montellano, 2nd ed., Plenum Press, New York, 1995.
9. J. Limburg, V. A. Szalai, G. W. Brudvig, *J. Chem. Soc. Dalton Trans.* (1999) 1351.
10. V. K. Yachandra, K. Sauer, M. P. Klein, *Chem. Rev.* 94 (1996) 807.
11. G. C. Dismukes, *Chem. Rev.* 96 (1996) 2909.
12. D. P. Riley, *Chem. Rev.* 99 (1999) 2573.
13. E. A. Lewis, J. R. L. Smith, P. H. Walton, S. J. Archibald, S. P. Foxon, G. M. P. Giblin, *J. Chem. Soc. Dalton Trans.* (2001) 1159.
14. M. -L. Tong, S. -L. Zheng, J. -X. Shi, Y. -X. Tong, H. K. Lee, X. -M. Chen, *J. Chem. Soc. Dalton Trans.* (2002) 1727.
15. B. S. Garg, M. R. P. Kurup, S. K. Jain, Y. K. Bhoon, *Transition Met. Chem.* 13 (1988) 92.
16. P. Bindu, M. R. P. Kurup, J. I. Bhat, *J. Electrochem. Soc. India*, 48 (1999) 154.
17. R. P. John, A. Sreekanth, H. -K. Fun, M. R. P. Kurup, *Polyhedron*, 24 (2005) 601.

18. A. Usman, I. A. Razak, S. Chantrapromma, H. -K. Fun, A. Sreekanth, S. Sivakumar, M. R. P. Kurup, *Acta. Cryst.* C 58 (2002) m461.
19. H. A. Tang, L. F. Wang, R. D. Yang, *Trans. Met. Chem.* 28 (2003) 395.
20. M. B. Ferrari, G. G. Fava, C. Pelizzi, P. Tarasconi, G. Tori, *J. Chem. Soc. Dalton Trans.* (1987) 227.
21. V. Philip, V. Suni, M. R. P. Kurup, M. Nethaji, *Spectrochim. Acta Part A*, in press.
22. B. A. Reul, S. S. Amin, J. -P. Buchet, L. N. Ongemba, D. C. Crans, S. M. Brichard, *Br. J. Pharm.* 126 (1999) 467.
23. D. S. Greco, *Diabetes 57th Sci. Sessions* (1997) 1274.
24. K. H. Thompson, J. H. McNeill, C. Orvig, *Chem. Rev.* 99 (1999) 2561.
25. J. H. McNeill, V. G. Yuen, H. R. Hoveyda, C. Orvig, *J. Med. Chem.* 35 (1992) 1489.
26. A. Sreekanth, R. P. John, M. R. P. Kurup, XXXVth International Conference on Coordination Chemistry (2002) Heidelberg, Germany.
27. A. Sreekanth, S. Sivakumar, M. R. P. Kurup, *J. Mol. Struct.* 655/1 (2003) 47.
28. V. Philip, E. Manoj, M. R. P. Kurup, M. Nethaji, submitted.
29. V. Suni, M. R. P. Kurup, M. Nethaji, *Spectrochim. Acta Part A*. in press.
30. V. Philip, V. Suni, M. R. P. Kurup, *Acta Crystallogr. C* 60 (2004) o856.
31. J. K. Swearingen, W. Kaminsky, D. X West, *Transition Met. Chem.* 27 (2002) 724.
32. A. Usman, I. A. Razak, S. Chantrapromma, H. K. Fun, V. Philip, A. Sreekanth, M. R. P. Kurup, *Acta Crystallogr. C* 58 (2002) o652.
33. C. Duan, X. You, T. C. Mak, *Acta Crystallogr. C* 54 (1998) 1395.
34. A. B. P. Lever, *Inorganic Electronic Spectroscopy*, 2nd ed., Elsevier Science Publishers B. V., Netherlands, 1984.
35. M. R. P. Kurup *in* Stereochemical Investigations on Transition Metal Complexes of Biologically Active Substituted 2-acetylpyridine-thiosemicarbazones, Ph. D. Thesis, University of Delhi, 1988.
36. K. B. Pandeya, R. Singh, P. K. Mathur, R. P. Singh, *Transition Met. Chem.* 11 (1986) 347.

37. B. T. Allen, *J. Chem. Phys.* 43 (1965) 3820.
38. R. P. John, *in* Structural and Biological Investigations of Metal Complexes of some Substituted Thiosemicarbazones, Ph.D. thesis, Cochin University of Science and Technology, Kochi, 2002.
39. K. Nakamoto *in* Infrared and Raman Spectra of Inorganic and Coordination Compounds, 4th ed., John Wiley & Sons, New York, 1986.

CHAPTER 5

Ni(II) complexes of di-2-pyridyl ketone *N*(4)-cyclohexyl- and *N*(4)-phenylthiosemicarbazones – Syntheses, structural and spectral investigations

Nickel occurs as Ni(I), Ni(II) or Ni(III) in biological systems such as the active sites of certain hydrogenases and dehydrogenases [1]. Hence the nickel species in various coordination environments are of interest to inorganic biochemists. Some nickel complexes of thiosemicarbazone derivatives are observed to exhibit antitumour activity [2]. Complexes of Ni(II) with Schiff bases derived from 4-amino-5-sulfanyl-1,2,4-triazoles are reported to exhibit antibacterial and antifungal activity [3]. The nickel complexes of dithiadiiminoamine and dithiabis(thiosemicarbazone) ligands are found to exhibit redox behaviour [1]. There are also some reports on the Ni(II) complexes of substituted thiosemicarbazones [4, 5] and their di-2-pyridyl ketone derivatives [6–8]. The mono- and bis-chelated nickel complexes of di-2-pyridyl ketone derivatives of *S*-methyldithiocarbazate are observed to have antifungal and antibacterial properties [9]. The coordination complexes of nickel are also studied for their magnetic behavior. For instance, the magnetic properties of Ni(II) complexes of diazomesocyclic ligands are carried out by Bu *et al.*, [10] and these compounds are observed to be antiferromagnetic. Complexes of cubane-type with $[\text{Ni}_4\text{O}_4]^{n+}$ cores are also reported with di-2-pyridyl ketone [11]. Similarly, conformationally rigid molecular squares of $[\text{Ni}(\text{HL})]_4^{4+}$ are prepared from bis[phenyl(2-pyridyl)methanone]-thiocarbazone and their magnetic studies reveal antiferromagnetic characteristics [12]. However, a dinuclear nickel complex containing triethylene tetramine and tricyanomethamide is found to exhibit ferromagnetic attributes [13]. Some trinuclear nickel complexes of 3,5-dialkyl-1, 3, 4-triazole compounds containing N-bridging isothiocyanate ligands are also observed to be ferromagnetic [14]. However, the magnetic studies of nickel complexes of di-2-pyridyl ketone *N*(4)-substituted thiosemicarbazones have never been attempted before and here we carry out some preliminary efforts towards it.

5.1. Stereochemistry of the complexes

Nickel compounds are observed to be less stable at higher oxidation states, and only Ni(II) occurs in the ordinary chemistry of the element. Stereochemistry and electronic structures of Ni(II) complexes vary with the coordination numbers ranging from 3 to 6. The principal geometries of Ni²⁺ complexes are octahedral and square planar. Some trigonal bipyramidal, square pyramidal and tetrahedral complexes are also known. Octahedral complexes are formed when Ni(II) exhibits its maximum coordination number of 6 and a coordination number of 4 is revealed in tetrahedral and square planar complexes.

5.1.1. Ni(L¹)₂·2H₂O (14)

The elemental analyses revealed a Ni(L¹)₂·2H₂O stoichiometry for the compound **14** synthesized. However, the single crystals prepared from the compound revealed a composition containing one molecule each of water and DMF in it.

Crystal studies

Single crystals suitable for X-ray diffraction of the compound Ni(L¹)₂·2H₂O are grown by room temperature slow evaporation of a 1:1:1 solution of the complex in methanol, chloroform and dimethylformamide. Similar to that of compound **9**, there are two crystallographically independent molecules in the asymmetric unit of Ni(L¹)₂·0.5(H₂O)0.5(DMF) (Fig. 5. 1).

The molecule with the atom numbering scheme is given in Fig. 5. 2. The structural refinement parameters are given in Table 5.1. and the selected bond distances and bond angles are given in Table 5.2. The bonding parameters in the crystallographically independent molecules in the asymmetric lattice bear almost identical features. In addition to the two Ni(L¹)₂ moieties, there are two solvent molecules, i.e., one molecule each of water and DMF in the lattice.

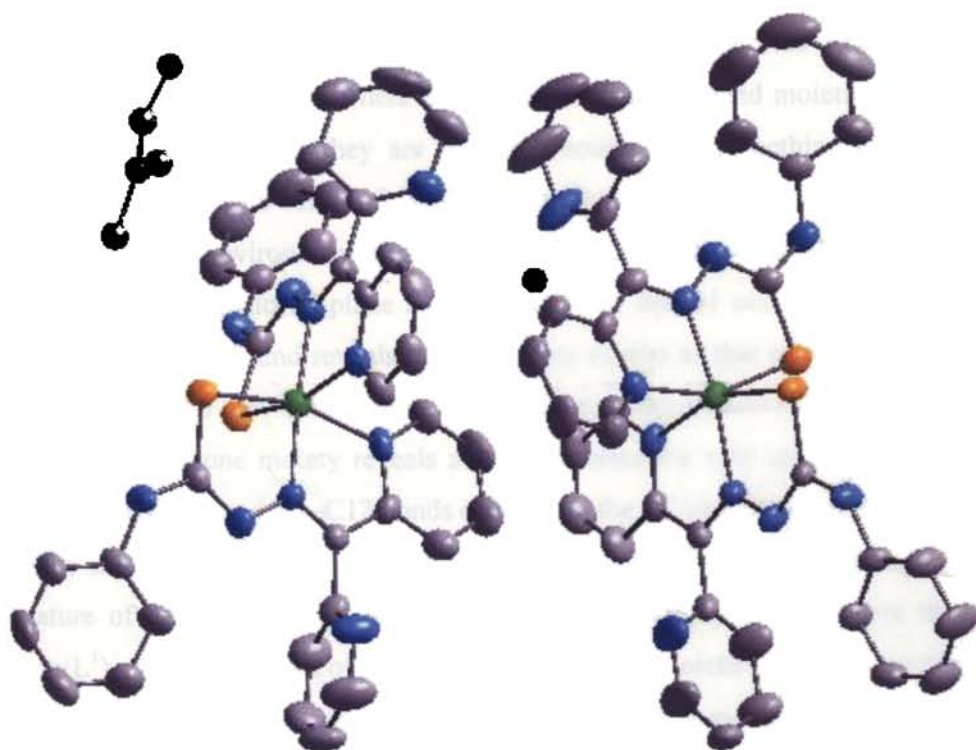


Fig. 5. 1. Molecular structure of the compound $\text{Ni}(\text{L}^1)_2 \cdot 0.5(\text{H}_2\text{O}) \cdot 0.5(\text{DMF})$. Hydrogen atoms are omitted for clarity

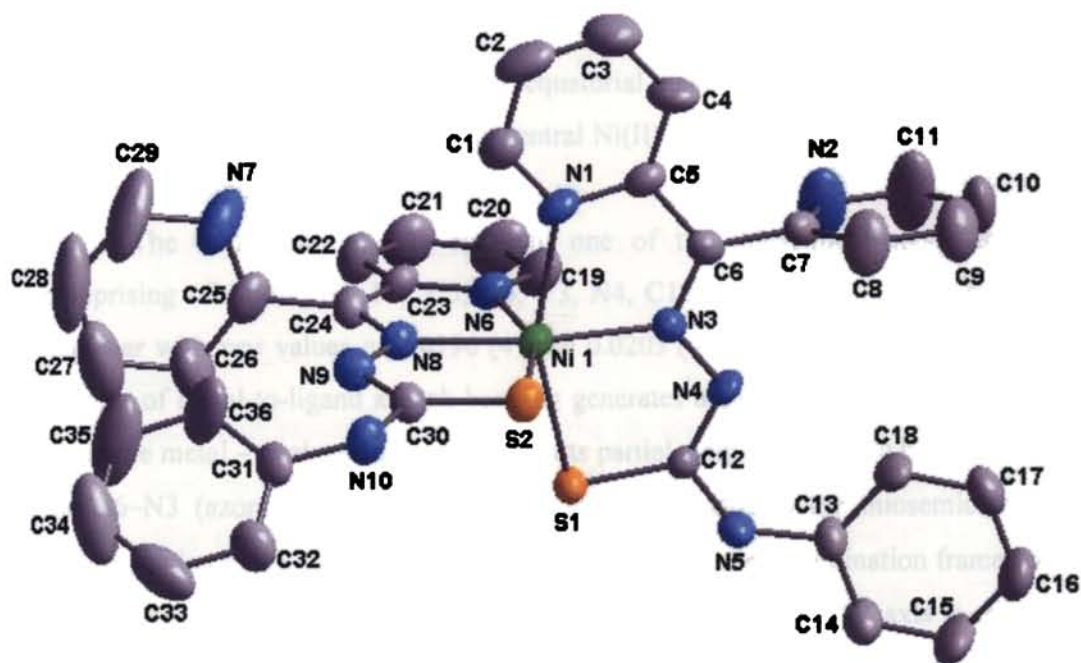


Fig. 5. 2. Molecular structure of $\text{Ni}(\text{L}^1)_2$ in the unit cell. The ellipsoids are shown with 50% probability and the hydrogen atoms are omitted for clarity

The bond distances and angles from single crystal X-ray diffraction studies reveal that the independent units of molecules exist in a distorted octahedral geometry around the metal center. There are two deprotonated ligand moieties of HL^1 around each metal center and they are bonded through the azomethine nitrogen, pyridyl nitrogen and thiolate sulfur of each of the thiosemicarbazone moieties thus effecting a six-coordinate environment about the metal center. The atoms N3, N6, N8 and S2 constitute the equatorial plane and the atoms N1 and S1 occupy the axial positions. The present compound reveals many features similar to that of the $Mn(L^1)_2$ complex discussed in the previous chapter. For instance, in the present Ni(II) complex also, the thiosemicarbazone moiety reveals an *ZZ* conformation with *cis* configurations about both the C6–N3 and N4–C12 bonds contrary to the *ZE* conformation in the free ligand. Here the S1–C12–N4–N3 torsion angle value is $2.9(7)^\circ$, which reveals a more *cis* nature of the thiocarbonyl S1 atom with the hydrazinic N3 atom here than that of $Mn(L^1)_2$. Similar to that of $Mn(L^1)_2$, the two ligand moieties in the present compound also are aligned almost perpendicular to each other, as revealed from the dihedral angle of $85.55(1)^\circ$ of the C6/N3/N4/C12/N5/S1 plane with that of the C24/N8/N9/C30/N10/S2 plane. The distortion from ideal octahedral stereochemistry is suggested by the values for the orthogonal bite angles N1–Ni1–N3 ($77.62(18)^\circ$); S1–Ni1–N3 ($79.99(13)^\circ$); N6–Ni1–N8 ($77.65(18)^\circ$) and S2–Ni1–N8 ($80.25(13)^\circ$). The maximum mean plane deviation of the equatorial plane consisting of N3, N6, N8, S2 and Ni1 is $0.0556(4) \text{ \AA}$ at N8 and the central Ni(II) atom is displaced out of this mean plane at a distance of $-0.0423(4) \text{ \AA}$.

The two metal chelate rings in one of the thiosemicarbazone moieties, comprising of atoms Ni1, N1, C5, C6, N3, N4, C12 and S1 are found to be almost coplanar with *rms* values of $0.0196(4)$ and $0.0203(4) \text{ \AA}$ respectively. A significant amount of metal-to-ligand π back bonding generates a delocalized conjugating effect along the metal – chelate rings which imparts partial single and double bond nature for the C6–N3 (azomethine) and N3–N4 (hydrazinic) bonds in the thiosemicarbazone moiety, owing to the extensive delocalization over the entire coordination framework.

The unit cell packing of the molecules viewed down the 'a' axis is shown in Fig. 5.3. The two independent molecules in the asymmetric unit constitute the

repeating unit of the crystal packing. The sets of two molecules repeat one-dimensionally in the lattice. The intermolecular $\pi - \pi$ interactions are observed at distances greater than 3.5 Å, and hence they contribute little towards the effective packing of the molecules in the lattice. However, some C–H--- π interactions, which are rather short, appear significant. The list of intermolecular interactions is given in Table 5.3.

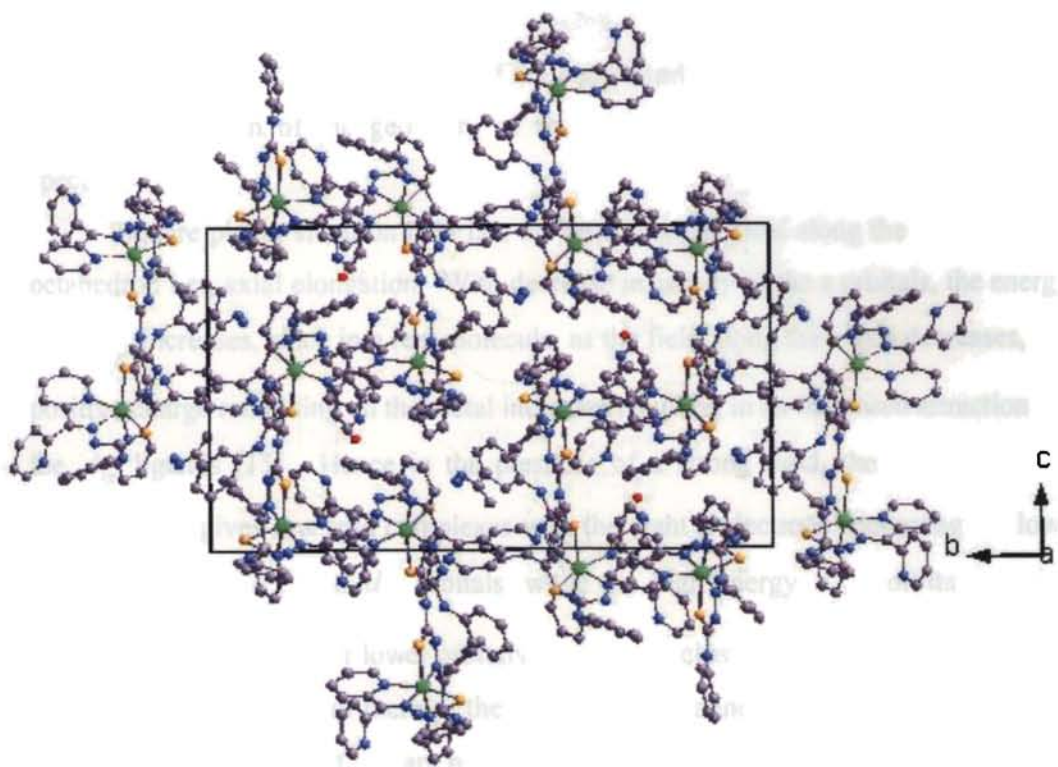


Fig. 5.3. Molecular packing diagram of $\text{Ni}(\text{L}^1)_2 \cdot 0.5(\text{H}_2\text{O}) \cdot 0.5(\text{DMF})$, the unit cell is viewed down the 'a' axis.

Spectral studies

A broad band around 3540 cm^{-1} in the IR spectrum is assigned to the –OH stretching vibrations of lattice water. The azomethine stretching band is shifted to 1562 cm^{-1} while the stretching vibration of the newly formed $\text{N}4=\text{C}12$ bond due to coordination through deprotonation appear as a sharp band at 1589 cm^{-1} . The $\delta(\text{CS})$ band observed at 806 cm^{-1} in the ligand is shifted to 745 cm^{-1} in the complex due to the coordination of the thiol form the thiosemicarbazone moiety. The compound is also characterized by solid-state electronic spectral techniques. The $\pi \rightarrow \pi^*$ and the

$n \rightarrow \pi^*$ transitions appear at 298 and 325 nm respectively. The ligand to metal charge transfer transitions are observed as a broad band at 441 nm. Weak shoulders at 551 and 587 nm correspond to the $d-d$ transitions. Selected electronic spectral data are given in Table 5.4.

5.1.2. $\text{NiL}^1\text{NCS}\cdot 2\text{H}_2\text{O}$ (15)

The compound is synthesized by the metathetical displacement of the acetate ion by thiocyanate anion in the Ni(II) complex. We were unable to obtain a single crystal suitable for X-ray diffraction of the compound, and hence the main tools used for the elucidation of the geometry of the molecule are IR, electronic and NMR spectra.

Square planar situation is in fact the limit of weak field along the 'z' axis of an octahedron i.e., axial elongation. With decrease in energy of the z orbitals, the energy of $d_{x^2-y^2}$ increases, since in a real molecule, as the field along the z axis decreases, the positive charge remaining on the metal increases resulting in an increased attraction for the d_{xy} ligands [15]. Hence in the presence of a strong field, the Ni^{2+} with a d^8 configuration gives low spin complexes with the eight d electrons occupying the low-energy d_{xz} , d_{yz} , d_{z^2} and d_{xy} orbitals, while the high energy $d_{x^2-y^2}$ orbital remains unoccupied [16]. The four lower orbitals are often so close together in energy, that the individual transitions from there to the upper d level cannot be distinguished. Hence the electronic spectra of d^8 square planar complexes with strong field ligands typically show a single band in the range of 400 – 600 nm. However, there are many examples where three transitions often in the form of weak shoulders or peaks are observed on each side of the main stronger absorption band. The electronic spectral data of the complexes are given in Table 5.4.

IR spectrum of compound 15 (Fig. 5.4.) shows a broad band near 3500 cm^{-1} supporting the presence of lattice water content consistent with the elemental analyses data. Another band is observed at 2095 cm^{-1} corresponding to the antisymmetric $\nu(\text{NCS})$ vibrations. The $\delta(\text{CS})$ band observed at 806 cm^{-1} in the ligand is shifted to regions near 751 cm^{-1} in the complex due to the enolization of thiosemicarbazone

moiety upon coordination. The azomethine stretching band in HL¹ suffers a negative shift of *ca.* 50 cm⁻¹ in the complex. A new sharp band at *ca.* 1595 cm⁻¹ is assigned to the stretching vibration of the newly formed N4=C12 bond in the thiolate form of thiosemicarbazone.

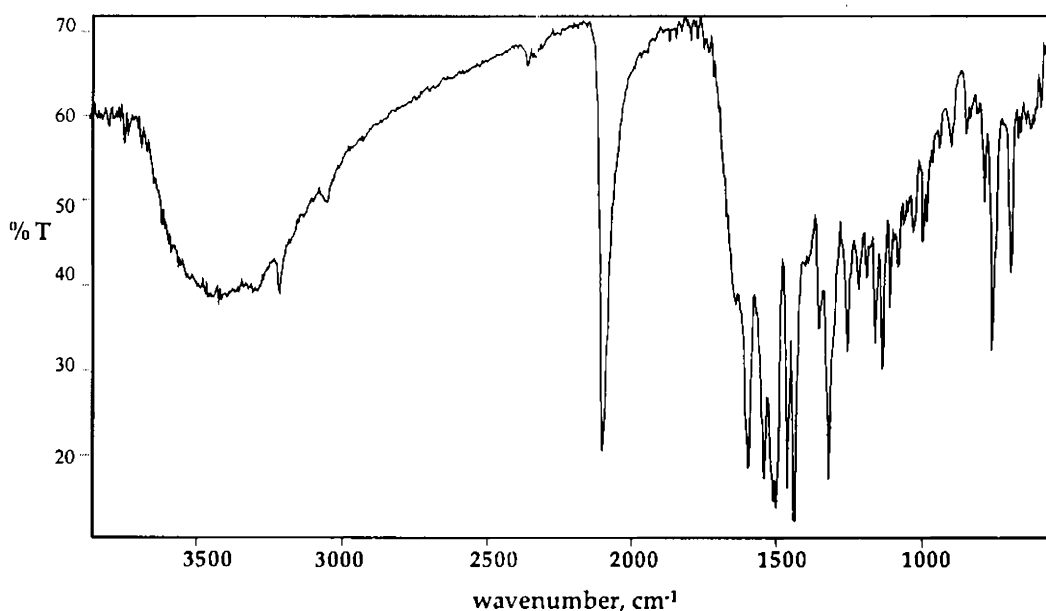


Fig. 5.4. IR spectrum of NiL¹NCS·2H₂O

The $\delta(\text{Ni}-\text{N}_{\text{NCS}})$ band at 498 cm⁻¹ shows that the thiocyanate group is N-bonded to the nickel centre. Another band at 438 cm⁻¹ is assigned to the $\nu(\text{NiN})$ vibration and it supports the coordination of the imine nitrogen. A medium band at 384 cm⁻¹ corresponds to the $\nu(\text{NiS})$ vibration confirming the coordination of thiolate sulfur. Coordination of the pyridyl nitrogen results in the $\nu(\text{NiN})$ band appearing as a strong band with two splits at 291 and 281 cm⁻¹.

The proton NMR spectrum of the compound **15** in DMSO is given in Fig.5.5. A sharp singlet at 14.55 ppm in the ¹H NMR of HL¹ is absent in the spectrum of the complex, which supports coordination of the thiosemicarbazone moiety in the thiolate form after enolization and deprotonation. The spectrum reveals three weak resonances at 9.25, 8.70 and 8.32 ppm, which do not reveal any coupling interactions in the ¹H-¹H COSY spectrum. Hence these may be assigned to the proton on the nitrogen at

N(4)-position of the thiosemicarbazone moiety, the resonance due to which splits into a triplet by quadrupole splitting. It is interesting to note that the coordination through the pyridyl nitrogen is clearly evidenced by the NMR spectra. The resonances corresponding to the protons on carbons adjacent to the pyridyl nitrogen are observed at 8.05 and 7.65 ppm in the complex, which are shifted from the corresponding values in the ligand HL¹. Both the resonances show correlation with the aromatic protons. The shift occurs due to coordination through one of the pyridyl nitrogen. However a slight shift in the resonance of the proton alpha to the uncoordinated pyridyl nitrogen may be attributed to the absence of hydrogen bonding interactions in the complex. The low intensity of the multiplets in the aromatic region may be attributed to the delocalization of electron density due to coordination in the complex. The overall quality of the spectrum is low due to the poor solubility of the sample in the deuteriated solvent.

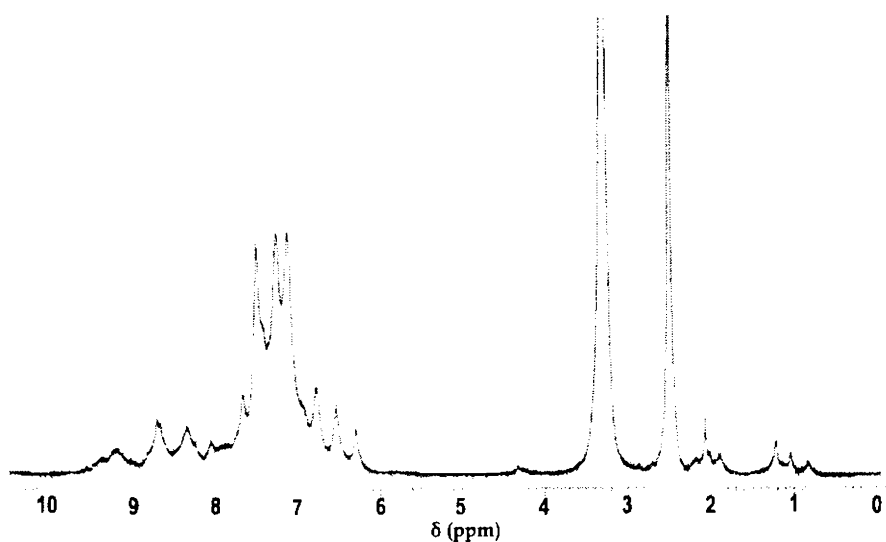


Fig. 5.5. ¹H NMR spectrum of NiL¹NCS·2H₂O

A very weak resonance at 4.3 ppm, which is more clearly observed in the COSY spectrum, indicates the presence of some water content in the solution of the complex. This may be either due to the lattice water content in the sample or due to dissolved water in DMSO. A sharp peak at 3.30 ppm corresponds to the solvent and another sharp peak at 2.5 ppm is assigned to dissolved water in the deuteriated

solvent [17]. A weak triplet centred around 2.05 ppm may be assigned to the resonance of the hydrogen bonded proton on nitrogen at the *N*(4) position, due to the presence of water content in the solution. The ^1H - ^1H COSY spectrum reveals some correlation between the peaks at 3.30 and 1.2 ppm, which helps to assign the weak peak at 1.2 ppm to that of the solvent, DMSO. Interestingly, the peak at 4.3 ppm shows some correlation with the solvent peak at 3.30 ppm, which also supports water content in the solution (Fig.5.6).

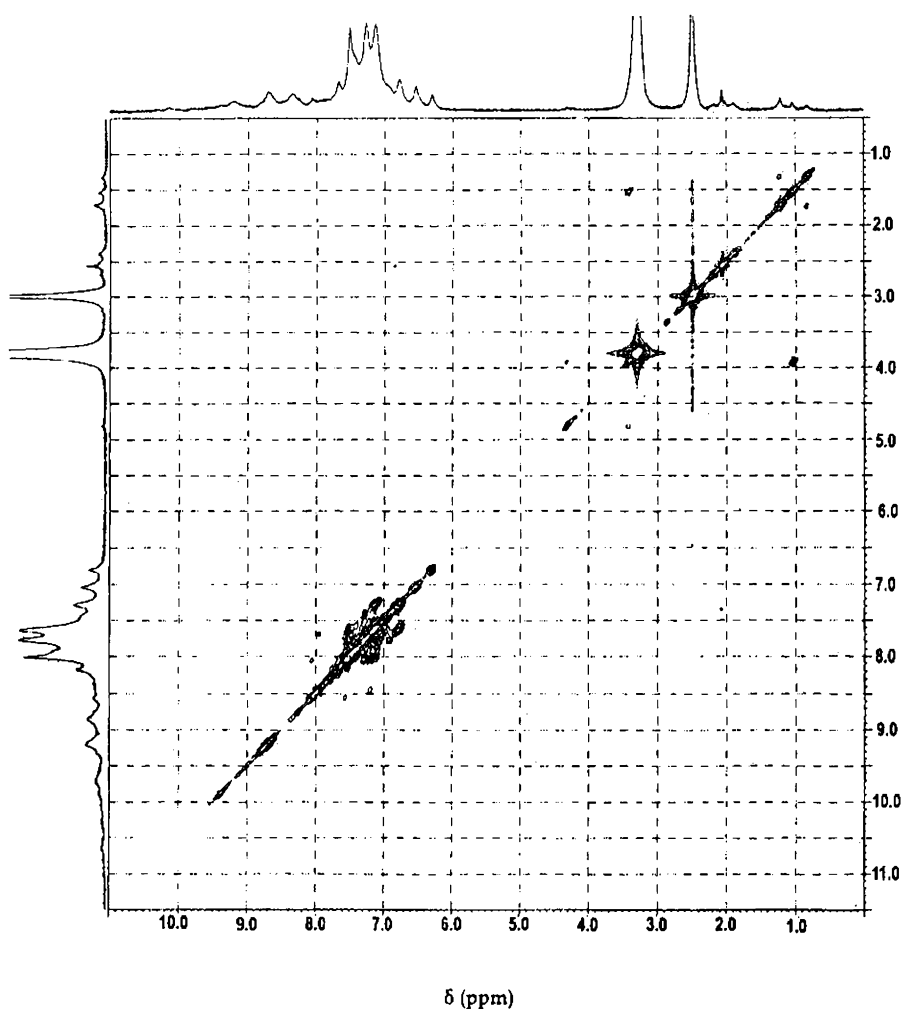


Fig. 5.6. ^1H - ^1H COSY spectrum of $\text{NiL}^1\text{NCS}\cdot 2\text{H}_2\text{O}$

5.1.3. NiL¹Cl·3H₂O (16)

The compound reveals a broad band around 3440 cm⁻¹ in the IR spectrum, which arises due to the symmetric and antisymmetric –OH stretching vibrations of lattice water. The azomethine stretching vibration is observed as a strong combination band at 1641 cm⁻¹. The δ(CS) band observed at 806 cm⁻¹ in the ligand is shifted to 749 cm⁻¹ in the complex due to the enolization of thiosemicarbazone moiety upon coordination. In the far IR region, the Ni–N_{azomethine} and Ni–S_{thiolate} stretching vibrations are observed as two strong bands at 421 and 376 cm⁻¹. A sharp band at 397 cm⁻¹ reveals the presence of terminal chlorine in the complex. The electronic spectral data are given in Table 5.4.

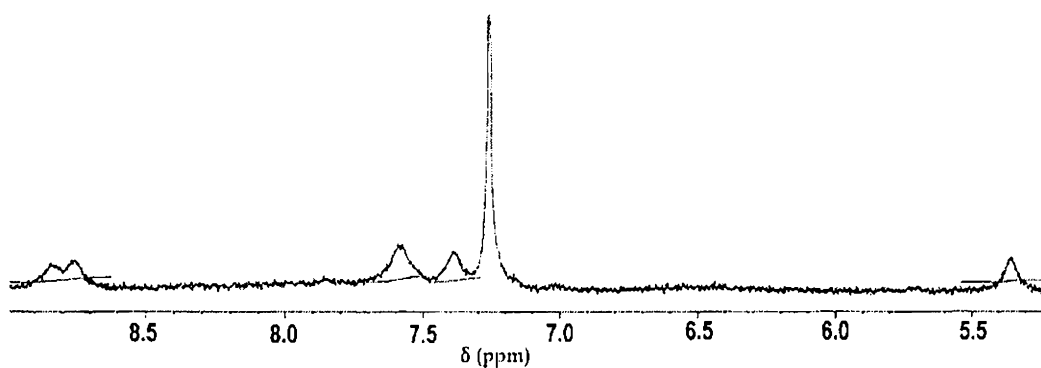


Fig. 5.7. ¹H NMR spectrum of NiL¹Cl·3H₂O

The ¹H NMR spectrum of compound **16** is very poorly resolved, perhaps due to the lack of solubility of the compound in CDCl₃. However, the sharp singlet at 14.55 ppm corresponding to the proton on imine hydrogen is absent in the present spectrum also, which provides proof for coordination of the thiolate form of HL¹ after deprotonation. The low solubility of the complex restricted our efforts to characterize the compound by ¹³C and ¹H-¹H COSY experiments. In the ¹H NMR spectrum also, only few broad peaks are visible, and their accurate assignment to respective protons is difficult. For instance, there is only a weak resonance near 8.5 ppm, which is a broad doublet and it may incorporate the resonances due to the N5H, C1H and C11H

protons. Due to the unavailability of the COSY spectrum, assignment of the peaks with the help of their observed coupling interactions could not be carried out. Similarly, there are only two weak multiplets at 7.59 and 7.40 ppm, which correspond to all the aromatic proton resonances. The low intensity nature of the peaks may also be attributed to the effect of a high electron delocalization due to complexation. A sharp peak at 7.26 corresponds to the CDCl_3 solvent. The lattice water content in the sample also shows a weak resonance at 5.36 ppm. The ^1H NMR spectrum of the compound $\text{NiL}^1\text{Cl}\cdot 3\text{H}_2\text{O}$ is shown in Fig. 5.7.

5.1.4. $\text{NiL}^1\text{N}_3\cdot 4.5\text{H}_2\text{O}$ (17)

Similar to compound 15, the compound 17 also is synthesized by the metathetical displacement of the acetate ion by azide anion in the Ni(II) complex. The IR spectrum of 17 (Fig. 5.8) reveals a sharp band at 2066 cm^{-1} corresponding to the asymmetric stretching vibrations of the coordinated azido group.

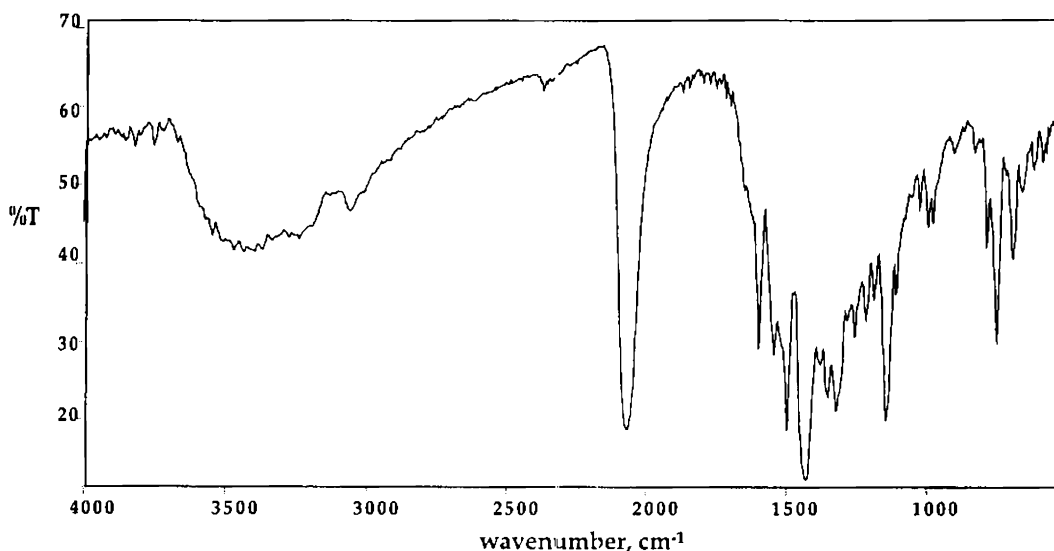


Fig. 5.8. IR spectrum of the compound $\text{NiL}^1\text{N}_3\cdot 4.5\text{H}_2\text{O}$

In the far IR region, the $\nu(\text{Ni}-\text{N}_3)$ bands are observed at 395 cm^{-1} . A band at 457 cm^{-1} is assigned to the $\nu(\text{NiN})$ vibrations supporting the coordination through the imine nitrogen. A medium band at 374 cm^{-1} indicates the $\nu(\text{NiS})$ vibrations due to

the coordination through thiolate sulfur. The stretching vibrations of the coordinated pyridyl nitrogen are observed at 298 and 285 cm^{-1} . Selected electronic spectral data are given in Table 5.4.

5.1.5. $\text{Ni}_2(\text{L}^1)_2\text{SO}_4 \cdot 4\text{H}_2\text{O}$ (18)

The elemental analyses data suggest a possible stoichiometry with two NiL^1 units and one sulfato moiety in the molecule. The IR spectrum is observed to be in accordance with a possible bridged stereochemistry, where the two NiL^1 units are connected through a sulfato group.

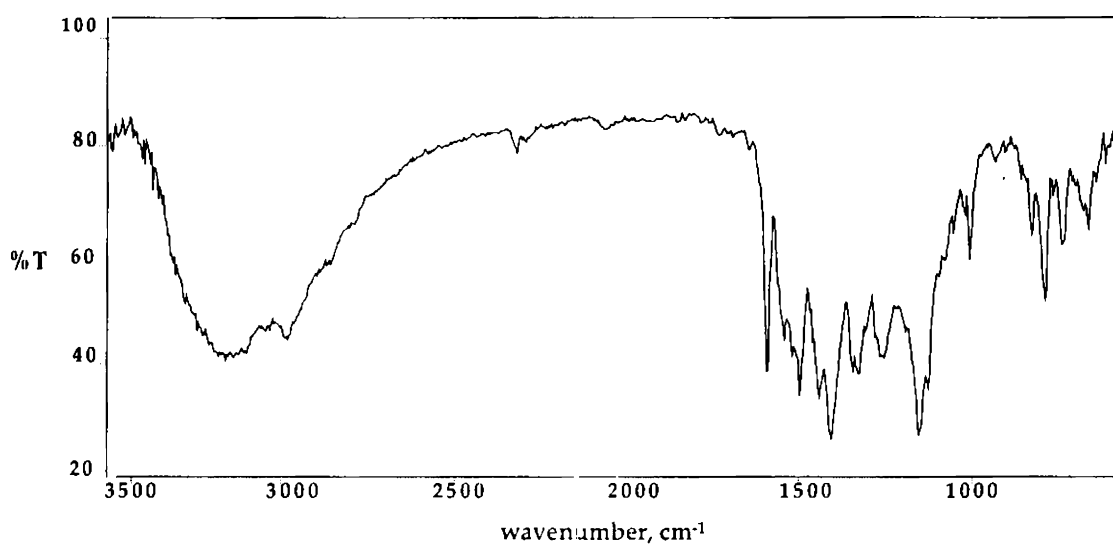


Fig. 5.9. IR spectrum of compound $\text{Ni}_2(\text{L}^1)_2\text{SO}_4 \cdot 4\text{H}_2\text{O}$

The IR spectrum of compound 18 reveals a broad band at 3235 cm^{-1} and a medium band at 3052 cm^{-1} , which can be assigned to the lattice water content and the mechanical coupling interactions involving the N(4)-H nitrogen (Fig. 5.9). We can distinguish the nature of the linkage of the sulfate anion in the complex depending upon the mode of coordination of the sulfate anion, i.e., whether unidentate, bidentate or bridged bidentate [18]. Complexation split the degenerate vibrations and all the ν_1 , ν_2 , ν_3 and ν_4 bands appear in the infrared spectra. The ν_1 and ν_2 vibrations are observed as weak bands at 979 and at 455 cm^{-1} respectively, which suggests the bridged bidentate nature of the sulfato anion in the complex. The ν_3 vibration is

observed at 1050 cm^{-1} , while the ν_3 vibrations are observed near 615 and 510 cm^{-1} , similar to the corresponding values of other complexes where the sulfate anion exists in the bridged bidentate form. The Ni-N_{azomethine} and Ni-S_{thiolate} stretching vibrations are observed at 418 and 385 cm^{-1} . The azomethine stretching vibration is observed as a strong combination band at 1541 cm^{-1} . The $\delta(\text{CS})$ band observed at 806 cm^{-1} in the ligand is shifted to regions near 789 cm^{-1} in the complex due to the enolization of thiosemicarbazone moiety upon coordination. Electronic spectral data are given in Table 5.4.

5.1.6. NiL²NCS·2H₂O (19)

The compound is synthesized by the metathetical displacement of the acetate ion by thiocyanate anion in the Ni(II) complex. The elemental analyses data, suggest a possible four-coordinate stoichiometry NiL²NCS·2H₂O for the compound. In HL², a distinct peak is observed at 3516 cm^{-1} in the IR spectrum, corresponding to the -OH stretching vibration of the hydroxyl group at C6. In the IR spectrum of the present compound, the intensity of this peak is observed to be reduced, giving support for a possible coordination through the oxygen atom of the hydroxyl group. The cyclohexyl stretching vibrations are observed at 2920 and 2830 cm^{-1} . A band near 2400 cm^{-1} in the spectrum is assigned to instrumental noise. The asymmetric stretching vibrations of the coordinated thiocyanato group appear as a sharp band at 2064 cm^{-1} . Since no bands are observed above 2100 cm^{-1} , a possible coordination through the sulfur atom of the thiocyanate group is ruled out. A medium $\nu(\text{Ni-N}_{\text{NCS}})$ band at 475 cm^{-1} in the far IR region further supports the N-bonded nature of the thiocyanate group. This is in accordance with the commonly observed trend that the elements of first transition series usually form M-N_{NCS} bonds. However, other factors such as the oxidation state of the metal, the nature of other ligands in the complex, and steric consideration are also found to influence the mode of coordination [18]. Bands due to the azomethine stretching and thiolate bending vibrations are shifted from that of the ligands due to coordination in the complex. The lattice water vibrations appear as several small bands around 3400 cm^{-1} , due to their variation in the extent of hydrogen bonding. Electronic spectral data are given in Table 5.4.

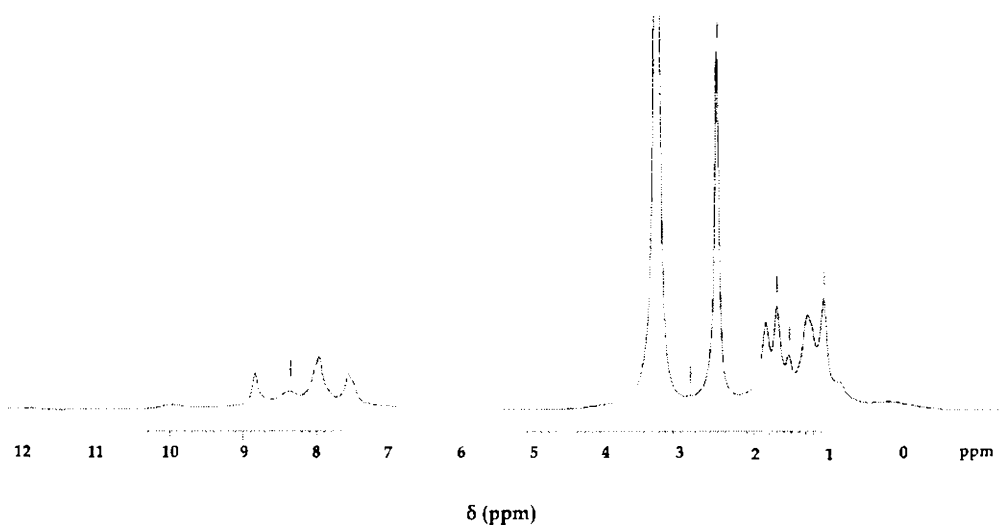


Fig. 5.10. ^1H NMR spectrum of $\text{NiL}^2\text{NCS}\cdot 2\text{H}_2\text{O}$

The ^1H NMR and the COSY spectrum of the compound **19** in DMSO are given in Figs. 5.10 and 5.11 respectively. Two medium peaks at 8.80 and 7.99 ppm correspond to the protons on carbons adjacent to the pyridyl nitrogens in the complex. The corresponding peaks are observed at 8.79 (C1H) and 8.60 (C11H) ppm respectively in HL^2 .

It may be noted that the C11H resonance is shifted in the complex due to coordination through the N1 nitrogen. A low intensity peak at 8.32 ppm is assigned to the proton on N3 nitrogen. This assignment is based upon the ^1H - ^1H COSY spectrum, which reveals no correlation peaks for the resonance at 8.35 ppm. However, another peak at 7.50 ppm which shows no correlation with the aromatic protons, but which gives cross peaks with the C13H resonance at 2.86 ppm is assigned to the proton on N5. It should be noted that the resonances of the protons attached to nitrogen atoms are shifted downfield in the complex, when compared to the corresponding N3H (7.84 ppm) and N5H (7.33 ppm) resonances in HL^2 . This can be attributed to the electron withdrawal from the thiosemicarbazone moiety upon complexation. The aromatic proton resonances appear overlapped in the peaks at 7.99 and 7.60 ppm. Two sharp peaks at 3.29 and 2.49 ppm correspond to the solvent DMSO and the dissolved water content in the deuteriated solvent respectively. The cyclohexyl protons other than

that on C13 show resonances in the range 1.52–1.83 ppm and 1.05–1.27 ppm corresponding to the equatorial and axial protons. The slight variation in these resonances from that of the ligand may be attributed to the changes in stereochemistry of the ligand moiety upon coordination. The electronic spectrum reveals the $\pi \rightarrow \pi^*$ and $n \rightarrow \pi^*$ transitions of the pyridyl and imine functions and the charge transfer transitions. The electronic spectral data are given in Table 5.4.

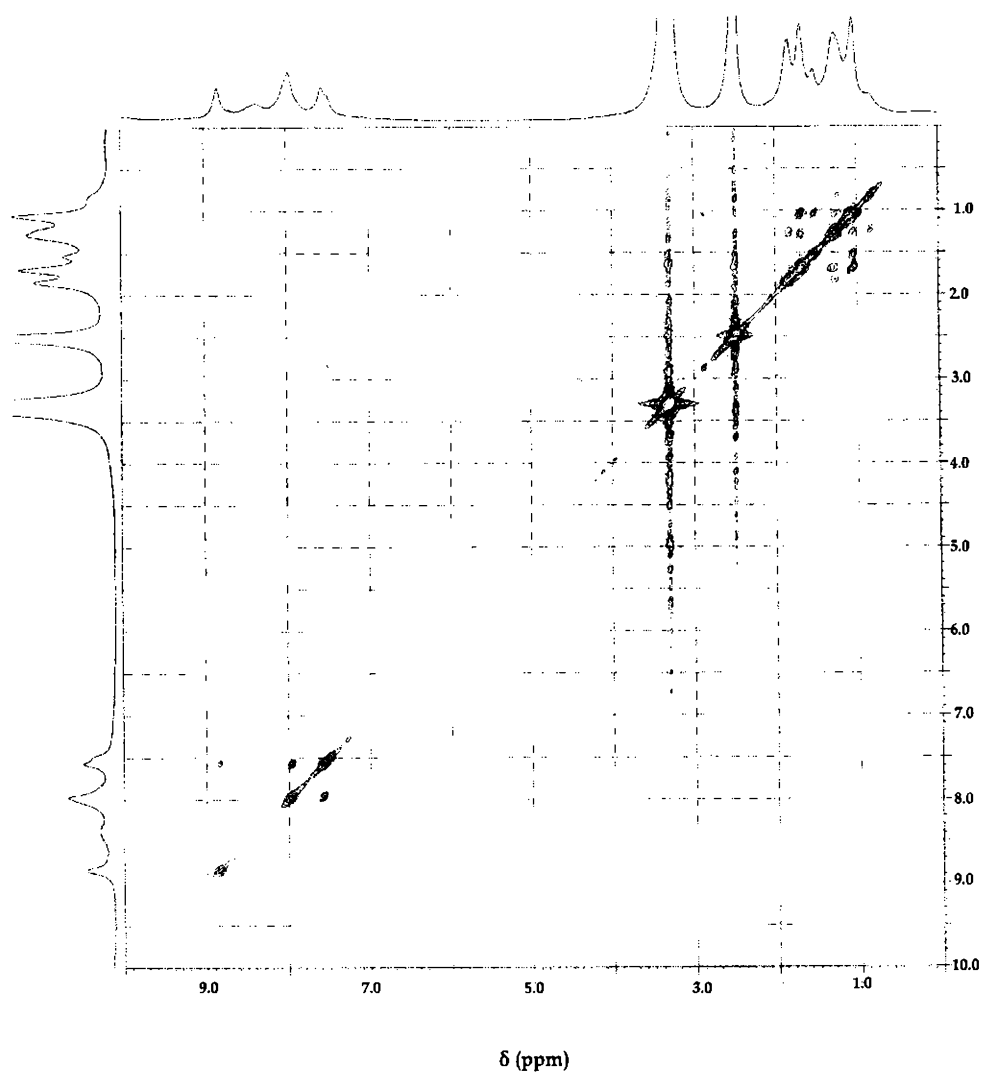


Fig. 5.11. ^1H - ^1H COSY spectrum of $\text{NiL}^2\text{NCS}\cdot 2\text{H}_2\text{O}$

5.1.7. $\text{NiL}^2\text{ClO}_4 \cdot 2\text{H}_2\text{O}$ (20)

Perchlorate ion is a weakly coordinating ligand and usually its complexes are prepared in non-aqueous solvents [18]. Lots of studies were carried out to investigate the mode of coordination of the perchlorate anion. It was established that the same symmetry selection rules as that of sulfato complexes could be applied to perchlorate ion also. However, the IR spectral assignments point towards a unidentate nature of the perchlorato anion in the present complex (Fig. 5.12). The characteristic stretching vibration ν_4 of the coordinated perchlorate anion is observed at 975 cm^{-1} [19]. Some weak bands are observed at 3400 and 3300 cm^{-1} region, and a weak band near 3510 cm^{-1} can be attributed to the $\nu(\text{OH})$ vibrations at C6-OH, the intensity of which is reduced due to a possible coordination to the metal center. Bands around 3300 cm^{-1} are due to the presence of non-hydrogen bonded lattice water. A weak band at 3050 cm^{-1} correspond to the stretching vibrations of the $N(4)\text{-H}$ nitrogen.

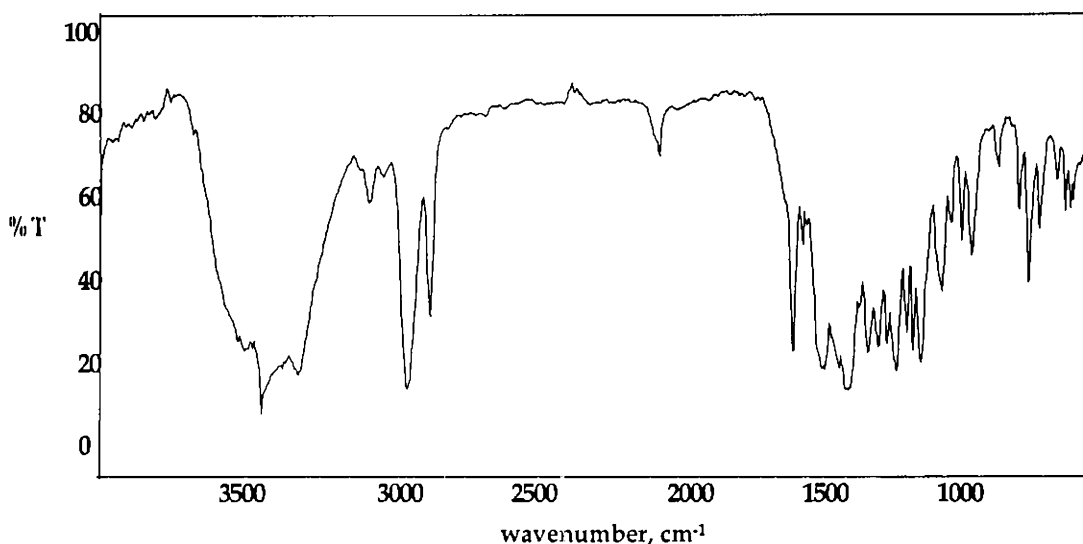


Fig. 5.12. IR spectrum of compound $\text{NiL}^2\text{ClO}_4 \cdot 2\text{H}_2\text{O}$

The azomethine stretching vibrations are observed as a strong combination band at 1554 cm^{-1} . The $\delta(\text{CS})$ band observed at 802 cm^{-1} in the ligand is shifted to 733 cm^{-1} in the complex due to the enolization of thiosemicarbazone moiety upon

coordination. The cyclohexyl stretching vibrations are observed as sharp bands at 2932 and 2850 cm^{-1} . A band near 2050 cm^{-1} in the spectrum is assigned to instrumental noise. The far IR spectrum reveals the $\nu(\text{NiN})$ band at 465 cm^{-1} supporting the coordination through the azomethine nitrogen. The $\nu(\text{NiS})$ vibration of the coordinated thiolate sulfur is observed as a medium band at 363 cm^{-1} . Coordination of the pyridyl nitrogen results in the $\nu(\text{NiN})$ band appearing as a strong band with two splits at 265 and 257 cm^{-1} .

In the solid-state electronic spectrum, the $\pi \rightarrow \pi^*$ and the $n \rightarrow \pi^*$ transitions appear as a broad band with two shoulders at 302 and 326 nm which correspond to the two transitions respectively. However, the ligand to metal charge transfer transitions are more clearly observed in the electronic spectrum, as a strong peak at 443 nm. The $d-d$ transitions appear as very weak shoulders at 557 and 590 nm (Table 5.4).

The ^1H NMR spectrum of the compound **20** (Fig. 5.13) is better resolved when compared to that of **19**. This may be due to the better solubility of the present compound in DMSO (Fig. 5.14).

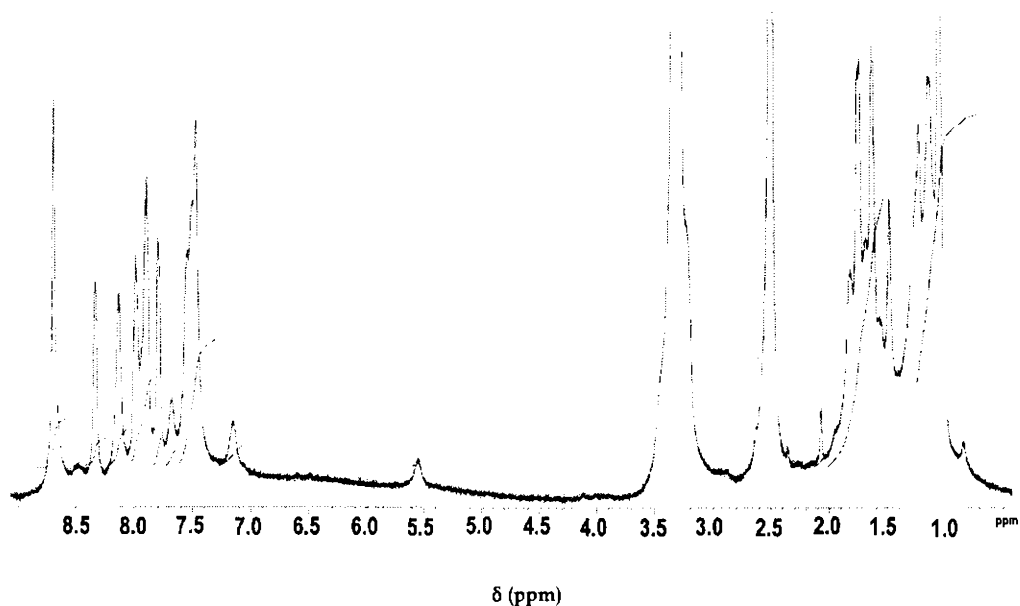


Fig. 5.13. ^1H NMR spectrum of $\text{NiL}^2\text{ClO}_4 \cdot 2\text{H}_2\text{O}$

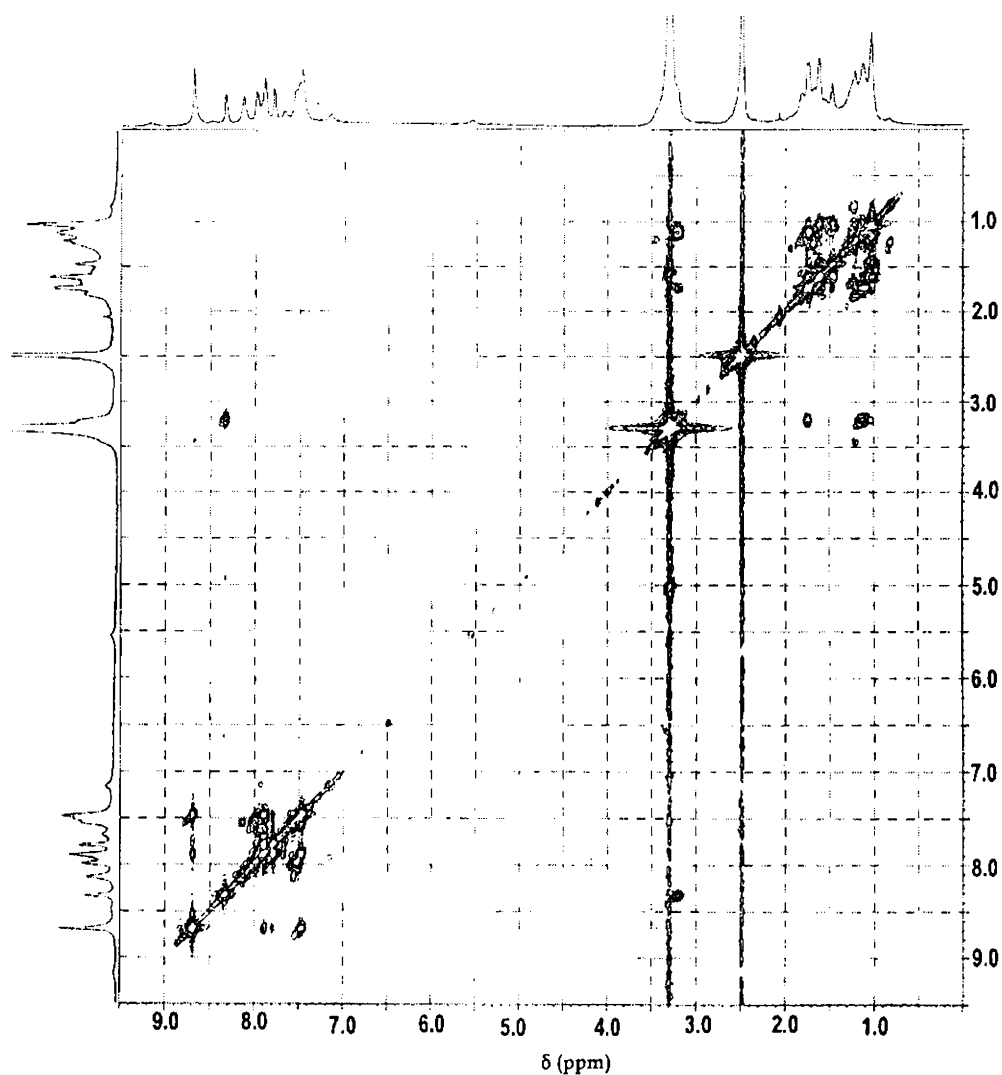


Fig. 5.14. ^1H - ^1H COSY spectrum of $\text{NiL}^2\text{ClO}_4 \cdot 2\text{H}_2\text{O}$

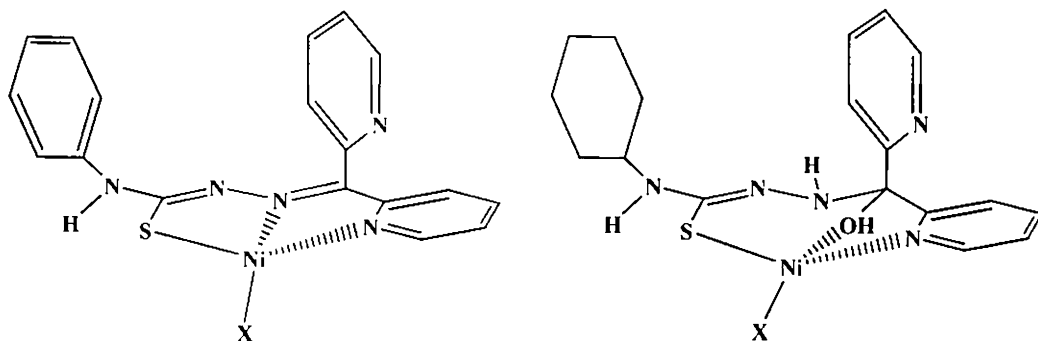
The peaks at 8.70 and 8.10 ppm may be assigned to the alpha proton resonances on pyridyl rings and they show interaction with the aromatic protons. One of the alpha proton resonances is shifted as a result of coordination of one of the pyridyl nitrogens. The peaks in the range 7.98 – 7.47 ppm correspond to the protons in the aromatic region. Another peak at 7.15 ppm, which gives no correlation peaks at all, is assigned to the N3H proton. A low intensity peak at 5.50 ppm can be assigned to the coordinated –OH group at C6. However, there are two sharp peaks at 3.30

and 2.50 ppm corresponding to the deuteriated solvent and the dissolved water content in the solvent. The peak around 3.25 ppm is assigned to the C13H proton, based upon its correlation interaction with the cyclohexyl axial protons. The equatorial and axial protons other than C13H on the cyclohexyl moiety show their resonances in the range of 1.03 – 2.10 ppm and they reveal extensive coupling interactions between each other.

5.1.8. NiL²Cl·0.5H₂O (21)

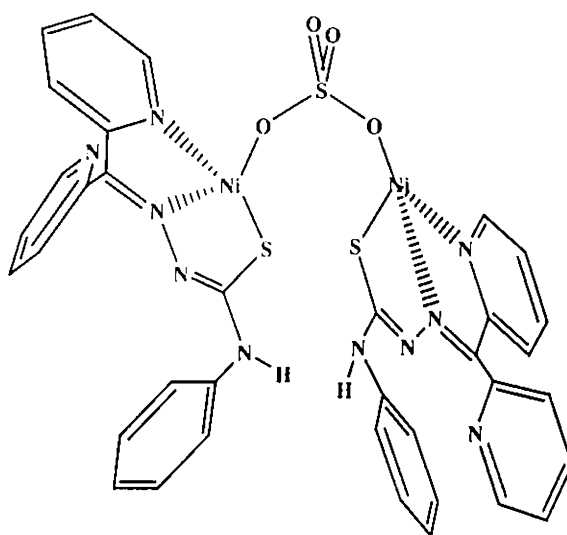
A broad band centred on 3400 cm⁻¹ establishes the presence of hydrogen bonded lattice water content in the samples. There is no intense band around 3510 cm⁻¹, which supports coordination through the oxygen of C6-OH. The cyclohexyl stretching vibrations appear as two sharp bands at 2929 and 2852 cm⁻¹. The azomethine stretching vibration is observed as a combination band at 1642 cm⁻¹, while the newly formed N4=C12 bond due to enolization of the ligand resonate at 1562 cm⁻¹. In the far IR region, the $\nu(\text{NiN})$ vibration involving the azomethine bond, and the $\nu(\text{NiS})$ vibration of the thiolate bond are observed at 421 and 353 cm⁻¹ respectively. The terminal chloro ligand reveals a sharp band corresponding to $\nu(\text{NiCl})$ vibration at 347 cm⁻¹. The solid-state electronic spectrum reveals the $\pi \rightarrow \pi^*$ and $n \rightarrow \pi^*$ transitions as one broad peak at 317 nm. The S \rightarrow Ni and Py \rightarrow Ni charge transfer transitions appear as a broad band centered around 438 nm. The *d-d* transitions are rather weak, appearing as shoulders at 510, 559 and 589 nm (Table 5.4).

Based on these structural and spectral studies, the tentative structures for the complexes (15–21) in the solid state can be proposed as given in Fig. 5.15.



X = -NCS (Compound 15)
 -Cl (Compound 16)
 -N₃ (Compound 17)

X = -NCS (Compound 19)
 -ClO₄ (Compound 20)
 -Cl (Compound 21)



Compound 18

Fig. 5.15. Tentative structures of the complexes (15–21), omitting lattice water

5.2. Magnetochemistry of the complexes

A few elements such as Fe, Co, Ni and some lanthanides are ferromagnetic—that is, they show a permanent magnetic moment even in the absence of applied magnetic fields. The reason for the ferromagnetic behaviour of these metals is explained with the help of band theory, where the individual levels of a band correspond to MOs, which extend throughout the metal lattice. For the three-dimensional crystals calculations, instead of ‘bands’, another term ‘density of states’ is used, meaning the relative number of energy levels in an arbitrarily small energy increment. Experimentally, the density of states diagram for a metal can be obtained by photoelectron spectroscopy. The metal is prepared with a clean surface in an ultrahigh vacuum ($<10^{-9}$ torr) and is irradiated with monochromatic photons. A plot of the number of emitted electrons per absorbed photons versus kinetic energy has approximately the shape of the density of states diagram, assuming that the yield of the electrons is proportional to the electronic population [20]. In the case of transition metals, some of the overlapping AOs that form bands will be the *d* orbitals, which have more angular nodes and are thus more directional than the *s* or *p* orbitals. Consequently, there will be a relatively large number of AO combinations that have essentially non-bonding overlap and nearly the same energy. The *d* orbitals are to some degree buried in the *3s* and *3p* core, reducing the overlap and hence the binding energy integral is reduced. These effects tend to narrow the *d* band in bulk transition metals. In narrow bands containing a large number of orbitals with nearly the same energy and with the Fermi surface of separation between the filled and empty portions of the band being at the high-density region, a large number of electrons near the Fermi surface will have degenerate energy. This is commonly observed in transition metals with their *d* orbitals mostly but not completely filled, such as Fe, Co and Ni. We can represent this situation in a density of states diagram of nickel metal as shown in Fig. 5.16. We use a two-sided diagram in which one side shows the density of states available to electrons with spins up (α) and the other side shows the density of states available to electrons with spins down (β).

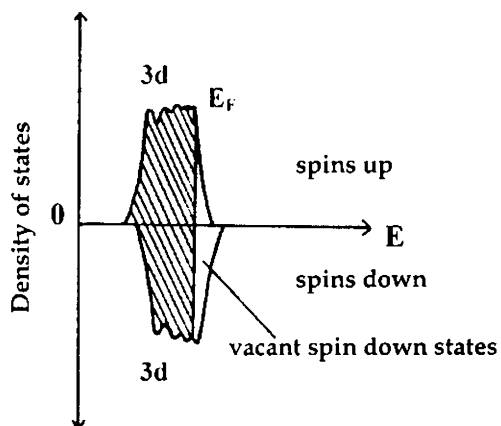


Fig. 5.16. Density of states diagram for the ferromagnetic Ni metal

The notable thing in the diagram is that the two bands are spontaneously displaced so that they are unequally filled. It can be seen that the Ni crystal has a substantial surplus of spin α electrons over spin β electrons. Thus more electrons are aligned one way than in the opposite way, and the metal has a permanent magnetic moment. This assigns ferromagnetic attributes to nickel.

Due to the extensive degeneracy of the electrons near the Fermi level, exchange energies become important in determining the spatial and spin properties of each electron. However, the thermal energy of the crystal tends to misalign the electronic spins and to bring the density of states bands together. Raising the temperature of a ferromagnet causes the magnetization to decrease. When the temperature reaches the Curie temperature, at which the thermal energy of the crystal tending to bring the bands together equals the exchange energy, the magnetisation is zero, and at temperatures above the Curie temperature, *eg.* 631 K for Ni, the metal is no longer ferromagnetic.

5.2.1. $\text{Ni}(\text{L}^1)_2 \cdot 2\text{H}_2\text{O}$

The magnetic susceptibility data for the compound $(\text{NiL}^1)_2 \cdot 2\text{H}_2\text{O}$ were collected at various temperatures between 80 and 293 K. A notable observation is that the effective magnetic moment values calculated were much reduced from the spin

only values and this suggested either an antiferromagnetic or paramagnetic interactions in the complex. In order to identify the actual magnetic attributes of the compound, the least square-fitting methods were applied. It was found that the efforts to fit the magnetic parameters into the theoretical values of Curie-Weiss equation were very unsuccessful. This prompted us to reach the conclusion that the present complex is paramagnetic with the anomalous magnetic moments explained through a possible spin-state equilibrium. This effect was observed earlier in Chapter 3 for the Cu(II) complex **2**. The variation of magnetic susceptibility with temperatures is plotted in Fig. 5.17.

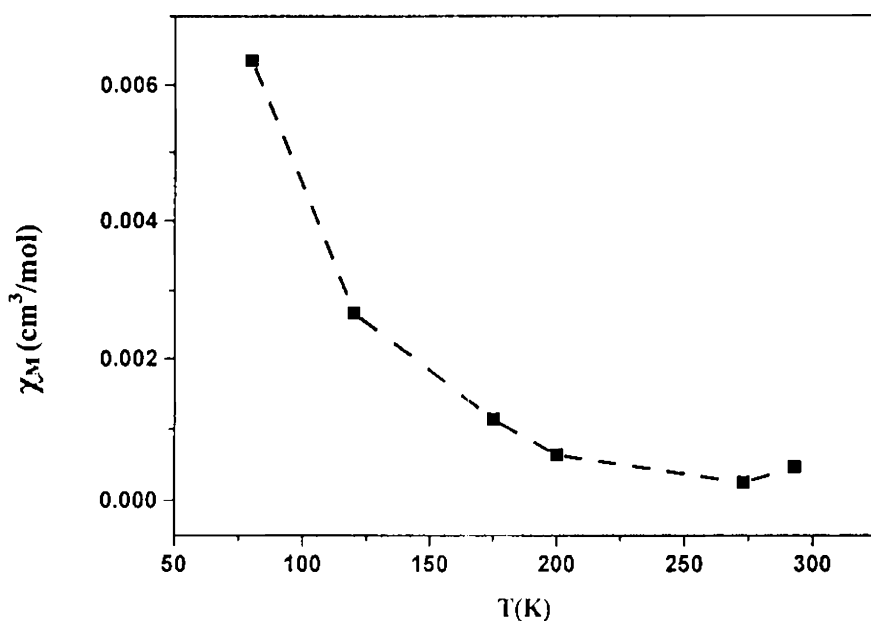


Fig. 5.17. Temperature dependence of χ_M for compound $\text{Ni}(\text{L}^1)_2 \cdot 2\text{H}_2\text{O}$

Eventhough Ni(II) complexes are mostly ferromagnetic in nature many Ni^{2+} complexes are also reported to exhibit this anomalous magnetic behaviour [21, 22]. This is because, the behaviour of the magnetically concentrated metallic lattice of a complex in a magnetic field can be quite different from that of an isolated molecule. In the present case, the compound is having an octahedral symmetry, where the Ni(II) ion exists in an orbitally nondegenerate ground state, $^3A_{2g}$ with the electronic configuration $t_{2g}^6 e_g^2$ and usually octahedral Ni(II) complexes are found to possess

effective magnetic moments near to the spin-only value for an appreciable range of temperature, since the non-degenerate ${}^3A_{2g}$ ground state denies appreciable orbital contribution to the effective magnetic moments. However, here the experimental magnetic moments lower than the spin-only values can be explained on the basis of the observed distortions from ideal octahedral geometry in the complex, which is substantiated by the single-crystal X-ray diffraction studies. In the case of tetragonally distorted octahedral complexes, the relative energies of the singlet and triplet states is very sensitive to the nature of the two ligands located axially, above and below the metal atom, and a possible spin-state isomerism can arise. As long as the effective binding strength of the axial ligands is close to that of the in-plane ligands, the structure is purely octahedral and the triplet state lies lowest in energy. As the axial ligand field strength is decreased, as in the case of a tetragonally elongated octahedron, the singlet state drops in energy relative to the triplet. Thus, at some particular point in relative axial and in-plane ligand field strengths, the singlet and triplet states should co-exist, providing some weak paramagnetic attributes to the compound. The absence of any intermolecular ferro- or antiferromagnetic interactions can also be accounted on the basis of the structure of the compound, where the bulky ligand units with strong ligand fields are likely to reduce the neighbouring interactions between adjacent molecules in the crystal lattice, thus assigning the compound magnetically dilute.

5.2.2. $\text{NiL}^1\text{N}_3 \cdot 4.5 \text{H}_2\text{O}$

In the case of compound $\text{NiL}^1\text{N}_3 \cdot 4.5 \text{H}_2\text{O}$, the magnetic susceptibility data at low temperatures revealed the effective magnetic moments higher than the spin only value of 2.83 B.M. and the values were observed to increase with decrease in temperature.

The magnetic susceptibility data collected at various temperatures between 80 and 298 K are plotted in Fig. 5.18 together with

the theoretical best-fit.

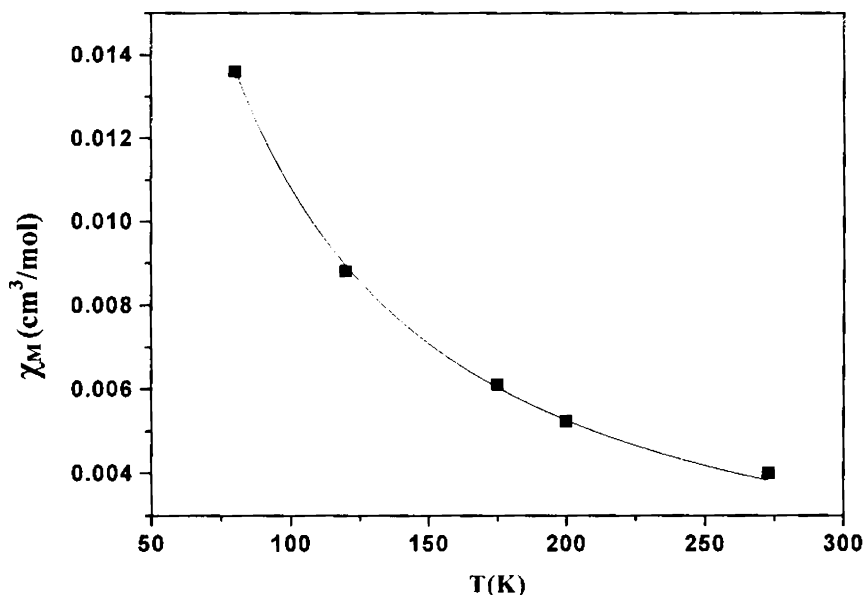


Fig. 5.18. Temperature dependence of χ_M for compound $\text{NiL}^1\text{N}_3 \cdot 4.5 \text{H}_2\text{O}$. The squares are the experimental points and the solid line is the theoretical best fit of the experimental data

The reason for the inherent ferromagnetic interactions are well accounted at the beginning of Part –II of this chapter. However, here the magnetic susceptibility data helps to assign a possible tetrahedral geometry for the four-coordinate complex, since the energy level distribution in a possible square planar structure would have predicted diamagnetic interactions at room temperature. The tetrahedral alignment of the energy levels provides a 3T_1 ground state with the electronic configuration $e_g^4 t_{2g}^4$, where an orbital contribution to the effective magnetic moment is expected. With decrease in temperature, the effective magnetic moment values are observed to increase, thus supporting the ferromagnetic interactions in the compound. Accordingly, the inherent parallel spin alignment of electrons of degenerate energy attributes the ferromagnetic interactions in the Ni(II) complex whereas the orbital contribution of the triply degenerate ground state assigns μ_{eff} values ~ 3.0 B.M.

5.2.3. $\text{Ni}_2(\text{L}^1)_2\text{SO}_4 \cdot 4\text{H}_2\text{O}$

Room temperature magnetic moment value for this compound was observed to be equal to 3.41 B.M. and at low temperatures, the μ_{eff} values are found to be much increased from the spin-only value. The magnetic susceptibility data are well-fitted into the modified Bleaney-Bowers equation (Fig. 5.19), with the best fit values of $2J = 51.20 \text{ cm}^{-1}$, $g = 2.534$, $N\alpha = -400 \times 10^{-6} \text{ emu}$ and ρ (impurity factor) = 0.4314 with $R \left\{ \sum (\chi_{\text{calc}} - \chi_{\text{obs}})^2 / \sum \chi_{\text{obs}}^2 \right\} = 2.5 \times 10^{-7}$.

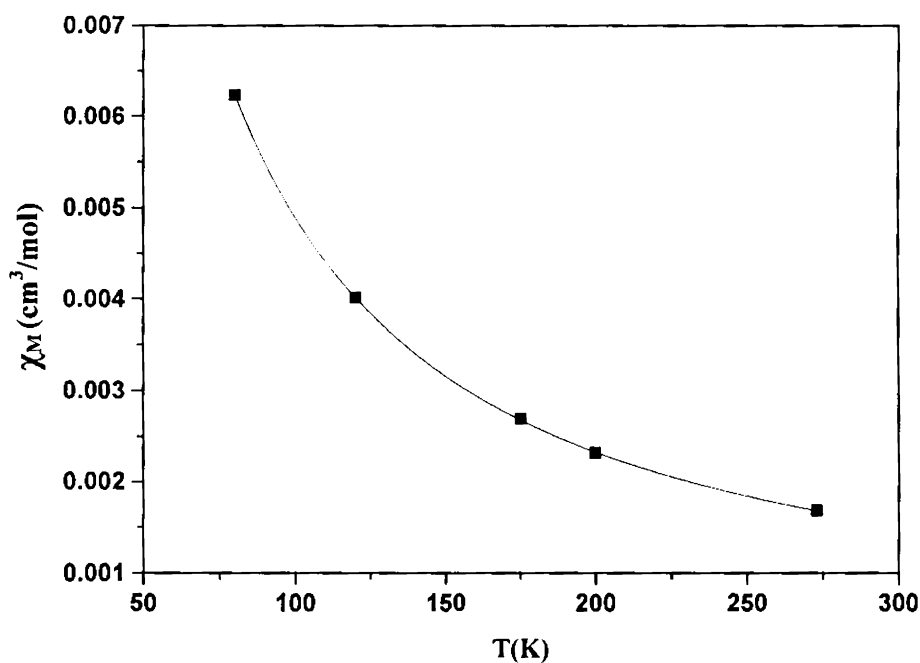


Fig. 5.19. Temperature dependence of χ_M for compound $\text{Ni}_2(\text{L}^1)_2\text{SO}_4 \cdot 4\text{H}_2\text{O}$. The squares are the experimental points and the solid line is the theoretical best fit of the experimental data

The weak ferromagnetic interactions in the present compound can be accounted on the basis of the proposed bridged structure of the complex. This usually occurs through the super-exchange interaction via the metal-ligand-metal pathway. Unlike in the case of an antiferromagnetic interaction, for the ferromagnetic interactions to occur, the ligand and metal orbitals involved in super exchange must be aligned orthogonal to each other. Here the proposed 90° exchange pathway may result from

the overlap of the non-bonding p orbital of the sulfur atom of the bridging sulfato group, the orthogonal d orbital of the interacting first Ni^{2+} atom and the orthogonal d orbital of the second Ni^{2+} atom through the Ni–S–Ni bridge, which leads to ferromagnetism. Unfortunately, in the present case, no single crystal of the compound could be isolated, which hinders detailed analyses of the interacting bond angles. However, since the spectral studies confirm the bridged nature of the complex, its ferromagnetic interactions can be reasonably accounted by the orthogonal super-exchange mechanism.

5.2.4. $\text{NiL}^2\text{Cl}\cdot 0.5\text{H}_2\text{O}$

The complex $\text{NiL}^2\text{Cl}\cdot 0.5\text{H}_2\text{O}$ (21) revealed magnetic interactions similar to compounds 2 and 14, where the experimental magnetic moments were much reduced from the spin-only values and the molar susceptibility values in the range 80–293 K returned no good-fit with the theoretical values (Fig. 5.20).

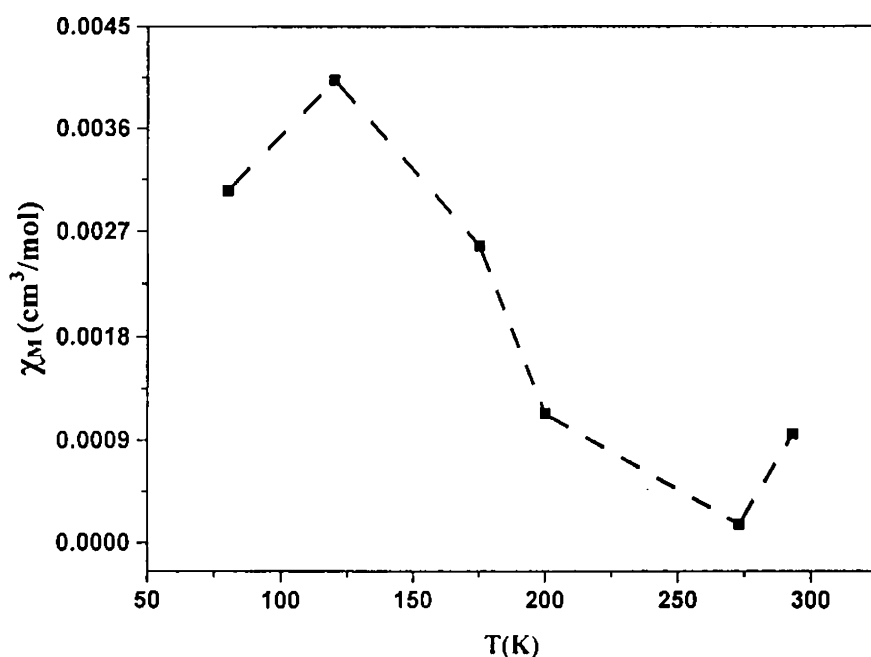


Fig. 5.20. Temperature dependence of χ_M for compound $\text{NiL}^2\text{Cl}\cdot 0.5\text{H}_2\text{O}$

Accordingly, the compound $\text{NiL}^2\text{Cl}\cdot 0.5\text{H}_2\text{O}$ is assigned to be magnetically dilute, and the inconsistent variation of the magnetic susceptibility values with temperature can be accounted on the basis of the weak paramagnetic nature of the complex. As mentioned earlier, the anomalous magnetic moment values can arise in square planar Ni(II) complexes through a thermally regulated singlet-triplet equilibrium. In $\text{NiL}^2\text{Cl}\cdot 0.5\text{H}_2\text{O}$, the nickel resides in a weak tetragonal field, and the magnetic moment is determined only by the thermal population of the low-lying paramagnetic level. Accordingly, depending upon the ligand field and consequent variation of the D_q values, in such systems, an equilibrium can arise from the thermal distribution between the singlet and triplet ground states with variation of temperature, and this attributes some amount of paramagnetic behaviour to square planar Ni(II) complexes at low temperatures. This effect is much dependent on the strength of the ligand field, and in square planar complexes, it is commonly observed in presence of anionic ligands like Cl^- and Br^- with moderate coordinating ability. With strong field ligands, the resultant complexes are diamagnetic and therefore have singlet ground states, whereas complexes of weak field ligands exhibit moments consistent with triplet ground state. In the case of moderately coordinating Cl^- and Br^- , the complexes are observed to possess magnetic moments intermediate between the two extremes of singlet and triplet ground states, which accounts for the observed spin-state equilibrium. A second contribution to this anomalous magnetic behaviour can arise from the magnetically non-equivalent sites in the unit cell, where the temperature and field dependent variation in the strength and orientation of the resultant spins can be observed.

5.2.5. $\text{NiL}^1\text{NCS}\cdot 2\text{H}_2\text{O}$, $\text{NiL}^1\text{Cl}\cdot 3\text{H}_2\text{O}$, $\text{NiL}^2\text{ClO}_4\cdot 2\text{H}_2\text{O}$ and $\text{NiL}^2\text{NCS}\cdot 2\text{H}_2\text{O}$

So far we have been discussing the paramagnetic and ferromagnetic Ni(II) complexes. The four-coordinate Ni(II) complexes usually exhibit another common magnetic behaviour, *viz.* diamagnetism. This occurs when the four-coordinate nickel complex favours a square planar geometry in the presence of a strong field. The present thiosemicarbazone ligands, with strongly electronegative nitrogen donor atoms

on the structural skeleton, with their electron density highly delocalized over a conjugated system, exert enough strong field for a square planar alignment of the ligands around the nickel atom. This results in low spin complexes with the eight d electrons occupying the low energy d_{xz} , d_{yz} , d_{z^2} and d_{xy} orbitals, while the high-energy $d_{x^2-y^2}$ orbital remains unoccupied. This assigns the diamagnetic attributes to the compound. Higher the strength of the surrounding field, greater will be the energy separation between the unoccupied $d_{x^2-y^2}$ orbital and other filled orbitals. The complex will also favour an unoccupied $d_{x^2-y^2}$ orbital since this will stabilise the complex as the lower occupied orbitals will drop in energy by a corresponding amount [16].

5.3. Experimental

Materials

Di-2-pyridyl ketone (Fluka), Ni(OAc)₂·H₂O (CDH), NiClO₄ (Fluka), NiSO₄ (Merck), NiCl₂·2H₂O (SD Fine), NaN₃ (Reidel-De Haen) and KSCN (BDH) were used as received. The solvent used, ethyl alcohol was repeatedly distilled before use.

Synthesis of ligands

Preparation of the ligands HL¹ and HL² was done as described previously in Chapter 2.

Preparation of complexes

Ni(L¹)₂·2H₂O (14): A solution of Ni(OAc)₂·H₂O (0.199 g, 1 mmol) in 10 ml of ethanol was added to an ethanolic solution of HL¹ (0.333 g, 1 mmol) and refluxed for four hours. The resulting brown product was washed with ethanol-water mixture followed by ether and dried over P₄O₁₀ *in vacuo*. Single crystals suitable for X-ray diffraction were grown by room temperature slow evaporation of a 1:1:1 solution of methanol, chloroform and dimethylformamide of the complex. Yield: 0.36 g (67 %). Elemental Anal. Found (Calc.): C, 55.83 (56.04); H, 5.09 (5.75); N, 17.71 (18.15)%.

NiL¹NCS·2H₂O (15): To ethanolic solutions of HL¹ (0.333 g, 1 mmol) Ni(OAc)₂·H₂O (0.199 g, 1 mmol) dissolved in ethanol (10 ml) was added and refluxed for the preparation of compound **15**. After fifteen minutes, aqueous solution of KSCN (0.097 g, 1 mmol) was added to the solution followed by a further refluxing for three hours. Dark brown product separated out was collected, washed with ether and dried *in vacuo*. Yield: 0.49 g (77%). Elemental Anal. Found (Calc.): C, 46.58 (47.03); H, 3.79 (3.74); N, 17.17 (17.32)%.

NiL¹Cl·3H₂O (16): A solution of NiCl₂·2H₂O (0.166 g, 1 mmol) in 10 ml of ethanol was added to ethanolic solution of HL¹ (0.333 g, 1 mmol) and refluxed for four hours. Brown product separated out was washed with ethanol followed by ether and dried over P₄O₁₀ *in vacuo*. Yield: 0.32 g (63%). Elemental Anal. Found (Calc.): C, 44.85 (44.98); H, 3.71 (4.19); N, 13.92 (14.57)%.

NiL¹N₃·4.5H₂O (17): To ethanolic solution of HL¹ (0.333 g, 1 mmol) 1 mmol of Ni(OAc)₂·H₂O (0.199 g) dissolved in ethanol (10 ml) was added and refluxed. Aqueous solution of NaN₃ (0.0651 g, 1 mmol) was then added to the solution followed by a further refluxing for three hours. Light brown product separated out was collected, washed with ether and dried *in vacuo*. Yield: 0.42 g (71%). Elemental Anal. Found (Calc.): C, 41.33 (42.05); H, 3.60 (4.51); N, 21.52 (21.79)%.

[Ni₂(L¹)₂(SO₄)·4H₂O (18): HL¹ (0.333 g, 1 mmol) was dissolved in ethanol (15 ml) and refluxed with a solution of NiSO₄ (0.223 g, 1 mmol) in 10 ml of water. Brown crystalline product separated out, which was filtered and washed with ether and dried over P₄O₁₀ *in vacuo*. Yield: 0.29 g (52%). Elemental Anal. Found (Calc.): C, 45.50 (45.50); H, 3.77 (3.82); N, 15.06 (14.74)%.

NiL²NCS·2H₂O (19): The preparation of the compound **18** is carried out in a similar way as that of compound **15**, except that the ligand HL² (0.339 g, 1 mmol) was used instead of HL¹. Yield: 0.45 g (70%). Elemental Anal. Found (Calc.): C, 44.90 (44.81); H, 4.66 (5.15); N, 16.70 (16.50)%.

NiL²ClO₄·2H₂O (20): A solution of NiClO₄ (0.171 g, 1 mmol) in 10 ml of water was added to HL² (0.339 g, 1 mmol) and refluxed for three hours. The resulting brown product was washed with ether and dried over P₄O₁₀ *in vacuo*. Yield: 0.21 g (42%). Elemental Anal. Found (Calc.): C, 39.31 (39.26); H, 4.74 (4.76); N, 12.75 (12.72)%.

NiL²Cl·0.5H₂O (21): Ethanolic solutions of HL² (0.339 g, 1 mmol) and NiCl₂ (0.129 g, 1 mmol) were mixed and refluxed continuously for four hours. Light brown product separated out, which was collected, washed with ethanol-water mixture followed by ether and dried *in vacuo*. Yield: 0.24 g (52%). Elemental Anal. Found (Calc.): C, 47.59 (47.04); H, 4.84 (5.04); N, 14.85 (15.24)%.

Table 5.1. Crystal data and structure refinement for $\text{Ni}(\text{L}^1)_2 \cdot 0.5(\text{H}_2\text{O}) \cdot 0.5(\text{DMF})$

Parameters	$\text{Ni}(\text{L}^1)_2 \cdot 0.5(\text{H}_2\text{O}) \cdot 0.5(\text{DMF})$
Empirical Formula	$\text{C}_{37.5}\text{H}_{32.5}\text{N}_{10.5}\text{NiOS}_2$
Formula weight (M)	796.07
Temperature (T) K	293(2)
Wavelength (Mo $K\alpha$) (Å)	0.71073
Crystal system	Monoclinic
Space group	$P2_1/n$
Lattice constants	
a (Å)	14.643(6)
b (Å)	29.365(11)
c (Å)	17.453(7)
α (°)	90.00
β (°)	104.476(8)
γ (°)	90.00
Volume V (Å ³)	7266(5)
Z	8
Calculated density (ρ) (Mg m ⁻³)	1.406
Absorption coefficient (μ) (mm ⁻¹)	0.696
$F(000)$	3192
Crystal size (mm)	0.35 x 0.33 x 0.31
θ Range for data collection	1.50-24.00
Limiting Indices	$-16 \leq h \leq 16, -33 \leq k \leq 33, -19 \leq l \leq 20$
Reflections collected	64276
Unique Reflections	11443 [$R_{\text{int}} = 0.1088$]
Completeness to θ	24.04 (99.8 %)
Absorption correction	Multi-Scan
Maximum and minimum transmission	0.8131 and 0.7907
Data / restraints / parameters	11443/0/1149
Goodness-of-fit on F^2	1.059
Final R indices [$I > 2\sigma(I)$]	$R_1 = 0.0784, wR_2 = 0.1447$
R indices (all data)	$R_1 = 0.1476, wR_2 = 0.1709$
Largest difference peak and hole (e Å ⁻³)	0.674 and -0.343

Table 5.2. Comparison of selected bond lengths (Å)
and bond angles (°) of HL¹ and Ni(L¹)₂·0.5(H₂O)0.5(DMF)

	HL ¹	Ni(L ¹) ₂ ·0.5(H ₂ O)0.5(DMF)
Ni1-N1		2.130(5)
Ni1-N3		2.030(4)
Ni1-S1		2.4360(18)
Ni1-N6		2.119(5)
Ni1-N8		2.030(5)
Ni1-S2		2.4296(18)
S1-C12	1.6763(12)	1.727(5)
N3-C6	1.2858(8)	1.304(7)
N4-N3	1.3573(10)	1.357(6)
N4-C12	1.3616(9)	1.314(7)
S2-C30		1.723(6)
N8-C24		1.297(7)
N9-N8		1.358(6)
N9-C30		1.325(7)
N1-Ni1-N3		77.62(18)
N1-Ni1-S1		157.49(12)
N1-Ni1-N6		90.03(17)
N3-Ni1-S1		79.99(13)
N6-Ni1-N8		77.65(18)
N6-Ni1-S1		90.13(12)
N6-Ni1-S2		157.90(13)
N6-Ni1-N3		96.27(18)
N8-Ni1-S2		80.25(13)
N8-Ni1-N1		97.05(18)
S2-Ni1-N1		93.05(12)

Table 5.3. H-bonding, π - π and CH \cdots π interaction parameters of the compound Ni(L')₂·0.5(H₂O)0.5(DMF)

H-bonding					
Donor \cdots H \cdots A	D-H (Å)	H \cdots A (Å)	D \cdots A (Å)	D-H \cdots A (°)	
N5-H5 \cdots S1	0.789	2.604	2.646	84.36	
C18-H18-N4	0.861	2.305	2.864	122.77	
C36-H36-N9	1.109	2.170	2.817	114.50	
N5A-H5A-S1A	0.809	2.579	2.607	82.96	
N10A-H102-S2A	0.791	2.525	2.632	88.98	
C36A-H36A-N9A	1.015	2.224	2.862	119.40	
π-π interactions					
Cg(I)-Res(I) \cdots Cg(J)	Cg-Cg(Å)	α °	β °		
Cg(13) [2] -> Cg(14) ^a	3.9396	10.65	24.98		
Cg(16) [1] -> Cg(18) ^b "	3.9148	22.61	16.87		
Equivalent position codes					
a=1+x, y, z					Cg(13)=N6, C19, C20, C21, C22, C23
b=1/2+x, 1/2-y, 1/2+z					Cg(14)=N6A, C19A, C20A, C21A, C22A, C23A
					Cg(16)=N7A, C25A, C26A, C27A, C28A, C29A
					Cg(18)=C13A, C14A, C15A, C16A, C17A, C18A
C-H$\cdots$$\pi$ interactions					
X-H(I) \cdots Cg(J)	H..Cg(Å)	X-H \cdots Cg (°)	X..Cg (°)		
C19-H19[2] -> Cg(1) ^a	2.8675	107.16	3.2766		
C19-H19[2] -> Cg(3) ^a	3.0398	100.47	3.3460		
C19A-H19A[1] -> Cg(5) ^a	2.8129	105.74	3.2129		
C1A-H1A[1] -> Cg(6) ^a	3.0189	106.78	3.4276		
Equivalent position code					
a=x, y, z					Cg(1)=N11, S1, C12, N4, N3
					Cg(3)=N11, N1, C5, C6, N3
					Cg(5)=N11A, S1A, C12A, N4A, N3A
					Cg(6)=N11A, S2A, C30A, N9A, N8A

Table 5.4. Electronic spectral data (nm) of Ni(II) complexes

Compound	$\pi \rightarrow \pi^*$	$n \rightarrow \pi^*$	Charge transfer	d-d
HL ¹	283	358	--	--
Ni(L ¹) ₂ ·2H ₂ O (14)	298	325	441 b	551 sh 587 sh
NiL ¹ NCS·2H ₂ O (15)	353	379	408 423 449	489 578 b
NiL ¹ Cl·3H ₂ O (16)	270 284	314	434 b	512 sh 558 sh
NiL ¹ N ₃ ·4.5H ₂ O (17)	299	322	417 sh 446 b	585 sh
[Ni ₂ (L ¹) ₂ (SO ₄)]·4H ₂ O (18)	279	298	402 s 462 b	570 sh 637 sh
HL ²	259 268	353 b	--	--
NiL ² NCS·2H ₂ O (19)	289	357 sh	381 b 398 sh 425 sh	538 sh 593 sh
NiL ² ClO ₄ ·2H ₂ O (20)	302	326	443 b	557 sh 590 sh
NiL ² Cl·0.5H ₂ O (21)	-	317 b	438 b	510 sh 559 sh 589 sh

b = broad, s = strong, sh = shoulder

References

1. V. V. Pavlishchuk, S. V. Kolotilov, A. W. Addison, R. J. Butcher, E. Sinn, J. Chem. Soc., Dalton Trans. (2000) 335.
2. M. Wang, L. -F. Wang, Y. -Z. Li, Q. -X. Li, Z. -D. Xu, D. -M. Qu, Transition Met. Chem. 26 (2001) 307.
3. M. S. Yadawe, S. A. Patil, Transition Met. Chem. 22 (1997) 220.
4. D. X. West, A. A. Nassar, F. A. EL-Saied, M. I. Ayad, Transition Met. Chem. 23 (1998) 423.
5. H. Beraldo, W. F. Nacif, L. R. Teixeira, J. S. Reboucas, Transition Met. Chem. 27 (2002) 85.
6. J. K. Swearingen, D. X. West, Transition Met. Chem. 26 (2001) 252.
7. J. K. Swearingen, W. Kaminsky, D. X. West, Transition Met. Chem. 27 (2002) 724.
8. V. Philip, V. Suni, M. R. P. Kurup, M. Nethaji, Polyhedron 23 (2004) 1225.
9. M. A. Ali, A. H. Mirza, M. Nazimuddin, H. Rahman, R. J. Butcher, Transition Met. Chem. 27 (2002) 268.
10. X. -H. Bu, M. Du, L. Zhang, D. -Z. Liao, J. -K. Tang, R. -H. Zhang, M. Shionoya, J. Chem. Soc., Dalton Trans. (2001) 593.
11. M. -L. Tong, S. -L. Zheng, J. -X. Shi, Y. -X. Tong, H. K. Lee, X. -M. Chen, J. Chem. Soc. Dalton Trans. (2002) 1727.
12. H. Cheng, D. Chun-ying, F. Chen-jie, L. Yong-jiang, M. Qing-jin, J. Chem. Soc., Dalton Trans. (2000) 1207.
13. R. Boca, M. Gembicky, R. Herchel, W. Haase, L. Jager, C. Wagner, H. Ehrenberg, H. Fuess, Inorg. Chem. 42 (2003) 6965.
14. G. A. van Albada, R. A. G. de Graaff, J. G. Haasnoot, J. Reedijk, Inorg. Chem. 23 (1984) 1404.
15. A. B. P. Lever, Inorganic Electronic Spectroscopy, 2nd ed., Elsevier Science Publishers B. V., Netherlands, 1984.

16. J. E. Huheey, E. A. Keiter, R. L. Keiter, *Inorganic Chemistry, Principles of Structure and Reactivity*, 4th ed., Harper Collins College Publishers, New York, 1993.
17. R. M. Silverstein, G. C. Bassler, T. C. Morrill, *Spectrometric Identification of Organic Compounds*, 4th ed., John Wiley & Sons, New York, 1981.
18. K. Nakamoto *in* *Infrared and Raman Spectra of Inorganic and Coordination Compounds*, 4th ed., John Wiley & Sons, New York, 1986.
19. M. R. P. Kurup *in* *Stereochemical Investigations on Transition Metal Complexes of Biologically Active Substituted 2-acetylpyridine thiosemicarbazones*, Ph. D. Thesis, University of Delhi, 1988.
20. W. L. Jolly *in* *Modern Inorganic Chemistry*, McGraw-Hill Book Company, New York, 1989.
21. S. L. Holt (Jr.), R. J. Bouchard, R. L. Carlin, *J. Am. Chem. Soc.* **86** (1964) 519.
22. S. C. Nyburg, J. S. Wood, *Inorg. Chem.* **3** (1964) 468.

CHAPTER 6

Syntheses and studies on some Co(II) and Co(III) complexes of di-2-pyridyl ketone *N*(4)-cyclohexyl- and *N*(4)-phenylthiosemicarbazones

The synthesis and reactivity of cobalt complexes of Schiff base ligands have played an important part in the development of coordination chemistry [1,2]. The cobalt complexes of tetradentate Schiff base ligands have been extensively used to mimic cobalamin (B₁₂) coenzymes [3-6], dioxygen carriers and oxygen activators [7-9] and enantioselective reduction [10]. Some Co(III) complexes with two amines in axial positions are also used as antimicrobial agents [11]. There have also been a large number of investigations on cobalt complexes based on the metal-radical approach for molecular magnets. For instance, the Co(II) complexes of the 4, 4, 5, 5 – tetramethyl-2-(2-pyridyl)-imidazolin-1-oxyl are observed to show ferromagnetic interactions [12]. Similarly, in a binuclear Co(II) complex with a chelated iminonitroxide radical, ferromagnetic couplings are observed between the adjacent Co(II) ions through azido bridges, while antiferromagnetic couplings are observed between the Co(II) ions and organic radicals [13]. Weak ferromagnetism is also observed in chiral three-dimensional oxalato-bridged Co(II) compounds [14]. Cobalt coordination polymers based on dicyanamide and pyrazine-dioxide derivatives are reported to display weak ferro- and antiferromagnetic coupling interactions [15]. Some low-spin Co(III) complexes of *N*-aryl-2-pyridylazophenylamines are diamagnetic, however, they display a reversible $\text{Co}^{\text{III}} \rightleftharpoons \text{Co}^{\text{II}}$ reduction at -0.40 V [16]. Certain cobalt complexes of pyridine-2-carbaldehyde thiosemicarbazone are observed to show cytotoxic activity [17]. Cobalt complexes of thiosemicarbazones are well reported [18-24], however, there are only two reports on cobalt complexes of di-2-pyridyl ketone thiosemicarbazones [25, 26]. Among them too, there are no reports on the studies of their magnetic behavior. Hence, some new Co(II/III) complexes of di-2-pyridyl ketone thiosemicarbazones are synthesized and characterized and the Co(II) complexes are magnetically characterized.

6.1. Stereochemistry of the complexes

Cobalt exhibits two important oxidation states as +2 and +3, and salts of Co(II) are more stable, as they are not easily oxidised to Co(III) state. However, in basic solutions, oxidation of Co^{2+} to Co^{3+} takes place relatively easily. It is usually found that when both oxidation states of an element are subject to complex formation, the overall formation constant is greater for the higher oxidation state and thus complexation makes it difficult to be reduced. Thus, Co(III) is stabilised by complexation and Co(II) forms relatively few complexes, which are not as stable as the corresponding complexes of Co(III). However, high spin six coordinate, high/low spin five coordinate and four coordinate complexes of Co(II) are widely reported. It is observed that Co(II) forms more tetrahedral complexes than any other transition metal ion, except Zn(II), due to its d^7 configuration, which is more favourable for taking up a tetrahedral geometry than an octahedral alignment. However, the difference in the stability between the two geometries of Co(II) is small so that there exists sometimes an equilibrium between the two structures.

The ground state in a Co^{2+} tetrahedral is 4A_2 and the possible transitions are ${}^4T_2 \leftarrow {}^4A_2$; ${}^4T_1(F) \leftarrow {}^4A_2$; and ${}^4T_1(P) \leftarrow {}^4A_2$. Usually, the ${}^4T_1(F) \leftarrow {}^4A_2$ and ${}^4T_1(P) \leftarrow {}^4A_2$ transitions appear as multiple absorption in the near infrared and visible regions respectively. These bands help to distinguish between tetrahedral and octahedral structures, since the latter shows less intense bands near 1000 and 500 nm corresponding to ${}^4T_{2g} \leftarrow {}^4T_{1g}$ and ${}^4T_{1g}(P) \leftarrow {}^4T_{1g}$ transitions. The electronic spectrum of four coordinate square planar complexes of Co(II) is similar to that of the low spin five coordinate Co^{2+} complexes. This gives rise to mainly two absorption bands corresponding to ${}^2E \leftarrow {}^2A_1$ at higher and ${}^2B_1 \leftarrow {}^2A_1$ at lower energy regions. In the case of Co^{3+} , six coordinate geometry make up the majority of known Co(III) complexes. They are invariably low spin and diamagnetic with ${}^1A_{1g}$ ground state. Electronic spectra of six-coordinate low spin Co(III) complexes usually show two bands corresponding to the spin allowed transitions ${}^1T_{1g} \leftarrow {}^1A_{1g}$ and ${}^1T_{2g} \leftarrow {}^1A_{1g}$.

6.1.1. $\text{Co}_2(\text{L}^1)_2\text{Cl}_2 \cdot 4\text{H}_2\text{O}$ (**22**)

The elemental analyses data reveal a $\text{CoL}^1\text{Cl} \cdot 2\text{H}_2\text{O}$ stoichiometry for the compound **22**. But the magnetic studies reveal antiferromagnetic interactions in the compound. However, the IR studies show no bridging characteristics for the chloride anion. Hence a structure similar to that of the copper complex **3** is suggested, where the non coordinating pyridyl nitrogen of the first molecule effects a bridged structure for the complex by getting involved in a coordinate bond with the Co(II) nucleus of the second molecule (see Fig. 6.9).

In the IR spectrum of **22**, the band at 3217 cm^{-1} may be assigned to the presence of the lattice water content in the sample, while the band at 3026 cm^{-1} is assumed to be due to the N(4)-H stretching vibration. The stretching vibration of the coordinated azomethine bond and that of the newly formed N=C bond are clearly distinguishable in the spectrum. The new N=C bond formed due to deprotonation show its stretching vibration at 1596 cm^{-1} , while the coordinated azomethine vibration is observed as a low intensity band at 1543 cm^{-1} . The coordinated thiolate vibration band appears at 757 cm^{-1} . The solid-state electronic spectrum reveals the $\pi \rightarrow \pi^*$ and $n \rightarrow \pi^*$ transitions as a broad peak at 267 nm. The charge transfer transitions are observed as a shoulder at 362 nm and as a broad peak at 445 nm. The $d-d$ transitions appear as shoulders around 547 and 579 nm.

Electron Paramagnetic Resonance studies

The X-band EPR spectrum of $\text{Co}_2(\text{L}^1)_2\text{Cl}_2 \cdot 4\text{H}_2\text{O}$ (**22**) in DMSO at 77 K is given in Fig. 6.1. The spectrum reveals axial features with the g values, $g_{\parallel} = 2.282$ and $g_{\perp} = 1.994$. The Co(II) nucleus has a nuclear spin of $7/2$ and hence eight hyperfine lines are expected in the EPR spectrum in the frozen state. It is interesting to note that in the perpendicular region, these hyperfine splittings are clearly resolved (Fig. 6.1). It should be noted that the EPR spectrum at 77 K reveals that $g_{\parallel} > g_{\perp}$, which is characteristic of four coordinate square planar complexes. However in the polycrystalline state, a five coordinate geometry is proposed around each Co(II)

nucleus based on magnetically concentrated nature of the complex. Hence it can be concluded that the bridging interactions are weakened in the frozen state at 77 K.

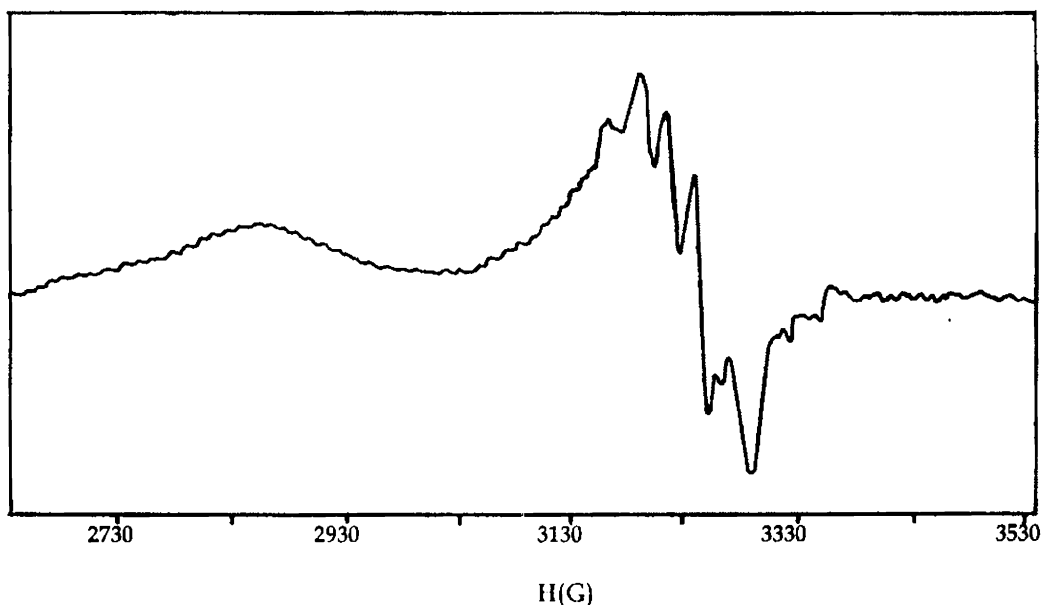


Fig. 6.1. EPR spectrum of $\text{CoL}_2\text{Cl}_2 \cdot 4\text{H}_2\text{O}$ at 77 K

6.1.2. $\text{CoL}^1(\text{NCS})_2 \cdot 3\text{H}_2\text{O}$ (23)

The elemental analyses data suggest a Co^{3+} metal centre with two thiocyanate groups in the molecule. Interestingly, the IR spectrum renders support for this stoichiometry which reveals some characteristic bands corresponding to a possible presence of more than one thiocyanate group. A strong band is observed near 2050 cm^{-1} , which is splitted into two at 2048 and 2089 cm^{-1} (Fig. 6.2). Another weak split is also observed at 2156 cm^{-1} . These all support the proposed stoichiometry of the compound and also suggest that the thiocyanate groups are N-bonded to the metal centre, since the characteristic bands are observed near or below 2150 cm^{-1} [27]. The azomethine stretching vibrations are observed as a weak band at 1560 cm^{-1} and the thiolate bending vibrations in the complex are observed as a medium band at 757 cm^{-1} , which are shifted from the corresponding values of 1592 and 806 cm^{-1} in the ligand,

thus supporting the coordinated nature of the complex. The electronic spectrum reveals the $\pi \rightarrow \pi^*$ transition at 287 nm and the $n \rightarrow \pi^*$ transitions as shoulders at 340 and 382 nm. The charge transfer transitions are observed as a shoulder at 455 nm and as a broad peak at 487 nm. The $d-d$ transitions appear as shoulders around 540 and 624 nm. However, the poor solubility of the compounds restricted their NMR studies.

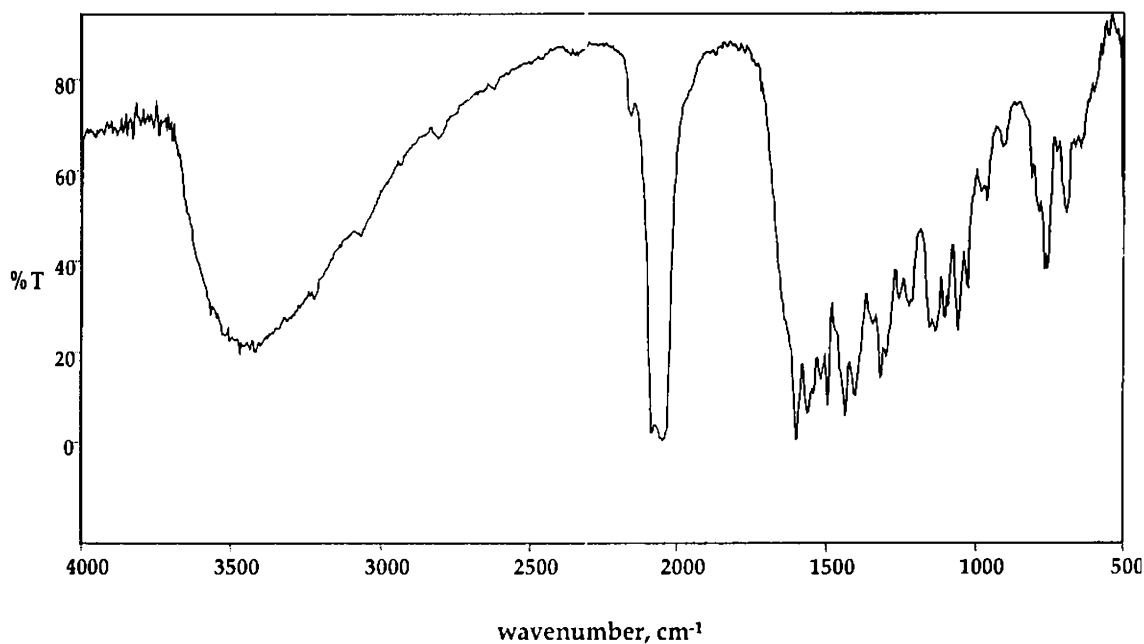


Fig. 6.2. IR spectrum of $\text{CoL}^1(\text{NCS})_2 \cdot 3\text{H}_2\text{O}$

6.1.3. $[\text{Co}(\text{L}^1)_2]\text{NO}_3 \cdot 3\text{H}_2\text{O}$ (24)

The elemental analyses suggest a possible stoichiometry where two ligand units are coordinated to the metal centre with a nitrate group in the outer sphere. The molar conductivity value is measured to be $50.08 \text{ ohm}^{-1}\text{cm}^2\text{mol}^{-1}$ in DMF, which is in the expected range for 1:1 electrolytes. The IR spectrum of the compound reveals an unsplit sharp band at 745 cm^{-1} (Fig. 6.3), and this is suggested to be the characteristic in-plane bending vibration band (ν_4) of a free $-\text{NO}_3^-$ ion [27]. Upon coordination, the ν_4 band is expected to split into two bands and a combination band, $\nu_4 + \nu_4$ may also be observed in the $1800 - 1700 \text{ cm}^{-1}$ region. Hence these support the non-coordinated

nature of the nitrate ion in the compound. Some weak bands near the 3300 and 3000 cm^{-1} region can be attributed to the stretching vibrations of the lattice water and the free $-\text{N}(4)\text{H}$ groups respectively. The bands due to azomethine stretching vibrations are shifted to 1543 cm^{-1} from a corresponding value of 1592 cm^{-1} in the ligand, the negative shift supporting the coordination of the thiosemicarbazone moiety. A weak band at 786 cm^{-1} can be assigned to the $\delta(\text{CS})$ vibrations of the coordinated thiolate sulfur. This is shifted from the corresponding value of 806 cm^{-1} in the ligand. The peaks in the electronic spectrum of the compound are also shifted from the corresponding values in the ligand, as a result of coordination. The electronic spectrum reveals the $\pi \rightarrow \pi^*$ and $n \rightarrow \pi^*$ transitions at 277 and 306 nm. The charge transfer transitions are observed as a broad peak at 458 nm and the $d-d$ transitions appear as shoulders around 529 and 577 nm.

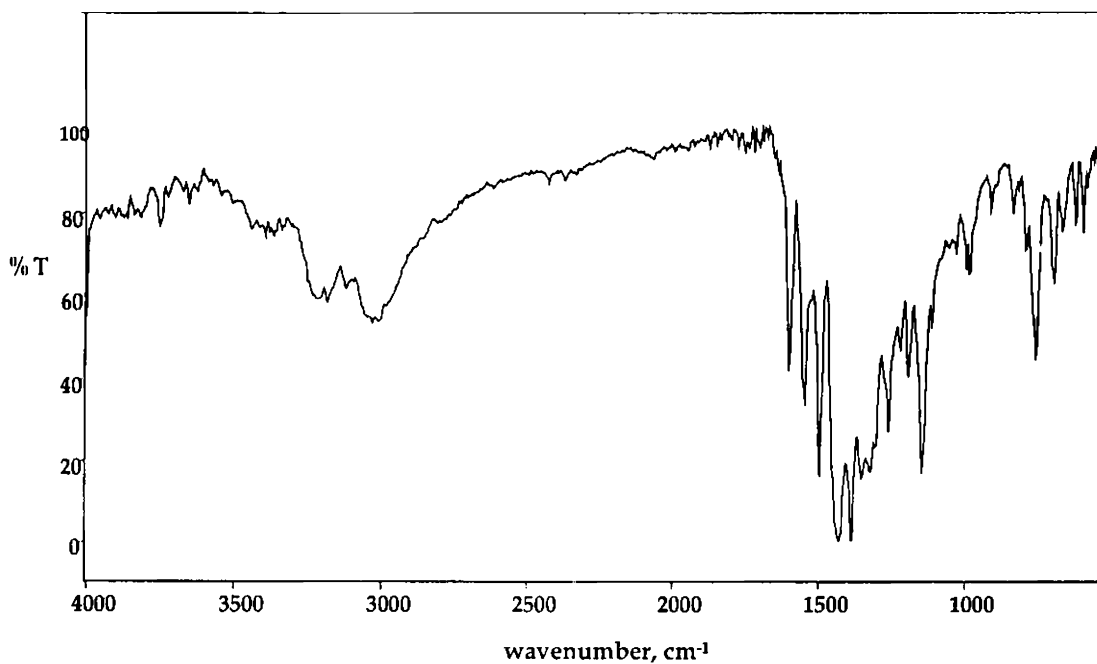


Fig. 6.3. IR spectrum of compound $[\text{Co}(\text{L}^1)_2]\text{NO}_3 \cdot 3\text{H}_2\text{O}$

6.1.4. $\text{CoL}^1\text{Br}_2 \cdot 4.5\text{H}_2\text{O}$ (25)

A broad band centred on 3420 cm^{-1} is consistent with the lattice water content in the sample. The $\nu(\text{NC})$ vibration of the newly formed $\text{N4}=\text{C12}$ bond due to

deprotonation of the thiosemicarbazone moiety appears as a sharp band at 1595 cm^{-1} . However, the azomethine vibration band is shifted to 1536 cm^{-1} as a result of coordination. The thiolate bending vibration, i.e., the $\delta(\text{CS})$ band is also shifted to 749 cm^{-1} in the complex from a value of 806 cm^{-1} in the free ligand, supporting coordination through the thiolate sulfur. The $\nu(\text{Co-N})$ of azomethine group is observed at 480 cm^{-1} while $\nu(\text{Co-S})$ of the thiolate sulphur is obtained at 375 cm^{-1} . The $\nu(\text{CoBr})$ vibrations of the terminal bromine groups appear 274 cm^{-1} . The solid-state electronic spectrum reveals the $\pi\rightarrow\pi^*$ and $n\rightarrow\pi^*$ transitions at 287 and 317 nm. The charge transfer transitions are observed at 401 nm and as shoulders at 428 and 465 nm. The $d-d$ transitions appear as shoulders around 502 and 526 nm.

6.1.5. $\text{CoL}^3\text{NCS}\cdot 2\text{H}_2\text{O}$ (26)

The IR spectrum of the compound is given in Fig. 6.4.

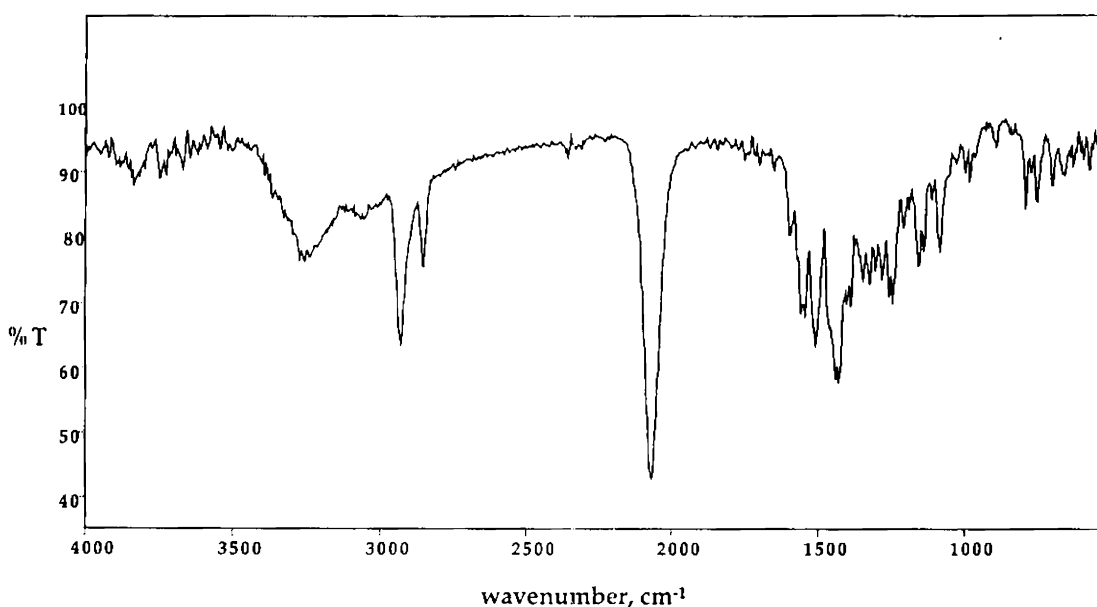


Fig. 6.4. IR spectrum of $\text{CoL}^3\text{NCS}\cdot 2\text{H}_2\text{O}$

A medium band centred on 3261 cm^{-1} is consistent with the lattice water content in the sample. A weak band around 3100 cm^{-1} can be assigned to the $\nu(\text{NH})$ vibration at the N(4)-H position. The cyclohexyl stretching vibrations appear as two

sharp bands at 2929 and 2852 cm^{-1} . A sharp band at 2067 cm^{-1} is characteristic of the N-coordinated thiocyanate group in the compound. The unsplit attribute of the band is in accordance with the presence of a single thiocyanate species in the compound, unlike in the case of compound **23**. Another interesting observation is that, unlike in other complexes, the band at 1593 cm^{-1} appears to correspond to the coordinated azomethine vibrations, based on its low intensity nature. Although negative shifts are commonly expected on coordination of the azomethine group, there are some reports on positive shifts too. The newly formed N=C bond due to enolization of the ligand resonate at 1555 cm^{-1} and the $\delta(\text{CS})$ bands appear at 747 cm^{-1} . The far IR results reveal the $\nu(\text{CoN}_{\text{azo}})$ and $\nu(\text{CoS})$ bands at 420 and 350 cm^{-1} . In the electronic spectrum, the intraligand transitions are observed as a broad peak at 306 nm and the charge transfer bands are observed at 404 nm. The $d-d$ transitions are rather weak, appearing as shoulders at 532 and 587 nm.

Electron Paramagnetic Resonance studies

The EPR spectrum of compound **26** in DMSO at 77 K is given in Fig. 6.5.

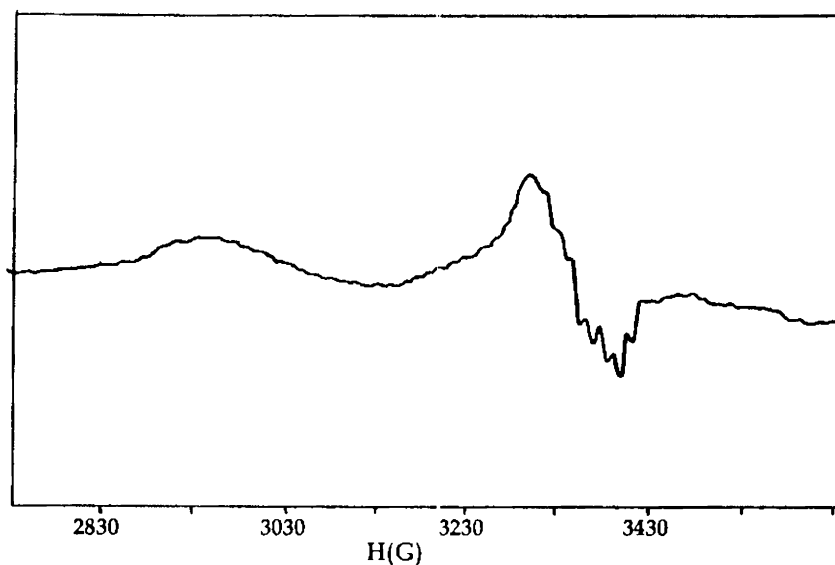


Fig. 6.5. EPR spectrum of $\text{CoL}^3\text{NCS}\cdot 2\text{H}_2\text{O}$ at 77 K

The EPR of $\text{CoL}^3\text{NCS}\cdot 2\text{H}_2\text{O}$ reveals features almost similar to that of compound **22**. The spectrum appears to be axial with two g values $g_{\parallel} = 2.299$ and

$g_{\perp} = 1.996$. Here also, the hyperfine splittings are more clearly resolved in the perpendicular region. Moreover, the value of $g_{\parallel} > g_{\perp}$, implies that the complex exists in a possible square planar geometry.

6.1.6. $[\text{Co}(\text{L}^3)_2]\text{ClO}_4$ (27)

In compound 27, the Co^{3+} nucleus appears to be six-coordinated with two ligand moieties where a perchlorate ion exists outside the coordination sphere. This stoichiometry is in accordance with the elemental analyses results. The molar conductivity value is measured to be $60.23 \text{ ohm}^{-1}\text{cm}^2\text{mol}^{-1}$ in DMF, which is in the expected range for 1:1 electrolytes. Further support for the non-coordinated nature of the perchlorate ion is given by the IR spectrum (Fig. 6.6). A strong unsplit band at 1082 cm^{-1} and a sharp band at 622 cm^{-1} can be assigned to the $\nu_3(\text{ClO}_4)$ and $\nu_4(\text{ClO}_4)$ vibrations of the free perchlorate anion [28, 29]. All these support the proposed stereochemistry for the compound.

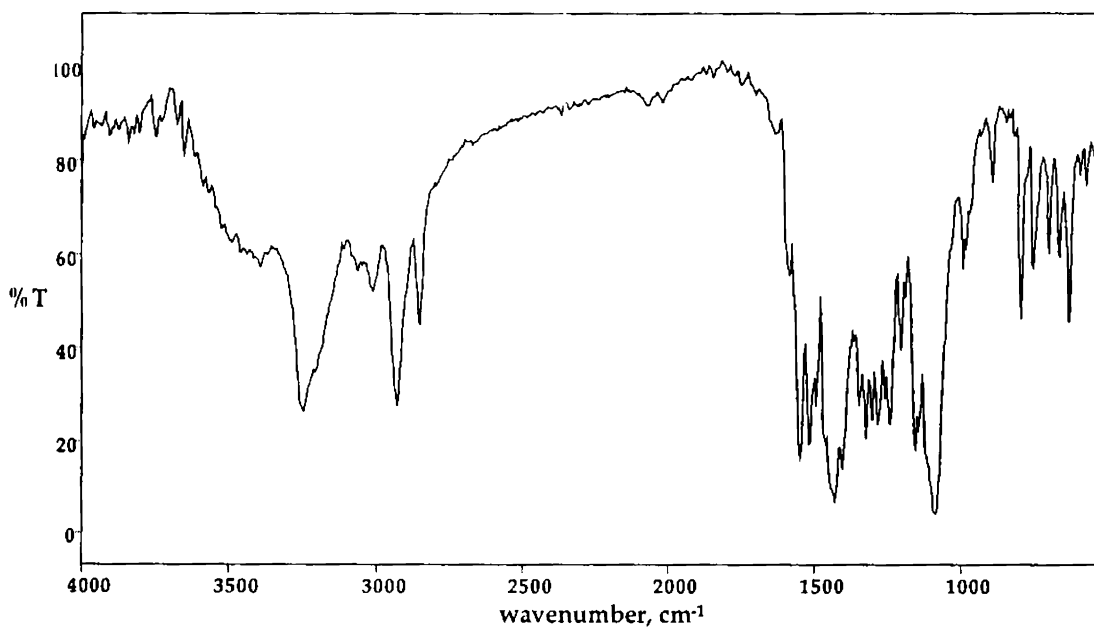


Fig. 6.6. IR spectrum of compound $[\text{Co}(\text{L}^3)_2]\text{ClO}_4$

The coordinated azomethine stretching bands are observed at 1543 cm^{-1} . The thiolate bending bands in the complex are observed at 745 cm^{-1} , which are also shifted

from the corresponding value in the ligand, due to coordination. An additional sharp band near 790 cm^{-1} may be attributed to some combination bands in the region. The electronic spectrum of the compound reveals the $\pi\rightarrow\pi^*$ and $n\rightarrow\pi^*$ transitions at 301, 321 and 385 nm. The charge transfer transitions are observed at 455 nm and as a shoulder at 470 nm. The $d-d$ transitions appear at 546 and 569 nm.

6.1.7. [Co(dpk)]Br·4H₂O (28)

The compound [Co(dpk)]Br·4H₂O (28) is the unexpected product obtained after the one-pot addition of CoBr₂ to the refluxing solution of di-2-pyridyl ketone with *N*(4)-cyclohexylthiosemicarbazide. Due to the low yield of the ligand HL³, the one-pot addition method was employed for the synthesis of its cobalt complexes. The product isolated, however, did not reveal the expected stoichiometry by elemental analyses, and attempts were made to crystallize the compound. Slow evaporation of a 1:1:1 mixture solution of methanol, chloroform and dimethylformamide yielded single crystals suitable for X-ray diffraction studies which revealed the [Co(dpk)]Br·4H₂O structure for the compound.

The molecular structure of the compound with the atom numbering scheme is given in Fig. 6.7. The structural data refinement parameters are given in Table 6.1. and the selected bond distances and bond angles are given in Table 6.2.

Here the di-2-pyridyl ketone itself acts as a ligand, by coordinating through a deprotonation of its gem-diol form. It is interesting to note that the *Co(dpk)* species in the compound reveals features close to that of an ideal octahedral stereochemistry. For instance, the four Co–N bond distances in the compounds are exactly the same, the value being 1.921(2) Å. However, both the Co–O bond distances are observed at 1.8913(19) Å, slightly less than the Co–N bond distances. This may be attributed to a possible axially compressed nature for the species. Another interesting observation is that all the O1–Co1–O1, N1–Co1–N1 and N2–Co1–N2 bond angles have turned out to be 180.00° from the crystal studies. This is very rarely observed in metal complexes of di-2-pyridyl ketone, and it implies that the metal center remains exactly in the same plane as that of the equatorial donor atoms, that is, the mean plane deviation of the

equatorial plane is zero. However, the molecule consists of an additional species of a bromide anion outside the coordination sphere. The bromide anion is positioned at a distance of 5.920 Å from the Co(III) center, and it is observed to be hydrogen bonded to four neighboring water molecules.

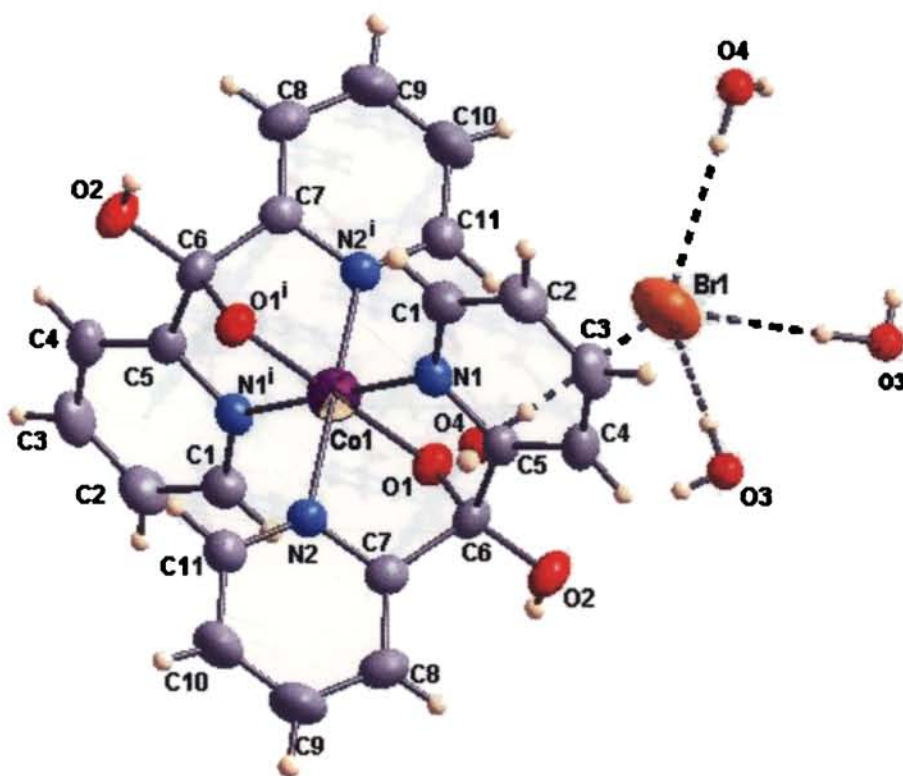


Fig. 6.7. Molecular structure of $[\text{Co}(\text{dpk})]\text{Br}\cdot 4\text{H}_2\text{O}$. The ellipsoids are shown at 50% probability

The packing of the molecules of **28** is shown in Fig. 6.8. The unit cell is viewed down the 'b' axis and a two-dimensional packing is effected in the lattice. The $\text{Co}(\text{dpk})$ units are arranged two-dimensionally in the lattice and the bromide anion and the water molecules interconnect the different $\text{Co}(\text{dpk})$ units through hydrogen bonding interactions. It is observed that the intermolecular $\pi - \pi$ and $\text{C}-\text{H}\cdots\pi$

interactions are rather weak, since they are observed at distances greater than 3.5 Å. The list of the intermolecular and hydrogen bonding interactions is given in Table 6.3.

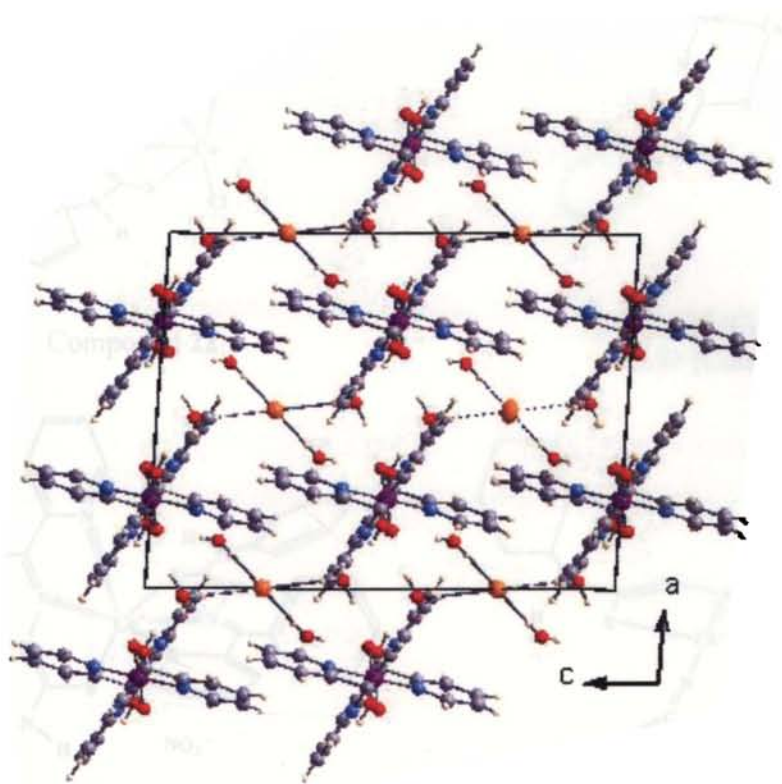
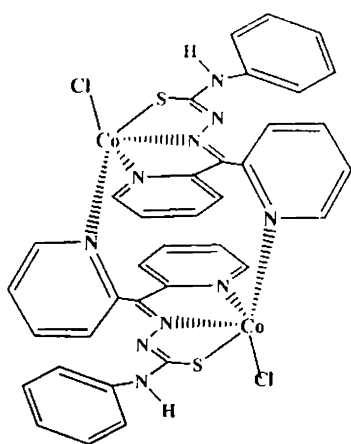
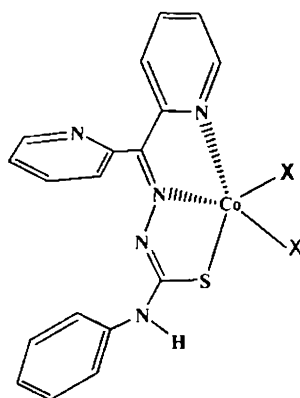
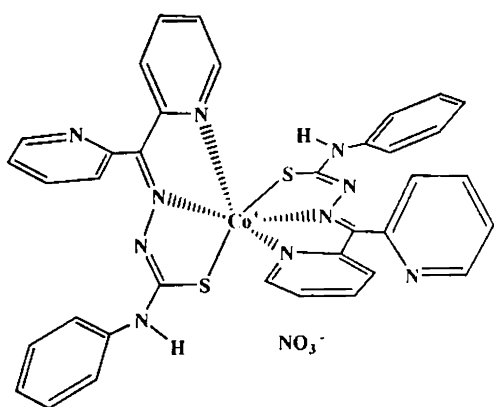


Fig. 6.8. Molecular packing diagram of $[\text{Co}(\text{dpk})]\text{Br}\cdot 4\text{H}_2\text{O}$

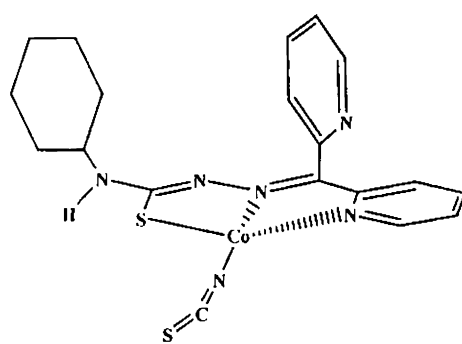
The stereochemistry of the various cobalt complexes (**22** – **27**) in the solid state can be proposed as given in Fig. 6.9.



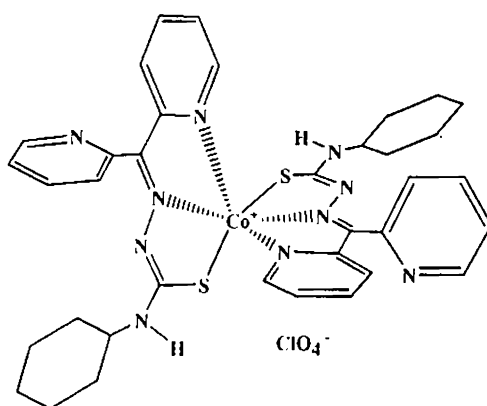
Compound 22

X = - NCS (Compound 23)
- Br (Compound 25)

Compound 24



Compound 26



Compound 27

Fig. 6.9. Tentative structures of the complexes (22 – 27) omitting the lattice water

6.2. Magnetochemistry of the complexes

The magnetic behavior of cobalt complexes is explained in a more or less similar approach as that of the corresponding nickel complexes, since both the metals possess some intrinsic ferromagnetic attributes. However, the cobalt complexes with azido and dicyanamido bridges are reported to exhibit ferro- and antiferromagnetic behavior. Monometallic cobalt complexes are also observed to show ferro- and antiferromagnetic behavior with radical ligands. For eg., a six-coordinate high-spin cobalt(II)-semiquinato complex is observed to show antiferromagnetic ordering at variable temperatures [30]. However, significant ferromagnetic interactions are observed in some heterobimetallic oxalato bridged $\text{Co}^{\text{II}}\text{Re}^{\text{IV}}$ complexes [31].

6.2.1. $\text{Co}_2\text{L}_2^1\text{Cl}_2\cdot 4\text{H}_2\text{O}$

The magnetic susceptibility data collected at various temperatures between 80 and 293 K are plotted in Fig. 6.10 together with the theoretical best-fit.

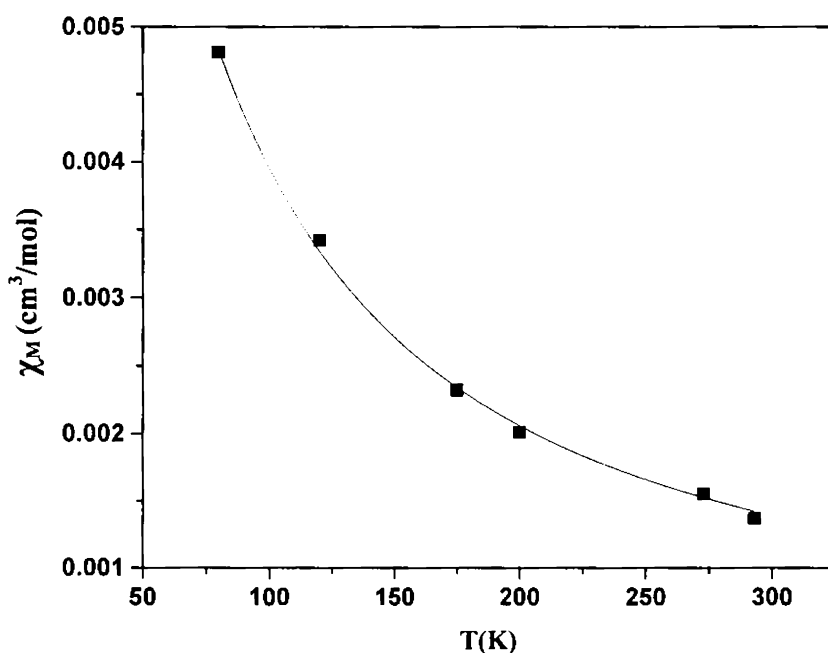


Fig. 6.10. Temperature dependence of χ_M for compound $\text{Co}_2\text{L}_2^1\text{Cl}_2\cdot 4\text{H}_2\text{O}$. The squares are the experimental points and the solid line is the theoretical best fit of the experimental data

At room temperature, the effective magnetic moment value was observed to be much reduced from the spin only value and fitting the experimental magnetic susceptibility values into the modified Bleaney-Bowers equation revealed the antiferromagnetic interactions. The best-fit values are $2J = -20.62 \text{ cm}^{-1}$, $g = 2.126$, $N\alpha = -400 \times 10^{-6} \text{ emu}$ and ρ (impurity factor) = 0.0028 with $R \left\{ \frac{\sum (\chi_{calc} - \chi_{obs})^2}{\sum \chi_{obs}^2} \right\} = 6.8 \times 10^{-4}$. The antiferromagnetic interactions in the compound can be explained through the proposed bridged structure (Fig. 6.9) of the compound, which support some exchange coupled interactions between two adjacent Co(II) nuclei through super exchange pathways. A similar effect is observed in compound 3 in chapter 3.

6.2.2. $\text{CoL}^3\text{NCS}\cdot 2\text{H}_2\text{O}$

For the compound $\text{CoL}^3\text{NCS}\cdot 2\text{H}_2\text{O}$, the magnetic susceptibility data were collected at various temperatures between 80 and 293 K (Fig. 6.11)

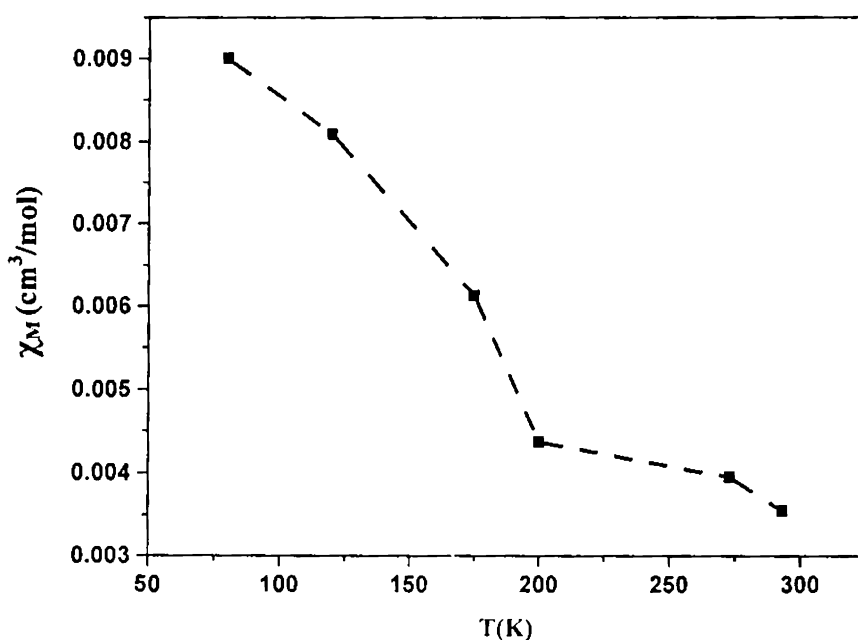


Fig. 6.11. Temperature dependence of χ_M for compound $\text{CoL}^3\text{NCS}\cdot 2\text{H}_2\text{O}$

It was observed that the effective magnetic moment values calculated are lower than the spin only values at all the experimental temperatures. However, the efforts to

fit the magnetic parameters into the theoretical values of different magnetic equations were very unsuccessful. Hence it is concluded that the present complex is paramagnetic with the anomalous magnetic moments explained through a possible spin-state equilibrium. This effect is discussed in detail in previous chapters.

6.3. Experimental

Materials

Di-2-pyridyl ketone (Fluka), $\text{CoCl}_2 \cdot 6\text{H}_2\text{O}$ (Merck), $\text{Co}(\text{OAc})_2 \cdot 4\text{H}_2\text{O}$ (BDH), $\text{Co}(\text{NO}_3)_2 \cdot 6\text{H}_2\text{O}$ (Merck), CoBr_2 (Aldrich), $\text{Co}(\text{ClO}_4)_2 \cdot 6\text{H}_2\text{O}$ (Aldrich), NaN_3 (Reidel-De Haen) and KSCN (BDH) were used as received.

Synthesis of ligands

Preparation of the ligands HL^1 and HL^3 was done as described previously in Chapter 2.

Preparation of complexes

$\text{CoL}^1\text{Cl} \cdot 2\text{H}_2\text{O}$ (22): $\text{CoCl}_2 \cdot 6\text{H}_2\text{O}$ (0.237 g, 1 mmol) in 15 ml of ethanol was added to an ethanolic solution of HL^1 (0.317 g, 1 mmol) and refluxed for four hours. Brown crystalline product separated out, which was filtered and washed with ether and dried over P_4O_{10} *in vacuo*. Yield: 0.36 g (65%). Elemental Anal. Found (Calc.): C, 46.83 (46.71); H, 4.11 (3.92); N, 15.40 (15.13)%.

$\text{CoL}^1(\text{NCS})_2 \cdot 3\text{H}_2\text{O}$ (23): For the preparation of compound **23**, at first, 1 mmol of $\text{Co}(\text{OAc})_2 \cdot 4\text{H}_2\text{O}$ (0.249 g) dissolved in ethanol (15 ml) was added to ethanolic solution of HL^1 (0.317 g, 1 mmol) and refluxed. Aqueous solution of KSCN (0.097 g, 1 mmol) was then added to the solution and further refluxed for three hours. Dark brown product separated out was collected, washed with ether and dried *in vacuo*. Yield: 0.38 g (55%). Elemental Anal. Found (Calc.): C, 42.89 (42.78); H, 3.62 (3.59); N, 16.98 (17.46)%.

[Co(L¹)₂]NO₃·3H₂O (24): A solution of Co(NO₃)₂·6H₂O (0.291 g, 1 mmol) in 10 ml of ethanol was added to HL¹ (0.317 g, 1 mmol) and refluxed for six hours. The resulting brown precipitate was washed with ether and dried over P₄O₁₀ *in vacuo*. Yield: 0.32 g (52%). Elemental Anal. Found (Calc.): C, 51.70 (51.49); H, 3.52 (4.08); N, 18.65 (18.35)%.

CoL¹Br₂·4.5H₂O (25): HL¹ (0.317 g, 1 mmol) was dissolved in ethanol (15 ml) and refluxed with CoBr₂ (0.218 g, 1 mmol) dissolved in 10 ml of hot water. Light brown product separated out was collected, washed with ether and dried *in vacuo*. Yield: 0.31 g (55%). Elemental Anal. Found (Calc.): C, 34.53 (34.20); H, 3.51 (3.67); N, 10.71 (11.08)%.

CoL³NCS·2H₂O (26) Co(OAc)₂·4H₂O (0.249 g, 1 mmol) dissolved in 10 ml methanol was added to the refluxing methanolic solution of di-2-pyridyl ketone (0.184 g, 1 mmol) and 4-cyclohexyl-3-thiosemicarbazide (0.173 g, 1 mmol). Fifteen minutes later, KSCN (0.097 g, 1 mmol) dissolved in 10 ml of water was added to the reaction mixture and further refluxed for three hours. Brown product separated out was collected, washed with ether and dried *in vacuo*. Yield: 0.40 g (58%). Elemental Anal. Found (Calc.): C, 46.22 (46.43); H, 4.72 (4.92); N, 17.80 (17.10)%.

[Co(L³)₂]ClO₄ (27): Ethanolic solution of Co(ClO₄)₂·6H₂O (0.365 g, 1 mmol) was added to the refluxing methanolic solution of di-2-pyridyl ketone (0.184 g, 1 mmol) and 4-cyclohexyl-3-thiosemicarbazide (0.173 g, 1 mmol) and further refluxed for three hours. The resulting brown precipitate was washed with ether and dried over P₄O₁₀ *in vacuo*. Yield: 0.35 g (49%). Elemental Anal. Found (Calc.): C, 50.73 (49.62); H, 5.19 (5.09); N, 16.85 (16.08)%.

[Co(dpk)]Br·3H₂O (28): The preparation of compound **28** was done in a similar way as that of compound **27** above, except that CoBr₂ (0.218 g, 1 mmol) was added instead of Co(ClO₄)₂·6H₂O. The obtained product was, however, unexpected and the elemental analyses data did not coincide with the expected structure.

Table 6.1. Crystal data and structure refinement for [Co(dpk)]Br·4H₂O

<i>Parameters</i>	[Co(dpk)]Br·4H₂O
Empirical Formula	C ₂₂ H ₂₆ N ₄ CoBrO ₈
Formula weight (M)	613.31
Temperature (T) K	293(2)
Wavelength (Mo K α) (Å)	0.71073
Crystal system	Monoclinic
Space group	C2/c
Lattice constants	
<i>a</i> (Å)	13.594(3)
<i>b</i> (Å)	10.666(2)
<i>c</i> (Å)	17.898(4)
α (°)	90
β (°)	93.886(4)
γ (°)	90
Volume V (Å ³)	2589.3(10)
Z	4
Calculated density (ρ) (Mg m ⁻³)	1.573
Absorption coefficient (μ) (mm ⁻¹)	2.258
<i>F</i> (000)	1248
Crystal size (mm)	0.45 x 0.34 x 0.33
θ Range for data collection	2.28-28.03
Limiting Indices	-17 $\leq h \leq$ 17, -13 $\leq k \leq$ 13, -20 $\leq l \leq$ 23
Reflections collected	10469
Unique Reflections	3016 [$R_{int} = 0.0567$]
Completeness to θ	27.53 (100 %)
Absorption correction	Multi-Scan
Maximum and minimum transmission	0.5210 and 0.4278
Data / restraints / parameters	3016 / 0 / 217
Goodness-of-fit on F^2	0.973
Final <i>R</i> indices [$I > 2\sigma(I)$]	$R_1 = 0.0521$, $wR_2 = 0.1056$
<i>R</i> indices (all data)	$R_1 = 0.0960$, $wR_2 = 0.1220$
Largest difference peak and hole (e Å ⁻³)	0.486 and -0.403

Table 6.2. Selected bond lengths (Å) and bond angles (°) of [Co(dpk)]Br·4H₂O

[Co(dpk)]Br·4H ₂ O	
Co1-N1	1.921(2)
Co1-N1'	1.921(2)
Co1-N2	1.921(2)
Co1-N2'	1.921(2)
Co1-O1	1.8913(19)
Co1-O1'	1.8913(19)
C6-O1	1.396(3)
C6-O2	1.382(4)
N1-Co1-N1'	180.00(13)
N2-Co1-N2'	180.00(15)
O1-Co1-O1'	180.00(0)
N1-Co1-N2	91.24(10)
N1-Co1-O1	82.86(9)
N1-Co1-N2'	88.76(10)
N1-Co1-N1	97.14(9)
N1-Co1-O1'	96.89(15)

Table 6.3. H-bonding, π - π and CH--- π interaction parameters of the compound [Co(dpk)]Br·4H₂O

H-bonding				
Donor---H---A	D-H (Å)	H---A (Å)	D---A (Å)	D-H---A (°)
O2-H2A---O4	0.800	1.816	2.602	166.98
O3-H3B---O2	0.676	2.280	2.948	169.80
O4-H4A---O1	0.860	1.863	2.703	165.23
π - π interaction				
Cg(I)-Res(1)---Cg(J)	Cg-Cg(Å)	α °	β °	
Cg(1) [1] -> Cg(1) ^a	3.7333	0.02	20.30	
Equivalent position code		Cg(1)=N1, C1, C2, C3, C4, C5		
a=-x, 1-y, 1-z				
CH--- π interactions				
X-H(I)---Cg(J)	H..Cg(Å)	X-H---Cg (°)	X..Cg (°)	
C3-H3[1] -> Cg(2) ^a	3.2197	122.90	3.8269	
C2-H2[1] -> Cg(2) ^a	3.2608	123.01	3.8341	
Cg(2)= N2, C7, C8, C9, C10, C11				

References:

1. S. Yamada, *Coord. Chem. Rev.* 190-192 (1999) 537.
2. M. Amirnasr, K. J. Schenk, A. Gorji, R. Vafazadeh, *Polyhedron* 20 (2001) 695.
3. M. M. Aly, *J. Coord. Chem.* 43 (1998) 89.
4. R. Cmi, S. J. Moore, L. G. Marzilli, *Inorg. Chem.* 37 (1998) 6890.
5. S. M. Polson, R. Cini, C. Pifferi, L. G. Marzilli, *Inorg. Chem.* 36 (1997) 314.
6. S. Hirota, E. Kosugi, L. G. Marzilli, O. Yamauchi, *Inorg. Chim. Acta* 275-276 (1998) 90.
7. A. E. Martell, D. T. Sawyer, *Oxygen Complexes and Oxygen Activation by Transition Metals*, Plenum Press, New York, 1988.
8. N. J. Henson, P. J. Hay, A. Redondo, *Inorg. Chem.* 38 (1999) 1618.
9. C. Benchini, R. W. Zoeliner, *Adv. Inorg. Chem.* 44 (1997) 263.
10. T. Nagata, K. Yoruzu, T. Yamada, T. Mukaiyama, *Angew. Chem., Int. Ed. Engl.* 34 (1995) 2145.
11. A. Botterher, T. Takeuchi, K. I. Meade, H. B. Gray, D. Cwikel, M. Kapon, Z. Don, *Inorg. Chem.* 36 (1997) 2498.
12. Y. Yamamoto, T. Suzuki, S. Kaizaki, *J. Chem. Soc. Dalton Trans.* (2001) 1566.
13. L. -Y. Wang, B. Zhao, C. -X. Zhang, D. -Z. Liao, Z. -H. Jiang, S. -P. Yan, *Inorg. Chem.* 42 (2003) 5804.
14. M. H. Molina, F. Lloret, C. R. Perez, M. Julve, *Inorg. Chem.* 37 (1998) 4131.
15. H. -L. Sun, Z. -M. Wang, S. Gao, *Inorg. Chem.* 44 (2005) 2169.
16. A. Saha, P. Majumdar, S. Goswami, *J. Chem. Soc. Dalton Trans.* (2000) 1703.
17. J. Garcia-Tojal, A. Garcia-Orad, A. A. Diaz, J. L. Serra, M. K. Urtiaga, M. I. Arriortua, T. Rojo, *J. Inorg. Biochem.* 84 (2001) 271.
18. P. Bindu, M. R. P. Kurup, *Synth. React. Inorg. Met.-Org Chem.* 30 (2000) 557.
19. P. Bindu, M. R. P. Kurup, *Indian J. Chem.* 38A (1999) 388.
20. R. P. John, A. Sreekanth, M. R. P. Kurup, S. M. Mobin, *Polyhedron* 21 (2002) 2515.

-
21. A. Sreekanth, U. L. Kala, C. R. Nayar, M. R. P. Kurup, *Polyhedron* 23 (2004) 41.
 22. H. Beraldo, W. F. Nacif, L. R. Teixeira, J. S. Reboucas, *Transition Met. Chem.* 27 (2002) 85.
 23. A. K. El-Sawaf, D. X. West, R. M. El-Bahnasawy, F. A. El-Saied, *Transition Met. Chem.* 23 (1998) 227.
 24. D. X. West, H. Beraldo, A. A. Nassar, F. A. El-Saied, M. I. Ayad, *Transition Met. Chem.* 24 (1998) 81.
 25. J. K. Swearingen, D. X. West, *Transition Met. Chem.* 26 (2001) 252.
 26. J. K. Swearingen, W. Kaminsky, D. X. West, *Transition Met. Chem.* 27 (2002) 724.
 27. K. Nakamoto *in* *Infrared and Raman Spectra of Inorganic and Coordination Compounds*, 4th ed., John Wiley & Sons, New York, 1986.
 28. M. R. P. Kurup *in* *Stereochemical Investigations on Transition Metal Complexes of Biologically Active Substituted 2-acetylpyridine-thiosemicarbazones*, Ph. D. Thesis, University of Delhi, 1988.
 29. B. H. Hathaway, A. E. Underhill, *J. Chem. Soc.* (1961) 3091.
 30. A. Caneschi, A. Dei, D. Gatteschi, V. Tangoulis, *Inorg. Chem.* 41 (2002) 3508.
 31. R. Chiozzone, R. Gonzalez, C. Kremer, G. De Munno, D. Armentano, F. Lloret, M. Julve, J. Faus, *Inorg. Chem.* 42 (2003) 1064.

CHAPTER 7

Zn(II) and Cd(II) complexes of di-2-pyridyl ketone N(4)-substituted thiosemicarbazones: Syntheses and spectral investigations

Complexes of the d^{10} metal ions such as Zn(II) and Cd(II) are of biological interest, since these metals are involved in many biomolecules. The chemical similarity of Zn(II) and Cd(II) suggests that the latter may displace the former from a critical site in the Zn(II) enzymes [1]. Considering the stereochemistry of the complexes, Zn(II) complexes are observed to be predominantly tetrahedral. Among the less common five-coordinate complexes, trigonal bipyramidal (*tbp*) geometry occurs more frequently than square-based pyramidal (*sbp*). Compared to this, Cd(II) cationic complexes are generally found in six- and four-coordination, while the five-coordinate complexes are less common and they include both *tbp* and *sbp* structures [2]. As regards to the Zn(II) and Cd(II) complexes of thiosemicarbazones, there are some interesting reports. For instance, metallic salts such as Zn(OAc)₂ and Cd(OAc)₂ are known to bring about ring-chain tautomerization of thiosemicarbazones derived from β -ketoesters and β -ketoamides [3]. During the reactions of Zn(OAc)₂ with thiosemicarbazones derived from β -ketoamides and esters in methanol, following the isolation of the corresponding Zn(II) thiosemicarbazones, the mother liquor afforded pyrazolonate complexes formed by the cyclization of the corresponding thiosemicarbazone [4]. It was also found that the cyclization is faster with Cd(OAc)₂ than with Zn(OAc)₂. In another report, Cd(II) complexes of the tripodal ligand, 1-(1-imidazolyl)-3,5-bis(imidazol-1-yl methyl)benzene are observed to exhibit anion-exchange properties [5]. Surprisingly, there are also some reports on the magnetic properties of Zn(II) complexes formed from free radicals. For instance, in the Zn(II) complex of IMP2y (4,4,5,5-tetramethyl-2-(2-pyridyl)-imidazolin-1-oxyl), a moderate intramolecular IMP2y–IMP2y antiferromagnetic interaction is estimated by the magnetic measurements [6]. Of the ‘through space’ and ‘through bond’ paths for transmission of the antiferromagnetic interaction, the former direct path has been assumed plausible for the above case. Zinc complexes of several ONS donor ligands

are reported to possess biological applications [7]. Ghosh and Parkin have designed some N_2S and NS_2 ligands, the zinc complexes of which can serve as structural models for the related zinc enzymes [8]. Spectral and biological studies have been carried out on metal complexes of 2,6-diacetylpyridine bis(*N*(4)-substituted thiosemicarbazone) [9, 10]. Mohan *et al.* reported that among the several M(II) complexes with 2,6-diacetylpyridine bis(thiosemicarbazone), only the Zn(II) complex showed a significant antitumour activity [11]. There are also some reports on one- and two-photon excited dual fluorescence properties of Zn(II) and Cd(II) complexes containing 4-dipropylaminobenzaldehyde thiosemicarbazones [12].

Mono- and bis-chelated Cd(II) complexes of di-2-pyridyl ketone Schiff base of *S*-methylthiocarbamate are reported to exhibit antibacterial and antifungal properties. It was observed that the mono-ligated Cd(II) complexes are four coordinate and tetrahedral while the bis-ligand complex is six-coordinate and octahedral [1]. However, there is only one report on Zn(II) complexes of di-2-pyridyl ketone thiosemicarbazone [13], and there are no previous reports on Cd(II) complexes of di-2-pyridyl ketone thiosemicarbazones. Hence an investigation into the stereochemistry of Zn(II) and Cd(II) complexes appeared to be quite interesting for us, and we synthesized and characterized some Zn(II) and Cd(II) complexes of di-2-pyridyl ketone thiosemicarbazones. However, the magnetochemistry of the present complexes is not pursued since the d^{10} configuration at the metal centre renders the complexes diamagnetic.

7.1. Stereochemistry of the complexes

7.1.1. ZnL^1Cl (29)

In the IR spectrum, a medium band at 3067 cm^{-1} correspond to the $\nu(\text{NH})$ vibrations at the *N*(4)-position of the thiosemicarbazone moiety (Fig. 7.1). The stretching vibration of the newly formed $N4=C12$ bond appears as a sharp band at 1598 cm^{-1} . The band corresponding to azomethine stretching vibration is shifted to 1543 cm^{-1} from a value of 1592 cm^{-1} in the free ligand. Coordination of the thiol form of the thiosemicarbazone moiety is also evidenced by a shift of the $\delta(\text{CS})$ band to 754

cm^{-1} in the complex from the corresponding value of 806 cm^{-1} in the ligand. A medium band around 310 cm^{-1} can be assigned to the stretching vibration of the terminal chlorine in the complex. In the electronic spectrum, the intraligand and charge transfer bands are observed at 273 and 425 nm respectively.

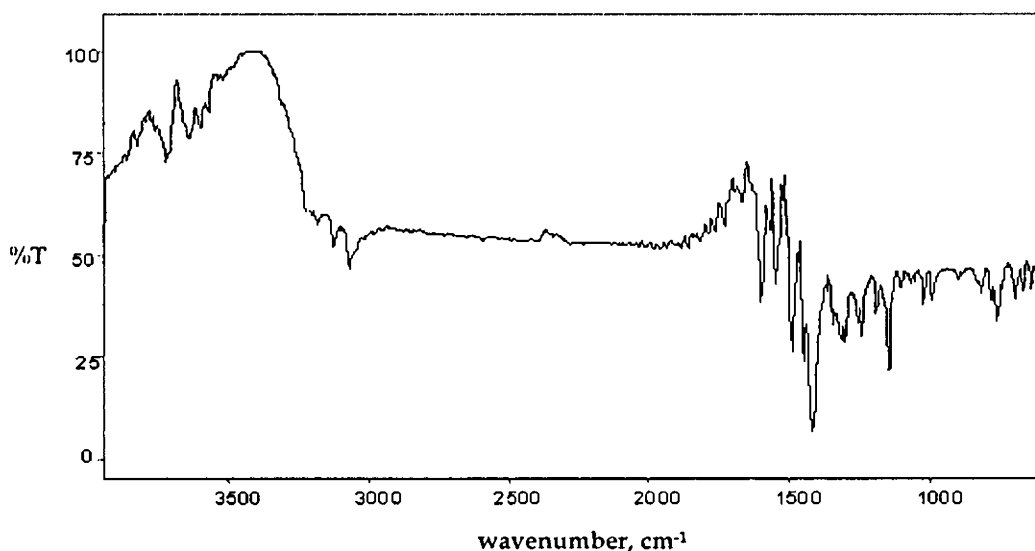


Fig. 7.1. IR spectrum of the compound ZnLCl

In the ^1H NMR spectrum, the resonance due to the imine nitrogen is absent, which provides support for the coordination of the thiosemicarbazone moiety by deprotonation of the thiol form. However, there are two resonances at 9.70 and 9.47 ppm in the spectrum of the complex, which integrates as one proton. These two peaks can therefore be regarded together as a doublet. However, these resonances show no correlation peaks in the ^1H - ^1H COSY spectrum, and hence they may be assigned to the proton at the $N(4)$ -position of the thiosemicarbazone moiety. Another interesting observation is that the resonances of the protons alpha to pyridyl nitrogen are observed to be shifted from the corresponding values in the ligand. Due to coordination, the electron density on the pyridyl ring is decreased. Hence all the aromatic proton resonances on the coordinated pyridyl ring are expected to be shifted to more downfield regions when compared to that of the ligand.

In the present case, there are two doublets, one centered at 8.81 ppm and another at 8.17 ppm, and these two integrate to give two protons and both the doublets show interaction with the aromatic protons. In the present complex, HL¹ coordinates as a tridentate ligand where one of the pyridyl rings is not involved in coordination. Hence the resonance due to the alpha hydrogen of the non-coordinating pyridyl nitrogen is expected to show more or less similar values as that in the ligand. Taking into consideration of this fact, the doublet at 8.81 ppm can be assigned to the α -proton on the non-coordinating pyridyl ring, and the resonance at 8.17 ppm may be assigned to the proton resonances on the carbon alpha to the coordinated pyridyl nitrogen (Fig. 7.2).

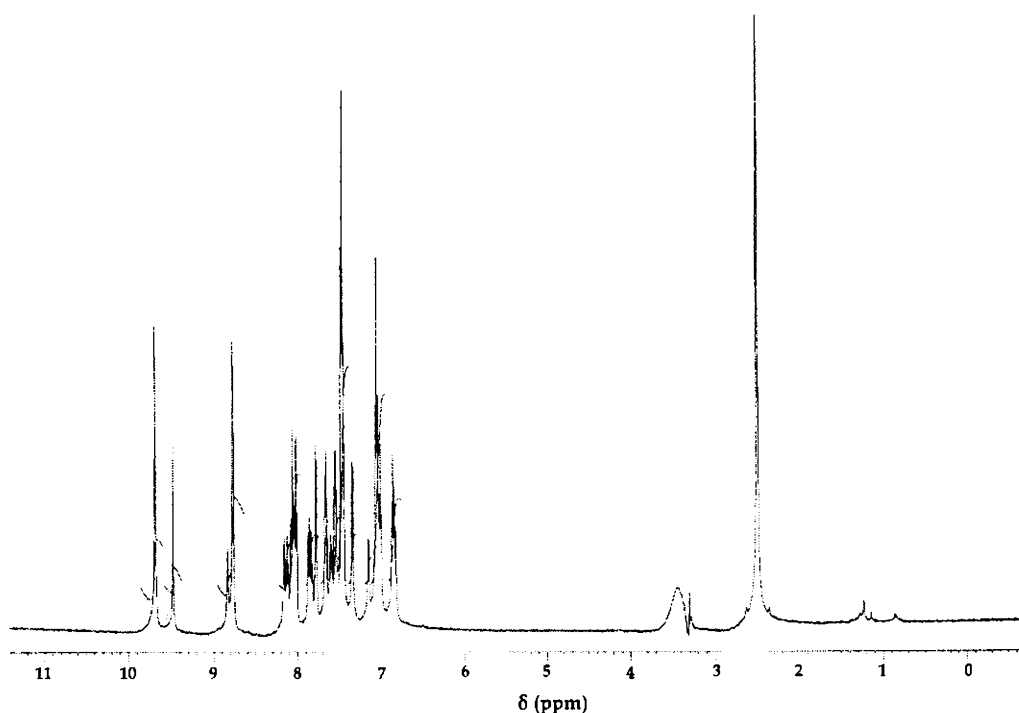


Fig. 7.2. ¹H NMR spectrum of ZnL¹Cl

Some of the aromatic proton resonances are shifted downfield as expected due to the coordination of one of the pyridyl nitrogens. The protons in the aromatic region show a wide range of ¹H-¹H coupling interactions, as observed in the COSY spectrum (Fig. 7.3). The region beyond 4 ppm shows only some solvent peaks. The peak at 3.5

ppm is assigned to the solvent DMSO and an additional sharp peak at 2.5 ppm is assigned to the dissolved water content in the deuteriated solvent [14].

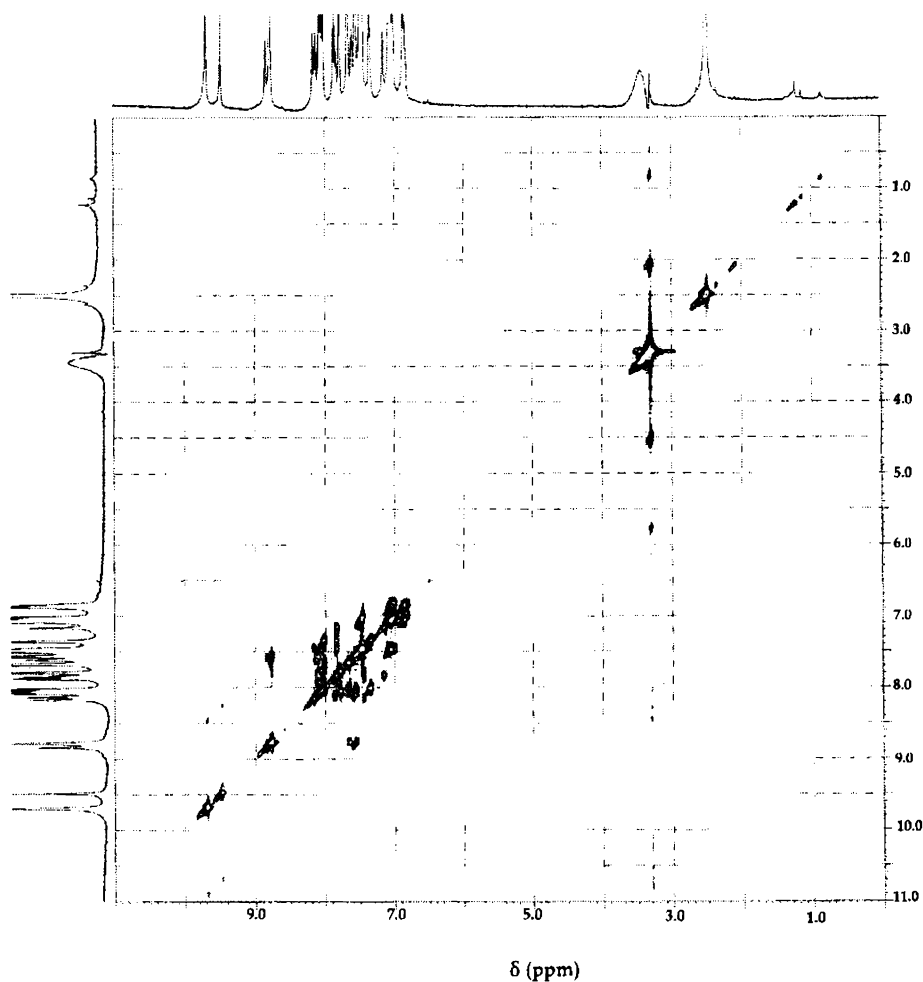


Fig. 7.3. ^1H - ^1H COSY spectrum of ZnL^1Cl

7.1.2. $\text{ZnL}^1\text{NCS}\cdot 2\text{H}_2\text{O}$ (30)

The compound **30** is synthesized by the metathetical displacement of the acetate ion by thiocyanate anion. IR spectrum of compound **30** (Fig. 7.4) shows a broad band near 3500 cm^{-1} supporting the presence of lattice water content consistent with the elemental analyses data. A sharp band is observed at 2073 cm^{-1} corresponding to the $\nu(\text{NCS})$ vibrations. Since the band is observed below 2100 cm^{-1} ,

it can be predicted that the thiocyanate group is coordinated to the metal centre through the nitrogen atom. A new sharp band at 1599 cm^{-1} is assigned to the stretching vibrations of the newly formed $\text{N}4=\text{C}12$ bond in the thiolate form of thiosemicarbazone. The azomethine stretching vibration band in HL^1 suffers a negative shift of *ca.* 30 cm^{-1} in the complex and is observed as a very low intensity band at 1565 cm^{-1} in the complex. The $\delta(\text{CS})$ band observed at 782 cm^{-1} in the present complex also supports coordination through the thiolate sulfur since it is shifted from a value of 806 cm^{-1} in the ligand.

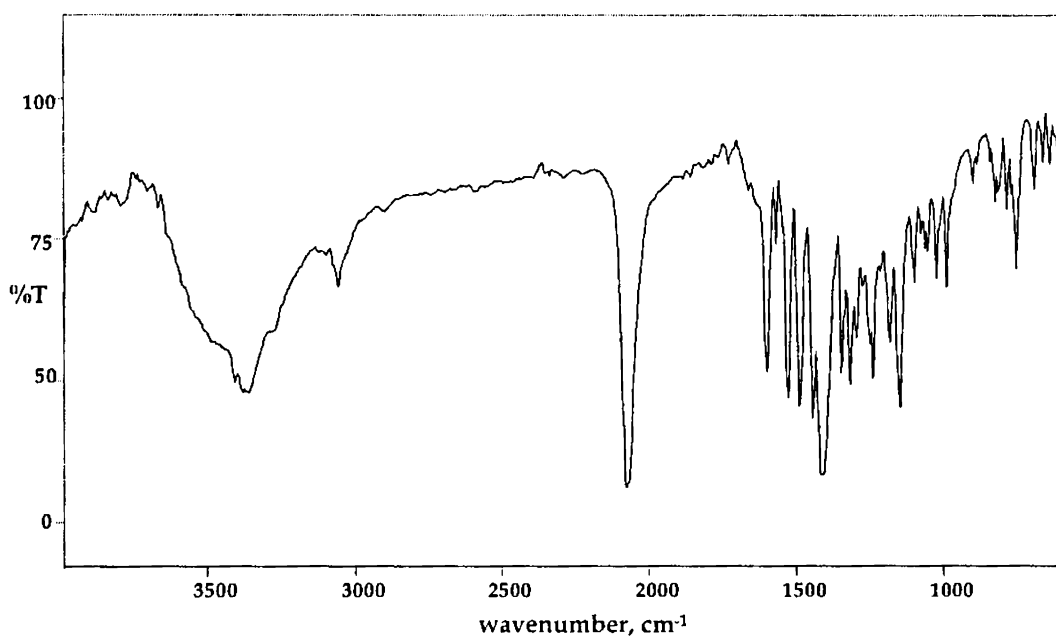


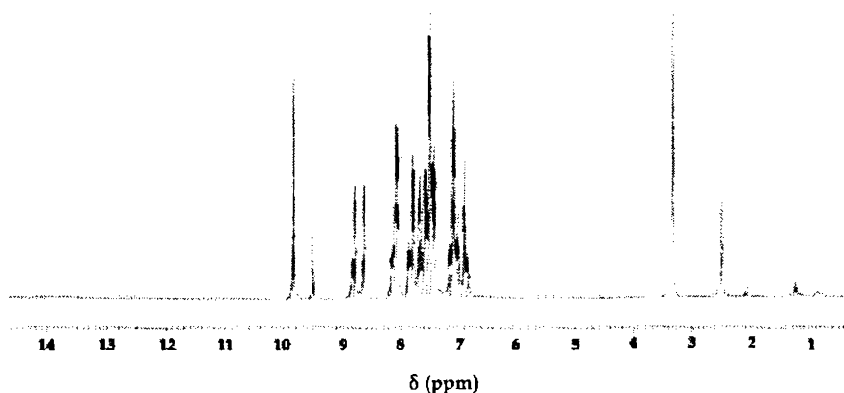
Fig. 7.4. IR spectrum of $\text{ZnL}^1\text{NCS}\cdot 2\text{H}_2\text{O}$

A $\delta(\text{NCS})$ band at 480 cm^{-1} also reveals that the thiocyanate group is N-bonded to the metal centre. The coordination of the imine nitrogen is indicated by a band around 430 cm^{-1} , which is assigned to the $\nu(\text{ZnN})$ vibrations. A medium band at 325 cm^{-1} correspond to the $\nu(\text{ZnS})$ vibrations confirming the coordination of thiolate sulfur and the $\nu(\text{ZnN}_{\text{py}})$ band of the coordinated pyridyl ring appears at 280 cm^{-1} . In the electronic spectrum, the intraligand and charge transfer bands are observed at 296 and 381 nm. The poor solubility of the compound in the deuteriated solvents restricted its NMR studies.

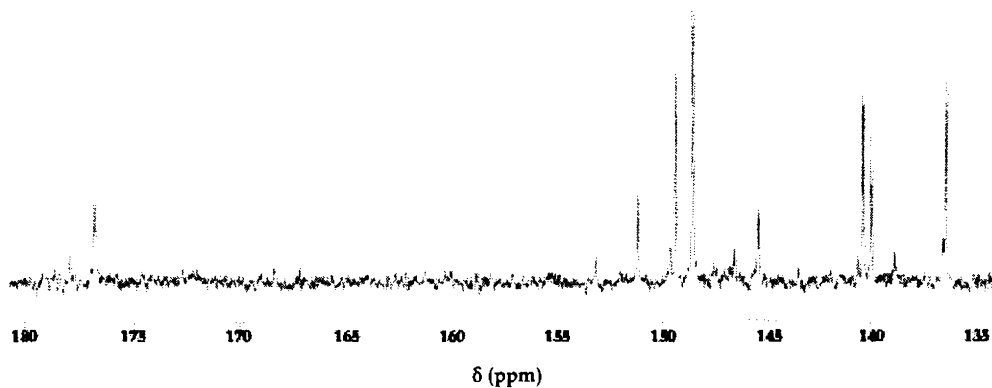
7.1.3. ZnL¹NO₃ (31)

The compound reveals a sharp band at 3059 cm⁻¹ in the IR spectrum corresponding to the $\nu(\text{NH})$ vibrations at the *N*(4)-position of the thiosemicarbazone moiety. The azomethine stretching and thiolate bending vibration bands are observed at 1545 cm⁻¹ and 780 cm⁻¹ respectively, which are shifted from the corresponding values in the free ligand. The new N4=C12 bond vibration is observed as a sharp band at 1597 cm⁻¹. According to Nakamoto [15], the NO₃⁻ ion can coordinate to a metal as a unidentate, symmetric and asymmetric chelating bidentate, or bridging bidentate ligand of various structures. It is rather difficult to differentiate these structures by vibrational spectroscopy since the symmetry of the nitrate ion differs very little among them (*C*_{2v} or *C*_s). The unidentate NO₃ group exhibits three NO stretching bands, viz., $\nu_3(B_2)$, $\nu_1(A_1)$ and $\nu_2(A_1)$ as expected of its *C*_{2v} symmetry, whereas the chelating bidentate NO₃ group exhibits three bands viz., $\nu_1(A_1)$, $\nu_3(B_2)$ and $\nu_2(A_1)$. For instance, in the complex Zn(*bt*)₂(NO₃)₂, where *bt* is benzothiazole, the nitrate group acts as a chelating bidentate with the $\nu_3(B_2)$ and $\nu_1(A_1)$ vibrations observed at 1485 and 1300 cm⁻¹ with the separation of the two highest-frequency bands being 185 cm⁻¹. However in the present case, it is difficult to assign the chelating nature of the nitrate group since distinct bands are observed at 1477, 1309 and 1021 cm⁻¹. Also, bands near similar regions appear in other complexes too. In addition to this, the use of far-IR spectra to distinguish unidentate and bidentate nitrate coordination is suggested to be controversial [15]. Hence, we are unable to assign the chelating nature for the nitrate group in this complex. However, supports for the coordinated behavior of the complex is obtained from the observed shifts in the stretching bands of the coordinating azomethine, pyridyl and thiolate linkages. In the solid-state electronic spectrum, the intra-ligand transitions appear as a broad peak at 354 nm and the charge transfer transitions appear 394 and 423 nm. It may be noted that the electronic spectrum reveals no distinct peaks above 450 nm, due to the absence of *d-d* transitions.

In the ¹H NMR spectrum (Fig. 7.5), two sharp peaks at 9.84 and 9.50 ppm integrate as one proton and they are assigned to N(4)H proton. Four resonances at 8.85, 8.79, 8.63 and 8.18 ppm integrate as two protons and they can be assigned to the α -proton resonances on the two pyridyl rings.

Fig. 7.5. ¹H NMR spectrum of ZnL¹NO₃

The proton resonances on the coordinated pyridyl rings are observed to be shifted here. The aromatic protons are also observed to be shifted downfield due to the decreased electron density on the coordinated pyridine ring. In the ¹³C NMR (Fig. 7.6), the resonance at 176.8 ppm due to the C6 carbon atoms almost unchanged, since it appeared at 177.4 ppm in the ligand (see Fig. 2.5). Similarly, the C12 carbon resonance at 151.14 ppm in the complex is also almost unshifted.

Fig. 7.6. ¹³C NMR spectrum of ZnL¹NO₃

However the α -carbon resonances on the pyridyl rings are shifted in the complex as a result of coordination. The four ¹³C resonances at 149.45, 148.53, 146.55 and 145.43 ppm are assigned to the four α -carbon atoms on the two pyridyl rings. Coordination decreases the electron density on one of the pyridyl rings, and as a result,

its carbon resonances are shifted downfield. An additional ^{13}C resonance at 140.01 is assigned to the carbon para positioned to the nitrogen atom in the coordinated pyridyl ring. A more intense peak at 140.42 ppm in the complex is assigned to the C13 carbon on the pyridyl ring, which is almost unshifted when compared to that of the ligand. Two more peaks at 138.88 and 136.41 ppm can be assigned to the downfield shifted carbon resonances on the coordinated pyridyl ring. Resonances in the 127.95-123.66 ppm region incorporate the pyridyl and phenyl ring carbons.

7.1.4. $\text{ZnL}^1\text{N}_3\cdot\text{CH}_3\text{OH}$ (32)

The compound **32** is synthesized by the metathetical displacement of the acetate ion by azido anion in the Zn(II) complex. The IR spectrum of **32** (Fig. 7.7) reveals a sharp band at 3269 cm^{-1} , which can be assigned to the symmetric and asymmetric stretching vibrations of the $-\text{OH}$ group of the methanol moiety in the lattice.

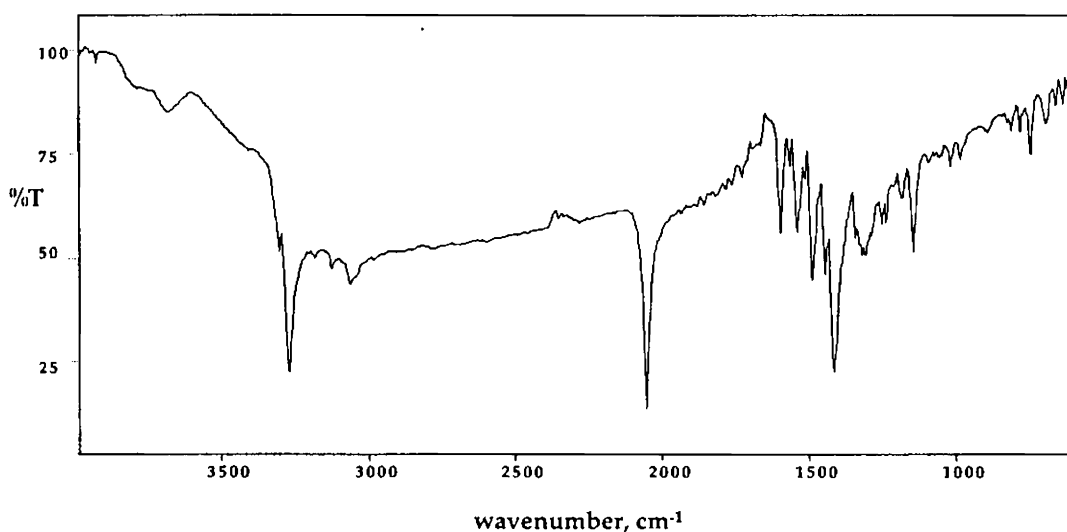


Fig. 7.7. IR spectrum of the compound $\text{ZnL}^1\text{N}_3\cdot\text{CH}_3\text{OH}$

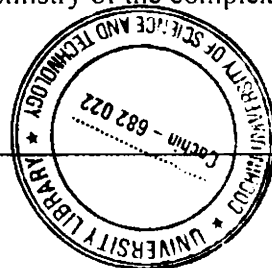
Another sharp band at 2052 cm^{-1} corresponds to the asymmetric stretching vibrations of the coordinated azido group. The coordinated azomethine stretching vibration is observed at 1538 cm^{-1} and the $\delta(\text{CS})$ band of the coordinated thiolate group appears at 748 cm^{-1} . Both these bands are shifted from their corresponding values of

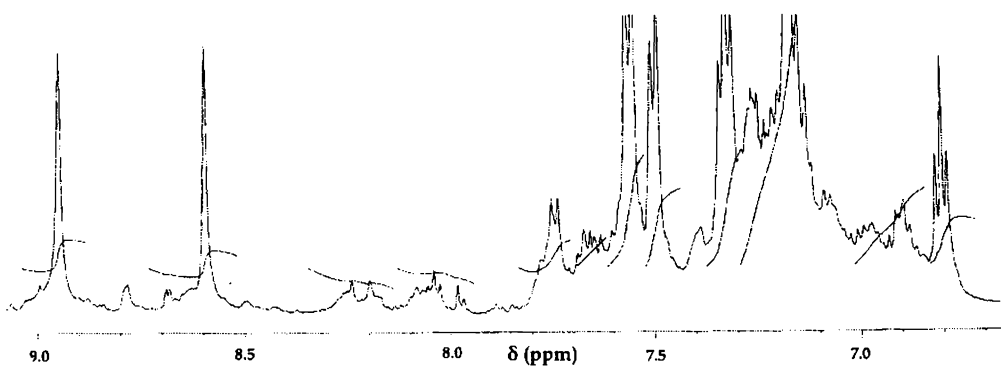
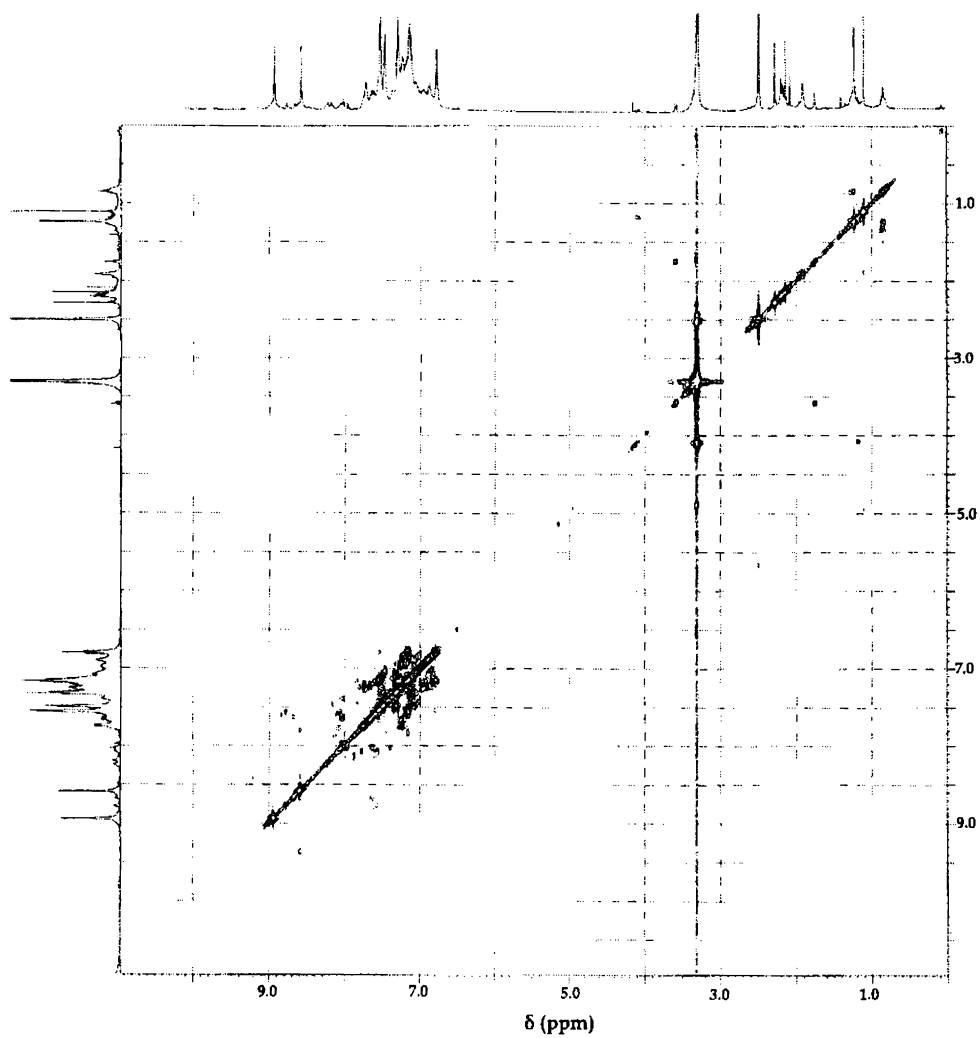
1592 and 806 cm^{-1} in the free ligand, which supports coordination. Medium bands observed at 460, 415 and 380 cm^{-1} can be assigned to the coordinated $\nu(\text{Zn}-\text{N}_3)$, $\nu(\text{ZnN}_{\text{azo}})$ and $\nu(\text{ZnS})$ vibrations. The solid-state electronic spectrum of the compound reveals the $\pi \rightarrow \pi^*$ and $n \rightarrow \pi^*$ transitions are observed at 345 and 382 nm. Peaks at 429 and 455 nm correspond to the charge transfer transitions. No transitions are observed beyond the region of 500 nm.

7.1.5. $\text{ZnL}^1\text{OAc}\cdot 1.5\text{H}_2\text{O}$ (33)

The acetato group can coordinate to metal ions to form unidentate, chelating bidentate or bridging bidentate complexes. In the IR spectrum of the compound, bands due to the azomethine stretching and the thiolate bending vibrations appear at 1530 and 760 cm^{-1} and are shifted from their corresponding values in the ligand. However, the assignment of bands due to the coordinated acetato group appears rather difficult here, since the characteristic $\nu(\text{C}=\text{O})$ and $\nu(\text{C}-\text{O})$ vibrations of the unidentate acetato group usually appear at regions near 1600 and 1400 cm^{-1} , where contributions from other stretching vibrations in the ligand moiety are also expected. The solid-state electronic spectrum of the compound reveals the $\pi \rightarrow \pi^*$ and $n \rightarrow \pi^*$ transitions as a broad peak at 352 nm. Another broad peak at 446 nm correspond to the $\text{M} \rightarrow \text{L}$ charge transfer transitions and the region beyond 600 nm is devoid of any transitions.

The ^1H NMR and the COSY spectrum of the compound 33 in DMSO are given in Fig. 7.8 and Fig. 7.9 respectively. The proton resonances of the compound 33 are of very low intensity, probably due to its low solubility in the solvent. Coordination by deprotonation of the thiolate form is indicated by the absence of $-\text{NH}$ resonances near 14.55 ppm. Interestingly, there are two sharp singlets at 8.95 and 8.58 ppm, which integrate as one proton. These show no correlation peaks in the $^1\text{H}-^1\text{H}$ COSY spectrum and hence these resonances correspond to the proton at the $N(4)$ -position of the thiosemicarbazone moiety. However, these resonances are shifted from a corresponding value of 9.55 ppm in the ligand, which can be attributed to the change in the conformation of the ligand and the overall stereochemistry of the complex.



Fig. 7.8. ^1H NMR spectrum of $\text{ZnL}'\text{OAc}\cdot 1.5\text{H}_2\text{O}$ Fig. 7.9. ^1H - ^1H COSY spectrum of $\text{ZnL}'\text{OAc}\cdot 1.5\text{H}_2\text{O}$

There is a low intensity doublet at 8.67 ppm and another doublet at 7.80 ppm, which show correlation with the aromatic protons. These can be assigned to the protons alpha to the pyridyl nitrogens in the uncoordinated and coordinated pyridyl rings. The aromatic proton resonances appear as multiplets in the region 7.65 – 6.80 ppm and they show wide coupling interactions in the $^1\text{H} - ^1\text{H}$ COSY spectrum. The lattice water content in the sample is revealed as two resonances at 4.1 and 3.6 ppm and they show correlation with the solvent peaks.

7.1.6. ZnL^1Br (34)

Nakamoto [15] suggests the MX stretching vibrations to appear in the regions of $300\text{--}200\text{ cm}^{-1}$ for the terminal M–Br bonds and in far-IR spectrum of the compound, there appear two medium bands near 240 and 230 cm^{-1} . The IR spectrum nevertheless gives enough support for coordination of the azomethine nitrogen and thiolate sulfur. The band due to azomethine stretching vibrations are shifted to 1542 cm^{-1} from a value of 1592 cm^{-1} in the ligand, whereas that of the thiolate bending vibrations are shifted to 750 cm^{-1} from a corresponding value of 806 cm^{-1} in the ligand HL^1 , as a result of coordination. Most of the other IR bands are observed similar to the other complexes in the series.

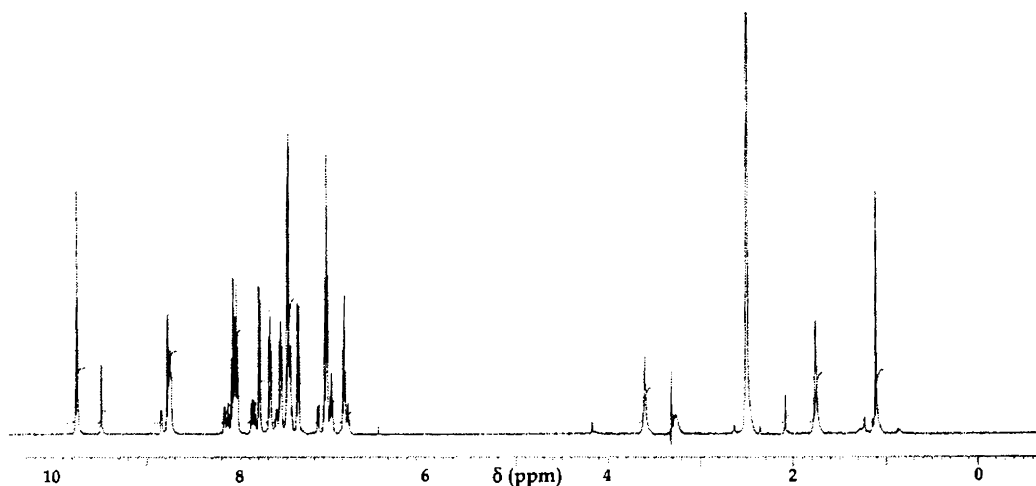


Fig. 7.10. ^1H NMR spectrum of ZnL^1Br

Two sharp singlets at 9.74 and 9.48 ppm (Fig. 7.10) integrate as one proton, and they show no correlation with the other proton resonances. Hence these can be

assigned to the $N(4)H$ proton of the compound. The α -proton resonances on pyridyl rings are observed as a double doublet at 8.83 ppm and 8.76 ppm and they show correlations with the aromatic protons in the COSY (Fig. 7.11).

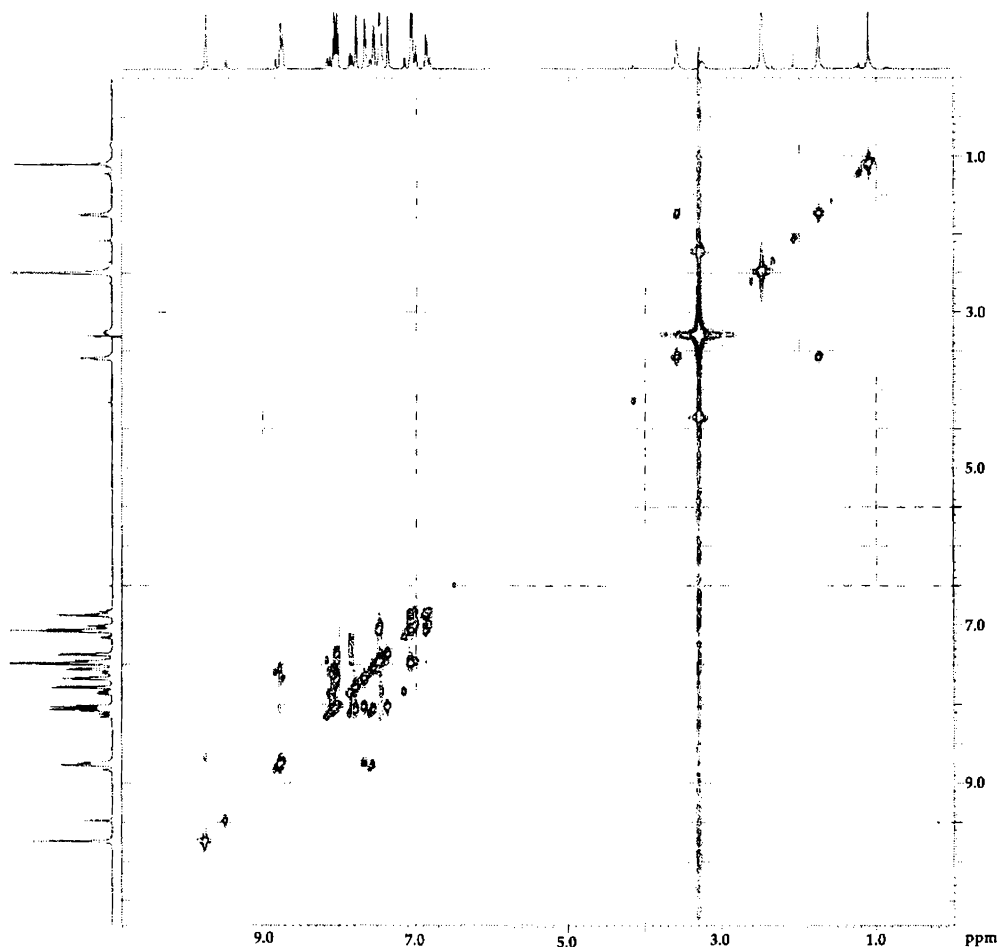


Fig. 7.11. 1H - 1H COSY spectrum of ZnL^1Br

It may be noted that the α -proton resonances are not much shifted due to coordination of one of the pyridyl nitrogens, but however, the intensity of one of the resonances appear largely reduced in the complex as the result of coordination. A triplet at 7.56 ppm gives no correlation with the aromatic protons, and hence it can be assigned to the proton resonances at the $N(4)$ position. The proton resonances on nitrogens can appear as triplets near 7.00 ppm due to nuclear quadrupole effects [14]. Contrary to the observation of multiplets in the previous compounds, the aromatic

proton resonances are clearly distinguished in the present compound and they show well defined coupling interactions. The lattice water content in the samples is revealed at 4.15 and 3.60 ppm.

7.1.7. ZnL^2Cl (35)

In the IR spectrum of the ligand, the C6–OH vibrations appear as a sharp band at 3510 cm^{-1} . However, they appear as low intensity bands around 3500 cm^{-1} in the present compound, as a result of coordination. A weak band at 3050 cm^{-1} correspond to the stretching vibrations of the N(4)–H nitrogen. The cyclohexyl stretching vibrations are observed as sharp bands at 2932 and 2850 cm^{-1} . The bands due to thiolate bending vibrations are shifted to 745 cm^{-1} as a result of coordination. Another medium band at 348 cm^{-1} correspond to the $\nu(\text{ZnS})$ vibrations of the coordinated thiolate sulfur. The $\nu(\text{ZnN})$ band of the coordinated pyridyl nitrogen appear at 299 and 287 cm^{-1} . In the solid-state electronic spectrum, the $\pi\rightarrow\pi^*$ and the $n\rightarrow\pi^*$ transitions appear as a broad shoulder at 322 nm . However, the charge transfer transitions appear more intense, as a strong peak at 418 nm . Only instrumental noise peaks are observed beyond 500 nm .

The ^1H NMR of compound ZnL^2Cl is given in Fig. 7.12. A broad quartet centred at 8.71 ppm integrates as two protons, which incorporate the resonance due to both the α - protons on the two pyridyl rings. The aromatic proton resonances are less resolved, appearing as multiplets in the $7.15 - 7.95\text{ ppm}$ region. However some of these resonances are shifted downfield due to coordination through one of the pyridyl nitrogens. The hydrogen bonded –OH proton resonances appeared at 5.30 ppm in the ligand HL^2 , whereas in the complex, it appears at 3.59 ppm , which supports coordination through C6-OH. The cyclohexyl C13H resonance is observed at 4.05 ppm , whereas the equatorial and axial proton resonances are observed as multiplets in the $1.55 - 1.90$ and $1.1 - 1.25\text{ ppm}$ range. The ^{13}C NMR spectrum of the compound is poorly resolved when compared to the ^1H NMR. Resonances at 149.20 , 148.87 , 148.65 , 146.26 ppm correspond to the α - carbons on the two pyridyl rings. Due to coordination by one of the pyridyl nitrogens the electron density on the ring is reduced and some of the aromatic carbon resonances are shifted downfield. Consequently, the

aromatic carbon resonances appear in the 123.33 – 139.75 ppm range. The cyclohexyl C13 resonance (see Fig. 2.9) is observed at 51.41 ppm. The other cyclohexyl carbons resonate at 32.26, 25.22 and 24.91 ppm.

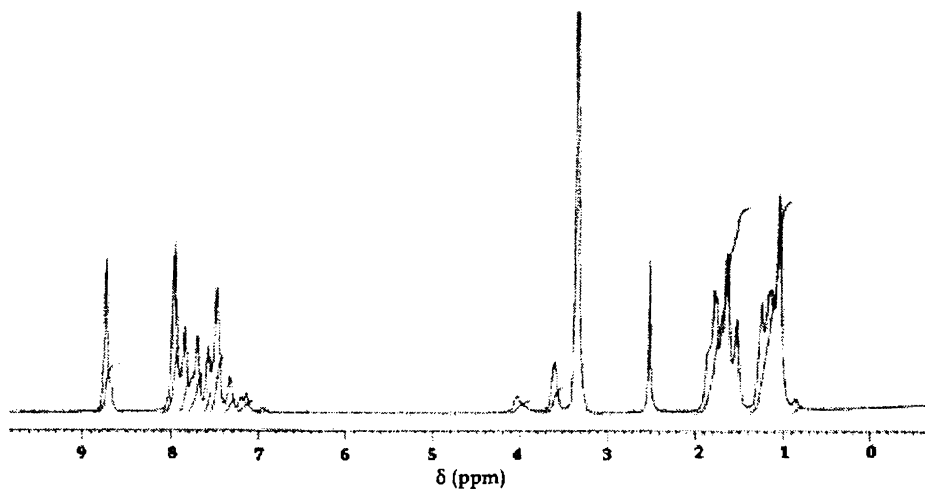


Fig. 7.12. ^1H NMR spectrum of ZnL^2Cl

7.1.8. $\text{ZnL}^2\text{NCS}\cdot 2\text{H}_2\text{O}$ (36)

Similar to the case of compound **35** above, the coordination through the oxygen of C6-OH is suggested by the presence of low intensity bands around 3500 cm^{-1} in the IR spectrum (Fig. 7.13).

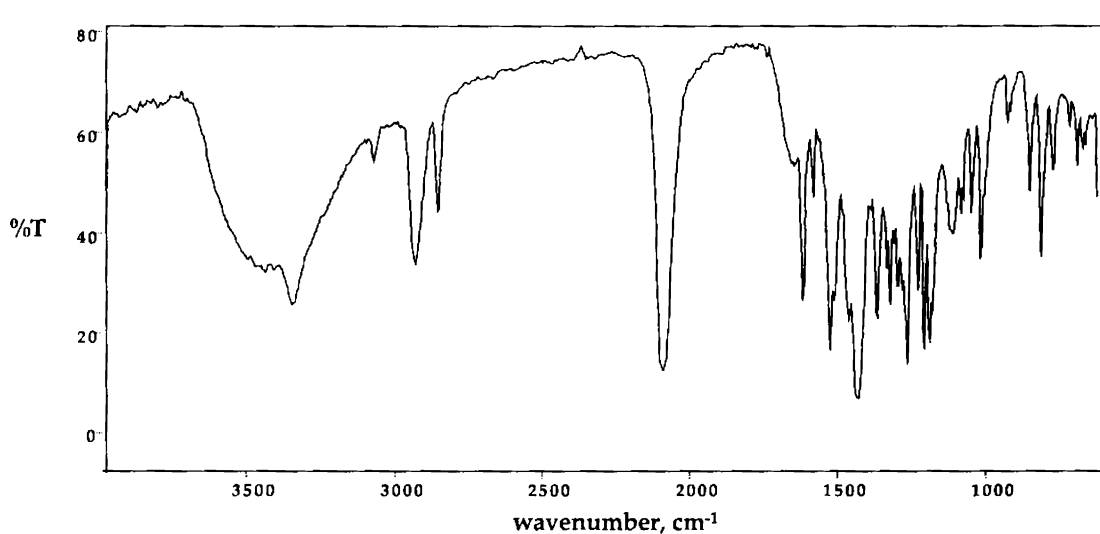


Fig. 7.13. IR spectrum of compound $\text{ZnL}^2\text{NCS}\cdot 2\text{H}_2\text{O}$

The cyclohexyl stretching vibrations appear as two sharp bands at 2928 and 2852 cm^{-1} . A sharp band is observed at 2076 cm^{-1} corresponding to the $\nu(\text{NCS})$ vibration. This reveals the N-coordinated nature of the thiocyanate group, since the band is observed below 2100 cm^{-1} . The band due to coordinated azomethine stretching vibration is observed at 1563 cm^{-1} and the $\delta(\text{CS})$ band of the coordinated thiolate group appear at 742 cm^{-1} . The newly formed $\text{N}4=\text{C}12$ bond due to enolization of the ligand resonate at 1598 cm^{-1} . In the far IR region, the $\nu(\text{Zn}-\text{S})$ vibration of the thiolate bond is observed at 375 cm^{-1} . The $\delta(\text{NCS})$ band is observed at 470 cm^{-1} . The intraligand transitions in the electronic spectrum are observed as a strong peak at 314 nm and the charge transfer transitions appear as a sharp peak at 411 nm.

In the ^1H NMR spectrum of the present compound (Fig. 7.14), there are no peaks beyond 9.0 ppm, which are devoid of coupling interactions. The resonances at 8.73 and 8.56 ppm, which show clear correlations with the aromatic protons can be assigned to the alpha proton on the uncoordinated and coordinated pyridyl rings similar to that of other molecules.

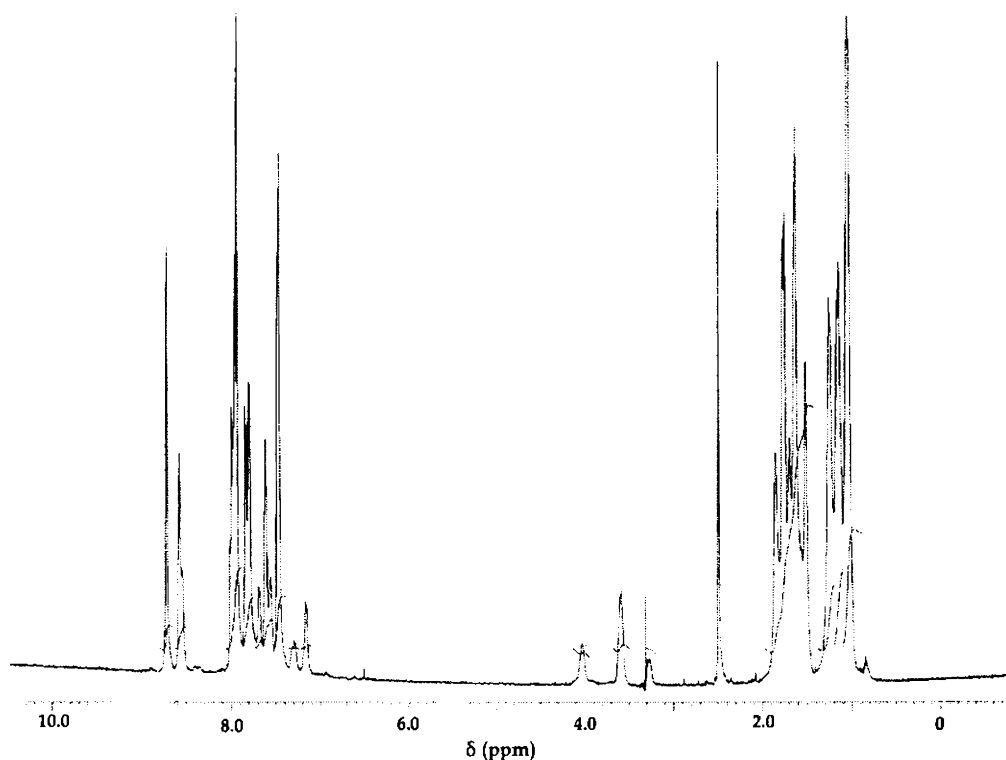


Fig. 7.14. ^1H NMR spectrum of $\text{ZnL}^2\text{NCS}\cdot 2\text{H}_2\text{O}$

However, the COSY spectrum helps to assign the $-\text{NH}$ protons (Fig. 7.15). It is observed that a triplet at 7.94 and a multiplet at 7.83 ppm reveal cross peaks with the resonances at 4.02 and 3.59 ppm respectively. The resonance at 3.59 ppm is assigned to the C13H resonance of the cyclohexyl moiety based on its correlations with the equatorial and axial cyclohexyl protons in the 1 – 2 ppm region. The N(4)H proton is expected to couple with the C13H proton in the cyclohexyl moiety. It is also previously observed that, due to quadrupole effects, the N(4)H resonance can appear as triplets in the aromatic region. Hence the triplet at 7.94 ppm is assigned to the N(4)H proton. It should be noted that, there is also a multiplet closely positioned at 7.99 ppm corresponding to the aromatic protons, and hence there are cross peaks observed in the COSY spectrum.

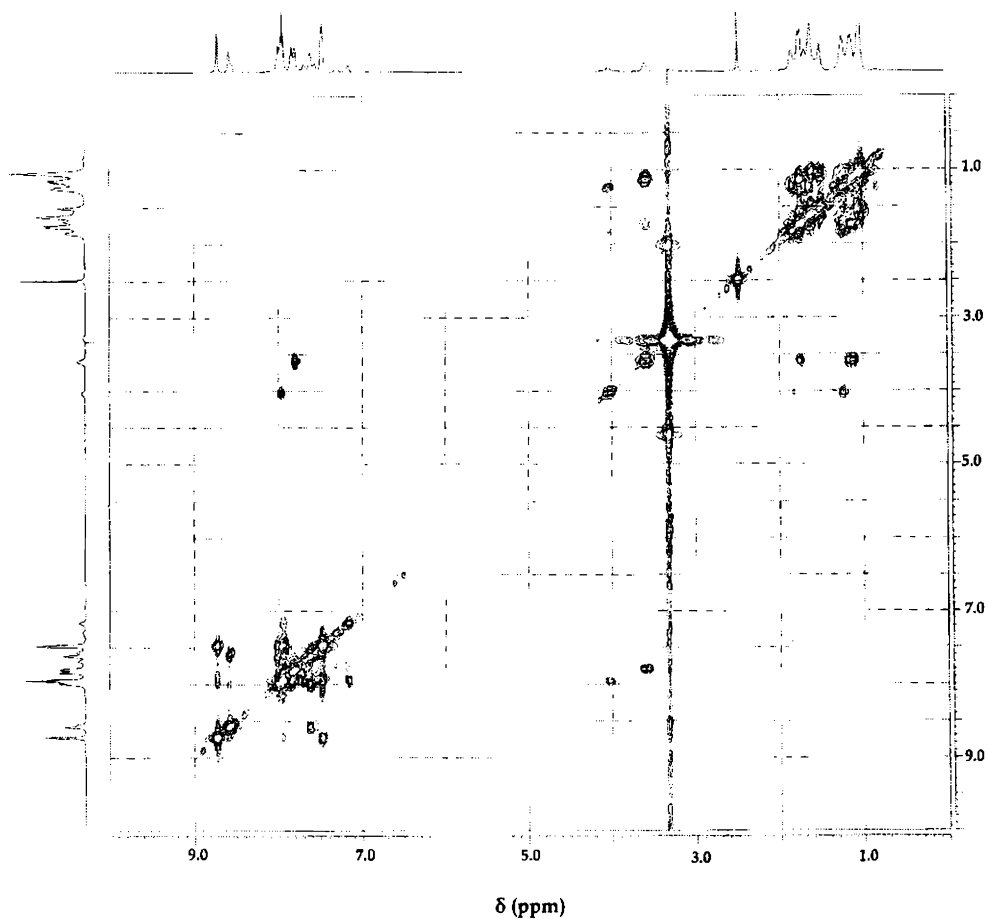


Fig. 7.15. ^1H - ^1H COSY spectrum of $\text{ZnL}^2\text{NCS}\cdot 2\text{H}_2\text{O}$

However, the multiplet at 7.83 ppm reveals no cross peaks in the aromatic region, but it shows correlation with the C6–OH proton resonance at 4.02 ppm. The C6–OH proton also reveals coupling interactions with the dissolved water content in the deuteriated solvents. Hence the multiplet at 7.825 ppm can be assigned to the resonances due to proton on nitrogen atom N3 adjacent to C6. The aromatic region is less resolved in the ^1H NMR and in the COSY, the coupling cross peaks appear crowded. The cyclohexyl equatorial and axial protons resonate as multiplets in the 1.85 – 1.5 and 1.24 – 1.04 regions respectively, and they reveal close coupling interactions between each other.

7.1.9. ZnL^2OAc (37)

In the IR spectrum, some weak bands near 3500 cm^{-1} region can be assigned to the asymmetric stretching vibrations of the coordinated –OH group at C6. Another weak band near 3100 is due to the $\nu(\text{CH})$ vibrations of the coordinated acetato group. The cyclohexyl stretching vibrations are observed at 2928 and 2852 cm^{-1} . The $\nu(\text{C}=\text{O})$ vibrations of the coordinated unidentate acetato group appear as a weak band near 1620 cm^{-1} . Another medium band at 1397 cm^{-1} correspond to the $\nu(\text{C}-\text{O})$ vibrations of the coordinated acetato moiety. The coordinated azomethine stretching $\nu(\text{CN})$ vibrations are shifted to 1554 cm^{-1} . The stretching vibrations of the newly formed $\text{N4}=\text{C12}$ bond appear as a sharp band at 1594 cm^{-1} . The coordination of the thiol form of the thiosemicarbazone moiety is evidenced by a shift of the $\delta(\text{CS})$ band to 733 cm^{-1} in the complex from a corresponding value of 802 cm^{-1} in the ligand. A medium band around 470 cm^{-1} is assigned to the $\delta(\text{CH})$ vibrations of the acetato group in the complex. The vibrations due to the coordinated thiolate group appear at 362 cm^{-1} . The $\nu(\text{ZnN})$ band of the coordinated pyridyl nitrogen appear at 298 cm^{-1} . The solid-state electronic spectrum reveals the intra-ligand $\pi\rightarrow\pi^*$ and the $n\rightarrow\pi^*$ transitions as two broad peaks at 300 and 322 nm . The charge transfer transitions appear as a broad shoulder at 379 nm and a small peak at 444 nm . The region beyond 500 nm is observed to be full of instrumental noise.

The ^1H and ^{13}C NMR resonances of the compound ZnL^2OAc are poorly resolved, perhaps due to the low solubility of the sample in DMSO. In the ^1H NMR, some broad multiplets are observed centred at 8.80, 8.46 and 8.01 ppm, which restrict their assignment to respective protons. The aromatic proton resonances also appear as a broad multiplet in the 7.11 – 7.90 ppm region. The cyclohexyl equatorial and axial protons appear as multiplets in the 1.5 – 1.9 and 1.1 – 1.35 ppm regions. In the ^{13}C NMR also the resonances are of very low in intensity. The C6 and C12 resonances are shifted to 177.05 and 175.20 ppm when compared to the corresponding values of 193.01 and 181.01 ppm in HL^2 . The observed shifts support coordination through the –OH and thiolate groups in HL^2 . The peaks at 149.30, 149.05, 148.72 and 147.90 ppm correspond to the α -carbon resonances on the pyridyl rings. The aromatic carbon resonances are shifted downfield and they appear in the 123.27 – 146.16 ppm region. The resonance of the cyclohexyl carbon C13 occurs at 51.15 ppm. Other cyclohexyl carbon resonances are observed in the 22.85 – 32.21 ppm range.

7.1.10. $\text{CdL}^1\text{Cl}\cdot 2\text{H}_2\text{O}$ (38)

In the IR spectrum, a weak band at 3378 cm^{-1} can be assigned to the asymmetric stretching vibrations of the lattice water. Another weak band near 3050 cm^{-1} is due to the $\nu(\text{NH})$ vibrations at the $N(4)$ -position of the thiosemicarbazone moiety. A sharp band at 1594 cm^{-1} can be assigned to the stretching vibrations of the newly formed $\text{N4}=\text{C12}$ bond. The azomethine stretching vibration appears as a low intensity band at 1548 cm^{-1} and is shifted from a value of 1592 cm^{-1} in the free ligand. The $\delta(\text{CS})$ vibration in the complex appears at 768 cm^{-1} and this also supports coordination since the band is shifted from a value of 806 cm^{-1} in the ligand. In the far IR region, the azomethine stretching vibration is observed at 488 cm^{-1} and the vibration due to the coordinated thiolate group appears at 332 cm^{-1} . The terminal chlorine stretching vibration appears as a medium band at 385 cm^{-1} . The $\nu(\text{CdN})$ band of the coordinated pyridyl nitrogen appear at 282 cm^{-1} . The solid-state electronic spectrum reveals the intra-ligand $\pi\rightarrow\pi^*$ and the $n\rightarrow\pi^*$ transitions at 301 and 343 nm.

The charge transfer transitions appear as a broad peak at 387 nm and two shoulders at 432 and 446 nm.

^1H NMR spectrum of the compound **38** in DMSO is given in Fig. 7.16. The resonance due to the imine nitrogen is absent, which provides support for the coordination of the thiosemicarbazone moiety by deprotonation of the thiol form. However, a doublet at 9.50 ppm is assigned to the N(4)-H proton, which is almost unshifted from the corresponding value in the ligand HL¹. A double doublet at 8.81 ppm and two doublets at 8.77 and 8.61 ppm together integrate as two protons. They can be considered as the resonances of the protons alpha to pyridyl nitrogens and they are shifted in the complexes due to coordination. The aromatic proton resonances appear as multiplets in the 6.80 – 8.28 ppm region. The region beyond 4 ppm reveals only some solvent peaks.

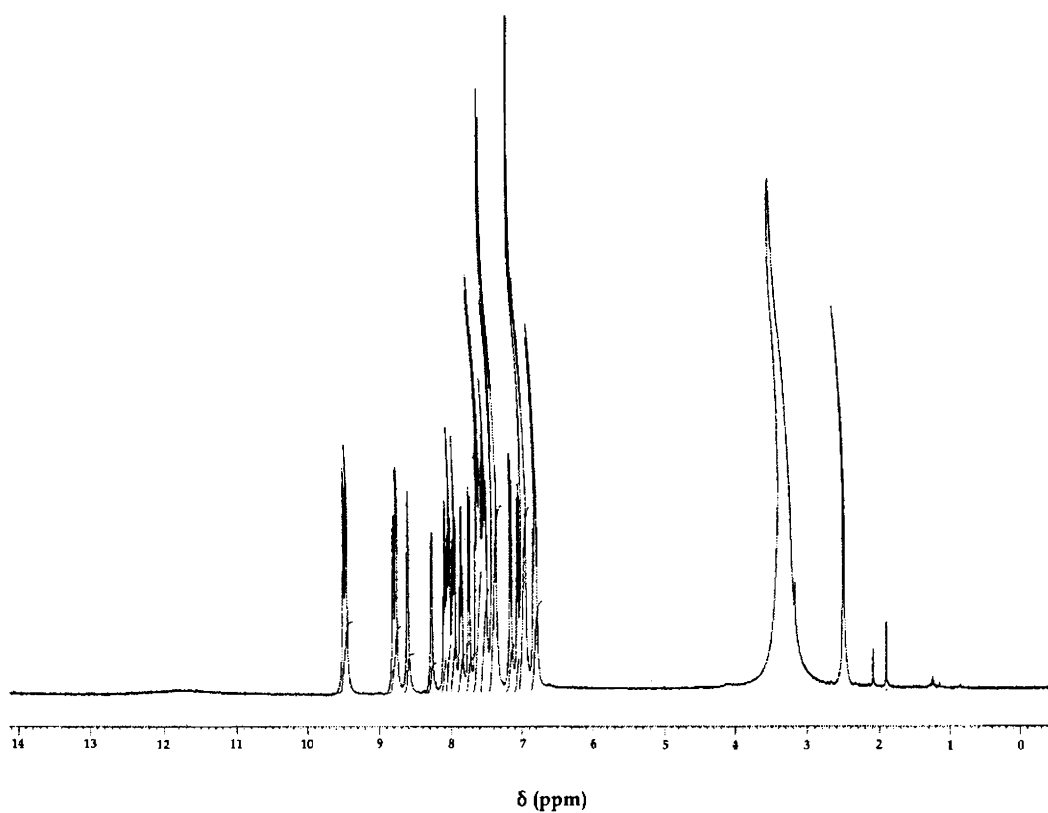


Fig. 7.16. ^1H NMR spectrum of $\text{CdLCl}\cdot 2\text{H}_2\text{O}$

7.1.11. $(\text{CdL}^1\text{NCS})_2$ (**39**)

The complex is synthesized by the metathetical displacement of the acetate ion in the Cd(II) complex by thiocyanate anion. IR spectrum of **39** is given in Fig. 7.17. There are no sharp bands around 3300 cm^{-1} supporting the absence of lattice water content in the sample, consistent with the elemental analyses data. However, a strong band observed near 2010 cm^{-1} corresponding to the $\nu(\text{NCS})$ vibrations is observed to be splitted into two sharp bands at 2057 and 2015 cm^{-1} . This suggests a possible bridged stereochemistry for the complex, which is further supported by the NMR results. This also indicates that the thiocyanate group is N-bonded to the metal centre through the nitrogen atom, since the band is observed below 2100 cm^{-1} . The observed shifts in the azomethine $\nu(\text{CN})$ band to 1549 cm^{-1} and thiolate $\delta(\text{CS})$ band to 740 cm^{-1} from that of the ligand evidence the coordination of the thiosemicarbazone moiety. In the electronic spectrum, the intra-ligand transitions are observed at 326 and 346 nm , while the $\text{M}\rightarrow\text{L}$ charge transfer transitions are observed at 420 and 445 nm .

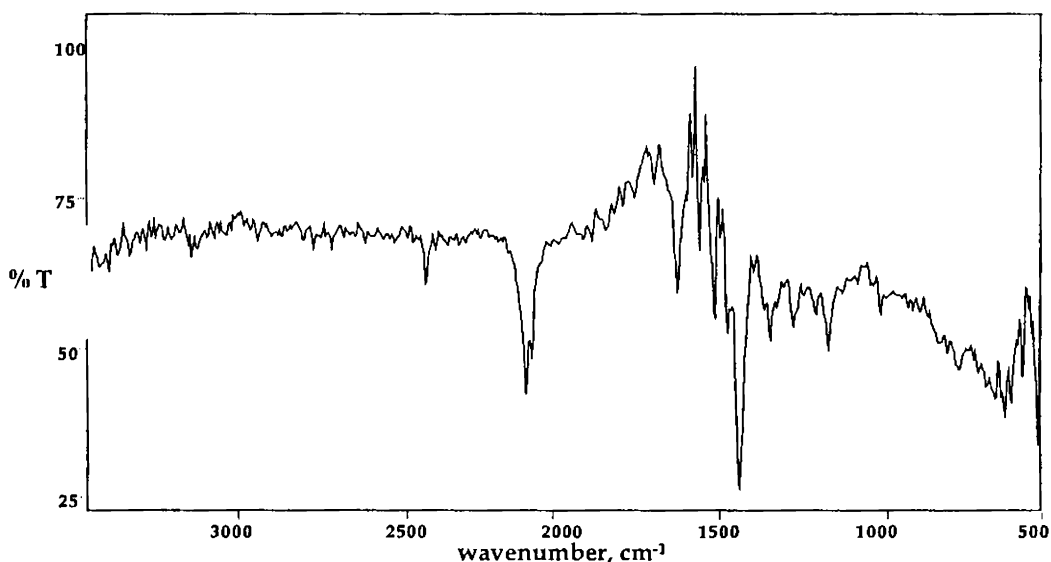


Fig. 7.17. IR spectrum of the compound $(\text{CdL}^1\text{NCS})_2$

Interestingly, the ^1H NMR spectrum gives support for the proposed dimeric structure. A sharp doublet at 9.50 ppm integrates as two protons and shows no

correlations with the aromatic protons. Hence it can be assigned to the $N(4)H$ resonances of the two possible ligand moieties in the molecule.

Also, there are four distinguishable resonances in the 8.82 – 8.04 ppm range, with their total integration summing up to 3.92. These resonances also show coupling interactions with the aromatic protons, and hence can be assigned to the four alpha protons on the four pyridyl rings (Fig. 7.18).

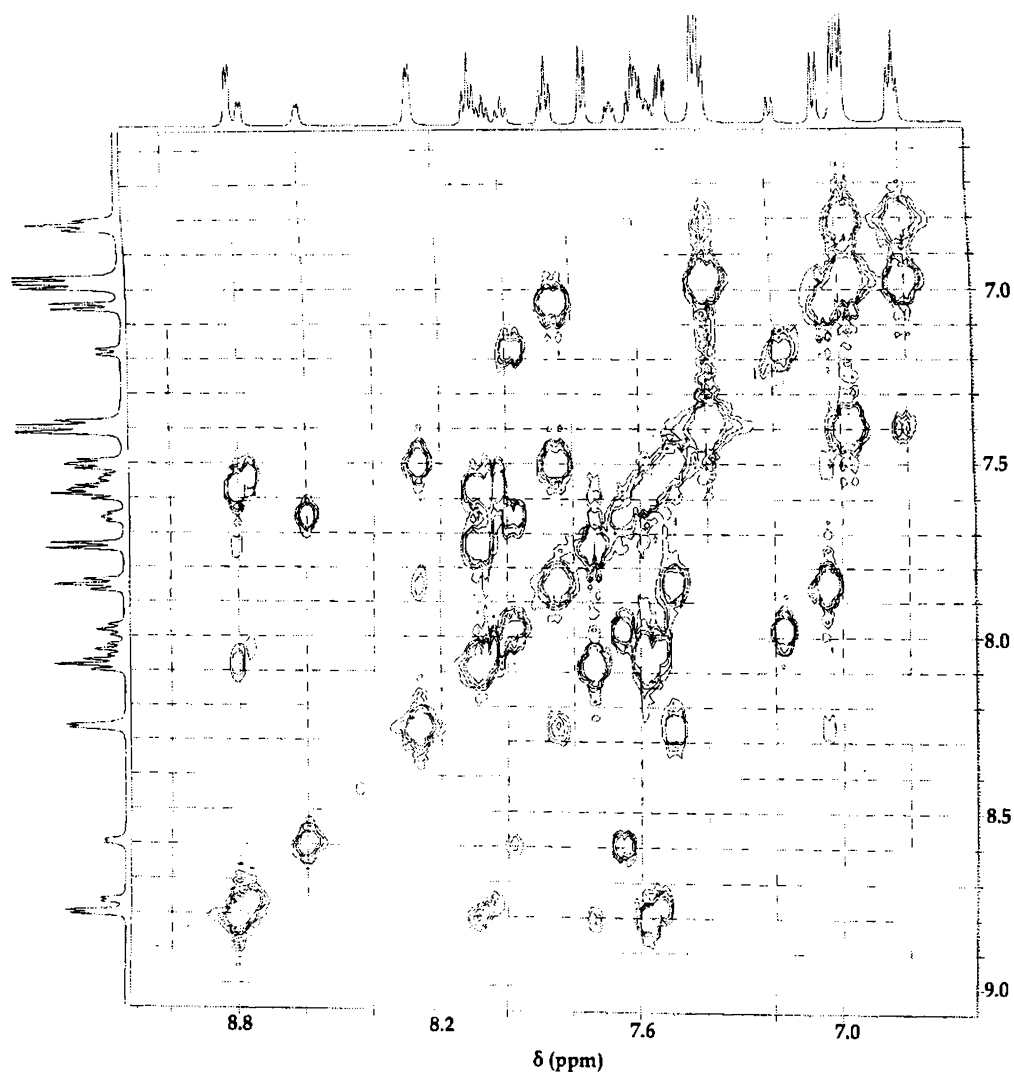


Fig. 7.18. 1H - 1H COSY spectrum of compound $(CdL^1NCS)_2$

The resonances at 8.80 and 8.60 ppm can be assigned to the protons on the non-coordinating pyridyl rings and other proton resonances in the range are shifted due to coordination. The aromatic region is better resolved with clearly distinguishable

peaks and they reveal close coupling interactions between each other. The region beyond 4 ppm reveals only some solvent peaks.

7.1.12. CdL^1N_3 (40)

The azido complex also is synthesized by the metathetical displacement of the acetate ion by azido anion in the Cd(II) complex. The IR spectrum of **40** reveals a broad band 3440 cm^{-1} , which can be assigned to the asymmetric stretching vibrations of the lattice water content in the sample. A sharp band at 2041 cm^{-1} corresponds to the asymmetric stretching vibrations of the coordinated azido group (Fig. 7.19). Another strong band at 1594 cm^{-1} corresponds to the stretching vibrations of the newly formed $\text{N}=\text{C}$ bond due to deprotonation. Due to coordination the azomethine stretching band is shifted by *ca.* 60 cm^{-1} and is observed as a low intensity band at 1529 cm^{-1} . The $\delta(\text{CS})$ band of the coordinated thiolate group appear as a medium band at 750 cm^{-1} , which is also shifted from the corresponding value in the free ligand.

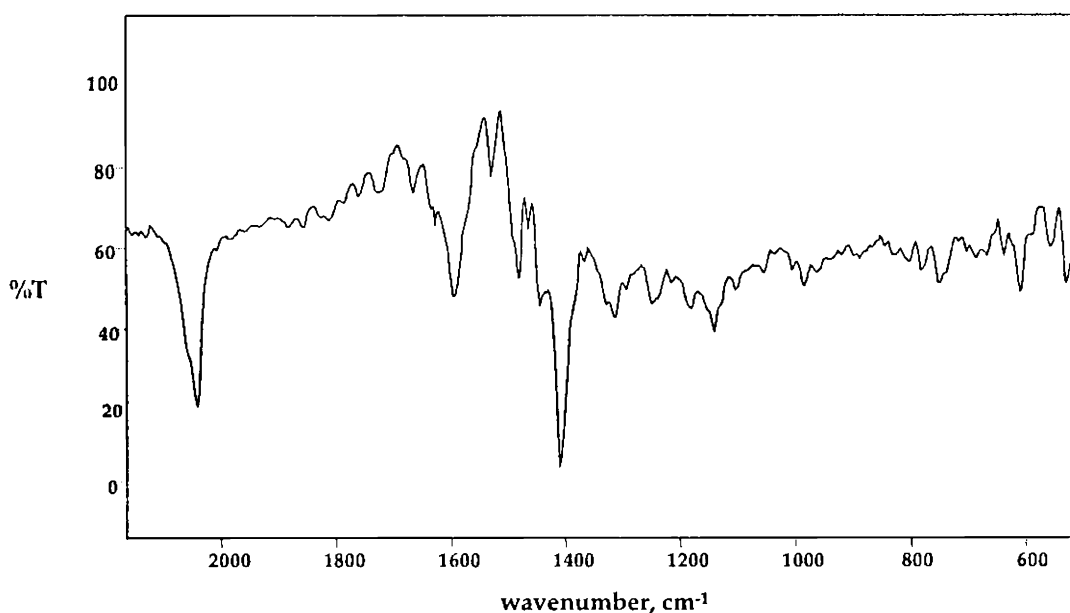


Fig. 7.19. IR spectrum of the compound CdL^1N_3

Medium bands observed at 463 , 434 and 376 cm^{-1} can be assigned to the coordinated $\nu(\text{Cd}-\text{N}_3)$, $\nu(\text{CdN}_{\text{azo}})$ and $\nu(\text{CdS})$ vibrations. In the solid-state electronic

spectrum, the intra-ligand $\pi \rightarrow \pi^*$ and the $n \rightarrow \pi^*$ transitions are observed as a sharp peak at 297 nm and two shoulders at 310 and 336 nm. The charge transfer transitions appear as a broad peak at 388 nm and a shoulder at 423 nm.

7.1.13. $\text{CdL}^1\text{Br}\cdot 2\text{H}_2\text{O}$ (41)

The lattice water content in the compound shows the asymmetric stretching vibrations at 3487 and 3379 cm^{-1} . The $\nu(\text{NH})$ vibration of the free N–H group at the *N*(4)-position of the thiosemicarbazone moiety is observed at 3060 cm^{-1} . The azomethine stretching band is shifted to 1528 cm^{-1} in the complex as a result of coordination. A sharp band at 1595 cm^{-1} is due to the $\nu(\text{NC})$ vibrations of the newly formed N=C bond. The band due to the bending vibration of the coordinated thiolate group appears at regions near 750 cm^{-1} , which is also shifted from a $\delta(\text{CS})$ band at 806 cm^{-1} in the ligand.

Unfortunately, due to the lack of solubility of the compound in the deuteriated solvents, the NMR studies of the present complex could not be carried out. However, in the solid-state electronic spectrum, intra-ligand transitions are observed at 341 and 372 nm, which are shifted from the corresponding values in the ligand, due to coordination and resultant electron delocalization. The charge transfer transitions appear as two shoulders at 447 and 497 nm and the charge transfer bands tails into the visible region.

7.1.14. $\text{CdL}^3\text{Cl}\cdot 2\text{H}_2\text{O}$ (42)

Several discrete bands are observed near 3400 cm^{-1} region in the IR spectrum, which may arise due to the association of thioamide groups in adjacent molecules in the solid sample. A broad band at 3230 cm^{-1} is in accordance with the lattice water content in the sample. The $\nu(\text{NH})$ stretching vibrations at *N*(4) give rise to a medium band at 3056 cm^{-1} . The cyclohexyl stretching vibrations are observed as two sharp bands at 2934 and 2853 cm^{-1} . A strong band at 247 cm^{-1} can be assigned to the terminal chlorine in the present compound. There is one more strong band in the 200–300 region, near 280 cm^{-1} in the spectrum, which can be assigned to the vibrations of

the coordinated pyridyl ring as it is observed in other complexes too. The azomethine stretching vibrations are observed at 416 cm^{-1} in the far IR region, while the $\nu(\text{CdS})$ vibrations are observed as a medium band at 370 cm^{-1} . The electronic spectrum reveals the intra-ligand transitions at 306 and 326 nm. The charge transfer transitions are observed at 388 and 402 nm and all the transitions are shifted from their corresponding values observed in the free ligand as a result of coordination.

^1H NMR spectrum of the compound $\text{CdL}^3\text{Cl}\cdot 2\text{H}_2\text{O}$ is given in Fig. 7.20. The spectrum is poorly resolved, may be due to the low solubility of the compound in DMSO. A doublet at 8.73 ppm integrates as one proton and is assigned to the N(4)-H resonance. A low intensity peak at 8.52 ppm and a doublet at 8.12 ppm integrate as two protons and they are assigned to the alpha proton resonances on the pyridyl rings and are shifted as a result of coordination. The aromatic proton resonances appear as weak multiplets in the 7.05 – 7.95 ppm region and they are poorly resolved. The cyclohexyl C13-H resonance appears at 3.34 ppm and the equatorial and axial proton resonances appear as multiplets in the 1.30–1.80 and 1.05–1.35 ppm regions respectively.

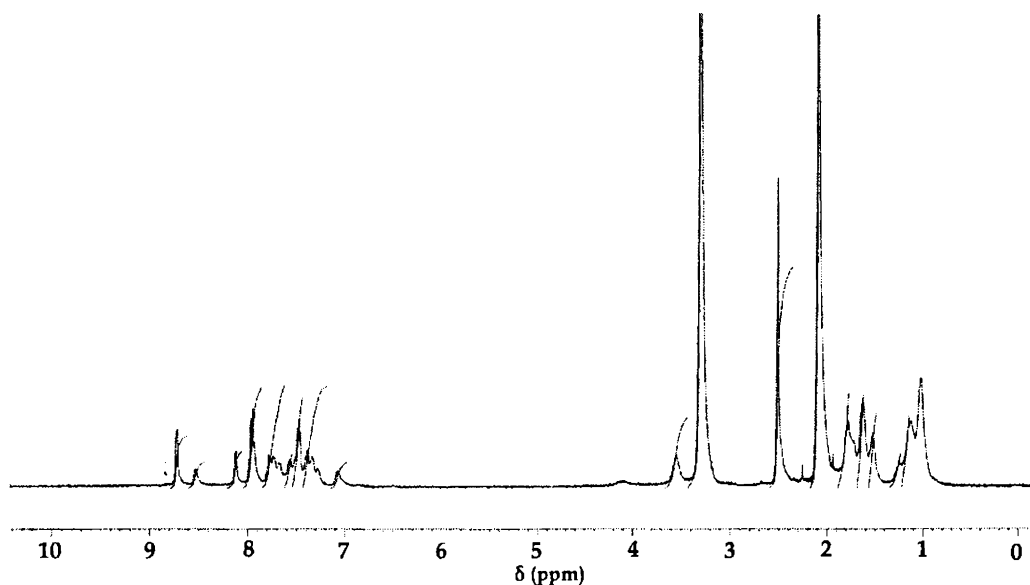


Fig. 7.20. ^1H NMR spectrum of compound $\text{CdL}^3\text{Cl}\cdot 2\text{H}_2\text{O}$

In the ^{13}C NMR spectrum of compound **42** (Fig. 7.21), the resonance at 177.02 ppm corresponds to the C6 carbon atom. A strong resonance at 153.80 ppm

corresponds to the C12 carbon resonance. Two weak resonances at 152.79 and 150.17 ppm belong to the non-protonated alpha carbon atoms on the pyridyl rings. The resonances at 149.07, 148.57 and 147.73 ppm correspond to the carbon atoms C1, C11 and C13 respectively. As a result of coordination the electron density on one of the pyridyl rings is decreased and hence the aromatic carbon resonances are shifted downfield. But the carbon resonances on the non-coordinated pyridyl and phenyl rings remain almost unshifted. Hence the other aromatic carbon resonances are observed in the 123.18 – 139.35 ppm region. The cyclohexyl carbon resonances are observed at 51.36 (C13), 32.24 (C16), 25.29 (C14 and C17) and 24.96 (C15 and C18) ppm.

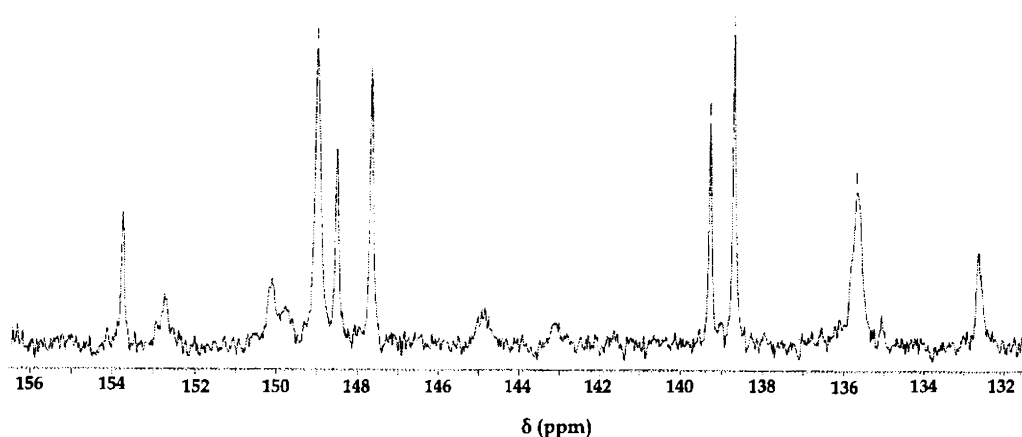


Fig. 7.21. ^{13}C NMR spectrum of compound $\text{CdL}^3\text{Cl}\cdot 2\text{H}_2\text{O}$

7.1.15. $(\text{CdL}^3\text{N}_3)_2$ (43)

The IR spectrum of the compound **43** reveals two strong bands, one at 2151 cm^{-1} and another at 2044 cm^{-1} , with a split at 2062 cm^{-1} (Fig.7.22). This is characteristic of the asymmetric stretching vibrations of a bridged azido group in a bimetallic complex. Since the elemental analyses data suggest a CdL^3N_3 stoichiometry for the compound, the geometry of the compound can be proposed as that in Fig. 7.27. The azomethine stretching band is shifted to 1564 cm^{-1} and the thiolate bending band is shifted to 741 cm^{-1} , supporting the coordinated nature of the thiosemicarbazone in the complex.

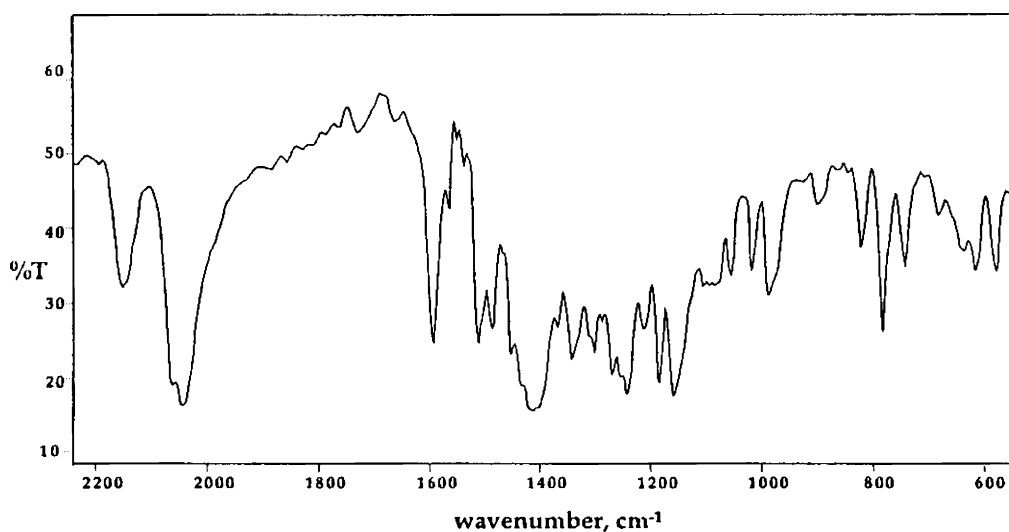


Fig. 7.22. IR spectrum of the compound $(\text{CdL}^3\text{N}_3)_2$

The electronic spectrum reveals the intra-ligand $\pi \rightarrow \pi^*$ and the $n \rightarrow \pi^*$ transitions at 314 and 357 nm. The charge transfer transitions are observed at 404 nm and as a shoulder at 442 nm. The ^1H NMR spectrum of compound **43** is poorly resolved and the ^1H - ^1H COSY spectrum is given in Fig. 7.23. The spectrum reveals features similar to that of compound **39** above. It is observed that the IR spectrum points towards a possible bridging structure for the compound. The ^1H NMR spectrum also gives more evidence for the bridged nature of the complex. Similar to compound **39** above, the proton resonances in the region 8.75–7.9 ppm show four peaks and their integration sums up to 3.65. This points to a possible presence of four alpha protons on the four pyridyl rings. Secondly, going through the COSY spectrum, we can see that there are four peaks at 7.65 and 7.55 ppm, which show no correlation interactions with the aromatic protons. Hence these protons can be assigned to the $N(4)$ -H hydrogens on the ligand moiety. Additionally, some of these peaks show correlation interactions with the cyclohexyl C13H proton resonance, which in turn shows interaction with the other cyclohexyl protons at 1.15 ppm. Hence the resonances at 7.65 and 7.55 ppm can be assigned to the $N(4)$ -H resonance on the two ligand moieties. The cyclohexyl equatorial and axial protons reveal their resonances as multiplets in the range 1.77 – 0.98 ppm.

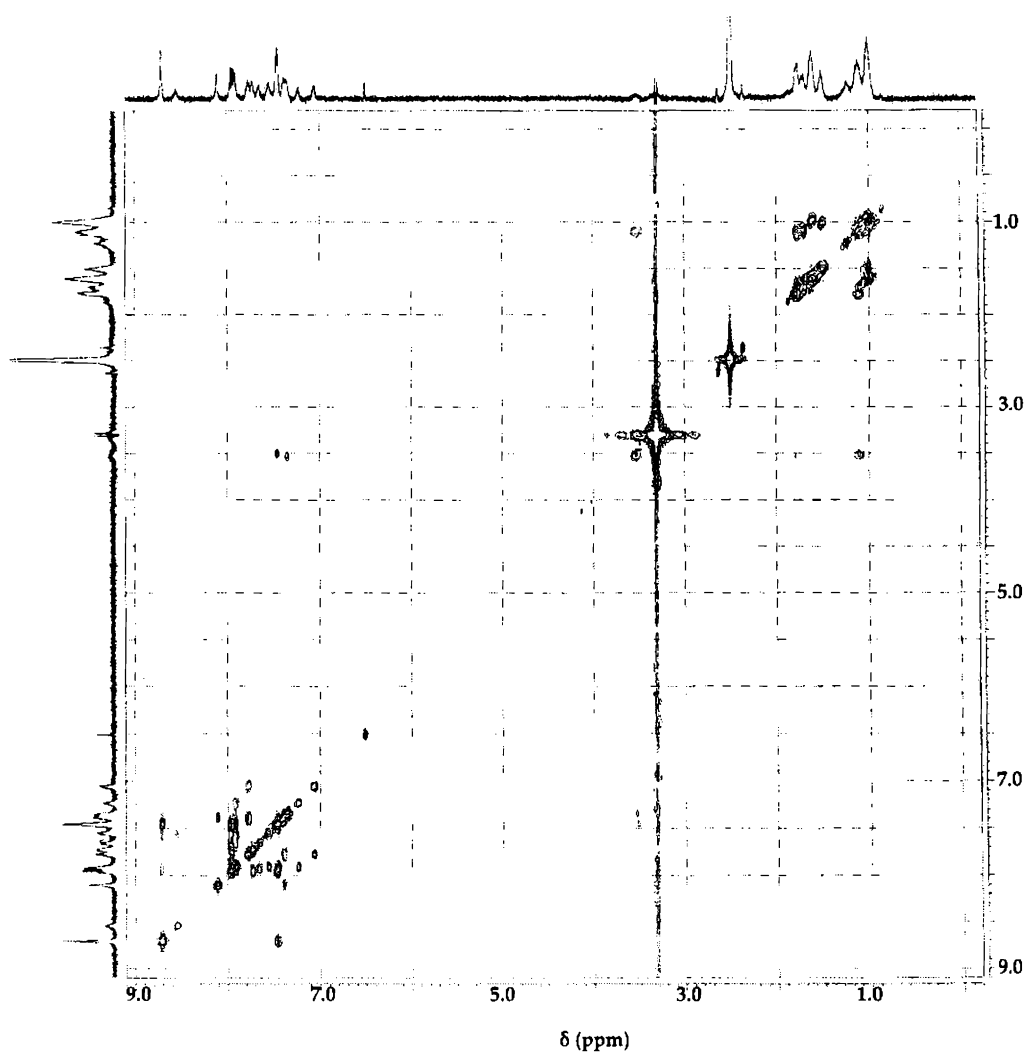


Fig. 7.23. ^1H - ^1H COSY spectrum of $(\text{CdL}^3\text{N}_3)_2$

7.1.16. $(\text{CdL}^3\text{NCS})_2$ (44)

The present compound reveals almost similar stereochemistry as that of the compound **43** mentioned above. The elemental analyses data suggest a stoichiometry with the empirical formula CdL^3NCS for the compound. However, the IR spectrum reveals some characteristic bands corresponding to a bridging NCS group (Fig. 7.24). A strong band, which is splitted into two sharp bands at 2062 and 2029 cm^{-1} is observed due to the asymmetric stretching vibrations of the thiocyanate group. Hence in accordance with the stoichiometric results, a stereochemistry as that given in

Fig.7.27 is proposed for the compound. The azomethine stretching vibrations are observed as a weak band at 1564 cm^{-1} and the thiolate bending vibrations in the complex are observed as a medium band at 743 cm^{-1} , which are shifted from the corresponding values in the ligand, thus supporting coordination.

However, the NMR studies of the present complex could not be carried out due to the lack of solubility of the compound. The electronic spectrum reveals the intra-ligand $\pi\rightarrow\pi^*$ and the $n\rightarrow\pi^*$ transitions at 298 and 323 nm. The charge transfer transitions are observed as a broad peak at 412 nm.

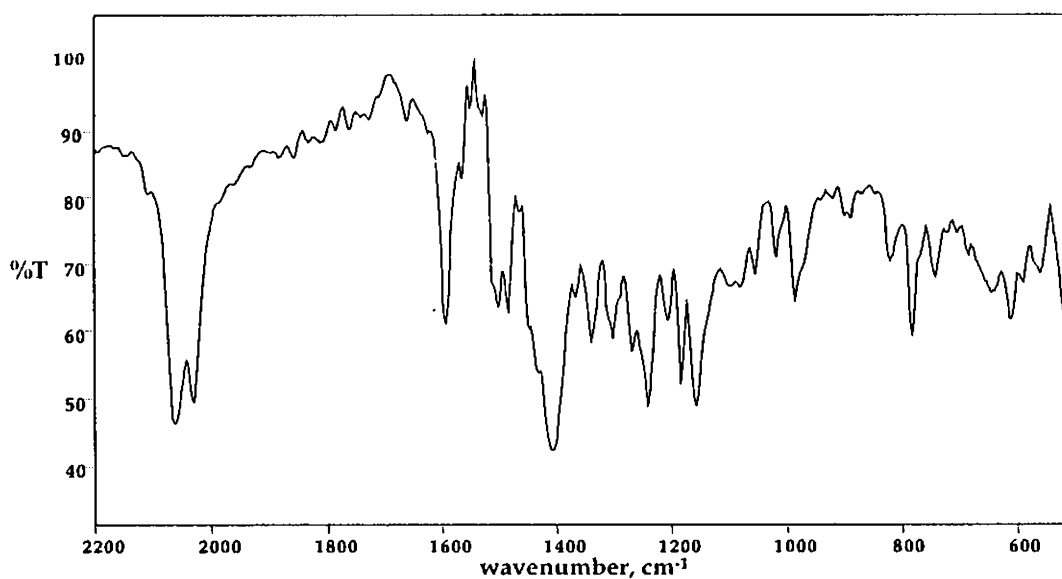


Fig. 7.24. IR spectrum of the compound $(\text{CdL}^3\text{NCS})_2$

7.1.17. $\text{CdL}^3\text{Br}\cdot 4\text{H}_2\text{O}$ (45)

Similar to compound 43 above, some discrete bands are observed near 3600 and 3400 cm^{-1} in the IR spectrum. These can be assigned either to the asymmetric stretching vibrations of lattice water or to the presence of associated thioamide functions in the solid state. The cyclohexyl stretching bands are observed at 2934 and 2853 cm^{-1} . The $\nu(\text{CN})$ vibrations of both the azomethine and the new $\text{N}4=\text{C}12$ bonds appear as a combination band near 1540 cm^{-1} in the complex. The thiolate bending vibrations are shifted to 746 cm^{-1} in the complex from a value of 801 cm^{-1} in the free

ligand. The $\nu(\text{CdBr})$ vibrations due to the terminal bromine appear 225 cm^{-1} . The azomethine stretching vibrations are observed at 448 cm^{-1} and the thiolate stretching vibrations are observed at 385 cm^{-1} in the far IR region. The solid-state electronic spectrum reveals the $\pi\rightarrow\pi^*$ and the $n\rightarrow\pi^*$ transitions at 304 and 326 nm. The charge transfer transitions are observed as shoulders at 399, 427 and 440 nm. The region beyond 475 nm appears to be devoid of any transitions, in accordance with the d^{10} configuration of Cd^{2+} metal centre in the complex.

7.1.18. CdL^3OAc (46)

The IR spectrum of the compound **46** revealed several discrete bands near 3000 cm^{-1} , which can be assigned to the $\nu(\text{CH})$ vibrations of the acetato group. It is interesting to note that a combination band is observed at 1500 cm^{-1} region of the IR spectrum, with four splittings at $1595, 1579, 1562$ and 1552 cm^{-1} (Fig. 7.25). This gives clear evidence for the presence of additional bands in this region corresponding to the $\nu(\text{C}=\text{O})$ and $\nu(\text{C}-\text{O})$ vibrations of the coordinated acetate group in the complex.

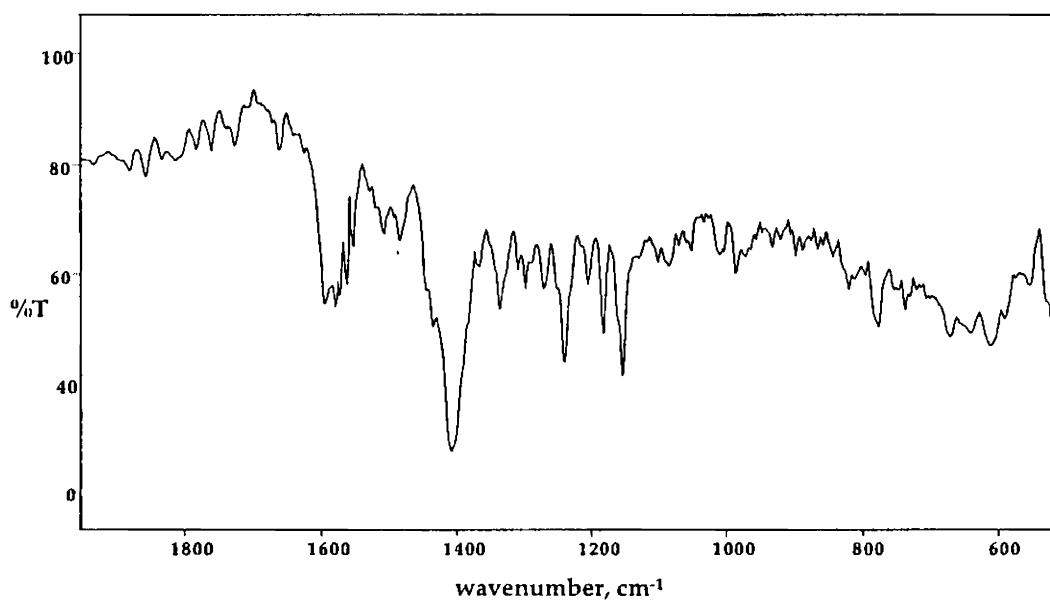
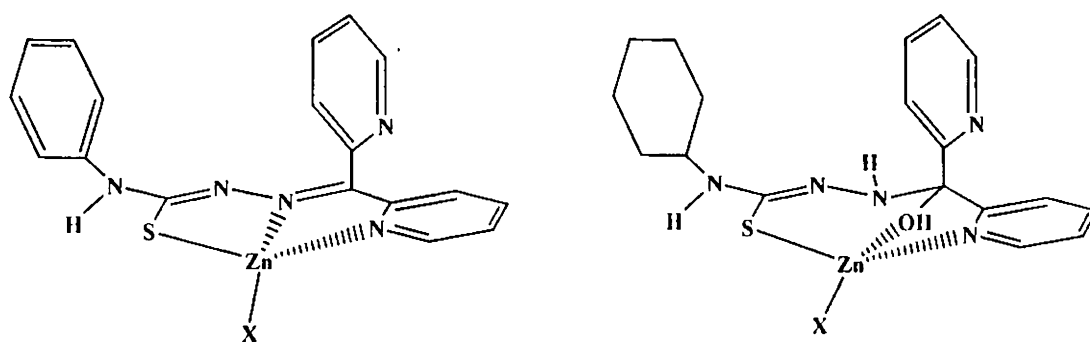


Fig. 7.25. IR spectrum of the compound CdL^3OAc

Thus, unlike in other acetato complexes in this series, the IR spectrum of compound **46** gives evidence for the coordinated acetato vibrations in the complex. The thiolate stretching bands are shifted to 777 cm^{-1} from the corresponding value in the free ligand, giving support for the coordination of the thiosemicarbazone moiety. The $\delta(\text{CH})$ vibrations of the acetato group is observed at 451 cm^{-1} . The $\nu(\text{CdS})$ bands due to coordinated thiolate group is observed at 390 cm^{-1} and the coordinated pyridyl ring vibration is observed at 275 cm^{-1} . The electronic spectrum reveals the intraligand transitions at 318 nm and the charge transfer transitions are observed as a strong peak at 414 nm and as a shoulder at 438 nm .

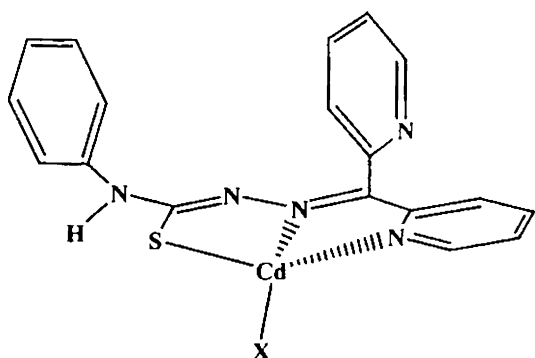
Based on these spectral studies, the tentative structures for the complexes can be proposed as given below: (Figs. 7.26 and 7.27)



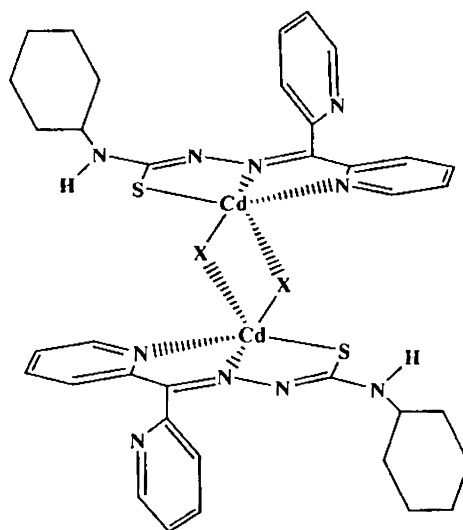
X = -Cl (Compound **29**)
 -NCS (Compound **30**)
 -NO₃ (Compound **31**)
 -N₃ (Compound **32**)
 -OAc (Compound **33**)
 -Br (Compound **34**)

X = -Cl (Compound **35**)
 -NCS (Compound **36**)
 -OAc (Compound **37**)

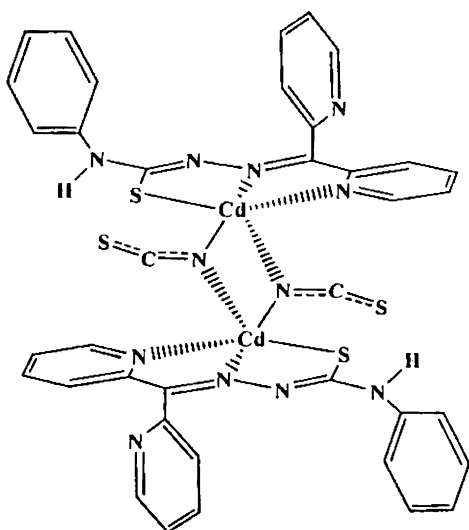
Fig. 7.26. Tentative structures of the Zn(II) complexes. Water of hydration and solvent molecules in the lattice are omitted for convenience.



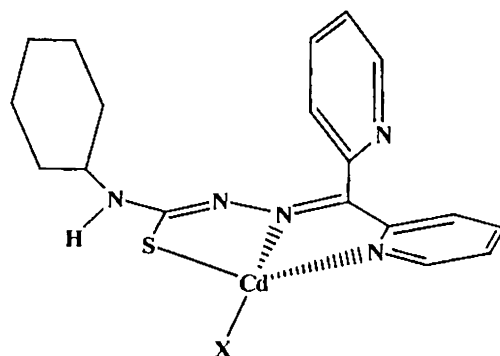
X = -Cl (Compound 38)
 -N₃ (Compound 40)
 -Br (Compound 41)



X = -N₃ (Compound 43)
 -NCS (Compound 44)



Compound 39



X = -Cl (Compound 42)
 -Br (Compound 45)
 -OAc (Compound 46)

Fig. 7.27. Tentative structures of the Cd(II) complexes. Water of hydration in the lattice is omitted for convenience.

7.2. Experimental

Materials

Di-2-pyridyl ketone (Fluka), $\text{Zn}(\text{OAc})_2$ (BDH), $\text{Zn}(\text{NO}_3)_2 \cdot 6\text{H}_2\text{O}$ (Merck), ZnBr_2 (Reidel-De Haen), ZnCl_2 (Merck), NaN_3 (Reidel-De Haen) KSCN (BDH) and methanol (Ranchem) were used as received.

Synthesis of complexes

ZnL^1Cl (29): Methanolic solution of HL^1 (0.333 g, 1 mmol) is mixed with ZnCl_2 (0.136 g, 1 mmol) and heated under reflux for four hours. Yellow crystalline product was then formed, which was separated, washed with ether and dried over P_4O_{10} *in vacuo*. Yield: 0.33 g (72%). Elemental Anal. Found (Calc.): C, 50.22 (49.90); H, 3.35 (3.26); N, 16.36 (16.16)%.

$\text{ZnL}^1\text{NCS} \cdot 2\text{H}_2\text{O}$ (30): To an ethanolic solution of HL^1 (0.333 g, 1 mmol), 1 mmol of $\text{Zn}(\text{OAc})_2$ (0.219 g) dissolved in methanol (10 ml) was added and refluxed for the preparation of compound 29. Aqueous solution of KSCN (0.097 g, 1 mmol) was then added to the solution followed by a further refluxing for three hours. Deep yellow product separated out was collected, washed with ether and dried *in vacuo*. Yield: 0.44 g (68%). Elemental Anal. Found (Calc.): C, 46.65 (46.39); H, 3.14 (3.69); N, 16.86 (17.06)%.

ZnL^1NO_3 (31): $\text{ZnNO}_3 \cdot 6\text{H}_2\text{O}$ (0.297 g, 1 mmol) dissolved in 20 ml methanol was added to HL^1 (0.333 g, 1 mmol) in methanol and refluxed for six hours. Yellow crystalline product separated out, which was washed with a small amount of cold dilute methanol followed by ether and dried over P_4O_{10} *in vacuo*. Yield: 0.36 g (58%). Elemental Anal. Found (Calc.): C, 46.96 (47.02); H, 3.09 (3.07); N, 17.59 (18.28)%.

$\text{ZnL}^1\text{N}_3 \cdot \text{CH}_3\text{OH}$ (32): Methanolic solution of $\text{Zn}(\text{OAc})_2 \cdot 2\text{H}_2\text{O}$ (0.219 g, 1 mmol) was added to HL^1 (0.333 g, 1 mmol) in methanol. After fifteen minutes, aqueous solution of sodium azide (0.130 g, 2 mmol) was added to the reaction mixture and further

refluxed for two hours. Bright yellow coloured product, which separated out, was filtered and washed with ether and dried over P_4O_{10} *in vacuo*. Yield: 0.38 g (56%). Elemental Anal. Found (Calc.): C, 48.27 (48.36); H, 3.29 (3.85); N, 23.55 (23.75)%.

ZnL¹OAc·1.5H₂O (33): Zn(OAc)₂·2H₂O (0.219 g, 1 mmol) dissolved in 10 ml methanol was added to a methanolic solution of HL¹ (0.333 g, 1 mmol). After two hours, yellow product separated out, was washed with ether and dried *in vacuo*. Yield: 0.33 g (60%). Elemental Anal. Found (Calc.): C, 49.04 (49.65); H, 3.69 (4.17); N, 14.52 (14.47)%.

ZnL¹Br (34): HL¹ (0.333 g, 1 mmol) was dissolved in methanol. ZnBr₂ (0.225 g, 1 mmol) dissolved in 10 ml methanol was added to the solution and refluxed for four hours. Yellow crystalline product of Zn₂L¹Br separated out was collected, washed with ether and dried *in vacuo*. Yield: 0.31 g (57%). Elemental Anal. Found (Calc.): C, 46.08 (45.26); H, 2.97 (2.95); N, 14.77 (14.66)%.

ZnL²Cl (35): The preparation of compound 35 was carried out by the same procedure as that of compound 29 above, except that HL² (0.339 g, 1 mmol) was used instead of HL¹. Yellow product formed was separated, washed with ether and dried over P_4O_{10} *in vacuo*. Yield: 0.29 g (62%). Elemental Anal. Found (Calc.): C, 47.85 (47.27); H, 4.76 (4.85); N, 15.51 (15.31)%.

ZnL²NCS·2H₂O (36): The preparation of compound 36 was carried out by the same procedure as that of compound 30 above, except that HL² (0.339 g, 1 mmol) was used instead of HL¹. Yellow crystalline product separated out was collected, washed with ether and dried *in vacuo*. Yield: 0.35 g (55%). Elemental Anal. Found (Calc.): C, 44.48 (44.23); H, 4.51 (5.08); N, 16.86 (16.29)%.

ZnL²OAc (37): To a solution of HL² (0.339 g, 1 mmol) in 10 ml methanol, methanolic solution of Zn(OAc)₂·2H₂O (0.219 g, 1 mmol) was added and refluxed. Deep yellow product separated out was washed with ether and dried *in vacuo*. Yield: 0.29 g (52%). Elemental Anal. Found (Calc.): C, 49.98 (49.95); H, 5.31 (5.24); N, 14.65 (14.56)%.

CdL¹Cl·2H₂O (38): Di-2-pyridyl ketone (0.184 g, 1 mmol) and 4-phenyl-3-thiosemicarbazide (0.167 g, 1 mmol) in methanol were mixed and refluxed continuously. After four hours, CdCl₂ (0.183 g, 1 mmol) dissolved in 10 ml methanol was added to the reaction mixture and the refluxing continued for further four hours. Bright yellow coloured product of compound 38 separated out was collected, washed with ether and dried *in vacuo*. Yield: 0.29 g (55%). Elemental Anal. Found (Calc.): C, 42.33 (41.87); H, 2.90 (3.51); N, 13.59 (13.56)%.

(CdL¹NCS)₂ (39): Di-2-pyridyl ketone (0.184 g, 1 mmol) dissolved in 5 ml methanol was mixed with methanolic solution of 4-phenyl-3-thiosemicarbazide (0.167 g, 1 mmol) and refluxed continuously for four hours. After that, Cd(OAc)₂·2H₂O (0.266 g, 1 mmol) was added to the solution and the refluxing continued. Fifteen minutes later, KSCN (0.097 g, 1 mmol) dissolved in 10 ml of water was added to the reaction mixture and further refluxed for three hours. Deep yellow product of 39 obtained was separated, washed and dried under *vacuo*. Yield: 0.41 g (58%). Elemental Anal. Found (Calc.): C, 44.31 (43.81); H, 2.80 (3.10); N, 16.44 (16.13)%.

CdL¹N₃ (40): Methanolic solution of Cd(OAc)₂·2H₂O (0.266 g, 1 mmol) was added to refluxing solution of di-2-pyridyl ketone (0.184 g, 1 mmol) with 4-phenyl-3-thiosemicarbazide (0.167 g, 1 mmol) in methanol. After fifteen minutes, aqueous solution of sodium azide (0.130 g, 2 mmol) was added to the reaction mixtures and further refluxed for two hours. Deep yellow coloured product separated out was filtered and washed with ether and dried over P₄O₁₀ *in vacuo*. Yield: 0.44 g (60%). Elemental Anal. Found (Calc.): C, 43.73 (44.41); H, 2.96 (2.90); N, 23.20 (23.02)%.

CdL¹Br·2H₂O (41): Di-2-pyridyl ketone (0.184 g, 1 mmol) and 4-phenyl-3-thiosemicarbazide (0.167 g, 1 mmol) dissolved in methanol were mixed and refluxed continuously. After four hours, CdBr₂·4H₂O (0.344 g, 1 mmol) dissolved in 10 ml methanol was added to the reaction mixture and the refluxing continued for further four hours. Yellow crystalline product of compound 41 separated out was collected,

washed with ether and dried *in vacuo*. Yield: 0.36 g (52%). Elemental Anal. Found (Calc.): C, 37.85 (38.55); H, 2.55 (3.24); N, 12.14 (12.49)%.

CdL³Cl·2H₂O (42): The preparation of compound **42** was carried out by the same procedure as that of **38** above, except that 4-cyclohexyl-3-thiosemicarbazide (0.173 g, 1 mmol) was used instead of 4-phenyl-3-thiosemicarbazide. Yellow crystalline product of CdL³Cl·2H₂O separated out was collected, washed with ether and dried over P₂O₅ *in vacuo*. Yield: 0.29 g (55%). Elemental Anal. Found (Calc.): C, 39.43 (40.01); H, 4.35 (4.85); N, 12.72 (12.96)%.

(CdL³N₃)₂ (43): Cd(OAc)₂·2H₂O (0.266 g, 1 mmol) in methanol was added to the refluxing solution of di-2-pyridyl ketone (0.184 g, 1 mmol) with 4-cyclohexyl 3-thiosemicarbazide (0.173 g, 1 mmol). After fifteen minutes, aqueous solution of sodium azide (0.130 g, 2 mmol) was added to the reaction mixture and further refluxed for two hours. Yellow product separated out was filtered and washed with ether and dried over P₄O₁₀ *in vacuo*. Yield: 0.42 g (56%). Elemental Anal. Found (Calc.): C, 43.38 (43.86); H, 4.20 (4.09); N, 22.69 (22.73)%.

(CdL³NCS)₂ (44): A procedure similar to that of **39** above was employed for the preparation of compound **44**, except that 4-cyclohexyl-3-thiosemicarbazide (0.173 g, 1 mmol) was used in place of 4-phenyl-3-thiosemicarbazide. Yellow product of **44** obtained was separated, washed and dried under *vacuo*. Yield: 0.41 g (55%). Elemental Anal. Found (Calc.): C, 44.11 (44.84); H, 3.98 (3.96); N, 16.36 (16.51)%.

CdL³Br·4H₂O (45): The preparation of compound **45** was carried out by the same procedure as that of **41** above, except that 4-cyclohexyl-3-thiosemicarbazide (0.173 g, 1 mmol) was used instead of 4-phenyl-3-thiosemicarbazide. Yellow crystalline product of CdL³Br·4H₂O separated out was collected, washed with ether and dried *in vacuo*. Yield: 0.39 g (56%). Elemental Anal. Found (Calc.): C, 35.40 (35.86); H, 4.55 (4.68); N, 11.33 (11.62)%.

CdL³OAc (46): Cd(OAc)₂·2H₂O (0.266 g, 1 mmol) dissolved in 10 ml methanol was added to the refluxing methanolic solution of di-2-pyridyl ketone (0.184 g, 1 mmol) and 4-cyclohexyl-3-thiosemicarbazide (0.173 g, 1 mmol). After four hours, bright yellow product separated out, which was washed with ether and dried *in vacuo*. Yield: 0.36 g (58%). Elemental Anal. Found (Calc.): C, 46.58 (47.11); H, 4.42 (4.55); N, 13.55 (13.73)%.

References:

1. M. A. Ali, A. H. Mirza, M. Nazimuddin, H. Rahman, R. J. Butcher, *Transition Met. Chem.* 27 (2002) 268.
2. Z. Li, Z. -H. Loh, S. -W. A. Fong, Y. -K. Yan, W. Henderson, K. F. Mok, T. S. A. Hor, *J. Chem. Soc. Dalton Trans.* (2000) 1027.
3. J. S. Casas, M. V. Castano, M. S. Garcia-Tasende, E. Rodriguez-Castellon, A. Sanchez, L. M. Sanjuan, J. Sordo, *Dalton Trans.* (2004) 2019.
4. J. S. Casas, M. V. Castano, E. E. Castellano, J. Ellena, M. S. Garcia-Tasende, A. Gato, A. Sanchez, L. M. Sanjuan, J. Sordo, *Inorg. Chem.* 41 (2002) 1550.
5. W. Zhao, J. Fan, T. Okamura, W. -Y. Sun, N. Ueyama, *New. J. Chem.* 28 (2004) 1142.
6. Y. Yamamoto, T. Suzuki, S. Kaizaki, *J. Chem. Soc. Dalton Trans.* (2001) 1566.
7. S. Padhye, G. B. Kauffman, *Coord. Chem. Rev.* 63 (1985) 127.
8. P. Ghosh, G. Parkin, *J. Chem. Soc. Chem. Commun.* (1998) 413.
9. M. Mohan, A. Agarawal, N. K. Jha, *J. Inorg. Biochem.* 34 (1998) 41.
10. M. Maji, S. Ghosh, S. K. Chattopadhyay, *Transition Met. Chem.* 23 (1998) 81.
11. M. Mohan, P. Sharma, M. Kumar, N. K. Jha, *Inorg. Chim. Acta* 125 (1986) 9.
12. Z. -M. Xue, Y. -P. Tian, D. Wang, M. -H. Jiang, *Dalton Trans.* (2003) 1373.
13. A. Sreekanth, S. Sivakumar, M. R. P. Kurup, *J. Mol. Struct.* 655 (2003) 47.
14. R. M. Silverstein, G. C. Bassler, T. C. Morrill, *Spectrometric Identification of Organic Compounds*, 4th ed., John Wiley & Sons, New York, 1981.
15. K. Nakamoto *in* *Infrared and Raman Spectra of Inorganic and Coordination Compounds*, 4th ed., John Wiley & Sons, New York, 1986.

Thiosemicarbazones are thiourea derivatives with the general formula $R_2N-C(S)-NH-N=CR_2$. In the solution state, the thiosemicarbazones exhibit the thione-thiol tautomerism similar to the keto-enol tautomerism, and in solution state the thiol form predominates and a deprotonation at the thiolate group in alcoholic medium enhances the coordination abilities of the thiosemicarbazones.

Accordingly, an unsubstituted thiosemicarbazone can function as a bidentate ligand by coordinating through the thiolate sulfur and the azomethine nitrogen, while the presence of additional donor sites with pyridyl derivatives in the ketonic part can render them potential tri-, quadri- or polydentate ligands. Hence an investigation into the stereochemistry of transition metal complexes of di-2-pyridyl ketone derivatives of *N*(4)-substituted thiosemicarbazones appeared quite interesting to us.

The magnetochemistry of metal complexes of di-2-pyridyl ketone is a current hot subject of research, which mainly owes to the excellent structural diversity of the complexes ranging from cubanes to clusters, with promising ferromagnetic outputs. There are many reports of single molecule magnets of di-2-pyridyl derivatives, however, all these reports were concerned with either the di-2-pyridyl ketone or its mono- or dimethylated anion as the principal ligand. Only few efforts were aimed at the magnetochemistry of metal complexes of thiosemicarbazones, and that too were concerned with the complexes of bis(thiosemicarbazones). However, as far as the monothiosemicarbazones are concerned, the magnetochemistry of transition metal complexes of di-2-pyridyl ketone thiosemicarbazones turned up quite unexplored. Consequently, an investigation into it appeared novel and promising to us and that prompted this study, which can be regarded as the initial step towards exploring the magnetochemistry of thiosemicarbazone complexes, especially of di-2-pyridyl ketone derivatives.

Four new ligands are prepared by modification of the procedures suggested by Klayman *et al.* and Scovill *et al.* Three of the ligands are isolated in the solid form while the fourth ligand remained in the solution form and hence a one-pot method was employed for the preparation of its metal complex. The ligands prepared are the following:

1. Di-2-pyridylmethanone *N*(4)-phenylthiosemicarbazone, HL¹
2. *N*(4)-cyclohexyl-2-[hydroxy(di-2-pyridyl)methyl]hydrazinecarbothioamide, HL²
3. Di-2-pyridylmethanone *N*(4)-cyclohexylthiosemicarbazone, HL³
4. *N*(4)-[di-2-pyridylmethylene]morpholine-4-carbothiohydrazide, HL⁴

We could successfully isolate single crystals suitable for X-ray diffraction for the first three ligands. The crystal system for the first ligand HL¹ is found to be monoclinic with space group *C*2/*c*. The second ligand HL² also turned out to be monoclinic with a different space group *P*2₁/*c*, while HL³ is observed to be triclinic with space group *P* $\bar{1}$. The azomethine and hydrazinic bond distances in HL¹ and HL² are observed to be intermediate between the values of corresponding formal single and double bond lengths, which substantiated the extended conjugation along the thiosemicarbazone skeleton. In the unit cell, all the three molecules are packed in a *zigzag* manner. In addition to the single crystal X-ray diffraction studies, the ligands are also characterized by spectroscopic methods such as IR, UV-Vis and 1-D and 2-D NMR methods. The two-dimensional NMR methods employed are ¹H-¹H correlation (COSY) and ¹H-¹³C (HMQC) techniques, which benefited towards the accurate assignment of individual peaks.

The ligands are made to complex with some transition metals such as Cu²⁺, Mn²⁺, VO²⁺, Ni²⁺, Co²⁺, Co³⁺, Zn²⁺ and Cd²⁺. The Cu(II) complexes prepared are characterized using IR, UV-Vis and EPR spectral studies. One of the Cu(II) complexes, CuTDCl₃ is observed to possess an unusual bimetallic structure, which is further supported by single crystal X-ray diffraction studies. Each Cu(II) centre exists in a square pyramidal geometry in CuTDCl₃ and the crystal system of the compound is monoclinic with space group *P*2₁/*c*. The compound is suggested to be formed by a simultaneous metal-induced cyclization and N-N bond cleavage. Previous observations were concerned with either the cyclization or the N-N bond cleavage alone, but a combination of both the rare phenomena during the formation of a coordination complex is observed for the first time. Among the other Cu(II) complexes, some of them revealed a possible dimeric stereochemistry. This is further

Summary and Conclusion

supported by the diamagnetic or magnetically concentrated attributes of the compounds and the presence of bands of bridged nature in the IR region. An effective exchange-coupled spin-pairing between two adjacent Cu(II) nuclei in a magnetically concentrated system through super-exchange pathways can lead to diamagnetic attributes. The magnetic behavior of the complexes is studied by measuring the magnetic susceptibility values at six different temperatures ranging from room temperature to liquid nitrogen temperature. The susceptibility values are then fitted into modified Bleaney – Bower's equation by least square fitting methods. The studies revealed that the bimetallic complex CuTbCl_3 is highly antiferromagnetic with a $2J$ value of -376 cm^{-1} . This can be attributed to two reasons, viz., the closer Cu–Cu distance ($2.9591(13) \text{ \AA}$) in the compound and the presence of the bridging chlorine and nitrogen atoms between the two Cu(II) nuclei in the molecule, which effect antiferromagnetic interactions in the compound through super-exchange pathways. Two other Cu(II) complexes also revealed antiferromagnetic behavior, while one revealed anomalous magnetic moments, and the others are observed to be diamagnetic. The diamagnetic nature of the Cu(II) complexes is explained through an effective antiferromagnetic exchange giving rise to a net spin-pairing effect.

The Mn(II) and VO(IV) complexes prepared are also characterized using IR, UV-Vis and EPR spectral studies. One of the Mn(II) complexes, $\text{Mn}(\text{L}^1)_2 \cdot \text{H}_2\text{O}$ is also studied by single crystal X-ray diffraction studies. There are two crystallographically independent molecules A and B, in the asymmetric unit of $\text{Mn}(\text{L}^1)_2(\text{H}_2\text{O})_3\text{DMF}$, with bond lengths and angles which agree with each other and are within normal ranges. The compound turned up with a distorted octahedral stereochemistry in a triclinic lattice with $P\bar{1}$ space group. The EPR studies of this complex revealed an isotropic g value at 2.021, while the two other manganese complexes $\text{Mn}(\text{L}^3)_2$ and $\text{Mn}(\text{L}^4)_2$ showed three g -tensors with values $g_1 = 5.691$, $g_2 = 2.871$, $g_3 = 2.021$ and $g_1 = 5.659$, $g_2 = 3.099$, $g_3 = 2.021$. This revealed less zero field splitting (ZFS) effects in $\text{Mn}(\text{L}^1)_2 \cdot \text{H}_2\text{O}$, while appreciable ZFS in the other two Mn(II) compounds. The axial zero field splitting parameter is calculated for the Mn(II) complexes, and it revealed very low value for $\text{Mn}(\text{L}^1)_2 \cdot \text{H}_2\text{O}$, which substantiated the above view point. The EPR spectra of the VO(IV) complexes turned out to be rhombic with three g -values and the

g -tensors showed lesser anisotropy, with values $g_1 = 2.015$, $g_2 = 1.995$, $g_3 = 1.943$ for $\text{VOL}^1(\text{acac})\cdot 2\text{H}_2\text{O}$ and $g_1 = 2.021$, $g_2 = 1.998$, $g_3 = 1.955$ for $\text{VOL}^2(\text{acac})$. The complexes are magnetically studied at various temperatures up to liquid nitrogen temperature, and the manganese complexes are observed to be antiferromagnetically coupled. However, since there is no direct contact or bridging atoms between the two Mn(II) atoms, the observed exchange coupled interactions can be accounted only on the basis of a quantum mechanical approach for a possible 'through space' interaction of the metal orbitals. In quantum mechanical considerations, the directional vectors in space are not confined to any particular axes or distances, and hence a net coupling of the moments is very nearly possible. However, the oxovanadyl complex studied showed no regular gradation with temperature and their magnetic susceptibility values failed to fit into different magnetic equations, and hence the compound is assumed to be possessing anomalous magnetic behavior.

The Ni(II) complexes prepared are mostly brown in color and we could successfully isolate single crystals suitable for X-ray diffraction for one of the compounds. The single crystal of $\text{Ni}(\text{L}^2)\cdot 2\text{H}_2\text{O}$ reveals two independent molecules in the asymmetric unit and the stereochemistry about Ni(II) is distorted octahedral. The crystal system is monoclinic and the space group is $P2_1/c$. This compound $\text{Ni}(\text{L}^2)\cdot 2\text{H}_2\text{O}$ reveals some anomalous magnetic behaviour, which is explained through a spin-state equilibrium possible in tetragonally distorted d^8 nickel complexes. However, two of the Ni(II) complexes are found to be weakly ferromagnetic with the $2J$ values near 50 cm^{-1} .

Some Co(II) and Co(III) complexes are also synthesized and characterized. Unfortunately, we could not isolate single crystals suitable for X-ray diffraction for the cobalt complexes of thiosemicarbazones. One of the Co(II) complexes revealed a well-resolved EPR spectrum with g values $g_{\parallel} = 2.282$ and $g_{\perp} = 1.994$, and this complex is also found to be having antiferromagnetic exchange interactions. Another Co(II) complex also revealed axial features in the EPR spectrum with g values $g_{\parallel} = 2.299$ and $g_{\perp} = 1.996$. However the compound is observed to possess anomalous magnetic moments. However, one of the compounds we synthesized turned up to be

[Co(*dpk*)₂]Br·4H₂O, where *dpk* stands for the gem-diol form of di-2-pyridyl ketone. A single crystal of this compound suitable for X-ray diffraction is isolated, which is found to exist in a monoclinic lattice with *C2/c* space group.

Zn(II) and Cd(II) complexes of HL¹ and HL³ are also prepared and characterized by different spectroscopic methods. Most of the complexes possess a four-coordinated stereochemistry. However, the IR and NMR data predict some possible dimeric attributes to few of the compounds, and hence a bridged structure is proposed for these compounds. Due to the presence of completely filled *d*-levels in Zn(II) and Cd(II), the complexes are observed to be diamagnetic in nature.

To conclude, we have synthesized some new thiosemicarbazones and their transition metal complexes and studied their structural, spectral and magnetic attributes. Some of the complexes revealed interesting stereochemistries and possible bridging characteristics with spectroscopic evidences. Unfortunately, single crystal X-ray diffraction studies could not be carried out for many of these interesting compounds due to the lack of availability of suitable quality single crystals. However, the magnetic studies provided support for the proposed stereochemistry giving evidences for their magnetically concentrated nature. The magnetic susceptibilities measured at six different temperatures in the 80–298 K range are fitted into different magnetic equations, which provided an idea about the magnetic behavior of the compounds under study. Some of the copper, oxovanadium, nickel and cobalt complexes are found to possess anomalous magnetic moments, i.e., they revealed no regular gradation with temperature. However, some other copper complexes are observed to be antiferromagnetic, due to super-exchange pathways. The manganese complexes and one of the cobalt complexes are also observed to be antiferromagnetic in nature. However, some nickel complexes have turned up to be ferromagnetic. Accordingly, the versatile stereochemistry and magnetic behavior of the complexes studied, prompt us to conclude that the transition metal complexes of di-2-pyridyl ketone thiosemicarbazones are promising systems for potential magnetic applications.

Curriculum vitae

Personal details

Birth 30th May 1978
Permanant address Sreyas, Vazhamuttom P.O., Omallur via, Pathanamthitta,
Kerala, India

Education

1993 S. S. L. C., Govt. V. H. S. School, Nandikara, Thrissur
(92.6%)
1993-1995 Pre-Degree, St. Mary's College, Thrissur
(83.3%)
1995-1998 B. Sc. Chemistry, Vimala College, Thrissur
(89.3%)
1998-2000 M. Sc. Hydrochemistry, Cochin University of Science and
Technology (81.9%, First class with distinction, 1st Rank)

Awards and honours

2000 Prof. Krishnan Nambeesan Memorial Award for securing
1st Rank in M. Sc. Hydrochemistry
2001 U-JRF from Cochin University of Science and Technology,
Kochi 682022
2002 KSCSTE-JRF in Chemistry from the Kerala State Council
for Science, Technology and Environment,
Thiruvananthapuram.

Positions of responsibility

Member, Organizing committee, National Symposium on Current Trends in Inorganic
Chemistry, CTIC-2004, Cochin University of Science and Technology

G9037

Research Publications

1. Structural and spectral studies of Ni(II) Complexes of di-2-pyridyl ketone N^4, N^4 - (butane-1, 4-diyl) thiosemicarbazone, V. Philip, V. Suni, M. R. Prathapachandra Kurup, M. Nethaji, *Polyhedron*, 23, 2004, 1225-1233.
2. Synthesis, spectral characterization and crystal structure of 2-benzoylpyridine $N(4)$ -cyclohexyl thiosemicarbazone, M. Joseph, V. Suni, C. R. Nayar, M. R. Prathapachandra Kurup, H. K. Fun, *J. Mol. Struct.*, 705, 2004, 63-70.
3. Structural, spectral and antimicrobial activities of Cu(II) complexes of 2-benzoylpyridine $N(4)$ -cyclohexyl thiosemicarbazone, M. Joseph, V. Suni, M. R. Prathapachandra Kurup, M. Nethaji, A. Kishore, G. Bhat, *Polyhedron*, 23, 2004, 3069-3080.
4. Dipyrin-2-ylmethanone $N(4)$ -methyl- $N(4)$ -phenylthiosemicarbazone, V. Philip, V. Suni, M. R. Prathapachandra Kurup, *Acta Crystallogr. C* 60, 2004, o856-o858.
5. 4-morpholinyl[2-[1-(2-pyridinyl)ethylidene]diazan-2-iumylidene]methanethiolate, H. -K. Fun, S. Chantrapomma, V. Suni, A. Sreekanth, S. Sivakumar, M. R. Prathapachandra Kurup, *Acta Crystallogr. E*, 61, 2005, o1337 - o1339.
6. Novel binuclear copper(II) complexes of di-2-pyridyl ketone $N(4)$ -methyl, $N(4)$ -phenylthiosemicarbazone: Structural and spectral investigations, V. Philip, V. Suni, M. R. Prathapachandra Kurup, M. Nethaji, *Polyhedron*, 24, 2005, 1133-1142.
7. Bis(μ -phenyl 2-pyridylketone N^4, N^4 -butane-1,4- diylthiosemicarbazonato)-bis[chlorocopper(II)], A. Sreekanth, V. Suni, R. P. John, M. Nethaji, M. R. Prathapachandra Kurup, *Acta Crystallogr. C* 61, 2005, m284 - m286.
8. Unusual Isolation of a hemiaminal product from 4-cyclohexyl-3-thiosemicarbazide and di-2-pyridyl ketone: structural and spectral investigations, V. Suni, M. Nethaji, M. R. Prathapachandra Kurup, *J. Mol. Struct*, 749/1-3, 2005, 177 - 182.
9. Structural and spectral perspectives of a novel thiosemicarbazone synthesized from di-2-pyridyl ketone and 4-phenyl-3-thiosemicarbazide, V. Suni, M. Nethaji, M. R. Prathapachandra Kurup, *Spectrochim. Acta*, in press.
10. Manganese(II) complexes of substituted di-2-pyridyl ketone thiosemicarbazones: structural and spectral studies, V. Philip, V. Suni, M. Nethaji, M. R. Prathapachandra Kurup, *Spectrochim. Acta*, in press.
11. Spectral characterization of iron(III) complexes of 2-benzoylpyridine $N(4)$ -substituted thiosemicarbazones, M. Joseph, A. Sreekanth, V. Suni, M. R. Prathapachandra Kurup, *Spectrochim. Acta*, in press.



Crystal studies

The molecular structure of HL¹ along with atom numbering scheme is given in Fig. 2.2. The crystal data and structural refinement parameters are given in Table 2.1 and selected bond lengths and angles are given in Table 2.2. The compound crystallizes into a monoclinic lattice with space group *C2/c*. The molecule exists in the *ZE* conformation of thiosemicarbazones since *Z* and *E* configurations are perceived with respect to C6–N3 and C12–N4 bonds respectively. A torsion angle of 171.58(5)° corresponding to the S1–C12–N4–N3 moiety confirms the *trans* configuration of the thiocarbonyl S1 atom [28]. The thiosemicarbazone skeleton comprising of atoms N3, N4, C12, S1 and N5 is almost planar with a maximum deviation of –0.0650(4) Å from the mean plane. The C6–N3 bond distance (1.2858(8) Å) is appreciably close to that of a C=N double bond (1.28 Å) [29], which confirms the azomethine bond formation.

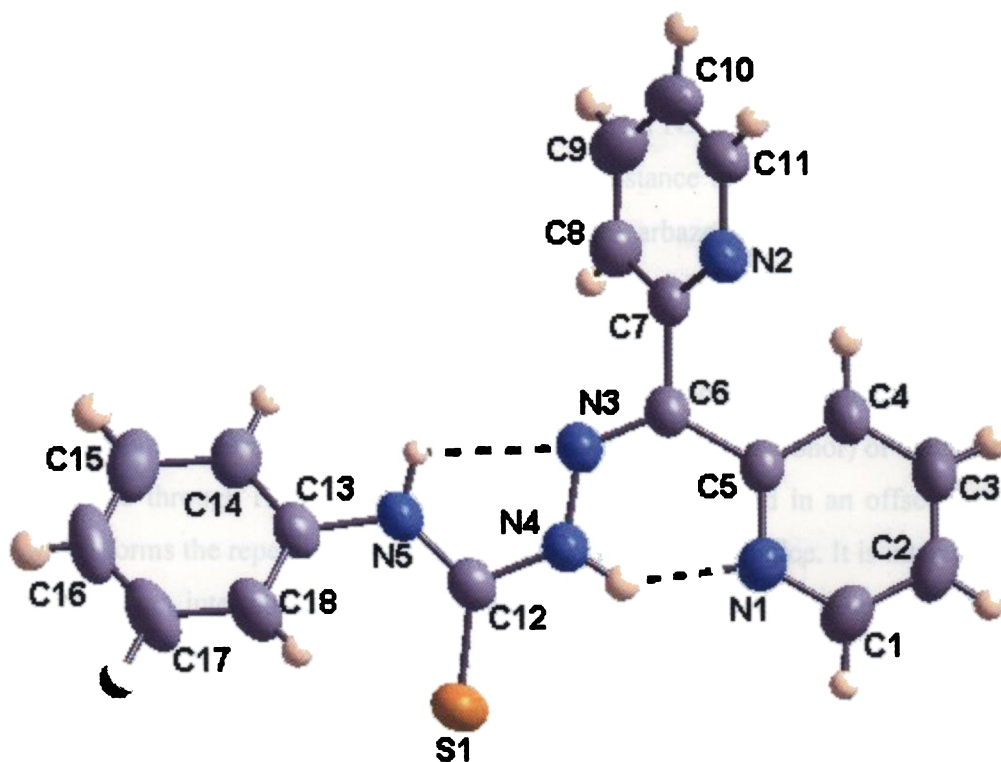


Fig. 2.2. Molecular structure of HL¹. Intramolecular hydrogen bonding interactions are shown as dashed lines

C11; $d_{Cg \cdots Cg} = 3.5809 \text{ \AA}$; ii = $-x, y, \frac{1}{2} -z$] are the shortest interactions observed of the type in the lattice. However, the two intramolecular hydrogen bonding interactions observed are much effective, operating at appreciably short distances, viz., N5–H5N \cdots N3ⁱⁱⁱ [$d_{D \cdots A} = 2.596(2) \text{ \AA}$; $\angle_{D-H-A} = 101.99^\circ$; iii= x, y, z] and N(4)–H(4)N \cdots N(1)ⁱⁱⁱ [$d_{D \cdots A} = 2.670(2) \text{ \AA}$; $\angle_{D-H-A} = 135.65^\circ$]. These intramolecular hydrogen bonding interactions have substantial effects upon the structural as well as spectral properties of the thiosemicarbazone.

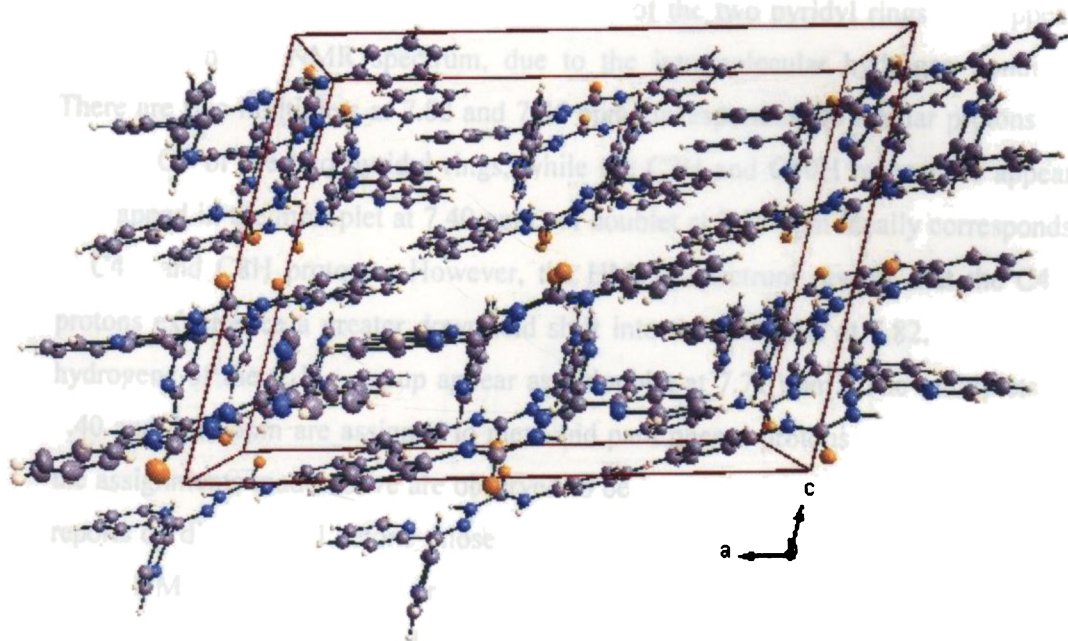


Fig. 2.3. Molecular packing diagram of HL¹, the unit cell is viewed down the 'b' axis

Spectral studies

Proton magnetic resonance spectroscopy is a helpful tool for the identification of organic compounds in conjunction with other spectrometric informations. The ¹H NMR spectrum of HL¹ along with the spectral assignments is given in Fig. 2.4. A sharp singlet, which integrates as one hydrogen at $\delta = 14.55$ ppm is assigned to the proton attached to the nitrogen atom N4, while another similar singlet at 9.55 ppm is assigned to the N5H proton. The downfield shifts of these protons are assigned to their hydrogen bonding interactions with adjacent

The COSY spectrum reveals the ^1H - ^1H coupling interactions in the molecule. It is usually plotted as three-dimensional contours, where the conventional spectrum is represented along the diagonal (Fig. 2.6). The cross-peaks along both the sides of the diagonal identify the nuclei that are coupled to each other. On the contrary, the protons that are decoupled from the adjacent ones due to the lack of α -protons will show no correlation in the spectrum. For instance, in the COSY spectrum of the present compound, absence of any off-diagonal peaks extending from 14.55 and 9.55 ppm confirm their assignment to N4H and N5H protons respectively. However, extending horizontal and vertical lines from 8.84 ppm [C1H] and 8.68 ppm [C11H] encounter cross-peaks at 7.40 ppm, where the C2H and C10H resonances are merged into multiplets along with the phenyl ring proton resonances.

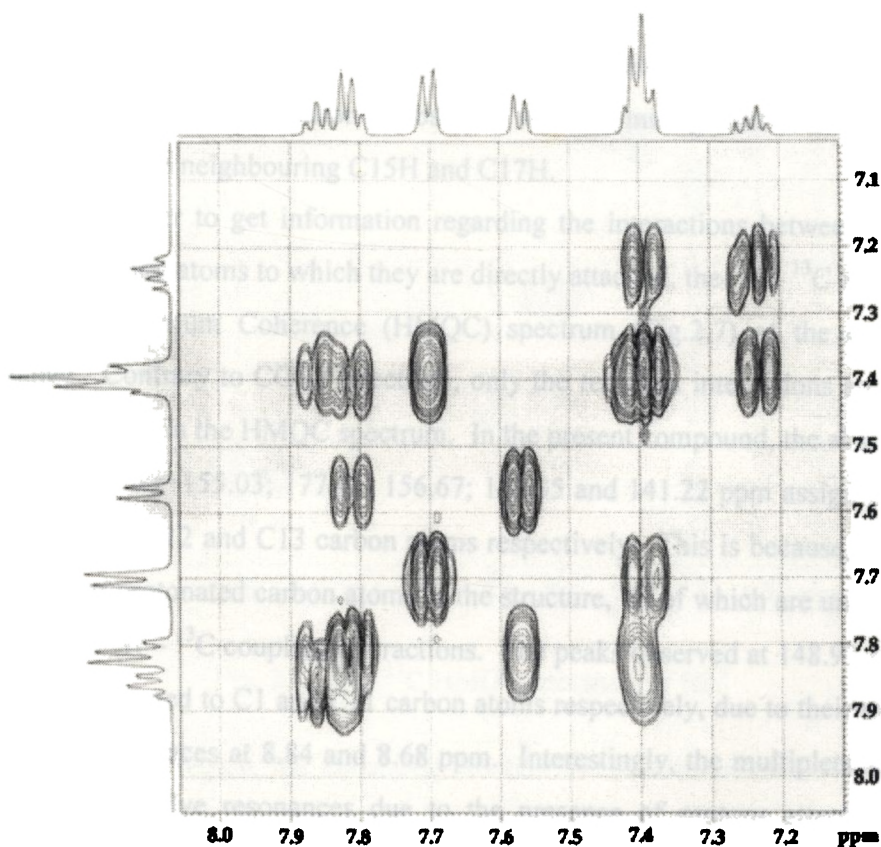


Fig. 2.6. ^1H - ^1H COSY spectrum of compound HL¹

transfer processes in the transition state during the condensation of di-2-pyridyl ketone with *N*(4)-cyclohexylthiosemicarbazone. A suggestive mechanistic approach would be that the double bond formation and the rehybridisation of carbon and nitrogen atoms from tetrahedral sp^3 structure of the hemiaminal intermediate to the planar sp^2 structure of the imine product lag behind other processes such as proton removal and electron delocalization in the transition state. As stated by Sayer and Jencks [39], the energetic advantage of maintaining significant overlap and bonding with the departing oxygen and hydrogen atoms in an sp^3 hybridised transition state is more than enough to offset the stabilization achieved through a carbon-nitrogen double bond by rehybridisation towards a planar sp^2 structure.

Crystal studies

The compound crystallizes into a triclinic lattice with space group $P\bar{1}$ and the molecular structure of HL² along with atom numbering scheme is given in Fig.2.9.

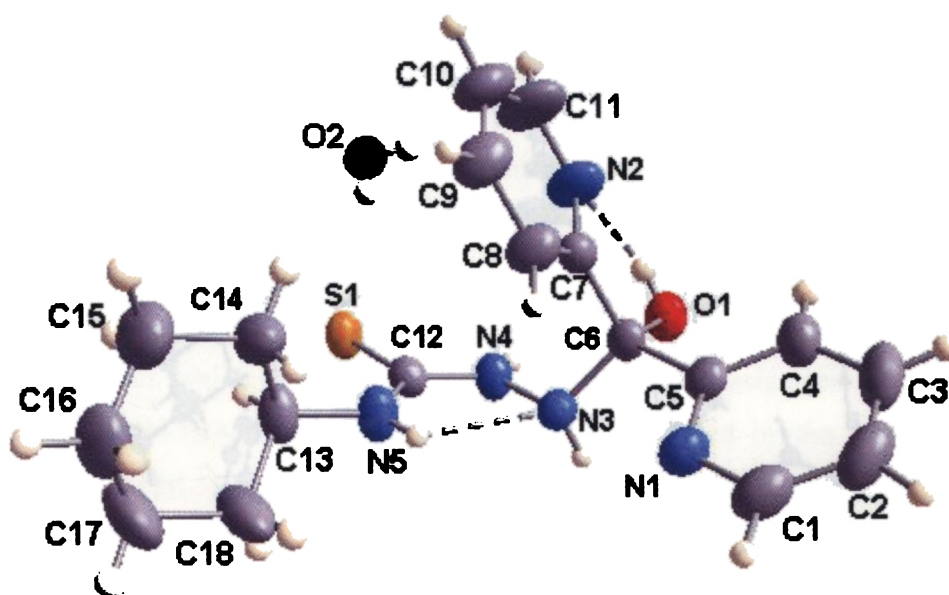


Fig. 2.9. Molecular structure of HL². The ellipsoids are drawn at 50% probability and the intramolecular hydrogen bonding interactions are shown as dashed lines

The crystal data parameters are given in Table 2.1 and selected bond distances and angles are given in Table 2.2. The molecule is non-planar as a whole, whereas the central moiety comprising of atoms N3, N4, C12, S1 and N5 is almost

planar with a maximum deviation of 0.0211(3) Å from the mean plane. A torsion angle of 177.86(11)° corresponding to the S1–C12–N4–N3 moiety confirms the trans configuration of the thiocarbonyl S1 atom [28]. Unlike the azomethine double bond in thiosemicarbazones, the C6–N3 bond distance (1.464(2) Å) is more close to that of a C–N single bond [29], supporting the hemiaminal structure of the compound. In order to minimize the steric strain, the bulky pyridyl groups are deviated farthest with a dihedral angle of 75.31(1)° between each other. The intramolecular hydrogen bonding interactions, *viz.*, N5–H401---N3 and O1–H101---N2 lead to the formation of two five membered rings comprising of atoms N3, N4, C12, N5, H401 and N2, C7, C6, O1, H101 respectively. Ring puckering analyses and least square planes calculations show that the cyclohexyl ring, Cg(3) adopts a chair conformation ($Q_T = 0.5404$ Å).

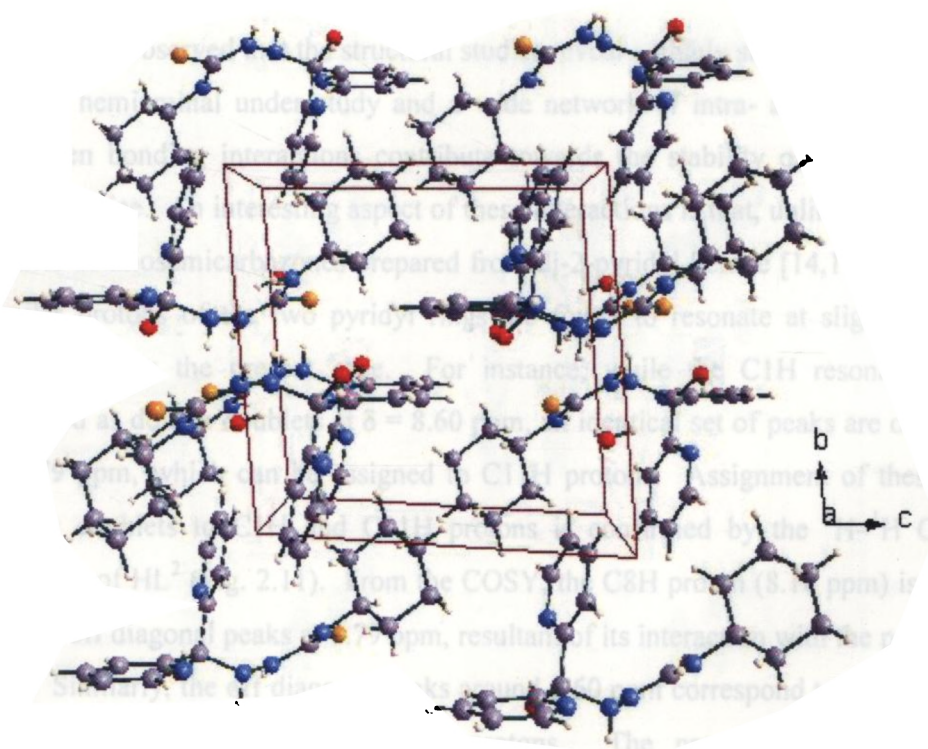


Fig. 2.10. Molecular packing diagram of HL², the unit cell is viewed down the 'a' axis

The molecular packing of compound HL² is shown in Fig. 2.10. The unit cell is viewed down the 'a' axis and the repeating unit consists of two molecules set

hydrogen bonding, which shifts the C11H resonance to more downfield compared to that of the C1H proton.

The molecule as a whole adopts a conformation in which the pyridyl ring with N2 is highly strained with active participation in the hydrogen bonding interactions. This results in a redistribution of electron density over the entire ring causing slight variations in the resonating frequencies of similar protons on the two pyridyl rings. Hence the C2H and C10H peaks are observed as triplets at 7.28 and 7.38 ppm respectively, while the C3H and C9H resonances are perceived as multiplets centred around 7.71 and 7.50 ppm respectively. Similarly, the doublets at 8.10 ppm and the doublet of a triplet at 7.90 ppm are assigned to C8 and C4 protons respectively. Assignment of these peaks to the respective protons is carried out with the help of ^1H - ^1H correlation data available from the COSY spectrum.

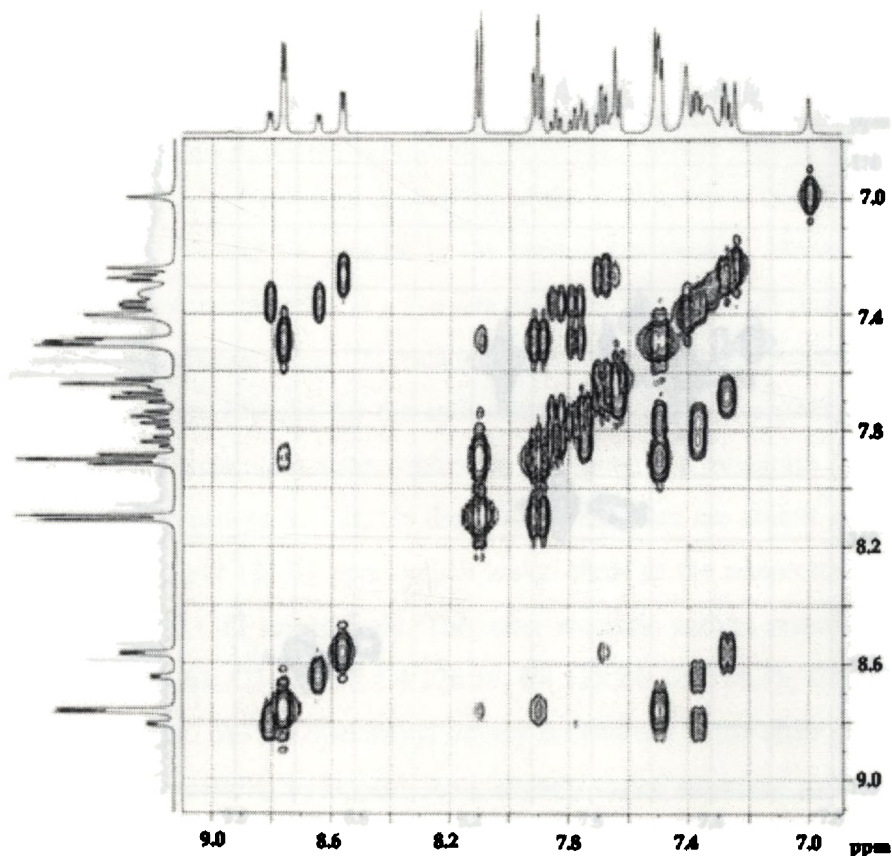


Fig. 2.11. ^1H - ^1H COSY spectrum of HL^2

Two sets of double doublets observed at 8.79 and 8.60 ppm for protons α to pyridyl nitrogens attribute interesting features to the compound under study. The ^1H NMR spectrum of the present compound follows strictly first order with well-separated chemical shift positions for protons with different environments. For example, the signal for C1H proton appears as a double doublet around 8.60 ppm due to the following coupling pattern observed between adjacent protons. At first, the proton at C1 couples with C2 proton, which splits the C1H signal into a doublet. But C1H also couples with C3H so that each line of the C1H is further split into two, giving a double doublet [33]. Although doublets and double doublets are reported previously [22] two well-defined sets of double doublets corresponding to two similar pyridyl protons are observed for the first time in substituted thiosemicarbazones.

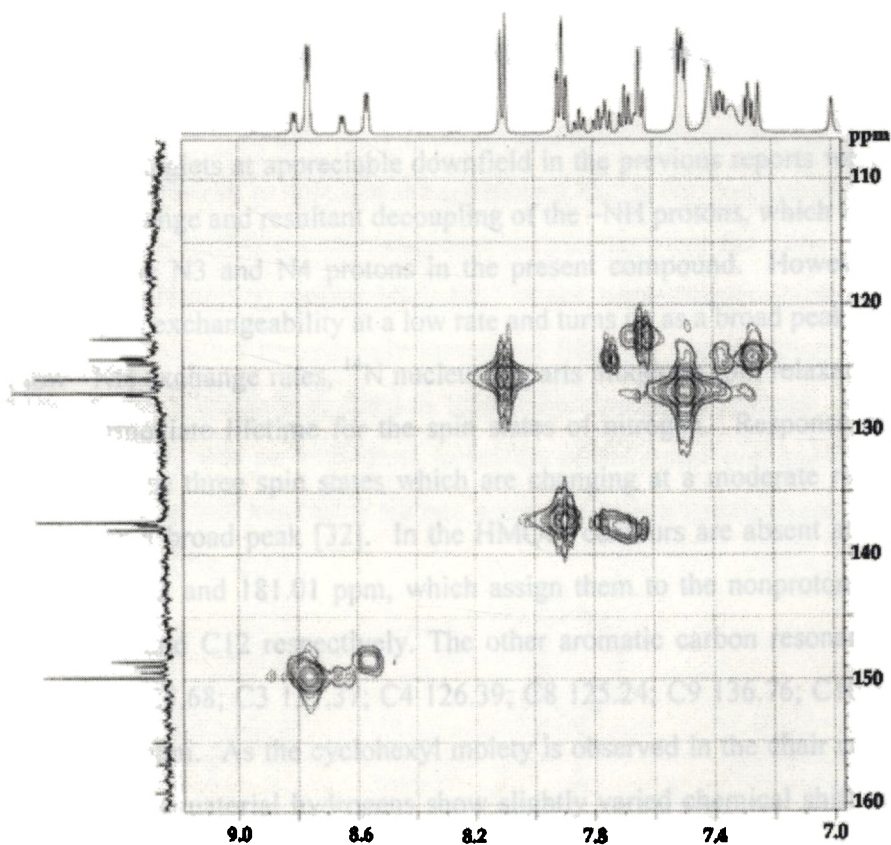


Fig. 2.12. $^1\text{H} - ^{13}\text{C}$ HMQC spectrum of HL^2

However, the yield of the compound HL^3 is observed to be very low. Hence for the preparation of some of the complexes of HL^3 , a one-pot method is employed successfully. Here, equimolar solutions of di-2-pyridyl ketone and *N*(4)-cyclohexylthiosemicarbazone are allowed to react for four hours, after that a solution of the stoichiometric amount of the metal salt is directly added to the solution and the refluxing continued for more than six hours, which produced the complexes in good yield.

Crystal studies

We could successfully isolate X-ray quality single crystals from a methanolic solution of the compound. The molecular structure of HL^3 along with atom numbering scheme is given in Fig. 2.14. The crystal data and structural refinement parameters are given in Table 2.1 and selected bond lengths and angles are given in Table 2.2.

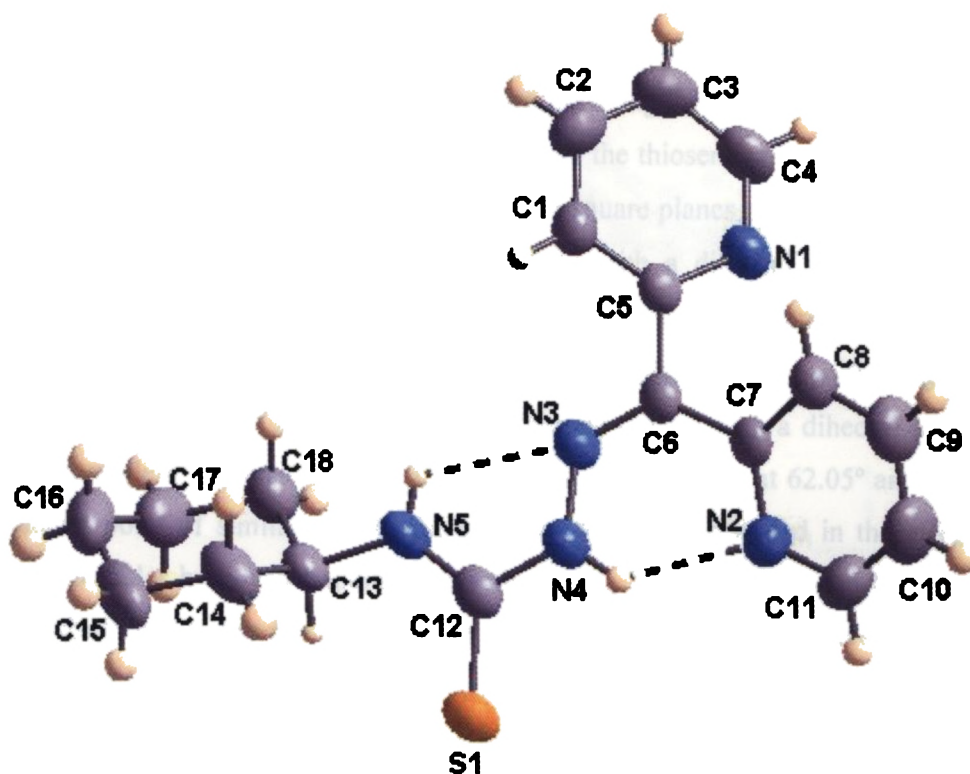


Fig. 2.14. Molecular structure of HL^3 . Ellipsoids are drawn at 50% probability and intramolecular hydrogen bonding interactions are shown as dashed lines

The molecular packing of HL³ is shown in Fig. 2.15. The unit cell is viewed down the 'a' axis. The repeating unit consists of a set of two molecules aligned in an offset fashion, which are aligned in such a way that the cyclohexyl rings of both the molecules are positioned close to each other. Each molecule repeats separately in a one-dimensional manner in the crystal lattice, and since these one-dimensional arrays are aligned in an offset fashion, a two-dimensional zig-zag packing is effected in the unit cell. The $\pi - \pi$ interactions observed in the crystal are rather weak, as they are observed at distances longer than 4.0 Å. Similarly, the C-H--- π interactions are also observed to be weak, since they are observed at distances greater than 3.7 Å. The intermolecular hydrogen bonding interactions are observed at a minimum donor-acceptor distance of 3.6 Å, which decreases the efficiency of the contact. However, the two prominent intramolecular hydrogen bonding interactions are observed in the crystal structure, viz., N5-H5A---N3ⁱ [$d_{D\cdots A} = 2.614$ Å; $\angle_{D-H-A} = 110.14^\circ$; $i = x, y, z$] and N4-H4A---N2ⁱ [$d_{D\cdots A} = 2.695$ Å; $\angle_{D-H-A} = 131.29^\circ$].

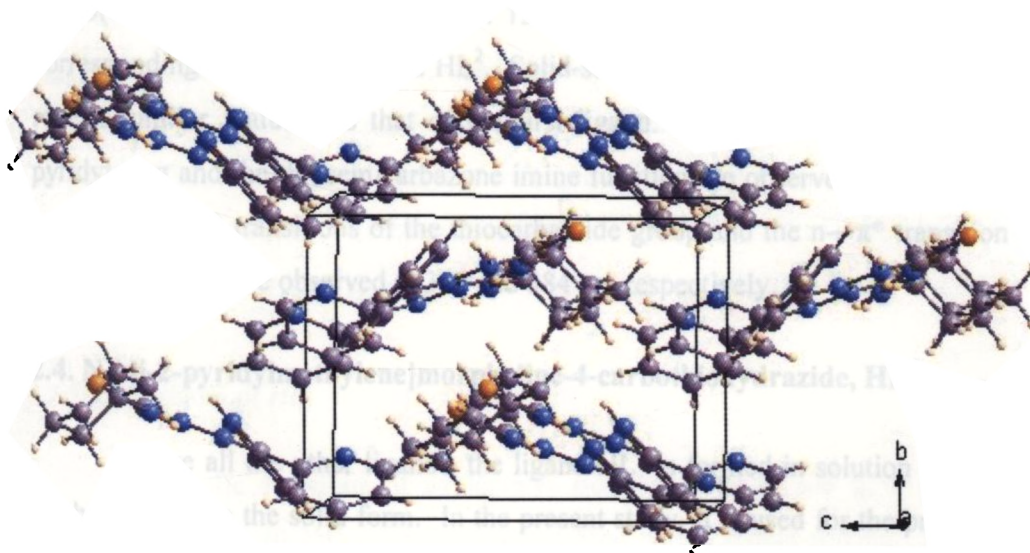


Fig. 2.15. Molecular packing diagram of HL³, the unit cell is viewed down the 'a' axis

Spectral studies

The compound is also characterized using infrared and electronic spectral studies. The low yield of HL³ denied the possibility for the NMR characterization of the compound. However, as far the structure of the compound is concerned, the

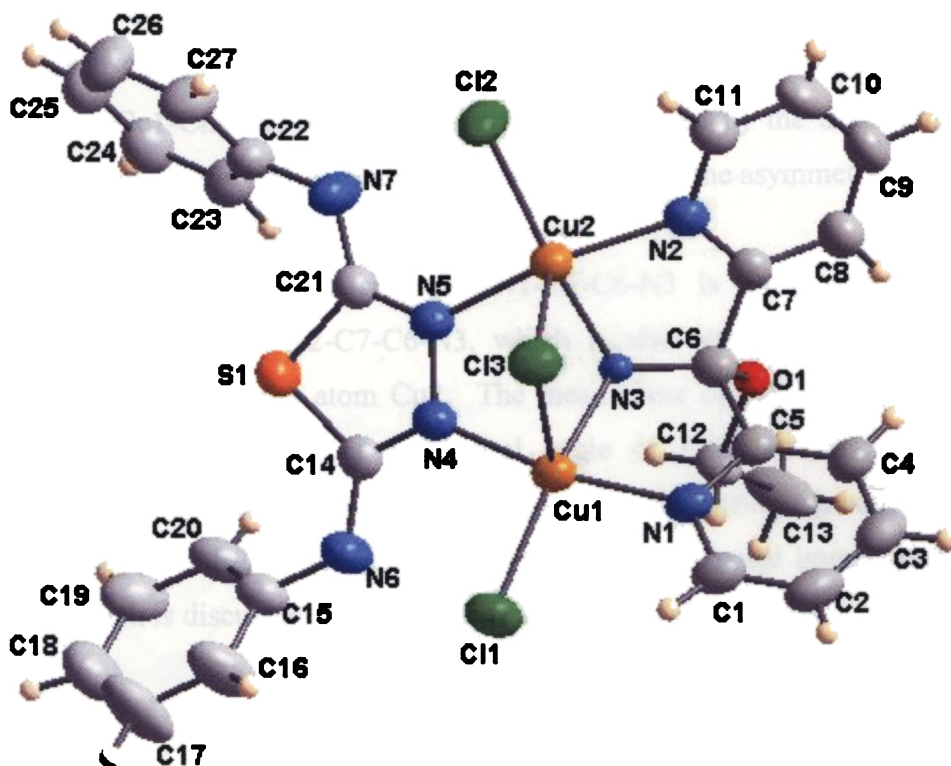


Fig. 3.1. Molecular structure of Cu_2TDCl_3 . The ellipsoids are drawn at 50% probability level

The skeletal structure at the metal centres can be regarded as two edge-sharing square pyramids. The $\text{Cu1}-\text{Cl3}-\text{Cu2}$ and the $\text{Cu1}-\text{N3}-\text{Cu2}$ angles are observed at $70.79(3)$ and $96.73(8)^\circ$ respectively and the bridging is found to be asymmetric with unequal apical bond lengths of the square pyramids ($\text{Cu1}-\text{Cl3} = 2.5790(13)$ Å; $\text{Cu2}-\text{Cl3} = 2.5347(17)$ Å). Also, Cu1 is $0.2132(4)$ Å out of the mean basal plane (atoms N1, N3, N4 and Cl1), whereas Cu2 is deviated at $0.2761(3)$ Å from its basal plane (atoms N2, N3, N5 and Cl2) towards the apical chlorine atom Cl3. This reveals greater pull on the chlorine Cl3 by Cu2 rather than Cu1, thus giving rise to asymmetry in bridging.

Interestingly, the overall structure of the molecule is composed of a number of six-membered and five-membered rings, mostly aromatic, which attribute much electron delocalization along the overall molecule, imparting stability to the structure. The thiadiazole ring is very nearly planar with a maximum deviation of $-0.0021(3)$ Å

at N5 from the mean plane, while the Cremer and Pople ring puckering analyses reveals that the two metal chelate rings, composed of N3, Cu1, N4, N5 & Cu2 and Cl3, Cu1, N4, N5 & Cu2 are observed to form envelopes on N3 and Cl3 respectively. The bridging plane Cu1-Cl3-Cu2-N3 is non-planar, as evidenced by the maximum mean deviation value of $-0.2961(5)$ Å. This is in accordance with the asymmetry in the Cu – Cl3 bonding suggested earlier.

Also, the metal chelate ring Cu1-N1-C5-C6-N3 is more puckered when compared to the ring Cu2-N2-C7-C6-N3, which is also attributed to the stronger Cu–Cl3 interaction of copper atom Cu2. The mean plane of the bridging Cu1-Cl3-Cu2-N3 moiety is positioned at a dihedral angle of $79.95(2)^\circ$ with the planar thiadiazole ring. However, the most interesting aspect of the bridging, coupled with a Cu1–Cu2 separation of $2.9591(13)$ Å is the strong spin-exchange interactions in the compound, which is discussed in detail at a later section of this chapter.

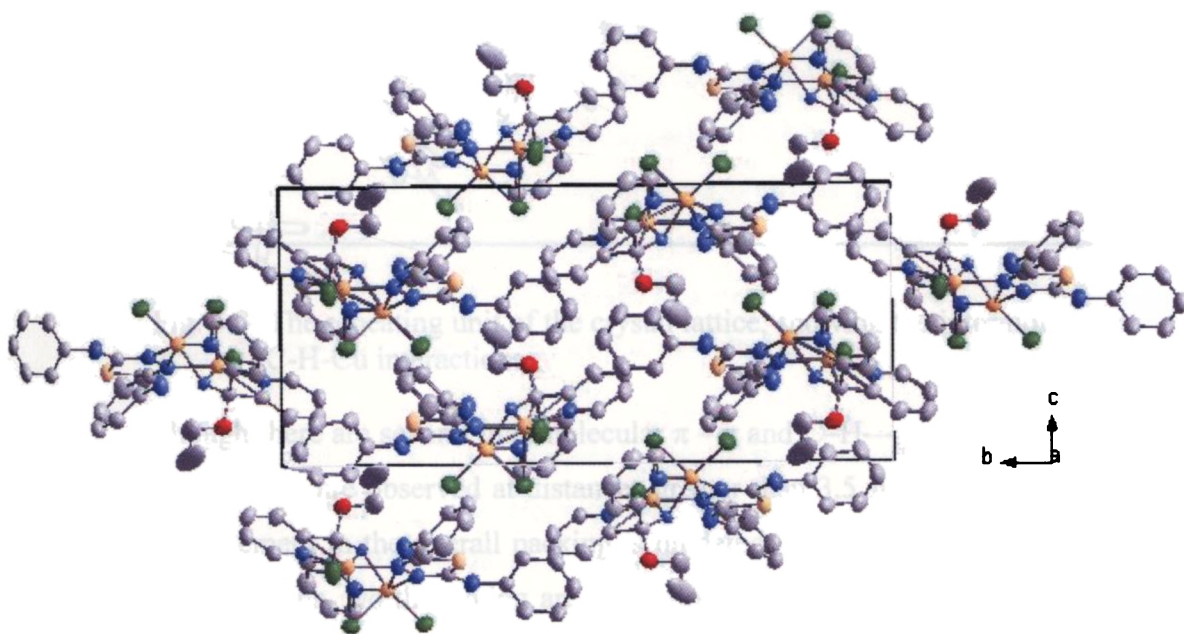


Fig. 3.2. Molecular packing diagram of Cu_2TdCl_3 , hydrogen atoms are omitted for clarity

Much stability is attributed to the structure through hydrogen bonding, $\pi - \pi$ and CH – π interactions in the crystal lattice. The molecular packing diagram of Cu_2TdCl_3 is given in Fig. 3.2, and the unit cell is viewed down the 'a' axis. The basic repeating unit in the crystal lattice is a set of two molecules, which are held together by

intermolecular C–H–Cu bonding interactions (Fig. 3.3) involving the hydrogens on C16 and C17 atoms of one molecule with the Cu2 atom of the adjacent molecule [C17–H17---Cu2 = 3.387 Å; C16–H16---Cu2 = 3.133 Å]. Two such adjacent units are then arranged in an offset fashion to each other, and in the crystal lattice, these two sets repeat one-dimensionally along the ‘c’ axis, contributing towards a zig-zag packing of the molecule.

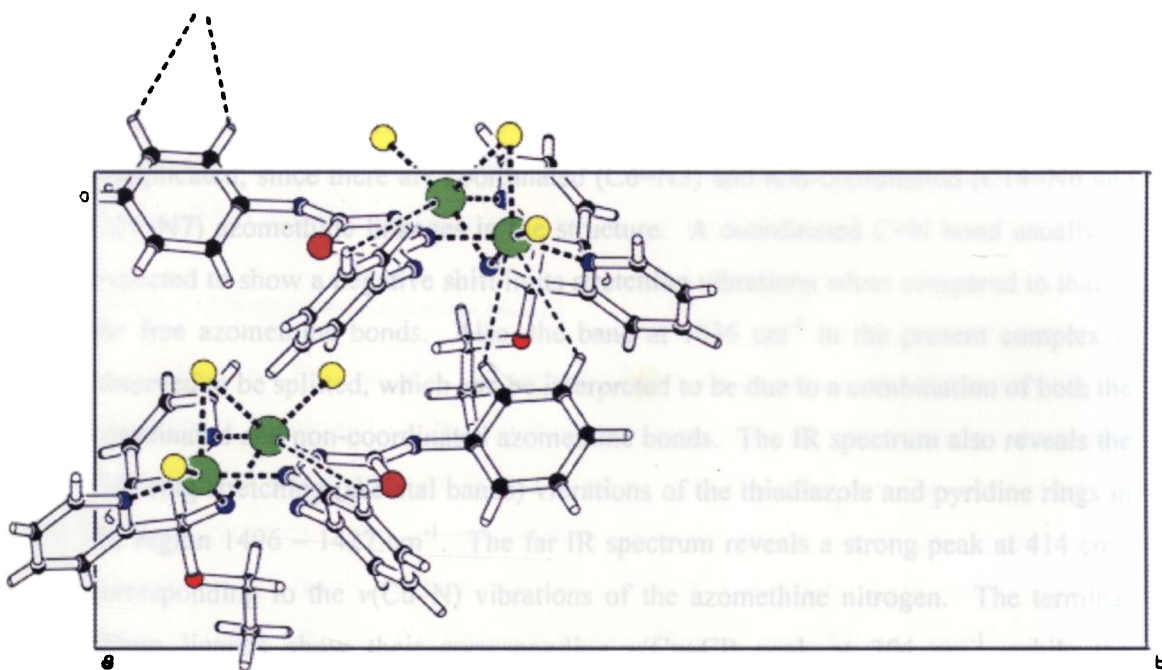


Fig. 3.3. The repeating unit of the crystal lattice, showing the intermolecular C-H-Cu interactions

Although there are several intermolecular $\pi - \pi$ and C–H--- π interactions in the lattice, most of them are observed at distances greater than 3.5 Å, due to which their effective involvement in the overall packing is hindered. Some of the weak C–H--- π and $\pi - \pi$ interactions, worth quoting are the following: C(12)–H(12A)–[1]–Cg(11)ⁱ [Cg(11): Cu(1), N(1), C(5), C(6), N(3); $d_{C(12)\cdots Cg} = 2.7987$ Å; $i = x, y, z$]; C(17)–H(17)–[1]–Cg(19)ⁱⁱ [Cg(19): N(2), C(7), C(8), C(9), C(10), C(11); $d_{C(17)\cdots Cg} = 3.5447$ Å; $ii = x, \frac{1}{2}-y, \frac{1}{2}+z$]; C(23)–H(23)–[1]–Cg(15)ⁱⁱⁱ [Cg(15): S(1), C(14), N(4), N(5), C(21); $d_{C(23)\cdots Cg} = 2.7987$ Å; $iii = x, \frac{1}{2}-y, -\frac{1}{2}+z$] and Cg(11)–[1]–Cg(19)ⁱ; $d_{Cg\cdots Cg} = 3.8363$ Å]. Three appreciable intra-molecular hydrogen bonding interactions are observed, viz., C(8)–H(8)---O(1)ⁱ [$d_{D\cdots A} = 2.797(1)$ Å, $\angle_{D-H-A} = 97.77^\circ$]; C(12) – H(12)B ---N(3)ⁱ

4.1. Stereochemistry of the complexes

The electronic structure of manganese reveals that it can have a maximum oxidation state of +7. However, the manganese complexes under the present study exist in the +2 oxidation state. The characteristic coordination number of Mn(II) is six in the present complexes, which corresponds to octahedral stereochemistry.

4.1.1. $\text{Mn}(\text{L}^1)_2 \cdot \text{H}_2\text{O}$ (9)

We could successfully isolate a single crystal suitable for X-ray diffraction for the compound, which revealed a distorted octahedral structure. Other major tools used for the characterisation include IR, electronic and EPR spectra.

Crystal studies

A single crystal suitable for X-ray diffraction was isolated by the slow evaporation of a solution of the compound in a 1:1:2 mixture of DMF, CH_2Cl_2 and acetone. There are two crystallographically independent molecules in the asymmetric unit of the compound (Fig. 4. 1).

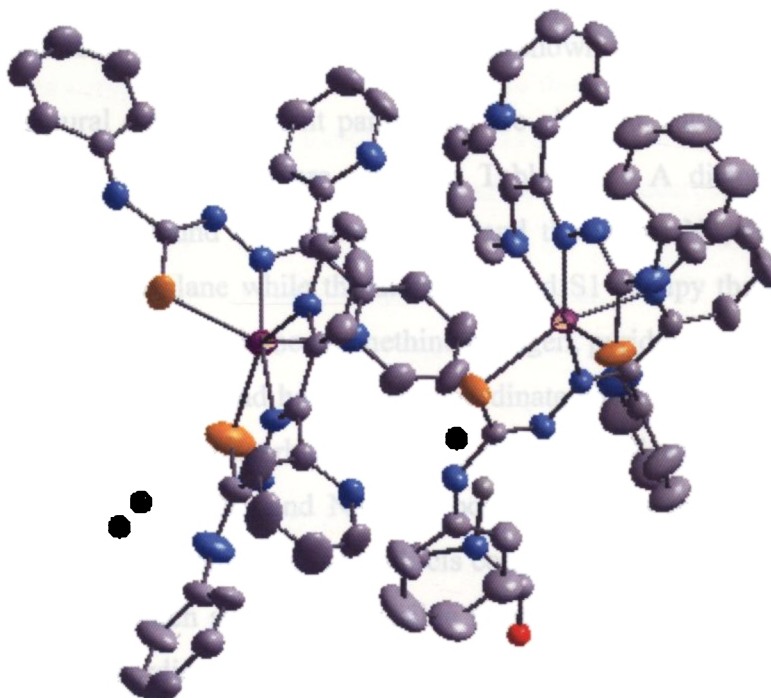


Fig. 4.1. Molecular structure of the compound $\text{Mn}(\text{L}^1)_2 \cdot 1.5(\text{H}_2\text{O}) \cdot 0.5(\text{DMF})$
Hydrogen atoms are omitted for clarity

There are four solvent molecules in the lattice, *viz*, three water molecules and one DMF molecule. The molecular structure of the compound with the atom numbering scheme is given in Fig. 4.2.

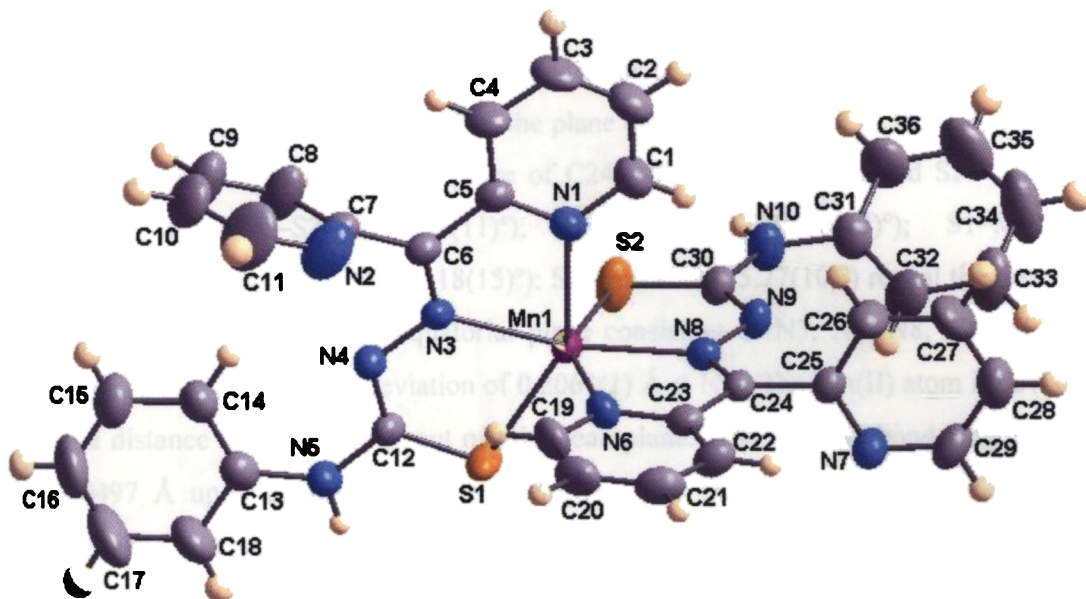


Fig. 4. 2. Molecular structure of one independent molecule $\text{Mn}(\text{L}^1)_2$ in the unit cell with the atom numbering scheme. The ellipsoids are shown with 50% probability.

The structural data refinement parameters are given in Table 4.1 and selected bond distances and bond angles are given in Table 4.2. A distorted octahedral geometry is observed around each metal center and the atoms N3, N6, N8 and S2 constitute the equatorial plane while the atoms N1 and S1 occupy the axial position. The coordination occurs through the azomethine nitrogen, pyridyl nitrogen and thiolate sulfur of two ligand moieties and hence a six-coordinate environment is present about the metal center. The thiosemicarbazone moiety in the free ligand [29] shows an *ZE* conformation about the C6–N3 and N4–C12 bonds, whereas in the present Mn(II) complex, it reveals an *ZZ* conformation with *cis* configurations about both the C6–N3 and N4–C12 bonds, which suggests a possible rotation occurs about the azomethine double bond during coordination. The S1–C12–N4–N3 torsion angle value of $-3.0(6)^\circ$ also evidences that the thiocarbonyl S1 atom is positioned *cis* to the hydrazinic N3 atom. *ZZ* conformation is rarely observed in complexes of di-2-pyridyl ketone derivatives of mono substituted thiosemicarbazones. Earlier, similar *ZZ* conformations

hydrogen bonding interactions are also significant and the list of the intermolecular interactions is given in Table 4.3.

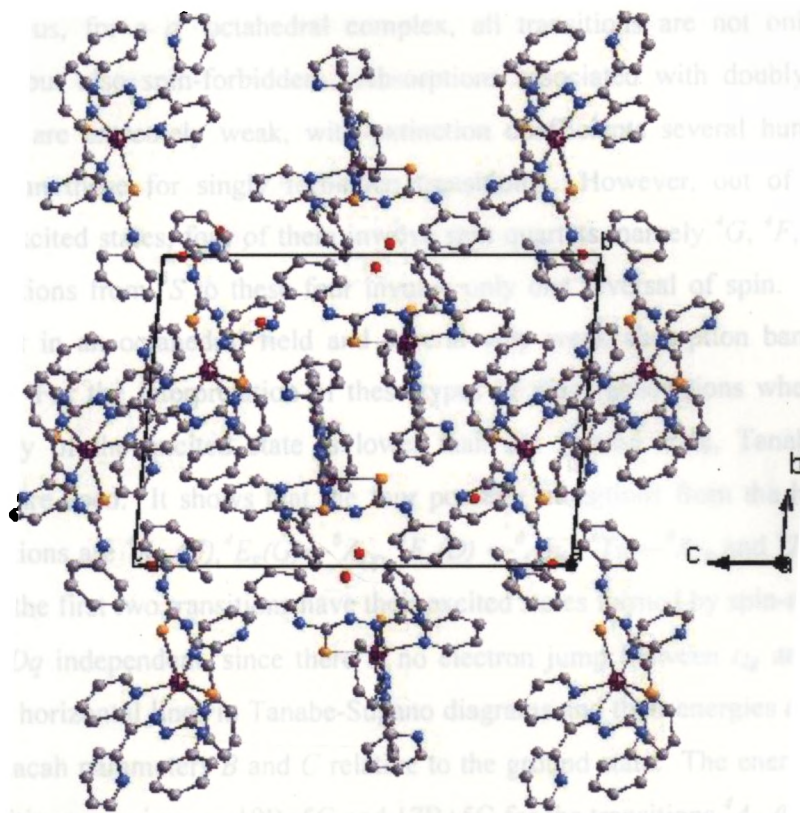


Fig. 4.3. Molecular packing diagram of $\text{Mn}(\text{L}^1)_2 \cdot 1.5(\text{H}_2\text{O})0.5(\text{DMF})$, the unit cell is viewed down the 'a' axis

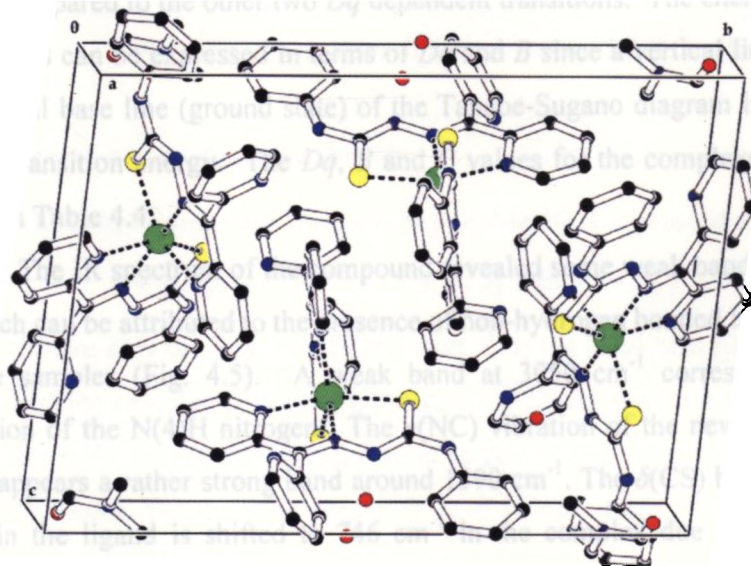


Fig. 4.4. The repeating unit in the lattice of $\text{Mn}(\text{L}^1)_2 \cdot 1.5(\text{H}_2\text{O})0.5(\text{DMF})$

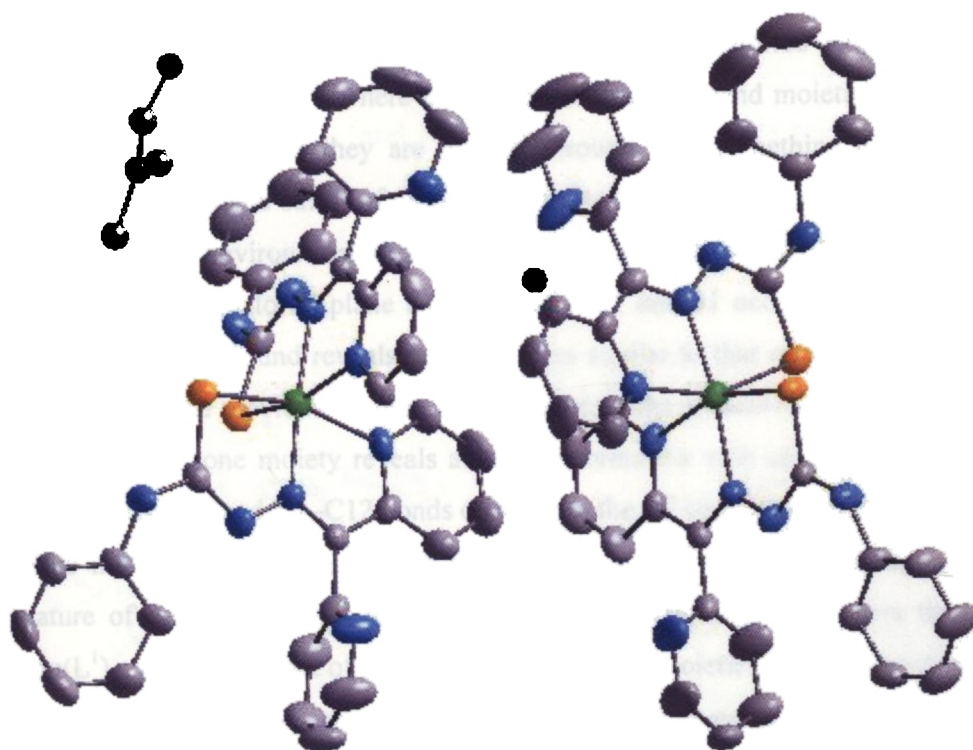


Fig. 5. 1. Molecular structure of the compound $\text{Ni}(\text{L}^1)_2 \cdot 0.5(\text{H}_2\text{O}) \cdot 0.5(\text{DMF})$. Hydrogen atoms are omitted for clarity

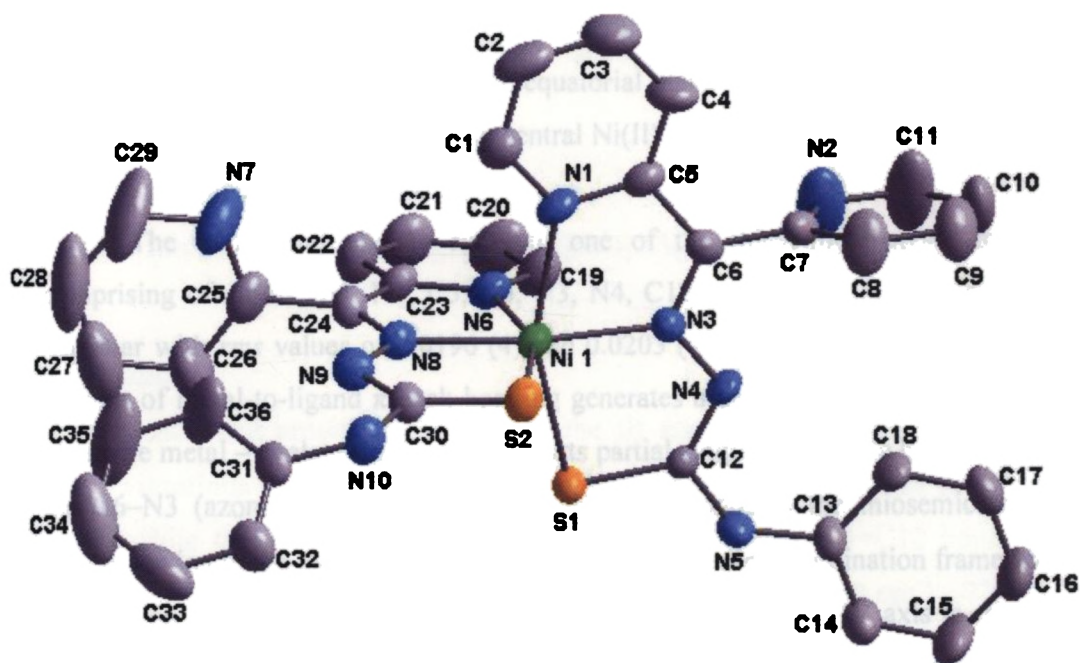


Fig. 5. 2. Molecular structure of $\text{Ni}(\text{L}^1)_2$ in the unit cell. The ellipsoids are shown with 50% probability and the hydrogen atoms are omitted for clarity

repeating unit of the crystal packing. The sets of two molecules repeat one-dimensionally in the lattice. The intermolecular $\pi - \pi$ interactions are observed at distances greater than 3.5 Å, and hence they contribute little towards the effective packing of the molecules in the lattice. However, some C–H--- π interactions, which are rather short, appear significant. The list of intermolecular interactions is given in Table 5.3.

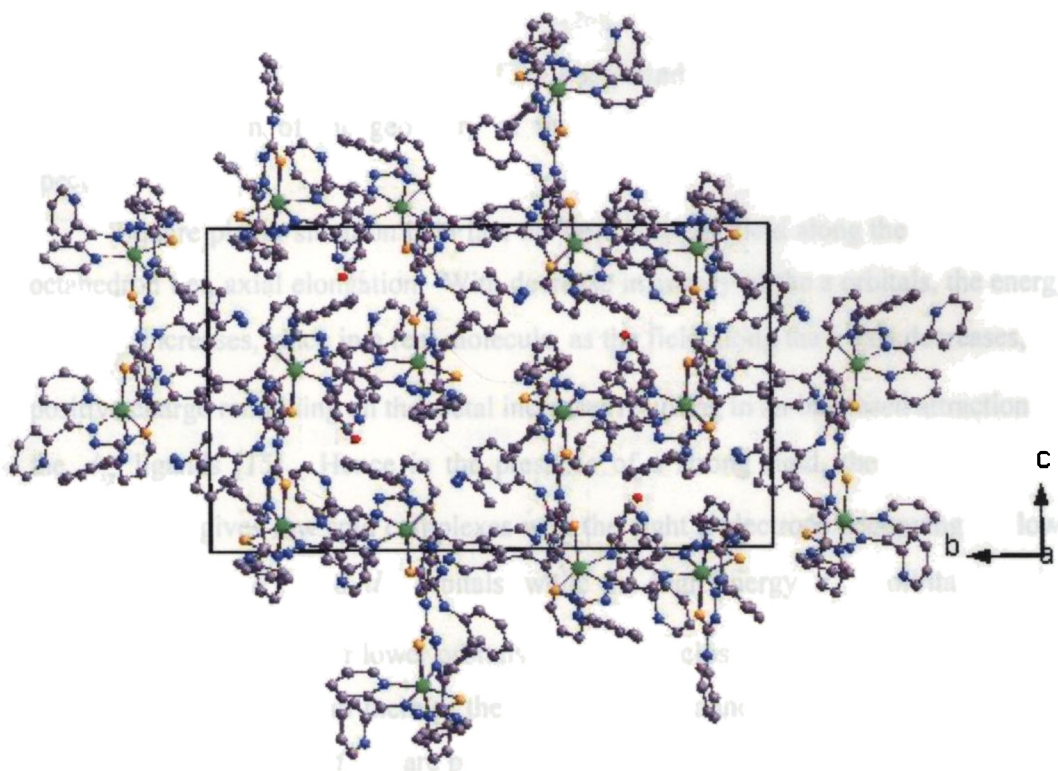


Fig. 5.3. Molecular packing diagram of $\text{Ni}(\text{L}^1)_2 \cdot 0.5(\text{H}_2\text{O}) \cdot 0.5(\text{DMF})$, the unit cell is viewed down the 'a' axis.

Spectral studies

A broad band around 3540 cm^{-1} in the IR spectrum is assigned to the –OH stretching vibrations of lattice water. The azomethine stretching band is shifted to 1562 cm^{-1} while the stretching vibration of the newly formed $\text{N}4=\text{C}12$ bond due to coordination through deprotonation appear as a sharp band at 1589 cm^{-1} . The $\delta(\text{CS})$ band observed at 806 cm^{-1} in the ligand is shifted to 745 cm^{-1} in the complex due to the coordination of the thiol form the thiosemicarbazone moiety. The compound is also characterized by solid-state electronic spectral techniques. The $\pi \rightarrow \pi^*$ and the

equatorial plane is zero. However, the molecule consists of an additional species of a bromide anion outside the coordination sphere. The bromide anion is positioned at a distance of 5.920 Å from the Co(III) center, and it is observed to be hydrogen bonded to four neighboring water molecules.

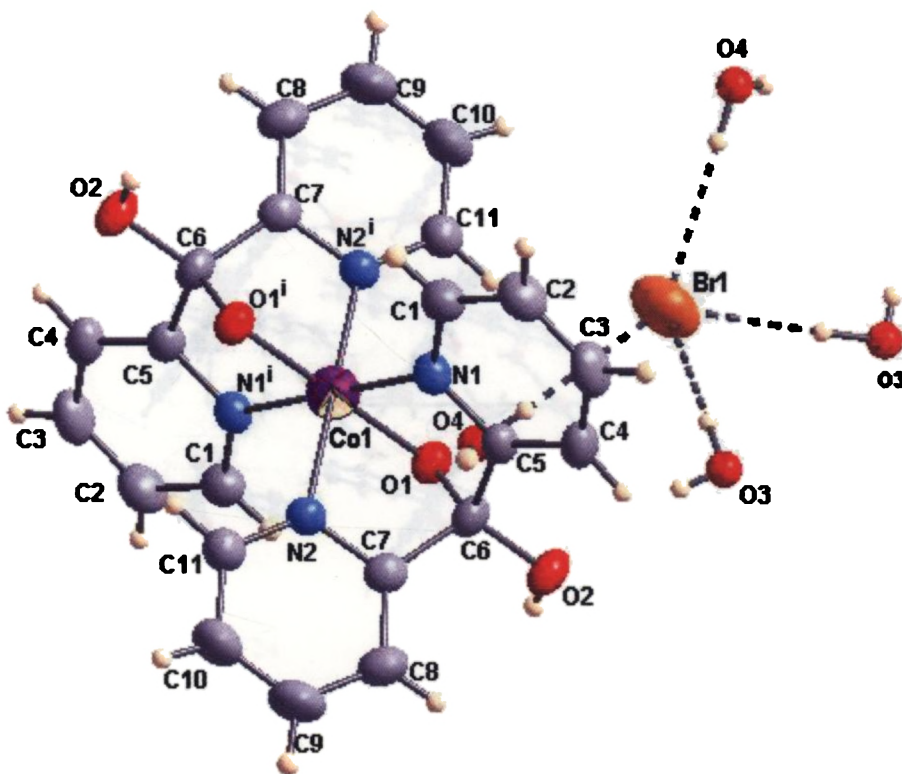


Fig. 6.7. Molecular structure of $[\text{Co}(\text{dpk})]\text{Br}\cdot 4\text{H}_2\text{O}$. The ellipsoids are shown at 50% probability

The packing of the molecules of **28** is shown in Fig. 6.8. The unit cell is viewed down the 'b' axis and a two-dimensional packing is effected in the lattice. The $\text{Co}(\text{dpk})$ units are arranged two-dimensionally in the lattice and the bromide anion and the water molecules interconnect the different $\text{Co}(\text{dpk})$ units through hydrogen bonding interactions. It is observed that the intermolecular $\pi - \pi$ and $\text{C}-\text{H}\cdots\pi$

interactions are rather weak, since they are observed at distances greater than 3.5 Å. The list of the intermolecular and hydrogen bonding interactions is given in Table 6.3.

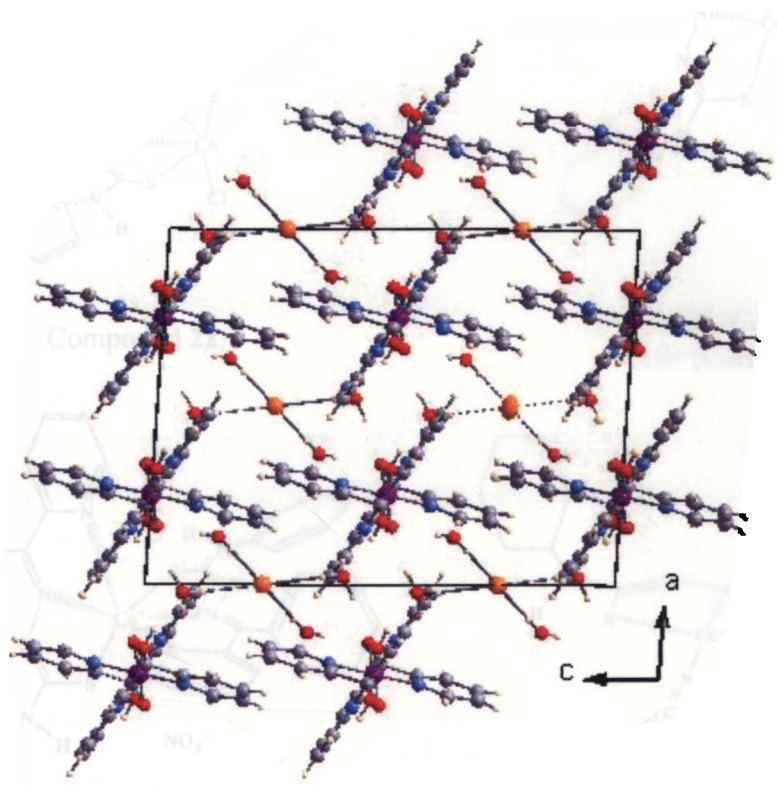


Fig. 6.8. Molecular packing diagram of $[\text{Co}(\text{dpk})]\text{Br}\cdot 4\text{H}_2\text{O}$

The stereochemistry of the various cobalt complexes (**22** – **27**) in the solid state can be proposed as given in Fig. 6.9.